# Synthesis of Heparan Sulfate Oligosaccharides to Study Heavy Metals Binding and Adjuvant Activity

A Thesis
Submitted in partial fulfilment of the requirements
for the degree of
**Doctor of Philosophy**

**By**
**Sandhya Namdev Mardhekar**
**20163464**

Under the guidance of
**Prof. Raghavendra Kikkeri**




**Indian Institute of Science Education and Research,**
**Pune - 411008**
**2022**

**I would like to dedicate my thesis to**
**My Mother**
**Ranjana**

# CERTIFICATE

This is to certify that the work incorporated in this thesis entitled "**Synthesis of Heparan Sulfate Oligosaccharides to Study Heavy Metals Binding and Adjuvant Activity**" submitted by **Sandhya Namdev Mardhekar** was carried out by a candidate at the Indian Institute of Science Education and Research, Pune under my supervision. The work presented here or any part of it has not been included in any other thesis submitted previously for the award of any degree or diploma from any other university or institution.



**Date**: 13/12/2022

**Prof. Raghavendra V. Kikkeri**
Professor
IISER, Pune

# DECLARATION

I hereby declare that the thesis entitled "**Synthesis of Heparan Sulfate Oligosaccharides to Study Heavy Metals Binding and Adjuvant Activity**" submitted for Doctor of Philosophy in Chemistry at Indian Institute of Science Education and Research, Pune, has not been submitted by me to any other university or institution. This work presented here was carried out at the, Indian Institute of Science Education and Research, Pune, India under the supervision of **Prof. Raghavendra Kikkeri**.



**Date**:

**Sandhya Namdev Mardhekar**
PhD Fellow (20163464)
IISER, Pune

# Acknowledgements

I truly believe that whatever and whomever we are today is the reflection of the people with whom we are surrounded and I feel so blessed that I surrounded by the right people who made me who I am today. And this short note is to remind them and me as well how much thankful I am to them. This list of people will be always unfinished because many people came into my life and helped me unknowingly.

If I have to start with my Ph.D. then the first person to whom I would like to express my sincere gratitude is my supervisor **Prof. Raghavendra Kikkeri**. Even though I had no idea about research he selected me with full belief that I will do my best in research, as time passed I realized his dedication to research is his first priority and it gave me a sense of understanding that I have to work hard throughout my Ph.D. and with consistency to fulfill his belief. I have been so fortunate to be able to work with an amazing supervisor who always strives to go above and beyond possibility in research. I always found him with a positive attitude. It is a pleasure working with him and I know he will go on to do great things in the field of glycobiology.

Thank You, Sir.

I would like to thank my collaborators, Dr. Mattan, from Hebrew University, Israel, Dr. Kavita Joshi from NCL, Pune, Prof. Nixon and Dr. Sandeep Mishra from IISER, Pune for their time and efforts. The thesis would not have been completed without their cooperation. I would also like to thank my RAC members, Prof. R. G. Bhat, from IISER, and Dr. D. Shanmugam from NCL, Pune, for their valuable suggestions.

I would like to thank CSIR, IISER Pune for providing me with financial support. My heartfelt thanks to Prof. Jayant Udgaonkar, Director IISER Pune, Prof. Nirmalya Ballav chair of chemistry, and Prof. H.N. Gopi, former Chair of Chemistry for providing excellent research facilities and for giving support during the pandemic days. A big thanks to all the chemistry technical team and instrument operators, especially Mr. Sandeep (for mass spectrometry, Mr. Sandeep and Nitin (for NMR), and Mr. Saurav (for FACS) for making the Ph.D. process much more comfortable.

I would like to thank my lab mates for their unlimited support throughout my Ph.D. Special thanks to my senior, Preeti Ma'am for teaching me the biological techniques and for the philosophical zone which is the peaceful and self-realizing time of my life, and Balamurugan

(*Tom*), for teaching me synthesis, because of him I felt very safe and happy in the lab. Also, Thanks to Prashant, from whom I learned consistency has its own way towards success, and from Suraj, I learned how to do focused and planned work even though on small scales which is almost invisible amount. Also big thanks to lab mates Rohan, Sivakoti, Harikrishna, Chethan, Vijendra,(hardworking), Trimbak, Deepak (humble), Amol, Rakesh (calm), Saurabh(passionate), Sharath, Haritha, Keerthana, Virendra (genuine), Ankita, Dipty, Sajid, Parvatalu, Remya for the joyful and unforgetful memories. Also thanks to Madhuri who showed me the way toward RK lab for my Ph.D., and supported me like a big sister during my initial days.

I am really grateful for having wonderful memories of my Ph. D. with my friend Neetu my homemade dinner partner who lighten-up my mood with her handmade food, Rashmi(sporty), Ruma (caring and hardworking), Saru (chirpy) and Special thanks to Roshani (like her name) for giving me positive vibes and spending nights in the lab with me. This list will be incomplete without my M. Sc. friend Ashwinee, with whom I spent the best days of my life. I believe cooking and gardening are the therapies for healing my body and soul she is my partner during this therapy so thank her.

With all respect, I would like to acknowledge my family, especially my parents who gave me the time of my life for completing my dream and to bloom in my own way. Thanks, for allowing me for everything without any restrictions. Also, I would like to say big thanks to my Sister Vidhya and Her husband Ramchandra for giving me financial support, you are so generous and so kind! Thank You. “It's hard to ask for help financially, but you didn't make me feel bad about it. I'm so grateful for your help. Thanks to my younger brother Vaibhav (Armyman) and his wife Dipty who gave me support and for being there when I needed someone, I truly don't know what I would have done without you.

Last but not least, Thank you to my friend, philosopher, and guide Pavan, for everything that he does for me. His to-do list for me will be always unfinished. I am grateful for your support and your presence in my life. Thank you for playing all my family member’s roles in their absence and making my life beautiful.

Thank you, God, for giving me an opportunity to meet these wonderful people and for giving me this satisfying life. (*ॐ नमः शिवाय*)

Thank you, **S@ndhy@** for holding you through everything.



Sandhya Mardhekar

# Contents

Abbreviations ……..10

Abstract……16

Publications ……18

## Chapter-1 Introduction

1.1 Abstract ……...20

1.2 Introduction ……....21

1.3 HS biosynthesis ……..….23

1.4 Heparan sulfate binding proteins ……....24

1.4.1 Growth factors ……..25

1.4.2 Antithrombin ……26

1.4.3 Chemokines ……..27

1.5 Conclusion ……..30

1.6 References……31

## Chapter-2 Synthesis of heparan sulfate oligosaccharides to study heavy metals binding

2.1 Abstract ……36

2.2 Introduction ……...37

2.3 Results and discussion ……...38

2.3.1 Synthesis of G-tetrasaccharides……...38

2.3.2 Preparation of HS-GCs ……41

2.3.3. HS-GC exposure to heavy metal ions……42

2.3.4 EIS measurements ……42

2.3.5 CA, CDS analysis ……..43

2.3.6 XPS analysis ……..43

2.3.7. Impedimentric response study to heavy metal ions ……44

2.3.8 CA, CPD and XPS surface analysis for I-6S and G-6S toward Cd2+ and Hg2+ …….49

2.4 Conclusion ……52

2.5 Experimental part ……..52

2.6 1H, 13C and DEPT NMRs ……71

2.7 References…….90

## Chapter-3 Glycosaminoglycan nanoprobes platform for tuning phenotypic cellular uptake

3.1 Abstract ……93

3.2 Introduction ……..94

3.3 Results and discussion……..95

3.3.1 Synthesis of HS and CS fluorescent conjugated nanoprobes ……95

3.3.2 physicochemical characterization of HS and Cs fluorescent conjugated nanoprobes…97

3.3.3 Quantification of sugar concentration on nanoparticle surface …….98

3.3.4 Cellular uptake studies …… ....99

3.3.5 Flow cytometry assay ……101

3.3.6 Quantification of CD44 expression level ……101

3.3.7 Homing of nanoprobes in cancerous and neural cells ……102

3.4 Conclusion ……..104

3.5. Experimental part ……...105

3.6 NMRs ……..111

3.7 References ……...115

## Chapter-4 Synthesis of carbohydrate based adjuvants

4.1 Abstract ……120

4.2. Introduction ……121

4.3 Results and discussion……..122

4.3.1 1$^{st}$ generation HS tetrasaccharides ……122

4.3.2 TLR4 and TLR2 activity of HS oligosaccharides…….123

4.3.3 Monosaccharide and disaccharide HS derivatives ……124

4.3.4 Synthesis of N-palmitic acid conjugated glucosamine derivatives -…….……125

4.3.5 Synthesis of N-acetate glucosamine derivatives ……...126

4.3.6 Synthesis of N-unsubstituted glucosamine derivatives …….127

4.3.7. Synthesis of glucose derivatives……127

4.3.8 Synthesis of galactose derivatives……...……...……...128

4.3.9. Synthesis of glucuronic acid derivatives……129

4.3.10 Synthesis of glucuronic acid disaccharide derivatives ……...…..130

4.3.11 TLR agonist activity of mono and disaccharides …….…...131

4.4 Conclusion ……..……..132

4.5 Experimental part ……..…132

4.6 NMRs …….…..150

4.7 References ……195

**Chapter-5 Pairing nanoparticles geometry with TLR agonists to modulate immune responses for vaccine development**

5.1 Abstract……..196

5.2 Introduction……197

5.3 Results and discussion……...……198

5.3.1 Synthesis of tripodal derivative of imidazoquinolin ……..…...198

5.3.2 Synthesis and characterization and quantification of AuNPs conjugates with CpG and tripodal imidazoquinolin adjuvants ……..….200

5.3.3 Cytokine production study …….……..202

5.3.5 Co-localization assay ……...204

5.4 Conclusion……...205

5.5 Experimental part …….……..205

5.6 NMRs …….…214

5.7 References …….….218

# Abbreviations

## A

| | |
|---|---|
| $Ac_2O$ | Acetic Anhydride |
| AcOH | Acetic Acid |
| AD | Alzheimer Disease |
| AF555 | Alexa Fluor 555 |
| AgOTf | silver trifluoromethanesulfonate |
| AM | Acetoxymethyl |
| AT | Antithrombin |
| ATP | Adenosine Triphosphate |

## B

| | |
|---|---|
| BAIB | Bis(acetoxy)iodobenzene |
| BACE-1 | Beta-site APP Cleaving Enzyme 1 |
| BE | Binding Energy |
| Bn | Benzyl |
| BMP-2 | Bone Morphogenetic Protein 2 |
| Bz | Benzoyl |

## C

| | |
|---|---|
| CA | Contact Angle |
| CAMs | Cell Adhesion Molecules |
| CBDs | Carbohydrate Binding Domains |
| CM5 | Carboxymethylated |
| CS | Chondroitin Sulfate |
| CV | Cyclic Voltammetry |
| CPD | Contact Potential Difference |
| CVDs | Cardiovascular Disease |

## D

| | |
|---|---|
| DCM | Dichloromethane |
| DDQ | 2,3-Dichloro-5,6-dicyano-1,4-benzoquinone |
| DMAP | 4-Dimethylaminopyridine |
| DMEM | Dulbecco's Modified Eagle's Medium |
| DMF | Dimethylformamide |
| DPPC | Diphenyl Phosphoryl Chloride |
| DS | Dermatan Sulfate |
| DTI | Direct Thrombin Inhibitor |

## E

| | |
|---|---|
| ECM | Extracellular Matrix |
| EDTA | Ethylenediaminetetraacetic acid |
| EGF | Epidermal Growth Factor |
| EGFR | Epidermal Growth Factor Receptor |
| EIS | Electrochemical impedance spectroscopy |
| ELISA | Enzyme-Linked Immunosorbent Assay |

## F

| | |
|---|---|
| FBS | Fetal Bovine Serum |
| FDA | Food and Drug Administration |
| aFGF | acidic Fibroblast Growth Factor |
| bFGF | basic Fibroblast Growth Factor |
| FGFR | Fibroblast Growth Factor Receptor |
| FITC | Fluorescein isothiocyanate |

## G

| | |
|---|---|
| GAGs | Glycosaminoglycans |
| Gal | Galactose |
| GalN | Galactosamine |

| | |
|---|---|
| GCE | Glassy Carbon electrode |
| GCP | Glassy Carbon Plates |
| GlcA | Glucuronic Acid |
| GFs | Growth Factors |
| GlcA | Glucuronic acid |
| GluN | Glucosamine |
| GPCRs | G-Protein Coupled Receptors |

## H

| | |
|---|---|
| HA | Hyaluronic acid |
| HCA | Hierarchical Cluster Analysis Hep Heparin |
| HR-ESI-MS | High Resolution Electrospray Ionisation Mass Spectrometry |
| HRP | Horseradish Peroxidase |
| HS | Heparan Sulfate |
| HSBPs | Heparan Sulfate Binding Proteins |
| HS-GC | Heparan Sulfate- Glassy Carbon Surfaces |
| HSPGs | Heparan Sulfate Proteoglycans |
| HSPI | HS-Protein nteractions |
| HUVECs | Human Umbilical Vein Endothelial Cells |

## I

| | |
|---|---|
| IdoA | Iduronic Acid |
| ITC | Isothermal Titration Calorimetry |

## K

| | |
|---|---|
| KS | Keratan Sulfate |

## L

| | |
|---|---|
| LiOH | Lithium Hydroxide |
| LMWH | Low Molecular Weight Heparin |

## M

| | |
|---|---|
| MAPK | Mitogen-activated Protein Kinases |
| MCP | Monocyte Chemoattractant Protein |
| MeI | Methyl Iodide |
| MS | Molecular Sieves |

## N

| | |
|---|---|
| NA | N-Acetyl |
| NAP-Br | 2-(Bromomethyl)naphthalene |
| NHS | N-Hydroxysuccinimide |
| NIS | N-Iodosuccinimide |
| NMR | Nuclear Magnetic Resonance |
| NU | N-Unsubstituted |

## P

| | |
|---|---|
| PBS | Phosphate Buffered Saline |
| PHF | Paired Helical Filaments |
| PMSF | Phenylmethane Sulfonyl Fluoride |
| PSGL-1 | P-Selectin Glycoprotein Ligand -1 |
| PTSA | p-Toluenesulfonic Acid |
| PVDF | Polyvinylidene Fluoride |
| py | Pyridine |

## R

| | |
|---|---|
| RE | Reference Electrode |
| RFU | Relative Fluorescence Units |
| RPTPσ | Receptor Protein Tyrosine Phosphatases |
| RT | Room Temperature |

**S**

| | |
|---|---|
| SAR | Structural-Activity Relationships |
| SD | Standard Deviation |
| SDS | Sodium Dodecyl Sulfate |
| SEM | Standard Error of the Mean |
| SPR | Surface Plasmon Resonance |

**T**

| | |
|---|---|
| TBAI | Tetrabutylammonium Iodide |
| TBDPS-Cl | tert-Butyldiphenylsilyl Chloride |
| TDW | Triple Deionized Water |
| TEM | Transmission Electron Microscopy |
| TEMPO | 2,2,6,6-Tetramethyl-1-piperidinyloxy free radical |
| THF | Tetrahydrofuran |
| T-HP | Texas red- Heparin |
| TLC | Thin-layer Chromatography |
| TMB | 3,3′,5,5′-Tetramethylbenzidine |
| TME | Tumor Microenvironment |
| TMSOTf | Trimethylsilyl trifluoromethanesulfonate |
| TMSSPh | Phenyl Trimethylsilyl Sulphide |
| TNBCs | Triple Negative Breast Cancer Cells |

**U**

| | |
|---|---|
| UFH | Unfractionated Heparin |

**V**

| | |
|---|---|
| VEGF | Vascular Endothelial Growth Factor |
| $V_{CPD}$ | CPD voltage |

**W**

| | |
|---|---|
| WE | working electrode |

## X

| | |
|---|---|
| XPS | X-ray Photoelectron Spectroscopy |

# Abstract

Heparan sulfate (HS) is a complex polysaccharide that is ubiquitous on all mammalian cell surfaces and extracellular matrices. The complexity of HS is encoded by broad sulfation patterns and uronic acid compositions. This pronounced structural heterogeneity of HS facilitates a wide range of biological activities. In the last two decades, carbohydrate chemists intensively pursued the synthesis of well-defined HS oligosaccharides to understand the structural-activity relationships (SARs). These studies revealed that sulfation codes and uronic acid variants synergistically modulate HS-protein interactions (HSPI). Furthermore, a growing number of studies associating the conformation plasticity of L-Iduronic acid, an uronic acid composition, provide a rationale to fine-tune the microenvironment to modulate the HSPI. In addition to traditional growth factors and chemokines binding, several non-canonical roles of HS are also reported, including HS binding to cell-penetrating peptides and metal ions. This thesis presents the synthesis of well-defined HS oligosaccharides and deciphers their binding affinity to heavy metal ions and toll-like receptors (TLRs). The thesis is divided into total of five chapters, and the summary of each chapter is outlined below.

In **Chapter 1**, a brief introduction is given about the cell surface glycans and discussed the structural heterogeneity of heparan sulfate, its biosynthesis and the current insight into the structure-activity relationship (SARs) of specific uronic acid-composed HS with growth factors, chemokines and anticoagulants proteins.

**Chapter 2** describes an efficient total synthesis of HS tetrasaccharide composed of glucuronic acid. The key features of synthesis include the divergent strategy to obtain 3-O sulfated and 6-O-sulfate HS tetrasccharides and evaluated their binding with heavy metal ions, such as lead(II), cadmium(II) and mercury(II), which are a common toxic pollutant. Here, we immobilized HS tetrasaccharides on electrodes using electrografting technique and exposed to Pb2+, Cd2+, and Hg2+ ions and the impedimetric response was monitored by EIS. The systematic analysis based on a combination of electrochemical and surface characterization methods showed that chelation ability and binding preference of the HS tetrasaccharide are strongly dependent on their sulfation pattern and uronic acid composition. This study shows that electrochemical analysis and suface science tools provide valuable insight into the effect of structural components on heparan sulfate and heavy metal ions.

**Chapter 3**, describes the synthesis of a large pool of structurally well-defined HS and chondroitin sulfate (CS) oligosaccharides encapsulated fluorescent gold nanoparticles and study their cellular homing. We hypothesized that sulfation pattern and hexosamine composition might tune to nanoparticle homing in cancer and neural cell lines. Confocal imaging studies with different aggregation level of cancer cells showed no such significant disparity in the recognition pattern. While, U-87, a glioblastoma cell showed almost exclusive uptake of CS-E nanoprobe over HS-based nanoprobes. Whereas, primary neural cells of hippocampal and olfactory bulb showed enhanced homing of CS-E nanoprobe. Further, mechanistic studies revealed receptor CD44 and caveolae-mediated endocytosis of nanoparticles. These results open a new avenue for generating a combinatorial library of GAG-nanoprobe to target specific cell lines to design drug delivery vehicles.

In **chapter 4**, the first systematic analysis of TLR4 activity of heparan sulfate and its mimics is reported. In addition, we describe the synthesis of glucosamine and uronic acid-based adjuvants, and investigate their TLR agonists activity.

**Chapter 5,** describes the synthesis of spherical, rod-, and star-shaped gold nanostructures appended with CpG and imidazoquinoline ligands to evaluate shape-dependent immune cell uptake and immune modulation. Star shaped AuNPs showed good immune responses and moderate uptake rate with all TLR agonists in contrast to the rod and spherical-shaped AuNPs is the key finding. These results open a new avenue for generating AuNPs-based vaccines.

# Publications

1. Bhoge, P. R.; **Mardhekar, S.**; Toraskar, S.; Subramani, B.; Kikkeri, R. Pairing nanoparticles geometry with TLR agonists to modulate immune responses for vaccine development. *ACS Appl Bio Mater*. ***(Accepted 2022)***. *DOI:* 10.1021/acsabm.2c00716
2. **Mardhekar. S.;** Subramani, B.; Samudra P.; Srikanth, P,; Mahida, V.' Boghe, P. R. Toraskar, S.; Abraham, N. M.; Kikkeri, R. Sulfation of heparan and chondroitin sulfate ligands enables cell specific homing of nanoprobes *Chem Eur. J.* ***(Accepted 2022)***. *DOI:* 10.1002/chem.202202622
3. Shitrit, A.; **Mardhekar. S**.; Alshanski, I.; Jain P, Raigawali, R.; Shanthamurthy, C. D.; Kikkeri, R.; Yitzchaik, S.; Hurevich, M. Profiling heparan sulfate-heavy metal ions interaction using electrochemical techniques. *Chem Eur J. (Accepted* **2022) DOI:** 10.1002/chem.202202193.
4. Anand, S.; **Mardhekar, S**.; Raigawali, R.; Mohanta, N.; **Jain, P**.; D. Shanthamurthy, C.; Gnanaprakasam, B.; Kikkeri, R., Continuous-Flow Accelerated Sulfation of Heparan Sulfate Intermediates. *Org. Lett.* **2020,** *22* (9), 3402-3406.
5. Subramani, B.; Shanthamurthy, C. D.; Maru, P.; Belekar, M. A.; **Mardhekar, S.;** Shanmugam, D.; Kikkeri, R. Demystifying a hexuronic acid ligand that recognizes toxoplasma gondii and blocks its invasion into host cells. *Org. Biomol. Chem*. **2019**, 17, 4535-4542.
6. Kikkeri, R.; Jain. P.; Shanthamurthy. C. D.; **Mardhekar, S.;** Kumar, N. V.; Raigawali, R.; Ben-Arye, S. L.; Padler-Karavani, V. Heparan Sulfate Compounds As Chemokine Inhibitors. PCT patent **(filed 2022).**

# CHAPTER- 1

## Introduction

## 1.1 Abstract

Regulating heparan sulfate (HS)-protein interactions *via* well-defined oligosaccharides are essential given their wide variety of proteins binding and their downstream biological activities. The sulfation patterns, uronic acid composition, oligosaccharide chain length and conformation plastic of L-iduronic acid underpins the structural heterogeneity of HS, strategies to encode these structural modifications using synthetic HS molecules are being intensively pursued. This chapter highlights the current state of the art in achieving synthetic HS with specific uronic acid composition and its molecular level interaction with various plasma, viral and bacterials proteins, and its applications.

## 1.2 Introduction

Heparan sulfate is a universal receptor/co-receptor for over 500 different proteins, which regulate a wide range of physiological and pathological processes.[1-2] The diverse biological functions of HS include binding to growth factors such as fibroblast growth factors (FGF), vascular endothelial growth factors (VEGF), epidermal growth factors (EGF) and mediate receptors clustering, which ultimately regulate cell proliferation, angiogenesis and cell differentiation process.[3-9] These singling events finally results in physiological function in the form of new blood vessel formation and wound healing. In the immune system, HS contributes to leukocyte rolling, adhesion and migration at the inflammatory site *via* binding to selectins.[3-14] HS on neutrophils binds to chemokines to release inflammatory signals. HS also serves as a receptor for several viruses and bacteria to adhere to the cell surface and infect. For example, SARS-CoV-2 spike protein interacts with both cellular heparan sulfate (HS) and angiotensin-converting enzyme 2 (ACE2) through its receptor-binding domain (RBD).[15-16] The binding between spike protein and HS shifts the conformation of the protein into trimeric form, activating the ACE2 receptor. Furthermore, aberrant expression of heparanase enzyme at the tumor site indicates structural modification of cell surface and extracellular matrix HS that facilitate tumor growth, immune evasion, and metastasis.[17]

HS is composed of repeating α(1-4) glycosidic linkage of glucosamine and uronic acid based disaccharides unit.[18-19] The large structural diversity of HS arises from the nature of sulfation patterns and uronic acid composition. The most prevalent sulfation patterns include *O*-sulfation at C-6 and C-3 of glucosamine and C-2 of uronic acid unit, and other notable sulfation is *N*-sulfation at glucosamine.[19] Further modification at uronic acid, which might be either D-glucuronic acid (GlcA) or L-iduronic acid (IdoA) results in 48 theoretical disaccharides. Among

them, 21 disaccharides are naturally occurring.[20] However, till date, biological functions of these modifications are not fully understood. Presumably, HS sequences can bind to more than one HS binding proteins and vice versa.[2] Overall, the level of HS heterogeneity of is so high that it is difficult to predict specific modification and rationalize the activity until we get all possible well-defined HS in hand. In such circumstances, unnatural modifications using bioisosteric groups are expected to improve the selectivity and sensitivity of HSPI.

In addition to the common HS modifications, the conformation plasticity of L-Iduronic acid yielded one more level of heterogeneity.[21] Due to advances in the NMR spectroscopy, it was possible to identify a unique $^{2}S_{0}$-conformation of IdoA, which was recently shown to fine-tune the HSPI, and we anticipate that the conformational plasticity results next level of micro-heterogeneity to differentiate HSPI.[22-31] In this chapter, we review the current understanding of the uronic acid composition of HS in structure-activity relation and their roles in cancer and immunology.

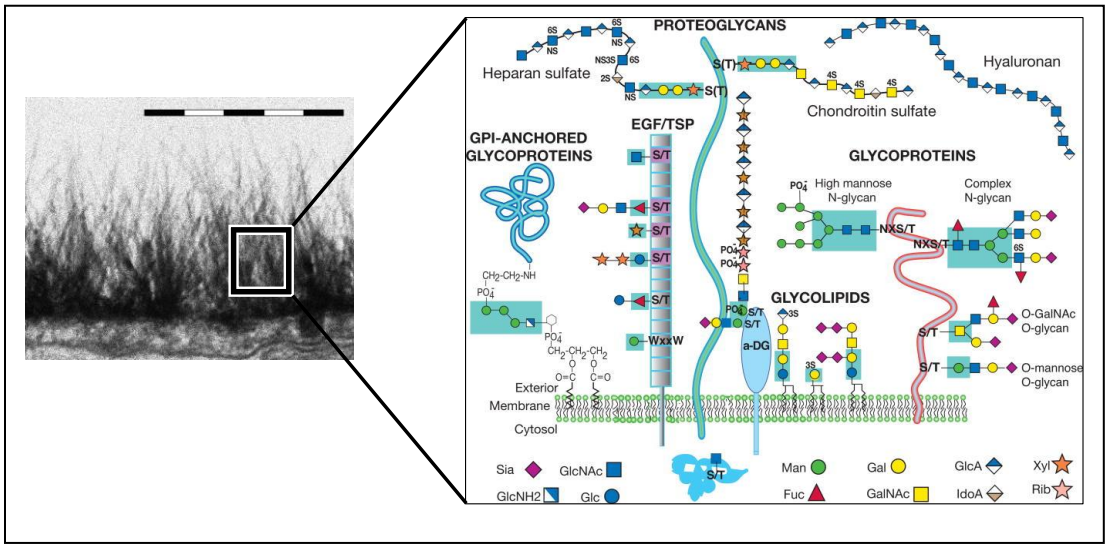



**Figure 1:** Cell surface representing different classes of mammalian glycans. (Adopted with permission from the (ref. 4)

**1.3 HS biosynthesis.**

The heparan sulfate (HS) biosynthesis is not encoded in the genome. Hence it is difficult to predict the exact structural outcome of the synthesis.[2] Generally, HS biosynthesis occurs at two different cellular compartments (endoplasmic reticulum (ER) and Golgi complex) and the availability and expression of various enzymes. HS biosynthesis begin at ER region, where the universal linker tetrasaccharide (Xyl-Gal-Gal-GlcA) is tethered on the core protein. First, xylose residue is glycosylated to serin amino acid of the core protein by the action of two xylotransferases (XYLT1 and XYLT2), followed by the action of galactosyltransferase (β4GalT7 and β3GalT6) resulting Xyl-gal-gal-linker (Figure 2)[28] The action of glucuronyltransferase I (GlcAT-1) furnished the glycosylation of glucuronic acid (GlcA) residue to the linker region. Then, the linker-conjugated proteoglycans are transferred to the golgi complex for HS polymerization and sulfation. The monosaccharide GlcNAc is glycosylated to the linker region by the action of exostosin like 2 (EXTL2) and EXTL3 glycosyltransferases initiator , followed by chain elongation *via* two more enzymes EXT1 and EXT2, which catalyses alternative glycosylation of GlcNAc and GlcA residues. Then, the resultant core HS polysaccharide undergoes a series of structural modifications including sulfation and epimerization to produce mature HSPGs. Initially, *N*-deacetylase/*N*-sulfotransferases 1-4 (NDSTs 1-4) regulate the deacetylation of GlcNAc and subsequently and incorporates *N*-sulfate moiety on glucosamine residue (GlcNS). This modification plays a pivotal role in all other sulfation and epimerization process. In addition, a fraction of glucosamine residues remains *N*-deacetylated or *N*-acetylated, leading to a wide range of structural heterogeneity. Subsequently, *N*-sulfated domain of HS at the reducing end undergoes the D-GlcA into L-IdoA epimerization in the presence of D-glucuronyl C5-epimerase (GLCE) and C2-sulfation of both GlcA and IdoA

residues by 2-O-sulfotransferases 1 (2OST1). 6-O-sulfotransferases 1-3 (6OSTs 1-3) and 3-O-sulfotraerenases 1-7 (3OSTs 1-7) mediate 6-O or 3-O sulfation of glucosamine moiety resulting the formation for mature HS proteoglyans and express at the cell surfaces.[32] Finally, the subset of mature HS polysaccharides undergoes post-synthesis reactions by 6-O-endosufatases (Sulf-1 and sulf-2) resulting the cleaveage of 6-O-sulfate residue from the core HSPG.

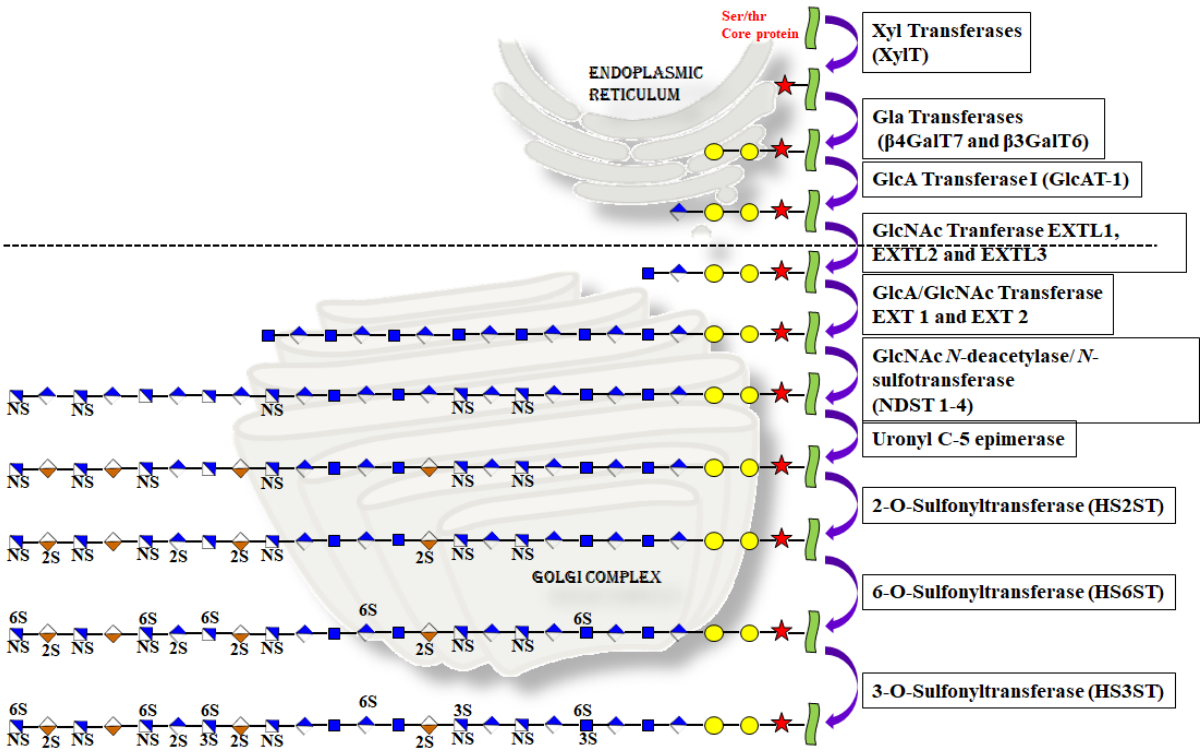



**Figure 2.** Biosynthesis of Heparan sulphate**.**

## 1.4 Heparan sulfate binding proteins

The inherent negative charges on HS involved in the plethora of proteins binding via ionic and hydrogen bond network. The sulfate and carboxyl residue on HS mediate ionic bonding with lysine and arginine residues in the proteins. Whereas, polar residues, such as asparagine, glutamine, and histidine of proteins bind to HS by hydrogen binding.[23-67]

The HSBPs are mainly classified based on their functions, which include blood coagulation factors; growth factors, chemokines and cytokines; extracellular proteins; transmembrane

signaling receptors and cell adhesion proteins (Figure 3). Given the structural similarities between HS and other GAGs family members, such as chondroitin sulfate and dermatan sulfate, HSBPs can also bind to CS and DS, with a binding affinity that is lower than that of HS. Typically, the binding affinity of HS with proteins is in the range of μM to nM concentration.

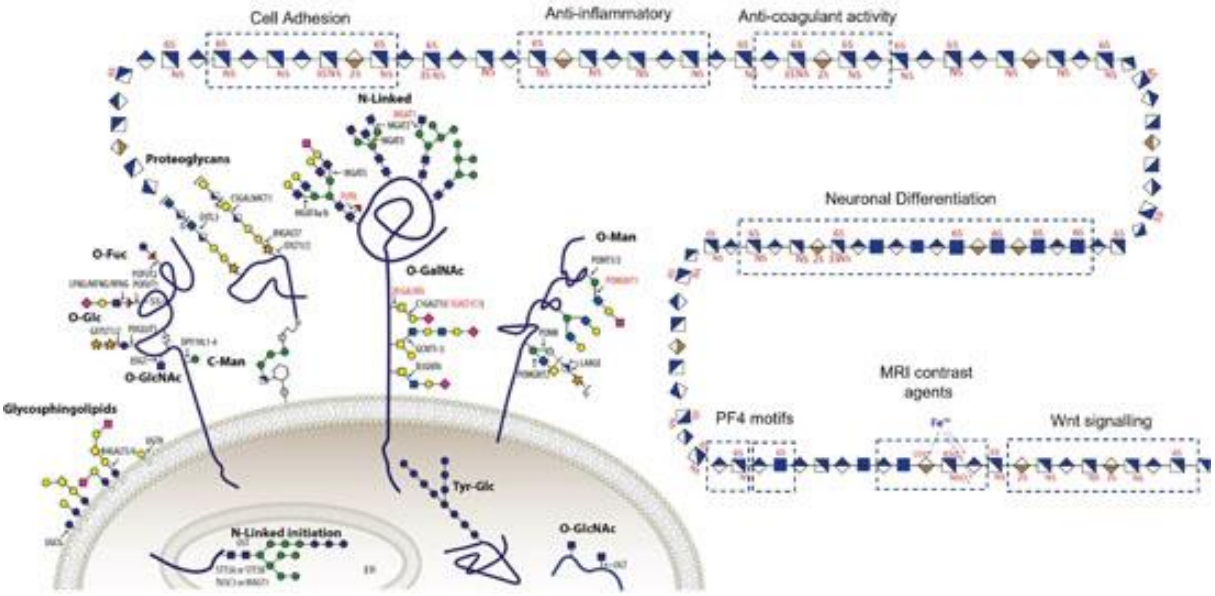



Figure 3. Heparan sulfate-proteins binding (Adopted from internet link https://icmm.ku.dk/english/research-groups/r-miller-group/).

### 1.4.1 Growth factors.

Heparan sulfate mediates activities of several growth factors and chemokines. The recent advances in the synthesis of well-defined heparan sulfate oligosaccharides allowed to understand structure-activity relation of various growth factors. The control over the sulfation pattern, uronic acid composition in the HS oligosaccharides led to the discovery of highly effective HS ligands for HS-binding proteins.[35] A variety of growth factors has been used for microarray high-through put analysis. Among them FGF (fibroblast growth factor) and VEGF (vascular endothelia growth factors) are most thoroughly studied proteins.[36] Seeberger et al. constructed heparin microarray to decipher the minimum heparin sequence required to bind FGF1, FGF-2, and FGF-4. They

observed that higher-oligosaccharides are essential for the activation of FGFs. Furthermore, Iduronate 2-*O*-sulfate and *N*-sulfate of glucosamine are critical for FGF-1 and FGF-2 binding. FGF-4 binds to L-idoA based hexasaccharide but less pronounce to its tetrasaccharide analog, indicating that increase in the oligosaccharide chain length induce strong binding.[27-28] Later, Hoffman et al. investigated the FGF10-HS oligosaccharides mediated BaF3 cells proliferation. They found that FGF10 requires C-6, C-2 and *N*-sulfated HS decasaccharide for maximum proliferation.[29] The pioneering with of Hung et al. of the synthesis of 48 disaccharides to study their binding affinity to FGF1 and FGF2 displayed the key structure-activity relation of HS.[20] Using the isothermal titration calorimetric (ITC), the binding affinity of HS disaccharide ligand was quantified. The SARs of FGF1 and FGF2 showed that 2-*O*-sulfated L-idoA is essential uronic acid residue for growth factors binding. Further, FGF2 showed preferred binding to 6-*O*-sulfo-N-sulfated glucosamine residue. Whereas, 3-*O*-sulfo-*N*-sulfated glucosamine residue was required for strong binding with FGF1. Boons and co-workers has synthesized library of 47 Heparan sulphate oligosaccharides and constructed a HS-microarray to revel the HS ligand requirement for binding with various proteins.[24-27] All highly sulphated compounds found to recognize FGF-2, while FGF2 preferentially bound to tri and tetra sulphated HS oligosaccharides containing iduronic acid moiety with 2-O sulfation. Natural heparan sulphate consists of high sulfation (NS) and low sulfation (NA) domains, which are of variable size and their contribution in HS for FGF-FGFR signalling was not well explored. Linhardt and co-workers showed that HS oligosaccharides with longer four and five disaccharide at non reducing end NS domain showed high binding with FGF-2 and low FGF1 recognition. Under physiological conditions trisulfated tetradecasaccharides of HS found to bind with VEGF165 with comparable affinity as that of heparin.[47]

### 1.4.2 Antithrombin

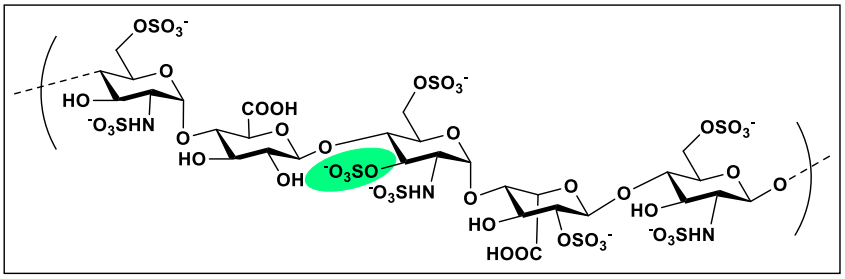



**Figure 4:** High affinity Heparin pentasaccharide for antithrombin binding.

Antithrombin III (AT III) is the serine protease inhibitor, broadly interact with thrombin and factor Xa, resulting in blood-coagulation cascade. AT III specifically binds to HS moiety and get activated.[40] Hence, it is very important to determine the structure-activity relationship to develop anti-coagulation drug molecules. The X-ray crystallography and NMR studies of AT III-HS interaction revealed that a pentasaccharide HS sequence is sufficient enough to cause effect anti-coagulation activity (figure 4).[41] Further SARs studies showed that four sulfations and two carboxyl acid residue are required for the binding of AT III. Crystallographic studies further revealed the importance of 6-O-sulfation, N-sulfation and 3-O-sulfation of glucamine. At the same time, 2-O-sulfation of L-IdoA and 6-O-sulfation of the reducing end glucosamine was found less important. However, 2-O-sulfation drive the L-IdoA into more stable $^{2}S_{0}$-conformation and this conformation plasticity was found pivotal for AT III/HS binding.

### 1.4.3 Chemokines

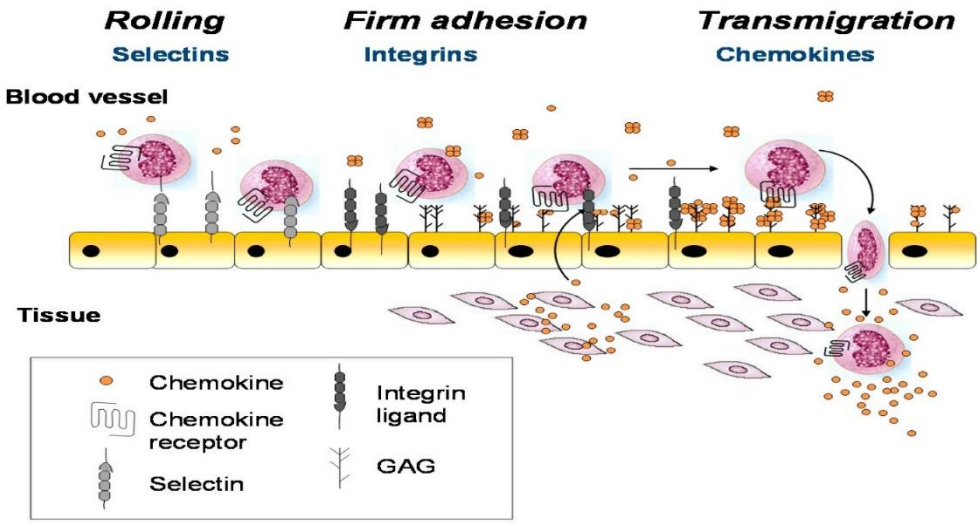



**Figure 5:** Role of GAGs in cell (leukocytes) recruitment during inflammation. (Adapted with permission from reference 46).

Chemokines are a special type of signalling proteins that facilitate leukocyte migration, angiogenesis, breast cancer metastasis, and leukocyte de- granulation also interact with heparin (Figure 5).[43-45] They mediate immune cell activity by producing inflammatory stimuli at the injury and infection site. There are more than 40 types chemokines, however they are broadly classified into two groups based on their primary and secondary structures. The main ligand recognized by the chemokines are heparan sulfate, chondroitin sulfate, which binds via ionic interactions. Hence, there is a growing interest to identify the HS ligands for chemokines. To determine the heparin-binding profiles of chemokines seebereger and Coworkers have used heparin chips containing a small library of synthetic heparin oligosaccharides with different sequences and sulfation group distribution. CCL21 found to strongly bind to hexasaccharide containing $GlcNSO_3$(6-$OSO_3$)-IdoA(2-$OSO_3$) repeating unit, on contrary CXCL12 binds poorly and CCL19 does not bind to this hexasaccharide at all. Monosaccharide 2,4-O-di-sulfated iduronic acid found to be the best binder for CXCL16 along with the hexa and tetrasaccharide

with trisulfated repeating unit GlcNSO3(6-OSO3)-IdoA(2-OSO3) but lack of N-sulfate and 6-O sulphate groups reduced the binding.[46]

Monosaccharide, 2,4-disulfated iduronic acid (Di-S-IdoA) binds with high affinity with CCL20 and significantly inhibited CCL20-heparan sulphate interaction which leads to leukocyte recruitment in the peribronchial region and bronchoalveolar lavage fluid (BALF) during airway hyperresponsiveness.[52-57]Miller et al. have shown the importance of presence of sulfation group either at C-6 of glucosamine or C-2 of IdoA for the binding with CCL2 chemokine. Presence of C-6 sulfate group in reducing end disaccharide increases the binding affinity with CCL2 by 200 folds.[58] Boons and Co-workers have used unprecedented library of 47 HS-oligosaccharides for the development of a microarray to examine ligand requirements for chemokines CCL2, CCL5, CCL7, CCL13, CXCL8, and CXCL10 binding. CCL2, CCL7, and CCL13 belonging to same chemokine subfamily exhibit clear differences in structure−binding relationships. CCL2, exclusively binds with highly sulfated compounds only without any preference for IdoA or GlcA, N-sulfate, 6-O-sulfate or 2-O-sulfate. CXCL10 and CCL5 showed a preference for 6-O-sulfates over 2-O-sulfates and binding do not tolerate GlcA at reducing end while strong response was observed on replacing GlcA with 2-OSO3 IdoA in non-reducing end disaccharide.[23-24]

Further Kikkeri and Co-workers synthesized series of N-unsubstituted (NU) and N-acetylated (NA) heparan sulfate tetrasaccharides to interrogate selective inhibition of structurally homologues chemokines. CCL13, CXCL12 and CCL21 finds to bind with non-sulfated as well as phosphorylated ligands, suggesting that the HS-based structure–activity relationship of these chemokines not necessarily depend on the sulfate group. While chemokine CCL2 strongly binds with 3, 6 sulfated NU domain tertrasaccharide while CCL5 found to bind selectively with 2,6

sulfated NU tetrasaccharide.[68] In another attempt Kikkeri and Co-workers synthesized tailor-made homooligouronic acid HS mimetics, wherein their sulfation patterns, conformational plasticity, and oligosaccharide chain length was analysed to modulate their binding with various chemokines using HS-microarray. Chemokines CCL28 and CCL13 modrate to strong binding with all HS mimetics. 4-sulfated tetrasaccharide showed weak binding towards CXCL12 and CCL21 chemokines. CXCL12 showed strong binding with 2,4 sulfated tetrasaccharide while very weak binding with CCL21 demonstrated importance of optimal homo-oligosaccharide chain length and sulfation code for molecular-level interaction.[69] CCL5 and CCL2 showed strong binding to high-sulfated HS mimetics, no binding to non-sulfated mimetics, and weak binding with a mono-sulfated ligand. Among these 2,4 sulfated HS mimetics showed strongest binding compared to 2-sulfated HS mimetics indicating that sulfation code, even number of IdoA units, and absolute 1C4-IdoA conformation are critical for CCL2 and CCL5 activation as 4-O-sulfation enhances the population of the $^{1}C_{4}$ geometry, and this conformer becomes exclusive upon additional 2-O-sulfation.

**1.5 Conclusion.**

Heparan sulfate are highly negatively charged polysaccharide ubiquitous on cell surface and extracellular matrix. They are involved in wide range of biological functions, including binding to growth factors, chemokines and regulate cellular activity. In addition to HS-protein interactions, the negative charge of the HS regulate various other characteristic binding which don't fit into HS mediated interactions. For example, Seeberger et al showed that cell surface HS can binds to positively charge cell penetrating peptides and antibiotics.[70] Hence, it is worth to understand this non-canonical interactions, which include metal chelation, cis-platin drug delivery.

## 1.6 References


1. J. M. Whitelock & R. V. Iozzo, *Chem. Rev.* **2005**, 105, 2745-2764.
2. D. Xu, & J. D. Esko, *Annu. Rev. Biochem.* **2014**, 83, 129–157.
3. T. J. Boltje & G. J. Boons, *Nat. Chem.* **2009**, 1, 611–622.
4. S. B. Dulaney& X. Huang, X *Advances in Carbohydrate Chemistry and Biochemistry* **2012**, **67**, 96-136.
5. J. D. Esko & U. Lindahl, *J. Clin. Invest.* **2001**, 108, 169–173.
6. Kreuger, J. & Kjellén, L. Heparan Sulfate Biosynthesis: Regulation and Variability. *J. Histochem. Cytochem.* **2012**, 60, 898–907.
7. V. Masola, G. Bellin, G. Gambaro & M. Onisto, *Cells* **2018**, 7, 236.
8. D. A. Pye, R. R. Vives, J. E. Turnbull, P. Hyde & J. T. Gallagher, *J. Biol. Chem.* **1998,** 273, 22936–22942.
9. R. V. Iozzo & L. Schaefer, *Matrix Biol.* **2015**, 42, 11–55.
10. M. P. Bevilacqua & R. M. Nelson, *J. Clin. Investig.* **1993,** *91* (2), 379-387.
11. R. P. McEver, *Curr. Opin. Immunol.* **1994,** *6* (1), 75-84.
12. K. E. Norgard-Sumnicht, N. M. Varki, A. Varki, *Science* **1993,** *261* (5120), 480-483.
13. A. Koenig, K. Norgard-Sumnicht, R. Linhardt, A. Varki, *J. Clin. Investig.* **1998,** *101* (4), 877-889.
14. K. Norgard-Sumnicht & A. Varki, *J. Biol. Chem.* **1995,** *270* (20), 12012-12024.
15. A. Milewska, M. Zarebski, P. Nowak, K. Stozek, J. Potempa, K. Pyrc, *J. Virol.* **2014**, *88* (22), 13221– 13230,
16. T. M. Clausen, D. R. Sandoval, C. B. Spliid, J. Pihl, H. R. Perrett, C. D. Painter, A. Narayanan, S. A. Majowicz, E. M. Kwong, R. N. McVicar, B. E. Thacker, C. A. Glass, Z. Yang, J. L. Torres, G. J. Golden, P. L. Bartels, R. N. Porell, A. F. Garretson, L. Laubach, J. Feldman, X. Yin, Y. Pu, B. M. Hauser, T. M. Caradonna, B. P. Kellman, C. Martino, P. Gordts, S. K. Chanda, A. G. Schmidt, K. Godula, S. L. Leibel, J. Jose, K. D. Corbett, A. B. Ward, A. F. Carlin, J. D. Esko, *Cell* **2020**, *183* (4), 1043– 1057
17. C. Reily, T. J. Stewart, M. B. Renfrow, J. Novak, *Nature Rev. Nephrol.* **2019**, 1. 123-145.
18. Z. Shriver, I. Capila, G. Venkataraman, R. Sasisekharan, In *Heparin-A Century of Progress*, Springer: 2012; pp 159-176.

19. D. L. Rabenstein, *Nat. Prod. Rep.* **2002,** *19* (3), 312-331.
20. Y. P. Hu, Y. Q. Zhong, Z. G. Chen, C. Y. Chen, Z. Shi, M. M. L. Zulueta, C. C. Ku, P. Y. Lee, C. C. Wang, S. C. Hung, *J. Am. Chem. Soc.* **2012,** *134* (51), 20722-20727.
21. M. Bernfield, M. Götte, P. W. Park, O. Reizes, M. L. Fitzgerald, J. Lincecum, M. Zako, *Ann. Rev. Biochem.* **1999,** *68* (1), 729-777.
22. Y. Xu, C. Cai, K. Chandarajoti, P. H Hsieh, L. Li, T. Q. Pham, E. M. Sparkenbaugh, J. Sheng, N. S. Key, R. Pawlinski, *Nat. Chem. Biol.* **2014,** *10* (4), 248-250.
23. X. Zhang, V. Pagadala, H. M. Jester, A. M Lim, T. Q. Pham, A.M. P. Goulas, J. Liu, R. J. Linhardt, *Chem. Sci.* **2017,** *8* (12), 7932-7940.
24. S. Arungundram, K. Al-Mafraji, J. Asong, F. E. Leach III, I. J. Amster, A. Venot, J. E. Turnbull, G. J. Boons, *J. Am. Chem. Soc.* **2009,** *131* (47), 17394-17405.
25. W. Lu, C. Zong, P. Chopra, L. E. Pepi, Y. Xu, I. J. Amster, J. Liu, G. J. Boons, *Angew. Chem. Int. Ed.* **2018,** *130* (19), 5438-5442.
26. L. Sun, P. Chopra, G. J. Boons, G.-J., Modular Synthesis of Heparan Sulfate Oligosaccharides Having N-Acetyl and N-Sulfate Moieties. *J. Org. Chem.* **2020**. 24, 16082-16094.
27. Y. Xu, Z. Wang, R. Liu, A. S. Bridges, X. Huang, J. Liu, *Glycobiology* **2012,** *22* (1), 96-106.
28. J. L. de Paz, C. Noti, P. H. Seeberger. *J. Am. Chem. Soc.* **2006,** *128* (9), 2766-2767.
29. M. L. Hecht, B. Rosental, T. Horlacher, O. Hershkovitz, J. L. De Paz, C. Noti, S. Schauer, A. Porgador, P. H. Seeberger, *J. Proteome Res.* **2009,** *8* (2), 712-720.
30. S. Maza, G. Macchione, R. Ojeda, J. López-Prados, J. Angulo, J. L. De Paz, P. M. Nieto, *Org. Biomol. Chem.* **2012,** *10* (10), 2146-2163.
31. S. B. Dulaney, X. Huang, *Adv. Carbohydr. Chem. Biochem.*, Elsevier: 2012; Vol. 67, pp 95-136.
32. K. Harter, M. Levine, S. O. Henderson, *West. J. Emerg.* **2015,** *16* (1), 11.
33. B. Dahlbäck, *The Lancet* **2000,** *355* (9215), 1627-1632.
34. J. Crawley, S. Zanardelli, C. Chion, D. Lane, *J. Thromb. Haemost.* **2007,** *5*, 95-101.
35. K. G. Mann, S. Butenas, K. Brummel, *Arterioscler. Thromb. Vasc. Biol.* **2003,** *23* (1), 17-25.

36. M. Di Nisio, S. Middeldorp, H. R. Büller, *N. Engl. J. Med.* **2005,** *353* (10), 1028-1040.
37. E. Gray, J. Hogwood, B. Mulloy, *Heparin-A century of progress*, Springer: 2012; pp 43-61.
38. T. K. Kishimoto, K. Viswanathan, T. Ganguly, S. Elankumaran, S. Smith, K. Pelzer, J. C. Lansing, N. Sriranganathan, G. Zhao, Z. Galcheva-Gargova, *N. Engl. J. Med.* **2008,** *358* (23), 2457-2467.
39. M. Guerrini, D. Beccati, Z. Shriver, A. Naggi, K. Viswanathan, A. Bisio, I. Capila, J. C. Lansing, S. Guglieri, B. Fraser, *Nature Biotechnol.* **2008,** *26* (6), 669-675.
40. C. A. van Boeckel, M. Petitou, *Angew. Chem. Int. Ed.* **1993,** *32* (12), 1671-1690.
41. B. E. Thacker, D. Xu, R. Lawrence, J. D. Esko, *Matrix Biol.* **2014,** *35*, 60-72.
42. P. Giangrande, *Int. J. Clin.* **2002,** *56* (8), 615-617.
43. N. Turner, R. Grose, *Nat. Rev. Cancer* **2010,** *10* (2), 116-129.
44. J. Amann, S. Kalyankrishna, P. P. Massion, J. E. Ohm, L. Girard, H. Shigematsu, M. Peyton, D. Juroske, Y. Huang, J. S. Salmon, *Cancer Res.* **2005,** *65* (1), 226-235.
45. K. Forsten-Williams, C. L. Chu, M. Fannon, J. A. Buczek-Thomas, M. A. Nugent, *Ann. Biomed. Eng.* **2008,** *36* (12), 2134-2148.
46. M. Mohammadi, S. K. Olsen, O. A. Ibrahimi, *Cytokine Growth Factor Rev.* **2005,** *16* (2), 107-137.
47. M. Maccarana, B. Casu, U. Lindahl, *J. Biol. Chem.* **1993,** *268* (32), 23898-23905.
48. P. Jemth, J. Kreuger, M. Kusche-Gullberg, L. Sturiale, G. Giménez-Gallego, U. Lindahl, *J. Biol. Chem.* **2002,** *277* (34), 30567-30573.
49. S. Ashikari-Hada, H. Habuchi, Y. Kariya, N. Itoh, A. H. Reddi, K. Kimata, *J. Biol. Chem.* **2004,** *279* (13), 12346-12354.
50. V. der Meer, E. Kellenbach, L. J. Van den Bos, *Molecules* **2017,** *22* (6), 1025.
51. S. Park, J. C. Gildersleeve, O. Blixt, I. Shin. *Chem. Soc. Rev.* **2013,** *42* (10), 4310-4326.
52. M. D. Disney, P. H. Seeberger, *Chem. Biol.* **2004,** *11* (12), 1701-1707.
53. C. Zong, A. Venot, X. Li, W. Lu, W. Xiao, J. S. L. Wilkes, C. L. Salanga, T. M. Handel, L.Wang, M. A. Wolfert, *J. Am. Chem. Soc.* **2017,** *139* (28), 9534-9543.
54. C. E. Hughes, R. J. Nibbs, *FEBS J.* **2018,** *285* (16), 2944-2971.
55. B. L. Farrugia, M. S. Lord, J. Melrose, J. M. Whitelock, *J. Histochem. Cytochem.* **2018,** *66* (4), 321-336.

56. A. E. Proudfoot, Z. Johnson, P. Bonvin, T. M. Handel, *Pharmaceuticals* **2017,** *10* (3), 70.
57. J. L. de Paz, E. Moseman, C. Noti, L. Polito, U. H. von Andrian, P. H. Seeberger, *ACS Chem. Biol.* **2007,** *2* (11), 735-744.
58. D. Raman, T. Sobolik-Delmaire, A. Richmond, *Exp. Cell Res.* **2011,** *317* (5), 575-589.
59. D. Aldinucci, A. Colombatti, *Mediators Inflamm.* **2014,** *2014*.
60. A. Müller, B. Homey, H. Soto, N. Ge, D. Catron, M. E. Buchanan, T. McClanahan, E. Murphy, W. Yuan, S. N. Wagner, *Nature* **2001,** *410* (6824), 50-56.
61. K. Iqbal, F. Liu, C. X. Gong, I. Grundke-Iqbal, *Curr. Alzheimer Res.* **2010,** *7* (8), 656-664.
62. M. Jouanne, S. Rault, A. S. Voisin-Chiret, *Eur. J. Med. Chem.* **2017,** *139,* 153-167.
63. K. Ley, *Trends Mol. Med.* **2003,** *9* (6), 263-268.
64. S. R. Barthel, J. D. Gavino, L. Descheny, C. J. Dimitroff, *Expert Opin. Ther. Targets* **2007,** *11* (11), 1473-1491.
65. D. Impellizzeri, S. Cuzzocrea, *Expert Opin. Ther. Targets* **2014,** *18* (1), 55-67.
66. M. P. Skinner, C. Lucas, G. Burns, C. Chesterman, M. C. Berndt, *J. Biol. Chem.* **1991,** *266* (9), 5371-5374.
67. R. M. Nelson, O. Cecconi, W. G. Roberts, *Science* **1993,** *261* (5120), 480-483.
68. P. Jain, C. D. Shanthamurthy, S. Leviatan Ben-Arye, R. J. Woods, R. Kikkeri, V. Padler-Karavani, *Chem. Sci.* **2021**, 12, 3674-3681.
69. C. D. Shanthamurthy, S. Leviatan Ben-Arye, N. V. Kumar, S. Yehuda, R. Amon, R. J. Woods, V. Palder-Karavani, *J. Med. Chem.* **2021**, 64, 3367-3380.
70. R. Wallbrecher, W. P. Verdurmen, S. Schmidt, P. H. Bovee-Geurts, F. Broecker, A. Reinhardt, T. H. ven Kuppevelt, P. H. Seeberger, R. Brock. *Cell. Mol. Life, Sci.* **2014**, 71, 2717-2729.

# CHAPTER- 2

## Synthesis of Heparan Sulfate Oligosaccharides to Study Heavy Metals Binding

## 2.1 Abstract

Heparan sulfate (HS) is a highly sulfated glycosaminoglycan found on the surface of every mammalian cell. It interacts with many proteins, drug molecules, and metal ions to mediate physiological and pathological processes. Heparan sulfate glycosaminoglycans provides extracellular matrix defense against heavy metals cytotoxicity. Despite rapid progress in the synthesis of HS oligosaccharides, their binding interactions with metal ions is unknown and identifying the precise glycan sequences that bind a particular heavy metal ion is a key for understanding those interactions. Here, we report the rational design and synthesis of *N*-acetate HS oligosaccharide analogs that selectively binds to heavy metals. HS oligosaccharides were synthesized by a divergent approach. The fully protected HS di and tetrasaccharide precursors were subjected to selective deprotection and sulfation to obtain a library of HS oligosaccharides. The electrochemical and surface characterization techniques were used to elucidate the relation between the tetrasaccharide analogs, uronic acid stereochemistry, and sulfation regiochemistry to heavy metal ions binding. A divergent strategy was employed to access a small library of structurally well-defined tetrasaccharides analogs with different sulfation patterns and uronic acid compositions. These tetrasaccharides were electrografted onto glassy carbon electrodes and their response to heavy metal ions was monitored by electrochemical impedance spectroscopy. The impedimetric response to heavy metal ions revealed that L-Iduronic acid composed of 6-*O*-sulfated HS tetrasaccharide showed strong selectivity to Hg(II) over Cd(II) or Pd(II) ions. While its D-glucuronic acid counterpart showed sensitivity binding to Cd(II) ions, the non-sulfated and 3-*O*-sulfated analogs showed weak binding to all three heavy metal ions. These prototype studies revealed a new insight into HS-metal binding, which is mainly unknown to date.

## 2.2 Introduction

Nature has developed a powerful defensive system in the form of extracellular matrix (ECM) to bind metal ions, small molecules, and biopolymers and thereby modulate their cellular response. The ECM is instrumental in various molecular recognition events that modulate cell fate and diseases.[1, 2] Delineating the structure-activity relation of ECM components is crucial for understanding these biological processes. The ECM is composed of two main classes of macromolecules: fibrous proteins and glycosaminoglycans (GAGs), including heparan sulfate (HS), chondroitin sulfate (CS), dermatan sulfate (DS), and hyaluronic acid (HA).[1-3] HS is highly heterogeneous, composed of disaccharide repeating units of D-glucosamine (GlcN) and uronic acid, which might be either D-glucuronic acid (GlcA) or L-iduronic acid (IdoA). In addition, HS heterogeneity is also derived from the degree and pattern of *O*- and *N*-sulfation/acetylation. Recent studies that utilize synthetic HS fragments, showed that the combination of specific sulfation code and uronic acid composition synergistically modulate protein binding.[4-6] This demonstrated the importance of synthetic HS oligosaccharides to define their structure-biological activity interplay.

Theoretically, HS tetrasaccharides can arrange as many as 2,304 combinations. Hence, identifying the active ligands requires a synthetic strategy. Although, several research groups have synthesized broad HS libraries to decipher active ligands for specific proteins,[7-11] their interaction with heavy metals ions is not well explored. Heavy metal ions such as $Pb^{2+}$, $Cd^{2+}$, and $Hg^{2+}$ are common pollutants near industrial infrastructure that are absorbed by the ECM components such as sulfated GAGs and cause severe damage.[12-16] Understanding the structural features that govern HS interactions with heavy metal ions is very important to tackle their toxicity effect.[17] There is only a limited set of analytical tools for studying those interactions due to deficient spectral characteristics,[18, 19] and very small heat release resulting from complexation.[20] Electrochemical impedance spectroscopy (EIS) is a label-free technique that is highly sensitive to changes in interfacial properties.[21] EIS translates changes in the packing of a ligand layer, induced by analyte binding, to a detectable signal.[20, 22, 23] We previously showed that peptide- and glycan-based EIS can serve as viable tool to trace metal ions.[20, 22, 24]

Here, we present a systematic study of the structural motifs effect on the interactions of HS with heavy metal ions. For this purpose, a novel library of HS tetrasaccharides analogs with a well-defined sulfation pattern and different uronic acid composition was synthesized (Figure 1). The

amino-functionalized HS were immobilized on glassy carbon (GC) surfaces by electrografting to prepare HS modified GC surfaces (HS-GC). The HS-GCs were exposed to $Pb^{2+}$, $Cd^{2+}$, and $Hg^{2+}$ ions, and the impedimetric response was monitored by EIS. Contact angle (CA), contact potential difference (CPD), and X-ray photoelectron spectroscopy (XPS) analyses were used as complementary methods to characterize the effect of HS structural motifs on heavy metal binding.

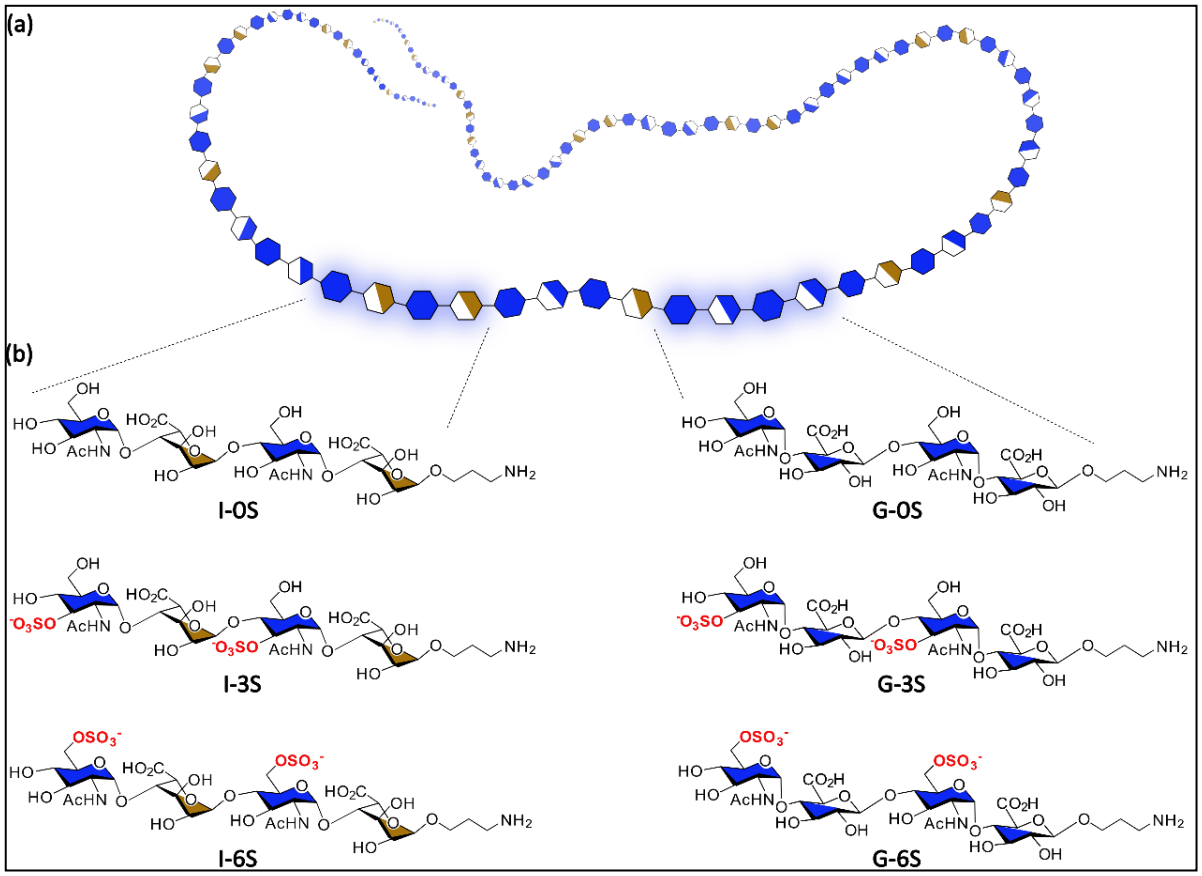



**Figure 1.** (a) Scheme of HS polymer; (b) Amino-functionalized HS tetrasaccharides with different sulfation and carboxylation.

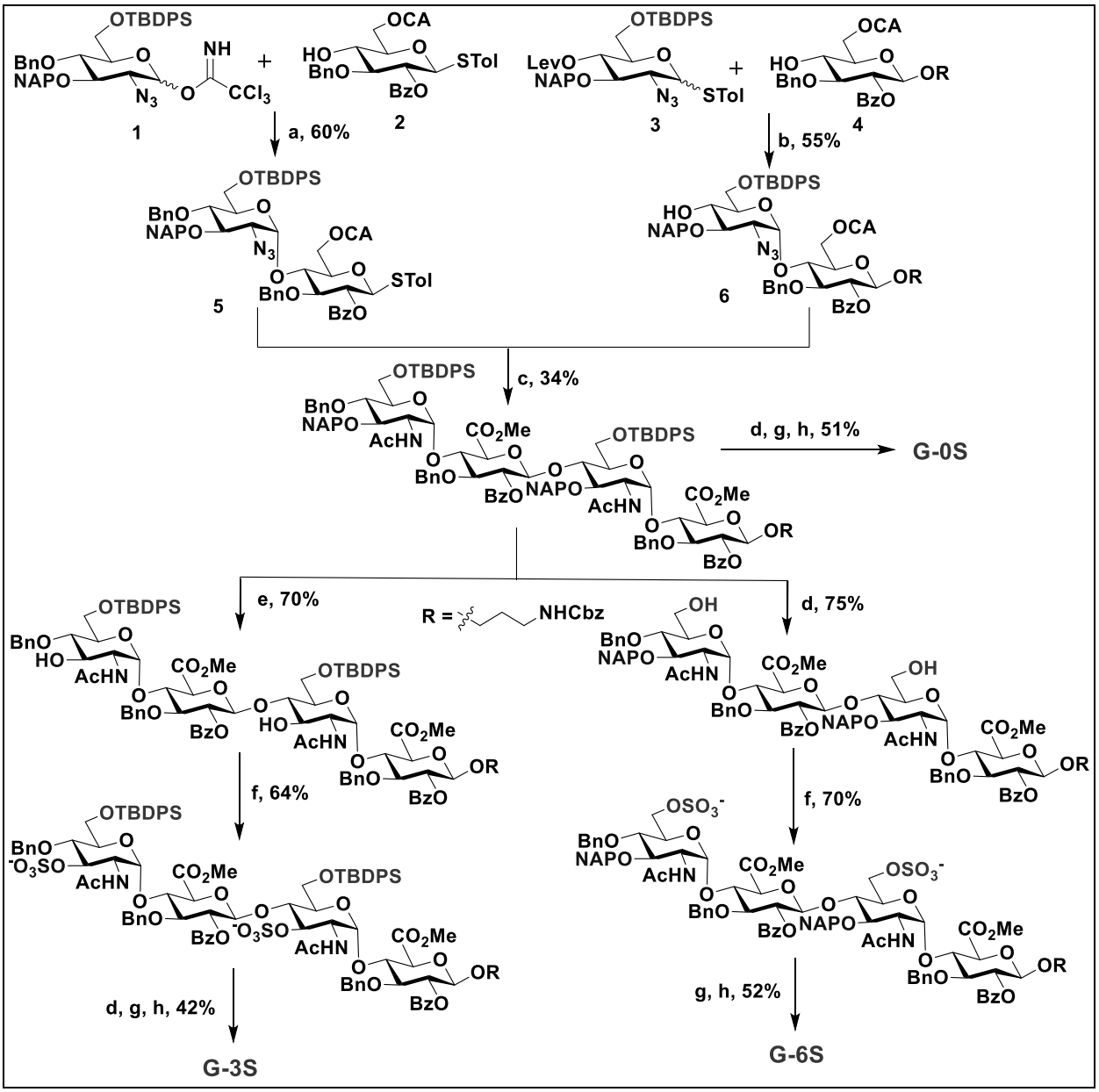
## 2.3 Results and Discussion

### 2.3.1. Synthesis of G- terasaccharides

#### i) Synthesis of G-tetrasaccharides precursor

To facilitate the structure-activity relation of HS with heavy metal ions, a small library of six HS tetrasaccharides was conceived with different sulfation and uronic acid composition. The synthetic design was to split the glycans library into two subclasses based on the uronic acid

type. The idea was that one precursor will enable the synthesis of all three GlcA-containing tetrasaccharides (**G**) while a second precursor will enable the synthesis of the IdoA-containing tetrasaccharides (**I**). Monosaccharide building blocks **1**–**4** were prepared as reported previously,[6, 25, 26] and were used to synthesize the **G** tetrasaccharides precursor **7** via a 7 steps procedure (Scheme 1, and in the Supporting Information). To enable later stage sulfation and derivatization, the *O*-6 hydroxyls of GlcN in **7** were protected with tetrabutyl diphenylsilyl (TBDPS) and *O*-3 hydroxyls were equipped with naphthylmethyl (Nap). TBDPS can be removed chemoselectively by using 70 % HF:py in the presence of benzyl (Bn), benzoyl (Bz), and Nap groups to enable selective *O*-6 sulfation. Nap can be selectively removed by 2,3-dichloro-5,6-dicyano-1,4-benzoquinone (DDQ) in the presence of Bz, Bn and TBDPS to enable selective sulfation on *O*-3. In addition to equipping the tetrasaccharide with suitable orthogonal protecting groups, the synthesis ensures the installation of two α-1, 2-cis glycosylation between GlcN and uronic acid residues. The common tetrasaccharide precursor **7** was then converted into desired sulfation patterns using divergent synthetic strategy. Briefly, Nap was removed using DDQ to provide *O*-3 free tetrasaccharide **9**. Sulfation in the presence of $SO_3.Me_3N$ in DMF provided sulfated protected tetrasaccharide **11**, which resulted in **G-3S** following three global deprotection steps. TBDPS removal from **7** provided the *O*-6 free tetrasaccharide **8**. Sulfation of *O*-6 free tetrasaccharide **8** provided the protected sulfated tetrasaccharide **10**, which was globally deprotected to provide **G-6S**. A three steps deprotection strategy provided the non-sulfated **G-0S** directly from tetrasaccharide **7**.




**Scheme 1**. Synthesis of G-tetrasaccharides: a) AgOTf in DCM, □ 40°C–RT, 40 min; b) i) NIS, TMSOTf in DCM, 20°C–RT, 10 min; ii) N2H4.H2O, AcOH in DCM, RT, 3 h; c) i) NIS, TMSOTf in DCM, □ 20 °C–RT, 10 min; ii) Thiourea in Py/MeOH (1 : 1), 80°C, 2 h; iii) TEMPO, BAIB in DCM/H2O (2 : 1), RT, 6 h; iv) MeI, K2CO3 in DMF, RT, 12 h; v) Zn dust, THF/AcOH/Ac2O (3 :2: 1), 0°C, 12 h; d) 70% HF.py in Pyridine, 0 °C–RT, 24 h; e) DDQ in DCM/H2O (18 : 1), RT, 2 h; f) SO3.Me3N in DMF, 60°C, 72 h; g) 1 M LiOH in THF/H2O (1 : 1), RT,18 h; h) H2, Pd(OH)2 in H2O, RT, 36 h.

## b) Glassy carbon Surface functionalisation and binding study with heavy metal ions:

The strategy of electrografting was chosen to prepare a platform in which the interaction of the HS tetrasaccharides with the heavy metal ions can be monitored. Electro-oxidative grafting of

aliphatic amines is a rapid single-step process to covalently immobilize amino-molecules on GC surface,[28] and proved as efficient modification strategy to prepare saccharide-based impedimetric sensors.[29] The amino-functionalized HS tetrasaccharides were electrografted on onto GC surfaces via electro-oxidative grafting conducted by cyclic voltammetry (CV). (Figure 2) shows an example of CV recorded for I-6S electrografting onto GC electrode (GCE) to prepare I-6S-GC. A corresponding anodic current peak that is correlated with electrografting reaction,[29] was observed during the first anodic scan at the potential of ~1 V. This peak was not followed by a reduction peak at the following reductive scan, indicating the irreversibility in the electrografting reaction. In addition, the anodic current peaks became unobservable in the successive scans,as usually observed during electrografting, which result in amono layer formation [28]

### 2.3.2 Preparation of HS-GC's:

GCE's and GCP's were manually polished on a micro-cloth pad (Buehler) with de-agglomerated alumina suspension (particle size: 0.05 µm, Buehler) and washed with TDW. GCPs polish was followed with sonication in triple deionized water (TDW) for 5 min at RT. The solutions of the HS tetrasaccharides were prepared by dissolving 0.1 mg of each in 3 mL 0.1 M KCl solution. The tetrasaccharides were electrografted onto the freshly polished GCE/GCP using CV by scanning over the potential range of 0.6 – 1.2 V for 5 cycles at the scan rate of 10 mV/s. After electrografting, the modified GC surfaces (HS-GC) were washed and kept in ammonium acetate (AA) buffer (50 mM AA in 0.1 M KCl, pH 6.7) for 60 min at 25 °C before exposure to the heavy metal ion.

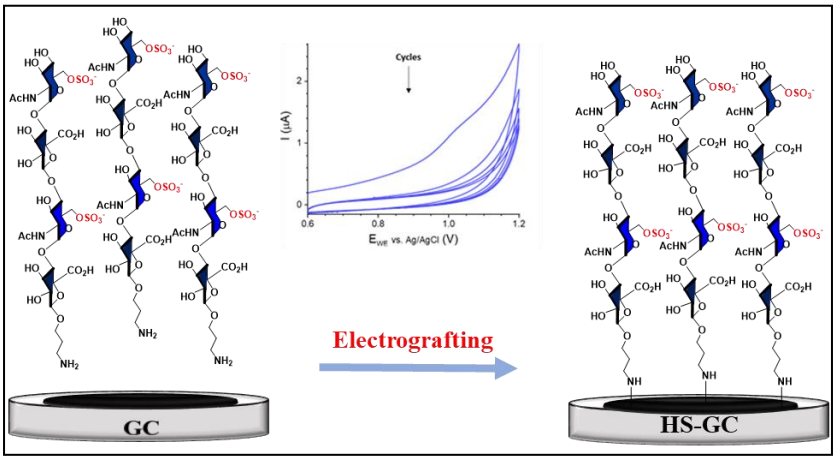


**Figure 2.** Electrografting of HS tetrasaccharides onto GC surface, demonstrated schematically by preparation of **G-6S-GC**; the inset is a representative CV recorded for **G-6S** electrografting.

### 2.3.3 HS-GC's exposure to heavy metal ions

EIS measurements were performed with ferricyanide/ferrocyanide redox active couple (1 mM $[Fe(CN)_6]^{3-}/[Fe(CN)_6]^{4-}$ in AA buffer), by applying a single sine AC potential with 10 mV amplitude superimposed with 0.21 V DC potential (vs. RE) and scanning over the frequency range of 100 kHz to 0.1 Hz. Solutions of $HgCl_2$, $CdCl_2$, and $Pb(NO_3)_2$ were prepared in AA buffer. The HS-GCs were exposed to the metal ions solutions in increase concentrations from 0.1 nM to 1 μM in an order of magnitude steps for 5 minutes each, then washed with TDW and kept in AA buffer for 5 minutes before measured. Nyquist plots of EIS measurements were fitted to the equivalent circuit of $R_S[(R_{CT}W)||Q]$, where $R_S$ is the solution resistance, $R_{CT}$ is the charge-transfer resistance of the layer, W is the Warburg diffusion element, and Q is the constant phase element of non-ideal capacitance.(Figure 3).

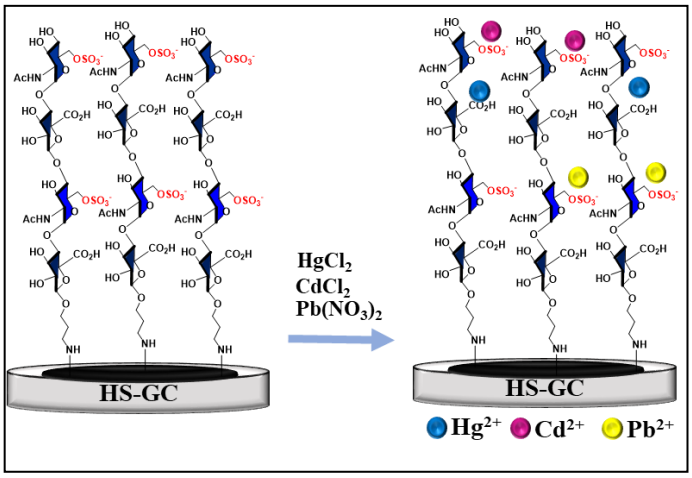



**Figure 3**. Exposure to heavy metal ions on G-6S-GC**.**

### 2.3.4 Binding interaction study:

#### EIS measurements:

EIS measurements prior and after electrografting were demonstrated for **I-6S-GC** and **G-6S-GC** showing an increase in the resistance to charge transfer ($R_{CT}$), from ~110 Ω for the bare GCE to 2278 Ω and 2439 Ω, respectively for the modified GCEs. The increase in the $R_{CT}$ correlates with the assembly of the negatively charged HS tetrasaccharides, which results from the electrostatic

repulsion and the limited transport of the negatively charged ferricyanide/ferrocyanide, redox active specie, to the electrode surface.

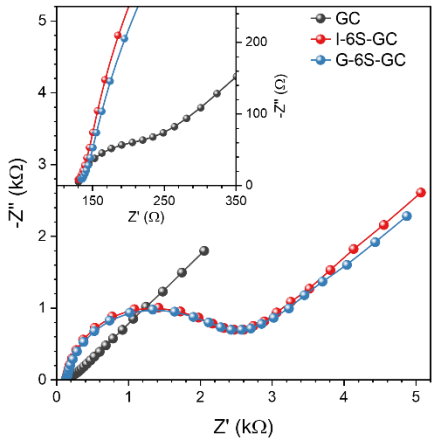



**Figure 4.** Nyquist plot of **I-6S-GC** and **G-6S-GC** prior (black, $R_{CT}$ = 113±3 Ω) and after electrografting of **I-6S** (red, $R_{CT}$ = 2280±2 Ω) and **G-6S** (blue, $R_{CT}$ = 2439±2 Ω); the inset is a magnification of 100 – 350 Ω and 0 – 250 Ω ranges of Z' and –Z'', respectively.

### 2.3.5 CA, CPD Analysis

CA measurements showed a decrease in hydrophobicity after electrografting, from 75(±1)° to 57(±1)° and 50(±1)° for **I-6S-GC** and **G-6S-GC**, respectively. This trend of decrease in hydrophobicity correlates with the assembly of the hydrophilic HS tetrasaccharides on the GC surface. CPD analysis showed an increase in the $V_{CPD}$ after electrografting with ΔCPD of 114(±5) mV for **I-6S-GC** and 136(±4) mV for **G-6S-GC**, indicating of a negative charge density on the surface that result in surface potential decrease that is translated to increase in the $V_{CPD}$.[21,30] CPD results correlate with the assembly of the negatively charged HS tetrasaccharides on the surface. Both CA and CPD analysis are in line with impedance spectroscopy results.

### 2.3.6 XPS Analysis

XPS was used to determine the presence of distinctive atomic features of the HS-GCs. XPS of **I-6S-GC** revealed increase in the measured signal in the N [1s] binding energy (BE) region. Deconvolution of XPS signal revealed the peaks at the BE of 398.2, 401.8, and 406.8 eV, that are correlated with amine electrografted GC surfaces,[18,22,25] in addition to increase of the main peak at the BE of 399.9 eV in comparison to the bare GC(Figure 5a). Quantification of XPS signal revealed an overall increase of nitrogen atomic concentration from 0.5(±0.2)% to

1.9(±0.3)% measured for bare GC and **I-6S-GC**, respectively. The presence of signal at BE of 168.2 and 169.4 eV, associated with S [2p], confirms the presence of the HS sulfate groups (Figure 5b ).

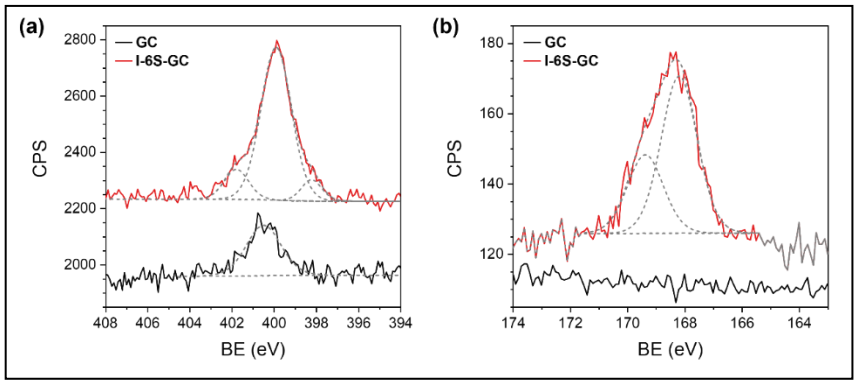



**Figure 5.** XPS spectra of bare **GC** (black) and **I-6S** modified **GC** (red) at the binding energy (BE) regions of: (a) N [1s], (b) S [2p] (dashed lines are fit components).

### 2.3.7 Impedimetric responses to heavy metal ions

After the preparation of the HS-GCs, they were exposed to increasing concentrations of $Pb^{2+}$, $Cd^{2+}$, and $Hg^{2+}$ ions and their response to the metal ions was monitored by EIS. Although heavy metal ions can be detected directly by CV, EIS is more sensitive as it benefits from the collective response of the monolayer induced by complexation. In addition, EIS require only a tiny amount of material to induce a detectable signal.[20,23] Those advantages make EIS a useful analytical tool to study heavy metal binding preferences of sulfated GAGs. In our previous work, the effect of HS tetrasaccharides sulfation on heavy metal ions binding was evaluated by modifying the oxide layer of GC using a multistep process and monitoring the complexation by EIS and CV.[20] This platform enabled the evaluation of sulfation degree effect on heavy metal ions binding preferences,[20] and to study the effect of sulfation on metal-ion mediated protein-GAGs interactions.[23]

Figure 6 a,c demonstrates Nyquist plots of **I-0S-GC, I-3S-GC, I-6S-GC** and **G-0S-GC, G-3S-GC, G-6S-GC** respectively response to increasing concentrations of $Pb^{2+}$, $Cd^{2+}$, $Hg^{2+}$ ions. In order to quantify the impedimetric response, resistance and capacitance components of the system were extracted, and since the changes in the capacitance were negligible, the response to the heavy metal ions was analyzed according to the changes in the $R_{CT}$. For ease of comparison,

$R_{CT}$ values after exposure to the heavy metal ions were normalized to the initial $R_{CT}$ of the HS-GCs before exposure.

Figure 6 b,d shows the dose-response analysis of **I-0S-GC, I-3S-GC, I-6S-GC** and **G-0S-GC, G-3S-GC, G-6S-GC** respectively to the three metal ions by normalized $R_{CT}$ ($NR_{CT}$), showing a stronger $NR_{CT}$ response toward $pb^{2+}$, $Hg^{2+}$ over $Cd^{2+}$ ions. The increase in $R_{CT}$ in response to the metal ions suggests that their binding by the anchored tetrasaccharides results in a substantial change in the monolayer density, probably due to conformational changes or inter-saccharide bridging leading to densification of the tetrasaccharides monolayer.[20,22]

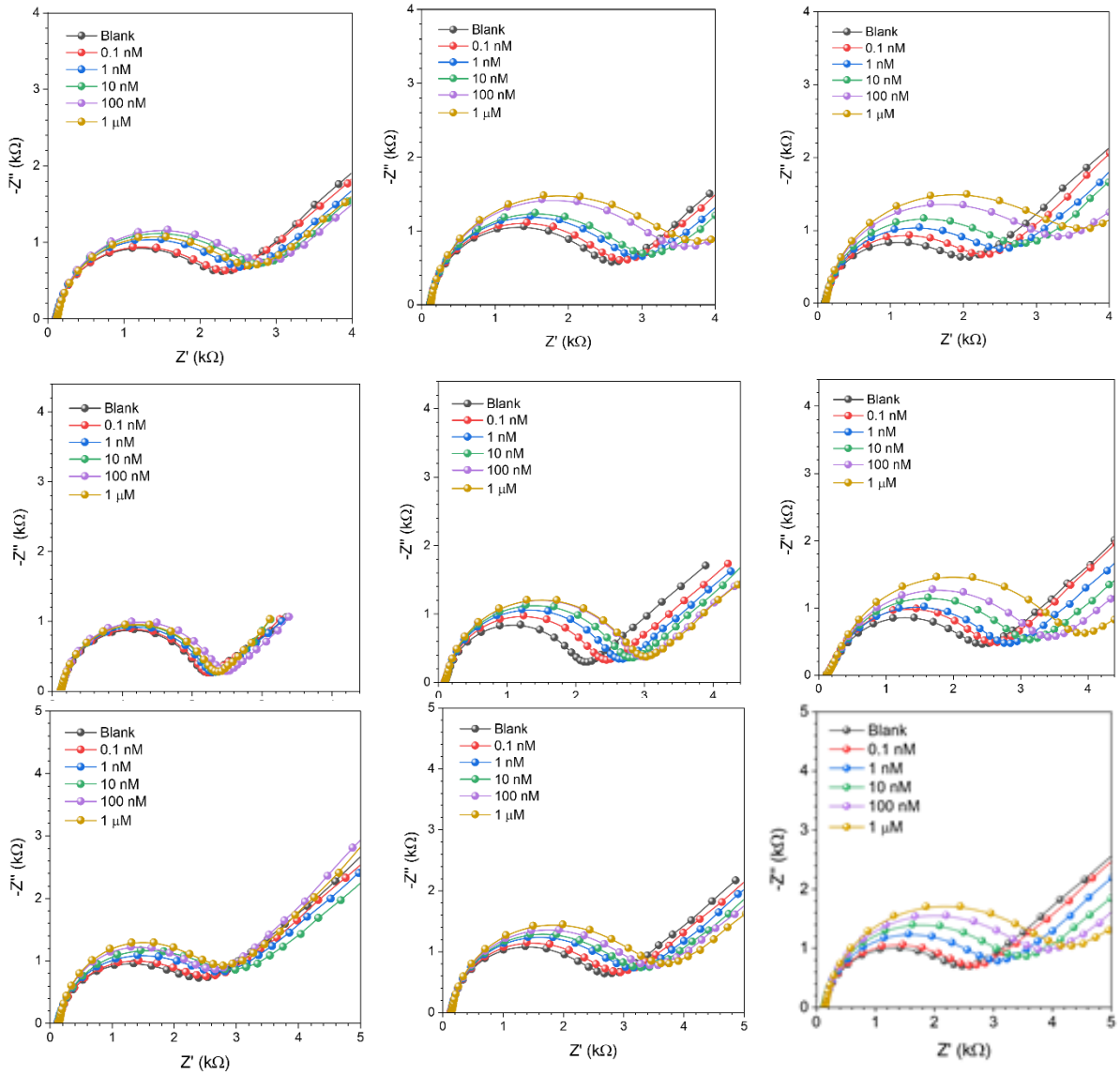



**Figure 6a.** Nyquist plots of (a) **I-0S-GC** (b) **I-3S-GC (c) I-6S-GC** electrodes to heavy metal ions: Representative Nyquist plots of response to increasing concentrations of (a) $Pb^{2+}$, (b) $Cd^{2+}$, and (c) $Hg^{2+}$ ions.

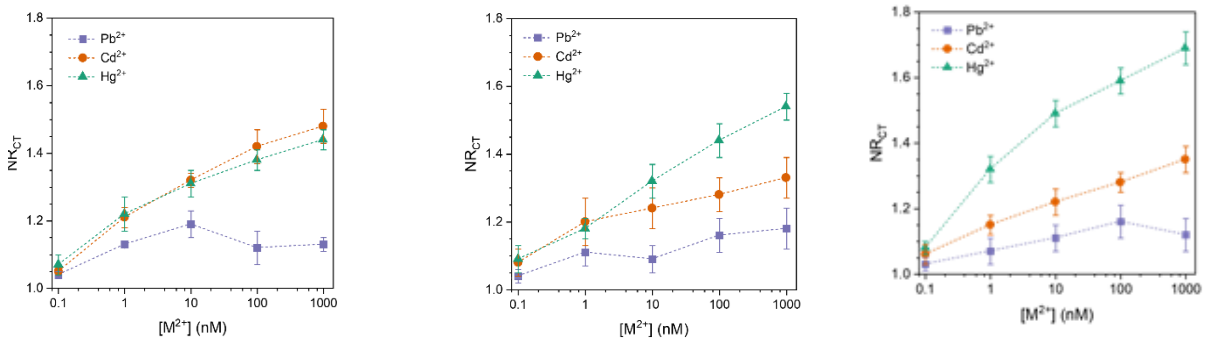



**Figure 6b**. Dose-response analysis of (a) **G-0S-GC** (b) **G-3S-GC (c) G-6S-GC** by $NR_{CT}$ to $Pb^{2+}$, $Cd^{2+}$, and $Hg^{2+}$ ions (N=10 for each data point).

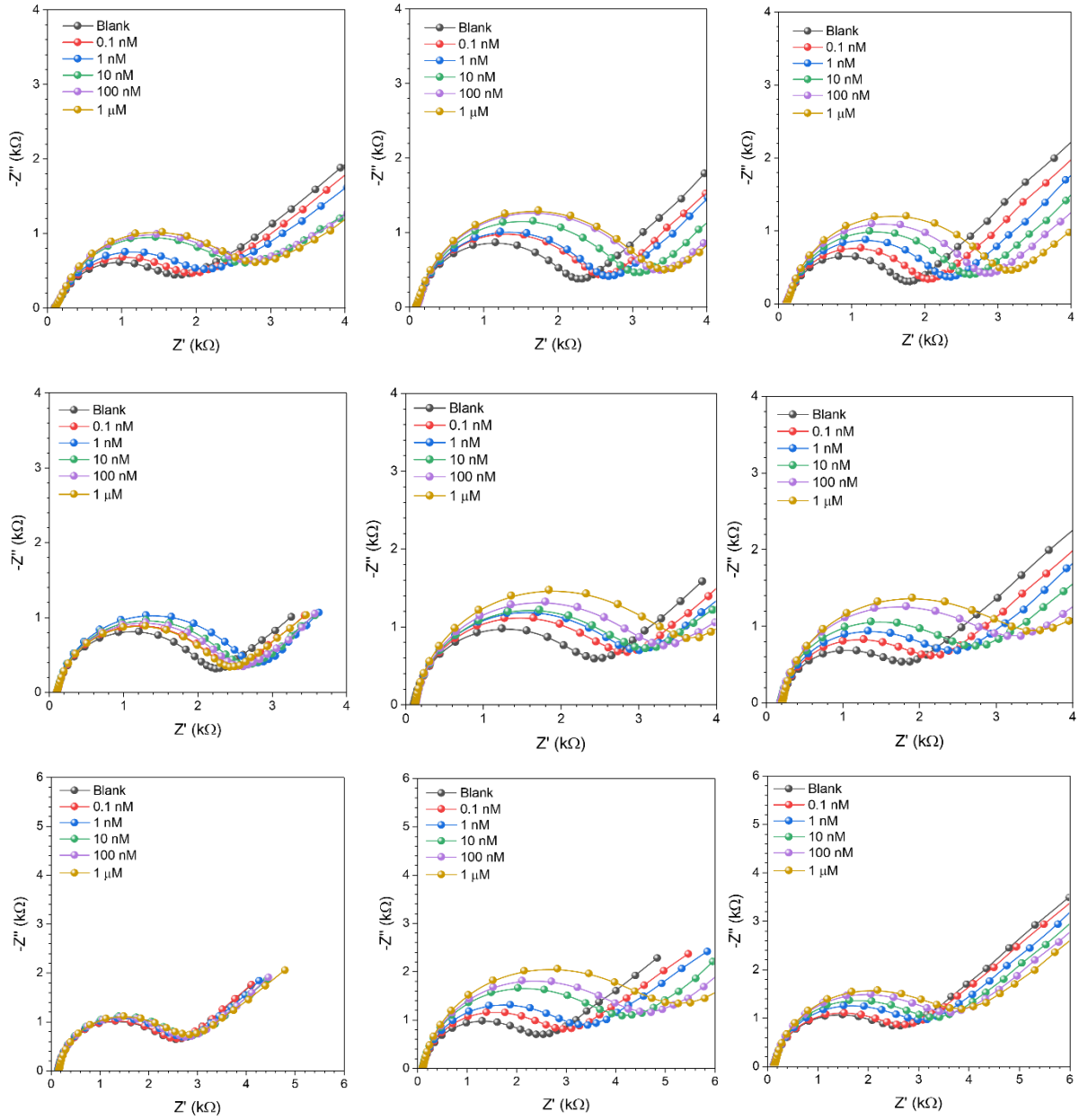


**Figure 6c.** Nyquist plots of (a) **G-0S-GC** (b) **G-3S-GC (c) G-6S-GC** electrodes to heavy metal ions: Representative Nyquist plots of response to increasing concentrations of (a) $Pb^{2+}$, (b) $Cd^{2+}$, and (c) $Hg^{2+}$ ions.

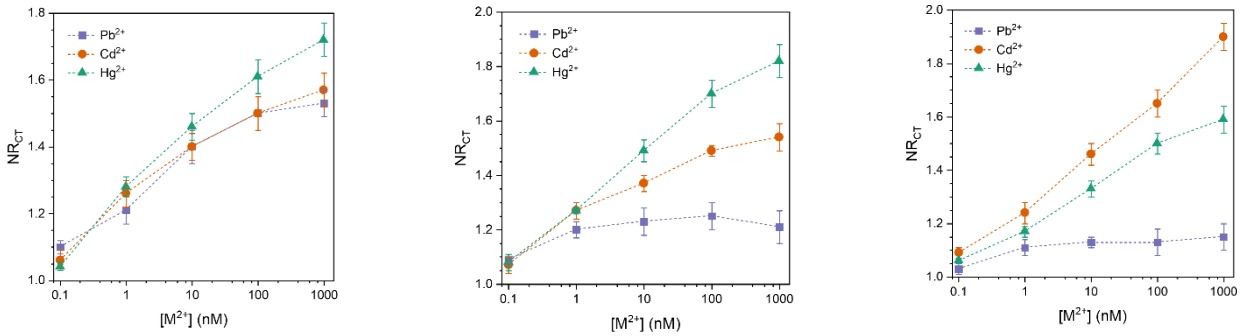



**Figure 6d**. Dose-response analysis of (a) **G-0S-GC** (b) **G-3S-GC (c) G-6S-GC** by $NR_{CT}$ to $Pb^{2+}$, $Cd^{2+}$, and $Hg^{2+}$ ions (N=10 for each data point).

The impedimetric response of all six glycans to the three metal ions was compared at a fixed concentration of 1 µM. To simplify the structural feature comparison, the results are presented based on stereochemistry, as uronic acid carboxylates pairs, and on the glycans sulfation regiochemistry (**n**) (Figure 7).

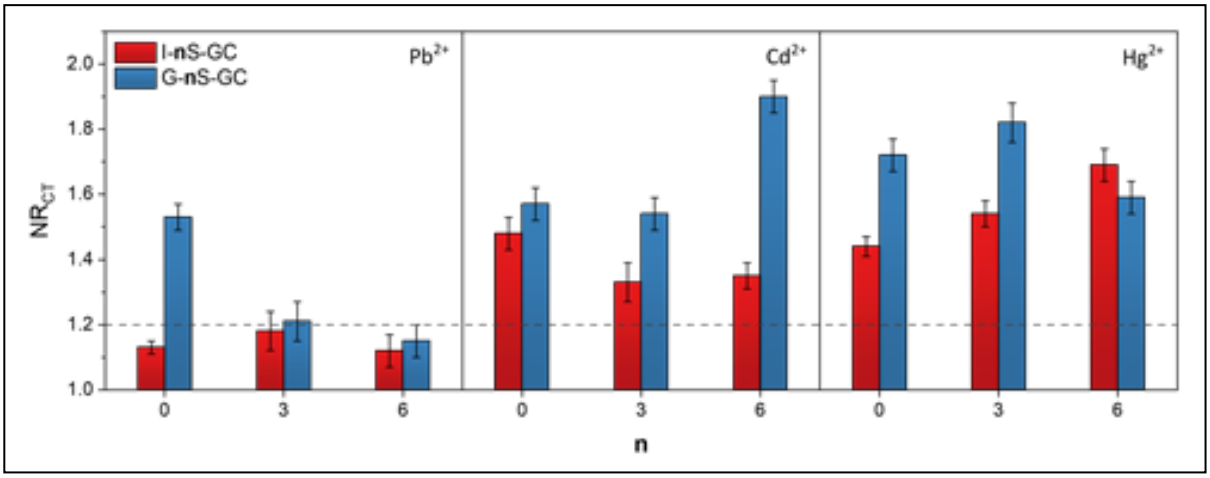
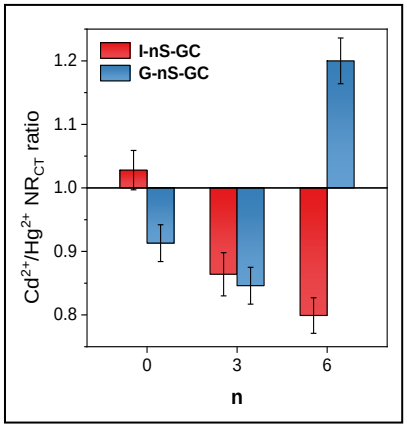



**Figure 7.** Impedimetric response of I-**n**S-GC and G-**n**S-GC glycan pairs vs. the sulfation index **n** in response to 1 µM of the heavy metal ions (only values above the dashed line are considered significant)

The analysis of the impedimetric study results highlights several characteristics. First, none of the glycans showed selectivity towards one of the metal ions. Second, only **G-0S** chelates the $Pb^{2+}$ ions while the other glycans showed a negligible response. For the G-**n**S tetrasaccharides,

the sulfation hinders $Pb^{2+}$ binding. The negligible response of **I-0S** indicates that the uronic acid stereochemistry is crucial to this ion binding suggesting that IdoA imposes a structure that prevents $Pb^{2+}$ binding. Third, most of the glycans showed preference to bind $Hg^{2+}$ over $Cd^{2+}$ ions. In the response to $Cd^{2+}$ ions, there was a preference for the G-**n**S glycans over the I-**n**S set. Significant binding preference of **G-6S** toward $Cd^{2+}$ ions was observed compared to **I-6S**, while only a moderate preference of **G-3S** was observed compared to **I-3S.** No significant preference was observed between the non-sulfated counterparts, **G-0S**, and **I-0S**. For $Hg^{2+}$ ions, moderate preference in binding was observed for **G-0S** and **G-3S** over their counterparts, **I-0S**, and **I-3S**, respectively. No preference was observed between **I-6S** and **G-6S**.

Two structural features affect the heavy metal ion binding preference: (i) sulfation pattern of the HS tetrasaccharides and (ii) uronic acid composition. To highlight the binding preference, $NR_{CT}$ values after exposure to $Cd^{2+}$ were divided by the $NR_{CT}$ values after exposure to $Hg^{2+}$ at the concentration of 1 µM, and the glycans $Cd^{2+}/Hg^{2+}$ $NR_{CT}$ ratio was plotted vs. the sulfation index **n** (Figure 8). For the non-sulfated glycans, a moderate preference of **G-0S** towards $Hg^{2+}$ was observed, while no preference was observed for **I-0S**. Both sulfated glycans **G-3S** and **I-3S** showed a preference towards $Hg^{2+}$ binding. On the contrary, dramatic effect of the uronic acid type on the ion binding preference for O-6 sulfated glycans was observed. **I-6S** showed a preference towards $Hg^{2+}$ ions while **G-6S** shows the opposite trend, high preference towards $Cd^{2+}$ ions binding. The above analyses show that both sulfation and uronic acid type affect the sensitivity and selectivity to heavy metal ions binding. This result demonstrates that the binding preference is not only sulfation pattern dependent, but also stereochemistry dependent, and that stereochemistry of the saccharides skeleton by itself is also a dominant factor in the binding preference of the HS tetrasaccharides (Figure 8).



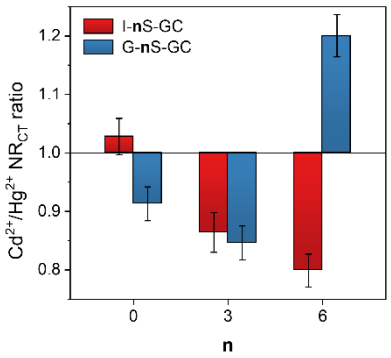



**Figure 8.** Binding preference study of I-**n**S and G-**n**S glycan pairs towards $Cd^{2+}$ and $Hg^{2+}$ ions represented by the $Cd^{2+}/Hg^{2+}$ $NR_{CT}$ ratio vs. the sulfation index **n** (measured at the concentration of 1 µM).

### 2.3.8 CA, CPD, and XPS surface analyses for I-6S and G-6S toward $Cd^{2+}$ and $Hg^{2+}$ ions:

The fact that for the same sulfation pattern an opposite binding preference toward $Cd^{2+}$ and $Hg^{2+}$ ions was achieved by uronic acid composition (**I-6S** and **G-6S)**, demanded further characterization by CA, CPD, and XPS surface analyses. CA measurements revealed an increase in hydrophobicity after exposure to the metal ions. For **I-6S-GC** the CA increased from 57(±1)° to 61(±1)° and 65(±2)° measured after exposure to $Cd^{2+}$ and $Hg^{2+}$ ions, respectively. For **G-6S-GC** the CA increased from 50(±1)° to 63(±2)° and 58(±3)° measured after exposure to $Cd^{2+}$ and $Hg^{2+}$ ions, respectively. Both monolayers exhibit a trend of a more hydrophobic interface following the metal ions binding preference, suggesting that the polar groups are now oriented inwards, facing the chelated ions, and exposing the more hydrophobic glycan moieties outwards. Our suggestion cannot distinguish between intra- and inter-molecular binding mechanisms where both binding modes will result in an increase of the measured impedance.

CPD measurements revealed a decrease in the $V_{CPD}$ measured after the exposure to the metal ions (Figure 9a). While electrografting of the negatively charged HS tetrasaccharides resulted in a positive ΔCPD, the exposure to the positively charged metal ions resulted in a negative ΔCPD. **I-6S-GC** showed ΔCPD of -31(±8) and -80(±9) mV, after exposure to $Cd^{2+}$ and $Hg^{2+}$ ions, respectively. **G-6S-GC** showed ΔCPD of -107(±9) and -43(±9) mV, after exposure to $Cd^{2+}$ and $Hg^{2+}$ ions, respectively. The ΔCPD magnitudes correlates with the observed preference towards the two ions as manifested also by increased $R_{CT}$ response and larger CA. This trend correlates with the expected addition of positive surface charge density due to the binding of the metal ions that leads to increase in surface potential and translated to decrease in the $V_{CPD}$.[21,30] According to CPD results, we assume that the increase in hydrophobicity observed by CA is a consequence of partial neutralization of the HS tetrasaccharides negative charge by the bounded of metal ions.

XPS analysis was used to identify and to quantify the presence of the metal ions on the surface of the two glycated monolayers. After exposure to $Hg^{2+}$ ions, the corresponding peaks were observed in the $Hg_{4f}$ BE region (Figure 9b), for both **I-6S** (BE: 101.5, 105.6 eV) and **G-6S** (BE: 101.9, 106.0 eV), and validated the presence of $Hg^{2+}$ ions on the surface. The fact that the corresponding peaks observed for **I-6S** were shifted toward lower BE by 0.4 eV in comparison to

**G-6S**, indicates that **I-6S** is a preferred ligand for $Hg^{2+}$ ions over **G-6S**. Deconvolution of the signal revealed two components for each peak, indicating two different chemical states of the $Hg^{2+}$ ions on the surface and suggesting that two kinds of complexes are formed between the HS tetrasaccharides and the metal ions. Interestingly, for **I-6S**, which showed a stronger $R_{CT}$ response to $Hg^{2+}$ ions, the lower BE components are significantly more dominant and the higher BE components are shifted towards lower BE by 0.3 eV in comparison to **G-6S**. This trend correlates with the increase of impedimetric signal of **I-6S** and **G-6S** in response to $Hg^{2+}$ ions binding. However, additional study of the complexes formed by the HS tetrasaccharides and $Hg^{2+}$ ions and the functional groups involved is required.

The presence of $Cd^{2+}$ ions was also validated by the corresponding peaks observed in the $Cd_{3d}$ BE region (Figure 9c), for both **I-6S** (BE: 405.5, 412.3 eV) and **G-6S** (BE: 405.0, 411.8 eV). Here also a correlation between BE and $R_{CT}$ response was observed. For **G-6S** the corresponding peaks were shifted toward lower BE by 0.5 eV in comparison to **I-6S**, indicating that the GlcA containing HS tetrasaccharides are preferred ligands for $Cd^{2+}$ ions over the IdoA containing ones.

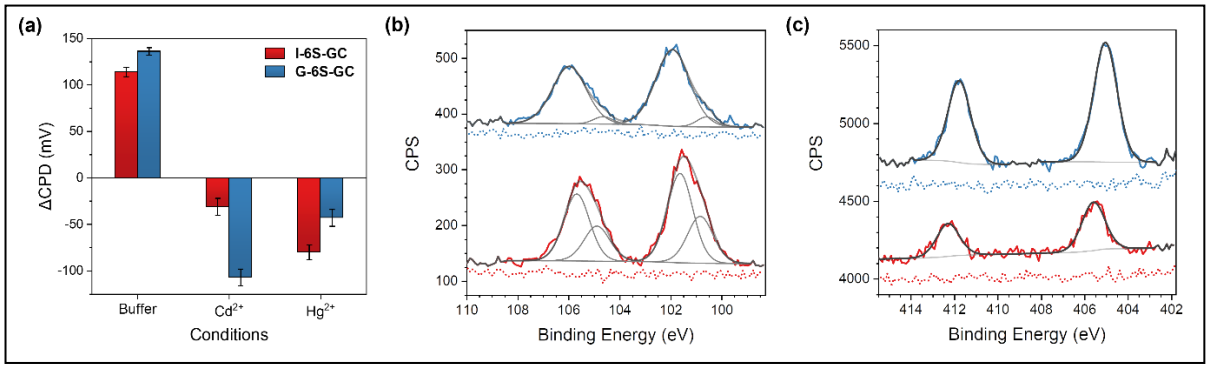



**Figure 9.** Surface characterizations of **I-6S** and **G-6S** modified GCs prior and after exposure to $Cd^{2+}$ and $Hg^{2+}$ ions: (a) CPD analysis (Buffer – after electrografting and exposure to buffer, $Cd^{2+}$/$Hg^{2+}$ – after exposure to 1 µM of each metal ion, ΔCPD values are in respect to the previous step); (b) XPS spectra of $Hg_{4f}$ BE region, and (c) $Cd_{3d}$ BE region (red – **I-6S**, blue – **G-6S**, doted/solid lines – before/after exposure to 1 µM of the metal ions, grey lines are fit components).

The ratio between the metal ions and sulfates on the glycated monolayers ($M^{2+}$/S ratio) was evaluated according to atomic concentrations quantified by XPS. For **I-6S**, the ratios of 0.23(±0.09) and 0.4(±0.1) were observed for $Cd^{2+}$/S and $Hg^{2+}$/S, respectively, and for **G-6S**, the

ratios of 0.5(±0.1) and 0.3(±0.1) were observed for $Cd^{2+}$/S and $Hg^{2+}$/S ions, respectively (Table 1). This reaffirms the binding preference trend observed by the impedance and surface potential measurements.

| **HS-GC / $M^{2+}$** | | **Atomic Concentration [%]*** | | | **$M^{2+}$/S Ratio** | |
|---|---|---|---|---|---|---|
| | | S [2p] | Hg [4f] | Cd [3d] | Hg/S | Cd/S |
| **I-6S-GC** | $Hg^{2+}$ | 0.10 ± 0.01 | 0.04 ± 0.01 | --- | 0.4 ± 0.1 | --- |
| | $Cd^{2+}$ | 0.13 ± 0.02 | --- | 0.03 ± 0.01 | --- | 0.23 ± 0.09 |
| **G-6S-GC** | $Hg^{2+}$ | 0.09 ± 0.01 | 0.03 ± 0.01 | --- | 0.3 ± 0.1 | --- |
| | $Cd^{2+}$ | 0.13 ± 0.02 | --- | 0.07 ± 0.01 | --- | 0.5 ± 0.1 |

*N=3

**Table 1.** Atomic concentrations by XPS of **I-6S-GC** and **G-6S-GC** after exposure to $Cd^{2+}$ and $Hg^{2+}$ ions.

XPS directly identify the metal ions on the surface and provide a quantitative evaluation of the atomic components. Additionally, XPS provide valuable information on the chemical environment of the metal ions. Lower atomic BEs of the metal ions correlate with higher binding affinity to a specific glycan as observed also by a larger impedance and a more negative ΔCPD. These BE shifts indicated that various glycans complexing the same metal ions exhibit different coordination sphere and highlighting the importance of uronic acid stereochemistry in the tetrasaccharides complexes formation within the monolayer.

The effect of GAGs sulfation pattern on heavy metal ions binding was previously demonstrated by us on an non-native HA system.[20] In the current study, we highlight the importance of the other GAGs molecular components on metal ion complexation and proved that EIS analyses can be applied to bio relevant HS fragments. Our results showed that although all HS tetrasaccharides have the same metal chelating groups,[33,34] their distinctive affinity towards metal ions is dictated by both sulfation regiochemistry and uronic acid stereochemistry. We assume that both sulfation pattern and uronic acid composition effect on the binding preference results from a combination of inter- and intra-molecular interactions, electrostatic interactions, and conformational differences, all leads to changes in the dielectric properties of the glycated

monolayers containing metal-ion complexes. Future study of GAGs-metal ion complexes by additional analytical methods will provide more profound insights

## 2.4 Conclusion

In this work, we described a rapid and facile modification of GC surfaces via electrografting of glycated monolayers. These label-free systems were used for impedimetric study of six HS tetrasaccharide analogs with three heavy metal-ions over modified glassy carbon surfaces. A systematic analysis based on a combination of electrochemical and surface characterization methods showed that chelation ability and binding preference of the HS tetrasaccharide are strongly dependent on their sulfation pattern and uronic acid composition. These observations can provide some hints on the interactions of native sulfated GAGs with heavy metal ions, and shed light on processes related to their accumulation in the ECM. Our system can be used in the future to the study biomedical relevant processes such as metal-ion mediated lectin binding to saccharides.

## 2.5 Experimental part:

### a) General information:

All reactions were performed under a nitrogen atmosphere with anhydrous solvents. Glycosylation reactions were performed with 4 Å molecular sieves that were flamed-dried under high vacuum. DCM was distilled with anhydrous phosphorus pentaoxide ($P_2O_{5)}$. Water was either distilled or Milli-Q-purified.

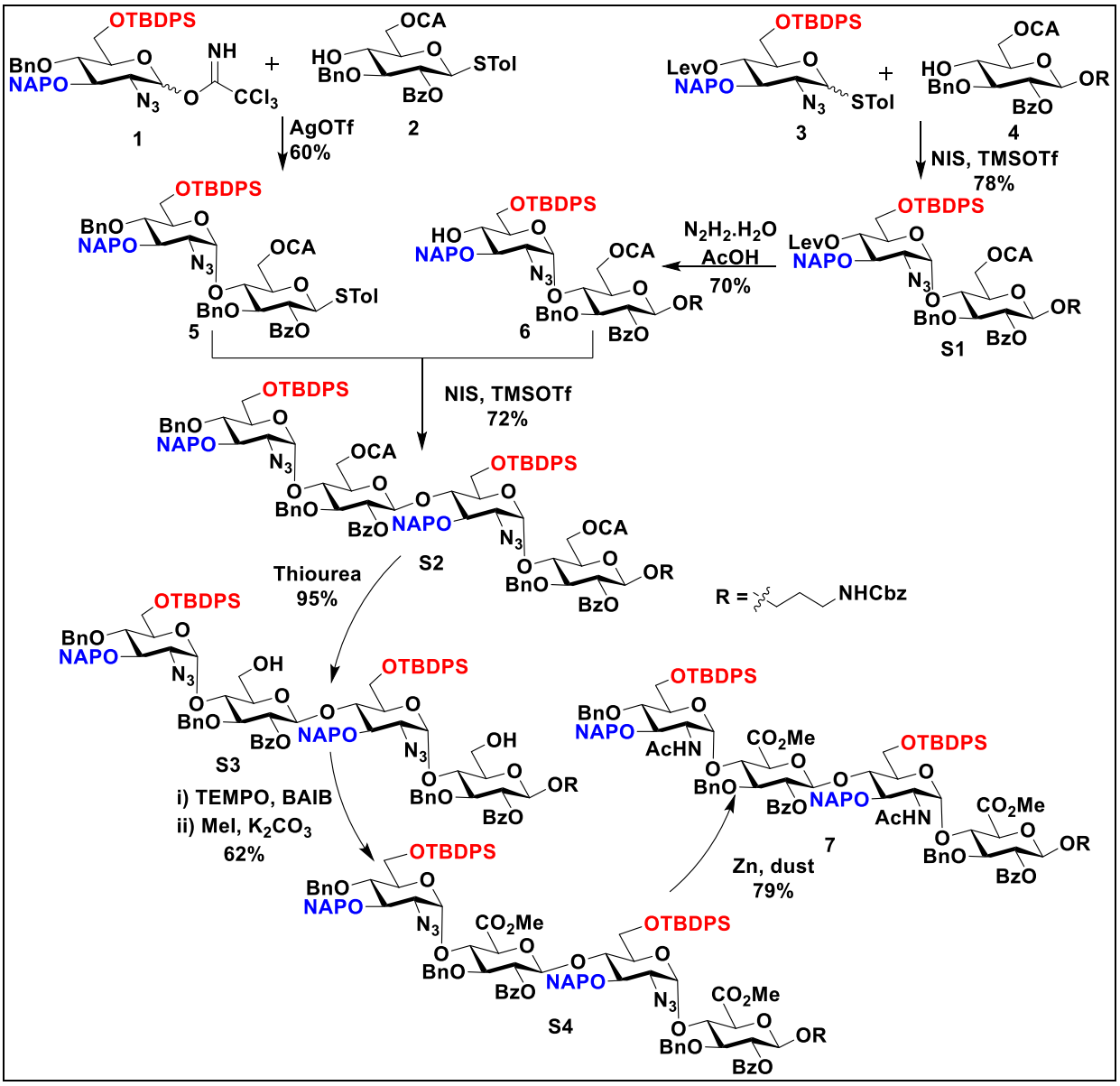
Flash column chromatography was carried out on Silica Gel 60 (100–200 mesh). TLC was performed on pre-coated glass plates of Silica Gel 60 F254 (0.25 mm, E. Merck); Reactions were visualized by UV light (254 nm) and executed by dipping into CAM or ninhydrin solution subsequent heating on a hot gun.

$^{1}$H-NMR and $^{13}$C-NMR spectra were recorded on a 400 or 600 MHz Bruker spectrometer at room temperature. Chemical shifts (in ppm) were calibrated with the solvent residual peak. Coupling constants (J) are reported in Hertz (Hz).

For the electrochemical section all chemicals used were reagent grade, purchased from Sigma-Aldrich (Merck), and used as received. TDW (18.3 MΩ·cm, EasyPure UV, Bedford) was used for all electrochemical experiments. Electrochemical experiments were performed with BioLogic SP-300 potentiostat, using a conventional three-electrode electrochemical cell of 3 mm diameter

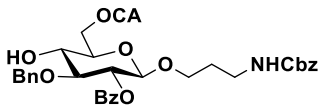
GCE as the working electrode (WE), Pt wire as the counter electrode (CE), and Ag/AgCl (KCl saturated) as the reference electrode (RE). For the surface characterization experiments GCP were used as the WE with the same three electrodes cell setup. CA measurements were carried with TDW using Attension Theta Lite goniometer (Biolin Scientific). Kelvin probe derived CPD measurements were performed with Kelvin Probe S vibrating gold grid electrode (WF ~ 4.8 eV), operated with Kelvin Control 07 unit (DeltaPhi Besocke, Julich, Germany), in a home-built faraday cage under argon gas atmosphere. $V_{CPD}$ was recorded with Keithley 2450 SMU. ΔCPD values represent the $V_{CPD}$ difference in respect previous step. XPS measurements were performed using Axis Supra$^{+}$ spectrometer (Kratos Analytical Ltd., Manchester, U.K.) with an Al $K_{\alpha}$ monochromatic x-ray source (1486.7 eV).

**b) Synthesis of G-disaccharide precursor:**




**Scheme S1.** Synthesis of **G**-tetrasaccharide precursor.

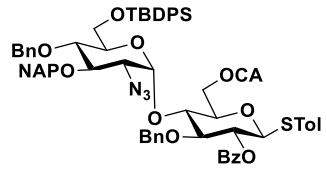
**_N_-benzyloxycarbonyl-3-aminopropyl-_O_-[2-_O_-benzoyl-3-_O_-benzyl-6-_O_-chloroacetyl-1-_β_-D-glucopyranoside] (4)**




To a solution of **2** (2.0 g, 3.59 mmol) and *N*-benzyloxycarbonyl-3-aminopropanol (0.90 g, 4.30 mmol) in anhydrous DCM (20 mL) under argon was added pre-activated 4 Å molecular sieves (1.0 g) and stirred at room temperature for 1 h. The reaction was cooled to -20 $^{o}$C and mixed

with NIS (0.88 g, 3.95 mmol) and TMSOTf (0.13 mL, 0.58 mmol). After completion of the reaction, the molecular sieves were filtered and organic layer was washed with sodium thiosulfate and brine and concentrated under reduced pressure. Purification was done by silica gel column chromatography (EtOAc/Hexane= 1/7, v/v) yielded 87% of compound **4**. $^{1}$H NMR (400 MHz, $CDCl_3$) δ 8.02 (d, *J* = 7.4 Hz, 2H), 7.56 (t, *J* = 7.4 Hz, 1H), 7.42 (t, *J* = 7.7 Hz, 2H), 7.37 – 7.27 (m, 5H), 7.23 – 7.16 (m, 5H), 5.26 – 5.19 (m, 1H), 5.03 (s, 2H), 4.73 (d, *J* = 9.4 Hz, 1H), 4.60 (d, *J* = 9.4 Hz, 1H), 4.53 (d, *J* = 8.0 Hz, 1H), 4.46 (d, *J* = 4.6 Hz, 1H), 4.06 (s, 1H), 3.86 (m, 1H), 3.71 – 3.60 (m, 2H), 3.58 – 3.49 (m, 2H), 3.13 (m, 2H), 2.56 (d, *J* = 2.6 Hz, 1H), 1.70 (m, 2H). $^{13}$C NMR (100 MHz, $CDCl_3$) δ 167.73, 165.32, 156.52, 137.68, 133.50, 129.83, 129.61, 128.68, 128.65, 128.58, 128.15, 101.22, 82.08, 74.82, 73.49, 69.89, 67.47, 66.53, 64.58, 40.81, 38.10, 29.51. HR-ESI-MS (*m/z*): $[M+Na]^+$, calculated for $C_{33}H_{36}ClNO_{10}Na$, 664.1925; found, 664.1933.

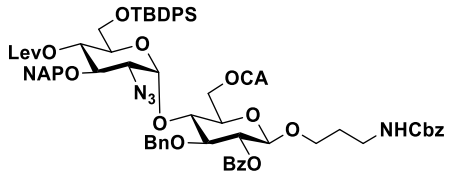
**4-Methylphenyl-[2-azido-4-*O*-benzyl-6-*O*-*tert*-butyldiphenylsilyl-2-deoxy 3-*O*-(2-naphthylmethyl)-*α*-D-glucopyranosyl]-(1→4)-2-*O*-benzoyl-3-*O*-benzyl-6-*O*-chloroacetyl-1-thio-*β*-D-glucopyranoside (5)**




To a solution of **1** (1.80 g, 2.20 mmol) and **2** (0.98 g, 1.76 mmol) in anhydrous DCM (20 mL) was added pre-activated 4 Å molecular sieves (0.9 g) and stirred at RT for 1 h under nitrogen atmosphere. Then at -40 $^{o}$C, AgOTf (3.96 g, 15.43 mmol) was added and stirred for 40 mins. After the completion of reaction molecular sieves filtered and organic layer was washed with saturated brine solution and concentrated under reduced pressure. Column chromatography (EtOAc/Hexane= 1/8, v/v), yielded 60% of **5**.$^{1}$H NMR (400 MHz, $CDCl_3$) δ 8.13 (d, *J* = 8.2 Hz, 2H), 7.89 – 7.79 (m, 4H), 7.64 (dd, *J* = 18.5, 7.5 Hz, 5H), 7.52 (q, *J* = 7.5, 6.4 Hz, 5H), 7.47 – 7.40 (m, 2H), 7.40 – 7.30 (m, 9H), 7.30 – 7.18 (m, 8H), 7.12 (d, *J* = 7.3 Hz, 2H), 5.58 – 5.53 (m, 1H), 5.30 (t, *J* = 9.1 Hz, 1H), 5.07 (q, *J* = 10.8 Hz, 2H), 4.95 – 4.68 (m, 5H), 4.61 (m, 1H), 4.20 (m,1H), 4.01 (m, 3H), 3.94 – 3.65 (m, 6H), 3.62 (d, *J* = 9.5 Hz, 1H), 3.34 (dd, *J* = 10.2, 2.4 Hz, 1H), 2.36 (s, 3H), 1.07 (s, 9H). $^{13}$C NMR (100 MHz, $CDCl_3$) δ 137.83, 135.91, 135.63, 135.19, 133.93, 133.46, 129.89, 129.81, 129.78, 129.56, 128.59, 128.53, 128.42, 128.32, 128.00, 127.78,

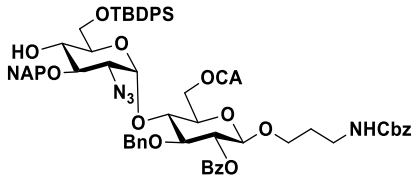
127.70, 127.64, 126.97, 126.11, 126.02, 98.03, 85.87, 84.59, 79.87, 76.22, 75.64, 75.23, 74.71, 73.67, 73.06, 72.63, 64.48, 63.33, 62.04, 40.50, 29.72, 26.91, 21.19, 19.33. HR-ESI-MS (*m/z*): $[M+Na]^+$, calculated for $C_{69}H_{70}ClN_3O_{11}SSiNa$, 1234.4087; found, 1234.4086.

**_N_-benzyloxycarbonyl-3-aminopropyl-_O_-[2-azido--6-_O_-_tert_-butyldiphenylsilyl-2-deoxy-4-_O_-levulinoyl-3-_O_-(2-naphthylmethyl)-_α_-D-glucopyranosyl]-(1→4)-_O_-2-_O_-benzoyl-3-_O_-benzyl-6-_O_-chloroacetyl-_β_-D-glucopyranoside (S1)**



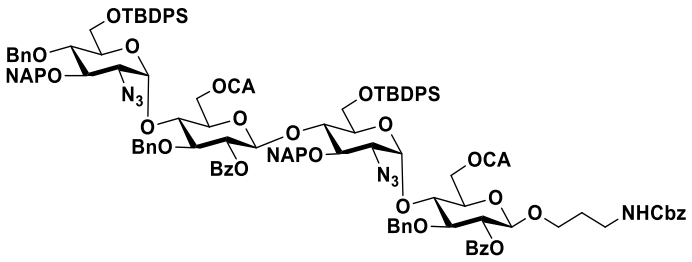

To a solution of **3** (1.8 g, 2.28 mmol) and **4** (1.17 g, 1.48 mmol) in anhydrous DCM (20 mL) was added preactivated 4 Å molecular sieves and stirred at room temperature for 1 h. Then at -20 $^oC$, NIS (0.10 g, 0.46 mmol) and TMSOTf (0.082 mL, 0.37 mmol) were rapidly added and stirred at the same temperature for 2 h. After the completion of the reaction molecular sieves were filtered, dissolved in DCM, and washed with sodium thiosulfate and brine and concentrated under reduced pressure. Silica gel column chromatography (EtOAc/Hexane= 1/7, v/v) yielded 78% of compound **S1**. $^1H$ NMR (400 MHz, $CDCl_3$) δ 8.03 (d, *J* = 7.3 Hz, 2H), 7.85 – 7.79 (m, 4H), 7.62 (m, 4H), 7.56 (t, *J* = 7.4 Hz, 1H), 7.48 – 7.37 (m, 7H), 7.36 (s, 1H), 7.33 (d, *J* = 4.5 Hz, 7H), 7.31 (s, 1H), 7.20 (d, *J* = 2.0 Hz, 2H), 7.17 (m, 2H), 5.58 (s, 1H), 5.29 (s, 1H), 5.23 (d, *J* = 10.5 Hz, 1H), 5.05 (s, 2H), 4.93 (d, *J* = 4.7 Hz, 1H), 4.83 (d, *J* = 11.4 Hz, 1H), 4.79 – 4.70 (m, 2H), 4.62 (m, 1H), 4.56 (d, *J* = 7.7 Hz, 1H), 4.17 (s, 1H), 4.02 (s, 2H), 3.91 (d, *J* = 2.3 Hz, 10H), 3.34 (m, 1H), 3.15 (m, 2H), 2.52 – 2.46 (m, 2H), 2.36 (s, 2H), 2.05 (s, 3H), 1.70 (q, *J* = 6.3 Hz, 2H), 1.01 (s, 9H). $^{13}C$ NMR (100 MHz, $CDCl_3$) δ 205.98, 171.17, 165.19, 156.45, 136.78, 135.72, 135.12, 133.49, 133.29, 133.14, 133.05, 129.75, 129.72, 128.60, 128.49, 128.43, 128.19, 128.03, 127.76, 127.64, 126.80, 126.10, 125.99, 125.94, 100.72, 97.48, 97.43, 82.93, 77.74, 74.75, 74.23, 73.74, 73.47, 73.34, 72.64, 72.53, 71.75, 70.17, 67.28, 67.14, 66.46, 64.62, 64.35, 62.90, 62.83, 62.18, 62.09, 40.56, 38.05, 37.66, 29.71, 29.69, 29.49, 27.91, 26.80, 19.29, 14.15. HR-ESI-MS (*m/z*): $[M+Na]^+$, calculated for $C_{71}H_{77}ClN_4O_{16}SiNa$, 1327.4690; found, 1327.4694.

**_N_-benzyloxycarbonyl-3-aminopropyl-_O_-[2-azido-6-_O_-_tert_-butyldiphenylsilyl-2-deoxy-3-_O_-(2-naphthylmethyl)-_α_-D-glucopyranosyl]-(1→4)-_O_-2-_O_-benzoyl-3-_O_-benzyl-6-_O_-chloroacetyl-_β_-D-glucopyranoside (6)**



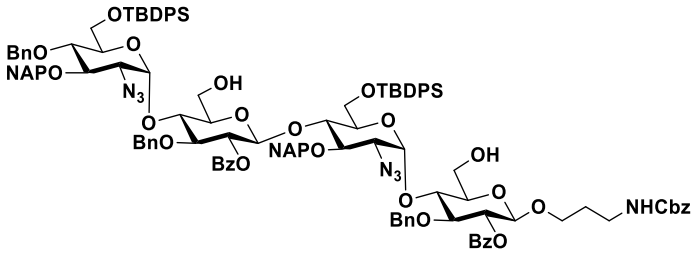

To a solution of **S1** (1.50 g, 1.14 mmol) in DCM (15 mL) under nitrogen was added glacial acetic acid (0.33 mL, 5.47 mmol) and $N_2H_4 \cdot H_2O$ (0.18 mL, 5.58 mmol) and stirred for 12 h at RT. the reaction mixture was extracted with DCM and washed with brine. Organic layer was concentrated and purified using column chromatography (EtOAc/Hexane= 1/6, v/v) yielded 70% of **6**. $^1$H NMR (400 MHz, $CDCl_3$) δ 8.03 (d, *J* = 7.2 Hz, 2H), 7.88 – 7.82 (m, 4H), 7.68 – 7.62 (m, 4H), 7.56 – 7.53 (m, 2H), 7.50 – 7.47 (m, 2H), 7.45 – 7.40 (m, 4H), 7.40 – 7.32 (m, 9H), 7.23 – 7.15 (m, 5H), 5.54 (d, *J* = 3.9 Hz, 1H), 5.31 – 5.25 (m, 1H), 5.05 (s, 5H), 4.78 (d, *J* = 10.4 Hz, 1H), 4.71 (d, *J* = 10.4 Hz, 1H), 4.62 (d, *J* = 11.5 Hz, 1H), 4.56 (d, *J* = 7.7 Hz, 1H), 4.18 (m, 1H), 3.99 (t, *J* = 8.6 Hz, 1H), 3.93 – 3.80 (m, 7H), 3.76 (m, 1H), 3.67 (m, 1H), 3.62 (dd, *J* = 8.6, 4.1 Hz, 1H), 3.57 – 3.50 (m, 1H), 3.27 – 3.06 (m, 3H), 2.65 (s, 1H), 1.70 (m, 2H), 1.05 (s, 9H). $^{13}$C NMR (100 MHz, $CDCl_3$) δ 165.17, 156.46, 136.80, 135.68, 135.59, 135.48, 133.46, 133.36, 133.13, 130.02, 129.99, 129.74, 129.47, 128.59, 128.49, 128.40, 128.37, 128.06, 128.02, 127.89, 127.83, 127.77, 127.72, 126.94, 126.17, 126.05, 126.00, 100.67, 97.85, 82.99, 79.36, 75.28, 74.34, 73.84, 73.60, 72.57, 72.32, 72.15, 67.31, 64.43, 63.83, 62.59, 40.53, 38.09, 29.48, 26.92, 19.27. HR-ESI-MS (m/z): $[M+Na]^+$, calculated for $C_{66}H_{71}ClN_4O_{14}SiNa$, 1229.4322; found 1229.4324.

**_N_-benzyloxycarbonyl-3-aminopropyl-_O_-[(2-azido-4-_O_-benzyl-6-_O_-_tert_-butyldiphenylsilyl-2-deoxy-3-_O_-(2-naphthylmethyl)-_α_-D-glucopyranosyl)-(1→4)-_O_-(2-_O_-benzoyl-3-_O_-benzyl-6-_O_-chloroacetyl-_β_-D-glucopyranosyl)-(1→4)-_O_-(2-azido-6-_O_-_tert_ butyldiphenylsilyl-2-deoxy-3-_O_-(2-naphthylmethyl)-_α_-D-glucopyranosyl)]-(1→4)-_O_-2-_O_-benzoyl-3-_O_-benzyl-6-_O_-chloroacetyl-_β_-D-glucopyranoside (S2)**



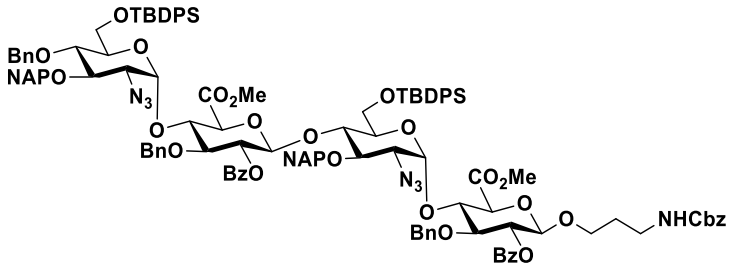
To a solution of **5** (1.50 g, 1.24 mmol), **6** (1.24 g, 1.02 mmol) in anhydrous DCM (20 mL) -20 $^{o}$C was added NIS (0.33 g, 1.48 mmol) and TMSOTf (0.02 mL, 0.13 mmol). Once reaction completed, molecular sieves were separated using celite filtration and organic layer was washed with sodium thiosulfate and brine. Finally, the organic layer was dried using anhydrous $Na_2SO_4$, concentrated and purified through silica gel column chromatography (EtOAc/Hexane= 1/7, v/v) yielded 72% of compound **S2**. $^{1}$H NMR (400 MHz, $CDCl_3$) δ 7.99 (d, *J* = 7.2 Hz, 2H), 7.86 – 7.76 (m, 8H), 7.76 – 7.70 (m, 4H), 7.66 – 7.60 (m, 6H), 7.56 – 7.49 (m, 6H), 7.49 – 7.44 (m, 4H), 7.42 (dd, *J* = 3.3, 1.5 Hz, 2H), 7.40 – 7.36 (m, 6H), 7.36 – 7.32 (m, 5H), 7.32 – 7.27 (m, 10H), 7.22 (t, *J* = 2.0 Hz, 2H), 7.20 – 7.15 (m, 7H), 7.14 – 7.09 (m, 2H), 5.55 (d, *J* = 3.8 Hz, 1H), 5.46 (d, *J* = 4.0 Hz, 1H), 5.38 (t, *J* = 8.7 Hz, 1H), 5.27 (d, *J* = 11.6 Hz, 1H), 5.21 – 5.15 (m, 1H), 5.08 (m, 5H), 4.90 – 4.80 (m, 4H), 4.74 (m, 2H), 4.61 (m, 2H), 4.43 (d, *J* = 7.8 Hz, 1H), 4.33 (d, *J* = 2.3 Hz, 2H), 4.18 (t, *J* = 9.3 Hz, 1H), 4.13 – 4.07 (m, 1H), 4.05 – 3.86 (m, 4H), 3.85 – 3.77 (m, 5H), 3.72 – 3.59 (m, 4H), 3.53 (d, *J* = 9.5 Hz, 2H), 3.50 – 3.44 (m, 2H), 3.41 (dd, *J* = 7.7, 4.7 Hz, 1H), 3.37 (s, 2H), 3.30 (d, *J* = 3.8 Hz, 1H), 3.29 – 3.25 (m, 1H), 3.25 – 3.18 (m, 2H), 3.14 (m, 1H), 3.10 – 3.02 (m, 1H), 1.66 (dt, *J* = 12.7, 7.1 Hz, 2H), 1.08 (s, 8H), 1.00 (s, 8H). $^{13}$C NMR (100 MHz, $CDCl_3$) δ 165.18, 156.45, 137.33, 135.95, 135.91, 135.86, 135.70, 135.62, 133.69, 133.44, 133.24, 132.88, 130.28, 130.10, 129.76, 129.71, 129.43, 128.81, 128.66, 128.57, 128.53, 128.47, 128.37, 128.34, 128.14, 128.03, 128.00, 127.97, 127.90, 127.86, 127.78, 127.77, 127.74, 127.70, 127.59, 126.95, 126.60, 126.14, 126.03, 126.00, 125.96, 125.75, 100.56, 99.98, 98.19, 97.75, 83.28, 82.97, 79.49, 76.30, 75.61, 75.21, 75.01, 74.78, 74.65, 74.21, 74.11, 73.83, 73.27, 73.05, 72.48, 72.17, 72.08, 67.23, 64.55, 63.26, 62.99, 62.53, 61.96, 60.84, 40.17, 29.71, 29.44, 26.98, 26.89, 19.39, 19.30. HR-ESI-MS (*m/z*): $[M+Na]^+$, calculated for $C_{128}H_{133}Cl_2N_7O_{25}Si_2Na$: 2316.8164; found 2316.8170.

**_N_-benzyloxycarbonyl-3-aminopropyl-_O_-[(2-azido-4-_O_-benzyl-6-_O_-_tert_-butyldiphenylsilyl-2-deoxy-3-_O_-(2-naphthylmethyl)-_α_-D-glucopyranosyl)-(1→4)-_O_-(2-_O_-benzoyl-3-_O_-benzyl-_β_-D-glucopyranosyl)-(1→4)-_O_-(2-azido-6-_O_-_tert_-butyldiphenylsilyl-2-deoxy-3-_O_-(2-naphthylmethyl)-_α_-D-glucopyranosyl)]-(1→4)-_O_-2-_O_-benzoyl-3-_O_-benzyl-_β_-D-glucopyranoside (S3)**



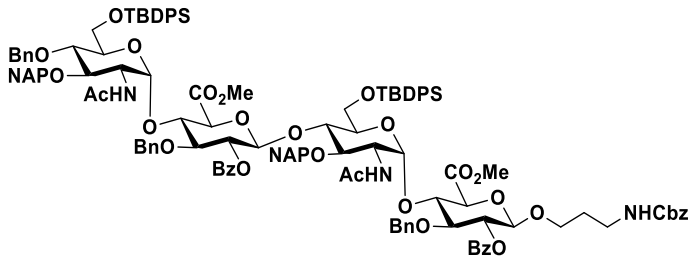

To a solution of **S2** (1.30 g, 0.56 mmol) in pyridine/MeOH (1:1, 15 ml) at 80 °C was added thiourea (0.16 g, 2.21 mmol) and stirred under nitrogen atmosphere for 6 h. After completion of the reaction, the solvent was evaporated, dissolved in EtOAc and washed with 1N HCl and brine solution. The organic layer was dried using anhydrous $Na_2SO_4$, filtered, concentrated, and purified through silica gel column chromatography (EtOAc/Hexane= 1/6, v/v), yielded 95% of **S3**. $^1$H NMR (400 MHz, $CDCl_3$) δ 8.02 (d, *J* = 7.5 Hz, 2H), 7.84 – 7.73 (m, 10H), 7.73 – 7.67 (m, 3H), 7.67 – 7.60 (m, 4H), 7.59 – 7.52 (m, 3H), 7.52 – 7.44 (m, 8H), 7.44 – 7.34 (m, 10H), 7.32 (d, *J* = 5.5 Hz, 6H), 7.30 – 7.28 (m, 4H), 7.26 (s, 1H), 7.24 (s, 1H), 7.22 (d, *J* = 4.1 Hz, 4H), 7.19 (s, 1H), 7.17 (m, 7H), 5.59 (d, *J* = 3.9 Hz, 1H), 5.50 (d, *J* = 3.7 Hz, 1H), 5.38 (t, *J* = 8.6 Hz, 1H), 5.27 – 5.18 (m, 2H), 5.08 – 5.01 (m, 5H), 4.95 – 4.73 (m, 6H), 4.65 (m, 2H), 4.50 (d, *J* = 7.8 Hz, 1H), 4.18 – 4.08 (m, 2H), 4.02 – 3.70 (m, 13H), 3.58 – 3.44 (m, 4H), 3.40 – 3.24 (m, 6H), 3.23 – 3.08 (m, 3H), 1.68 (m, 2H), 1.06 (s, 9H), 1.04 (s, 9H). $^{13}$C NMR (100 MHz, $CDCl_3$) δ 165.26, 165.09, 156.47, 138.08, 137.48, 136.73, 135.99, 135.92, 135.72, 135.68, 135.60, 135.37, 133.82, 133.55, 133.43, 133.37, 133.27, 133.13, 132.95, 132.43, 130.16, 129.96, 129.88, 129.79, 129.75, 129.59, 128.64, 128.60, 128.53, 128.48 (d, *J* = 1.9 Hz), 128.41, 128.33, 128.26, 128.09, 128.03, 127.86, 127.79, 127.72, 126.95, 126.52, 126.13, 126.08, 126.06, 126.02, 125.81, 101.00, 100.06, 97.92, 97.36, 83.63, 83.32, 79.85, 78.07, 77.78, 76.07, 75.66, 75.58, 75.14, 74.87, 74.55, 74.39, 74.00, 73.19, 72.70, 72.16, 72.05, 67.46, 66.50, 63.41, 62.97, 62.06, 61.77, 61.35, 60.89, 38.11, 29.52, 27.03, 26.90. HR-ESI-MS (*m/z*): $[M+H]^+$, calculated for $C_{124}H_{131}N_7O_{23}Si_2$, 2142.8508; found, 2142.8509.

**_N_-benzyloxycarbonyl-3-aminopropyl-_O_-[methyl(2-azido-4-_O_-benzyl-6-_O_-_tert_-butyldiphenylsilyl-2-deoxy-3-_O_-(2-naphthylmethyl)-_α_-D-glucopyranosyl)-(1→4)-_O_-(2-_O_-benzoyl-3-_O_-benzyl-_β_-D- glucopyranosyluronate)-(1→4)-_O_-(methyl(2-azido-3-_O_-(2-naphthylmethyl)-6-_O_-_tert_-butyldiphenylsilyl-2-deoxy-_α_-D-glucopyranosyl))]-(1→4)-_O_-2-_O_-benzoyl-3-_O_-benzyl-_β_-D-glucopyranosiduronate (S4)**




To a solution of **S3** (1.10 g, 0.52 mmol) in DCM/$H_2O$ (2:1, 12 mL) was added 2,2,6,6-tetramethyl-1-piperidinyloxyl free radical (TEMPO) (0.06 g, 0.41 mmol), and [Bis(acetoxy)iodo] benzene (BAIB) (1.67 g, 5.2 mmol) and stirred at RT for 6 h. The organic layer was washed with saturated $NH_4Cl$ solution and concentrated. Then, the crude product was dissolved in DMF (10 mL) and mixed with $K_2CO_3$ (0.21 g, 0.001 mmol), MeI (0.09 mL, 0.001 mmol), and stirred overnight at RT. On completion of reaction, reaction mixture extracted with EtOAc and brine. The organic layer was concentrated and purified through silica gel column chromatography (EtOAc/Hexane= 1/8, v/v) to get compound **S4** in 62% yield. $^1$H NMR (400 MHz, $CDCl_3$) δ 8.01 (d, *J* = 7.3 Hz, 2H), 7.86 – 7.73 (m, 13H), 7.70 – 7.62 (m, 7H), 7.60 – 7.37 (m, 19H), 7.35 – 7.27 (m, 18H), 7.18 (m, 14H), 5.49 (d, *J* = 3.7 Hz, 1H), 5.47 – 5.41 (m, 2H), 5.35 – 5.26 (m, 2H), 5.08 (d, *J* = 3.5 Hz, 2H), 5.04 (s, 3H), 4.99 (t, *J* = 6.0 Hz, 1H), 4.97 – 4.91 (m, 2H), 4.84 (m, 2H), 4.76 (m, 2H), 4.68 (d, *J* = 10.4 Hz, 1H), 4.57 – 4.51 (m, 2H), 4.27 – 3.87 (m, 12H), 3.85 – 3.67 (m, 6H), 3.44 (m, 2H), 3.33 (m, 1H), 3.23 (d, *J* = 3.9 Hz, 1H), 3.20 (s, 3H), 3.09 (m, 4H), 2.89 (s, 3H), 1.66 (m, 2H). $^{13}$C NMR (100 MHz,$CDCl_3$) δ 168.36, 167.66, 165.14, 164.68, 156.41, 138.36, 137.27, 137.20, 136.85, 135.94, 135.90, 135.70, 135.63, 135.60, 135.33, 133.92, 133.59, 133.53, 133.50, 133.39, 133.35, 133.12, 133.03, 132.93, 132.29, 130.21, 129.99, 129.75, 129.69, 129.61, 129.37, 128.99, 128.69, 128.60, 128.47, 128.44, 128.40, 128.39, 128.30, 128.22, 128.17, 128.02, 128.00, 127.98, 127.87, 127.83, 127.74, 127.70, 127.65, 127.52, 127.48, 127.35, 126.97, 126.80, 126.11, 126.07, 126.00, 125.64, 125.58, 100.84, 100.06, 98.03, 97.26, 82.94, 82.46, 79.73, 77.84, 77.26, 76.24, 75.76, 75.59, 75.04, 74.91, 74.88, 74.68, 74.28, 73.91, 73.65, 73.52, 73.48, 72.39, 71.54, 67.31, 66.37, 63.49, 62.61, 61.80, 60.50, 52.33, 51.77, 38.02, 29.72, 29.34, 19.42, 19.40. HR-ESI-MS (*m/z*): $[M+2H]^+$, calculated for $C_{126}H_{131}N_7O_{25}Si_2$, 2199.8890; found, 2199.8898.

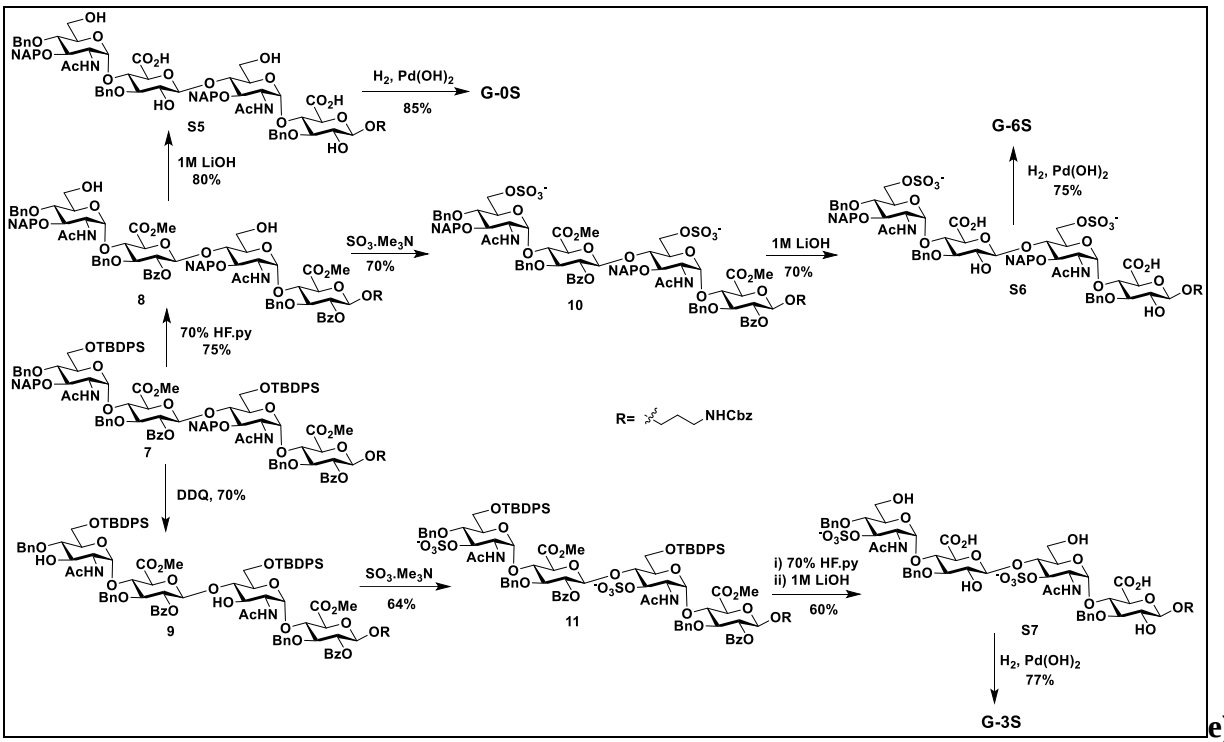
***N*-benzyloxycarbonyl-3-aminopropyl-*O*-[methyl(2-acetamido-4-*O*-benzyl-6-*O*-*tert*-butyldiphenylsilyl-2-deoxy-3-*O*-(2-naphthylmethyl)-*α*-D-glucopyranosyl)-(1→4)-*O*-(2-*O*-benzoyl-3-*O*-benzyl-*β*-D- glucopyranosyluronate)-(1→4)-*O*-(methyl(2-acetamido-6-*O*-*tert* butyldiphenylsilyl-2-deoxy-3-*O*-(2-naphthylmethyl)-*α*-D-glucopyranosyl))]-(1→4)-*O*-2-*O*-benzoyl-3-*O*-benzyl-*β*-D-glucopyranosiduronate (7)**




**S4** (0.9 g, 0.40 mmol) and zinc dust (1.07 g, 0.01 mmol). was dissolved in mixture of THF/AcOH/$Ac_2O$ (3:2:1, 12 ml) and stirred at RT for 12 h. Then solvent evaporated, and the residue was coevaporated with MeOH, Further residue was dissolved in EtOAc and washed with saturated $NaHCO_3$ and brine. Crude obtained on concentration of EtOAc layer was purified by column chromatography (EtOAc/Hexane= 1/6, v/v) to afford 79% of **7**. $^1$H NMR (400 MHz, $CDCl_3$) δ 8.02 (d, *J* = 7.6 Hz, 2H), 7.83 (d, *J* = 7.5 Hz, 2H), 7.71 – 7.65 (m, 7H), 7.61 (d, *J* = 6.7 Hz, 2H), 7.55 (t, *J* = 7.2 Hz, 2H), 7.41 (m, 11H), 7.32 (dd, *J* = 7.1, 2.7 Hz, 14H), 7.22 (dt, *J* = 5.3, 2.4 Hz, 6H), 7.17 (d, *J* = 2.8 Hz, 1H), 7.14 (dd, *J* = 5.9, 3.2 Hz, 3H), 6.39 (d, *J* = 8.0 Hz, 1H), 5.92 (m, 1H), 5.45 – 5.41 (m, 1H), 5.29 (t, *J* = 7.8 Hz, 1H), 5.05 (d, *J* = 8.2 Hz, 4H), 4.97 (d, *J* = 3.2 Hz, 2H), 4.81 (d, *J* = 7.9 Hz, 1H), 4.76 (m, 1H), 4.68 (d, *J* = 10.4 Hz, 1H), 4.61 (m, 3H), 4.54 (d, *J* = 7.0 Hz, 1H), 4.08 (t, *J* = 8.6 Hz, 4H), 4.00 (m, 1H), 3.95 (d, *J* = 9.4 Hz, 1H), 3.87 (m, 3H), 3.80 (m, 4H), 3.74 – 3.61 (m, 6H), 3.44 (s, 3H), 3.32 (d, *J* = 9.8 Hz, 1H), 3.28 (s, 3H), 3.16 – 3.09 (m, 2H), 3.06 (s, 1H), 2.95 (d, *J* = 3.6 Hz, 1H), 1.66 (d, *J* = 5.8 Hz, 2H), 1.50 (s, 3H), 1.36 (s, 3H), 1.09 (d, *J* = 3.8 Hz, 18H). $^{13}$C NMR (100 MHz, $CDCl_3$) δ 172.85, 170.97, 168.32, 167.75, 165.53, 165.26, 156.84, 139.03, 136.78, 136.33, 136.29, 136.12, 136.09, 134.30, 134.26, 134.06, 133.83, 133.47, 133.03, 130.46, 130.42, 130.24, 130.20, 130.14, 130.02, 129.64, 129.30, 129.22, 129.17, 129.10, 129.08, 129.02, 128.95, 128.90, 128.42, 128.36, 128.21, 128.14, 101.55, 100.82, 100.22, 99.30, 81.94, 81.59, 78.58, 78.52, 76.68, 75.86, 75.51, 75.37, 75.27, 74.93, 74.06, 73.51, 73.11, 71.96, 70.17, 67.77, 66.85, 62.80, 61.72, 55.19, 53.67, 53.47, 52.92,

38.36, 30.15, 29.79, 27.48, 27.40, 23.11, 22.58, 19.99, 19.83. HR-ESI-MS (*m/z*): $[M+2H]^+$, calculated for $C_{130}H_{139}N_3O_{27}Si_2$: 2231.9291; found, 2231.9293.

**Synthesis of deprotected G-tetrasaccharides**




**e)**

**General Experimental Procedures**

**General procedure A**

To a solution of TBDPS protected HS oligosaccharides (1 mmol) in pyridine (5 ml) was added 70% HF.py (5 mmol) at 0 °C and stirred at room temperature overnight. After completion, the reaction mixture was diluted with EtOAc and washed with 1 N HCl and brine. The organic layer was dried using anhydrous $Na_2SO_4$ and concentrated under reduced pressure. The residue was purified by silica column chromatography or sephadex LH-20 column depending on sulfate group in the starting material.

**General procedure B**

To a solution of NAP-protected HS oligosaccharides (1 mmol) in DCM/$H_2O$ (18:1, 10 mL) was added DDQ (5 mmol) and stirred under nitrogen atmosphere at 0 °C for 3-4 h. After the reaction completion, the mixgture was diluted with DCM and washed with brine. The organic layer was

concentrated under reduced pressure and the residue was purified by silica gel column chromatography (EtOAc/Hexane).

**General procedure C**

To a solution of 6-O or 3-O-hydroxyl group HS oligosaccharides (1 mmol) in DMF (5 mL) was added $SO_3 \cdot NMe_3$/ $SO_3 \cdot NEt_3$ (10 mmol per -OH) and stirred at 60 °C for 72 h. DMF was evaporated and the crude product was purified by column chromatography (MeOH/DCM).

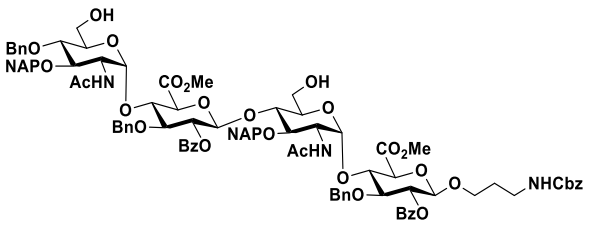
**General procedure D**

To a solution of HS oligosaccharides (1 mmol) in a mixture of THF/$H_2O$ (1:1, 4 ml) was added 1 M $LiOH \cdot H_2O$ (3 mmol) and stirred at RT for 15 h. After completion of the reaction, the reaction mixture was diluted with MeOH and neutralized using Dowex 50WX8 $H^+$ resin. The reaction was filtered and concentrated under reduced pressure and purified by bond elute C-18 column ($H_2O$/ACN).

**General procedure E**

To a solution of HS oligosaccharides (1 mmol) in $H_2O$ (4 ml) was added $Pd(OH)_2$ (10% per wt) and stirred for 24 h under hydrogen atmosphere. After reaction completion, the reaction mixture was diluted with $H_2O$, filtered and concentrated, and finally purified by bond elute C-18 column ($H_2O$/ACN).

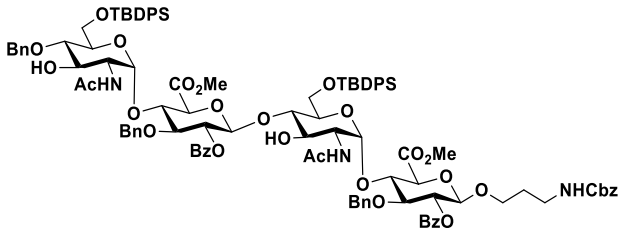
***N*-benzyloxycarbonyl-3-aminopropyl-*O*-[methyl(2-acetamido-4-*O*-benzyl-2-deoxy-3-*O*-(2-naphthylmethyl)-*α*-D-glucopyranosyl)-(1→4)-*O*-(2-*O*-benzoyl-3-*O*-benzyl-*β*-D-glucopyranosyluronate)-(1→4)-*O*-(methyl(2-acetamido-2-deoxy-3-*O*-(2-naphthylmethyl)-*α*-D-glucopyranosyl))]-(1→4)-*O*-2-*O*-benzoyl-3- O-benzyl-*β*-D- glucopyranosiduronate**




The TBDPS deprotection of compound **7** (0.22 mmol) was accomplished as described in the general procedure A yielded 75% of **8**. $^1$H NMR (400 MHz, $CDCl_3$) δ 8.04 (d, *J* = 7.5 Hz, 2H), 7.96 (d, *J* = 7.5 Hz, 2H), 7.82 (d, *J* = 8.9 Hz, 2H), 7.79 (s, 2H), 7.75 (t, *J* = 5.2 Hz, 3H), 7.70 (s, 1H), 7.60 (t, *J* = 7.4 Hz, 1H), 7.53 (d, *J* = 7.3 Hz, 1H), 7.50 – 7.44 (m, 5H), 7.44 – 7.39 (m, 5H),

7.37 (s, 1H), 7.33 (d, *J* = 3.2 Hz, 9H), 7.05 (m, 10H), 5.67 (m, 1H), 5.51 – 5.43 (m, 2H), 5.24 (t, *J* = 7.2 Hz, 1H), 5.14 – 5.07 (m, 2H), 5.06 – 4.92 (m, 6H), 4.86 (m, 1H), 4.76 (m, 1H), 4.71 – 4.66 (m, 2H), 4.57 (m, 3H), 4.42 (m, 2H), 4.27 (m, 1H), 4.19 – 4.13 (m, 2H), 4.09 (m, 1H), 4.04 (m, 1H), 3.92 (m, 1H), 3.88 – 3.81 (m, 3H), 3.79 (d, *J* = 6.5 Hz, 1H), 3.76 (s, 1H), 3.69 (m, 3H), 3.65 – 3.61 (m, 2H), 3.55 (m, 2H), 3.46 (d, *J* = 2.8 Hz, 6H), 3.29 (m, 1H), 3.18 – 3.09 (m, 2H), 2.12 (t, *J* = 6.2 Hz, 1H), 2.04 (s, 1H), 1.68 (d, *J* = 5.7 Hz, 2H), 1.42 (s, 3H), 1.40 (s, 3H). $^{13}$C NMR (100 MHz, $CDCl_3$) δ 170.25, 170.06, 168.43, 167.94, 165.02, 164.96, 156.55, 137.87, 136.73, 136.42, 136.38, 136.36, 135.71, 133.84, 133.61, 133.32, 133.22, 132.91, 132.82, 129.69, 129.65, 129.13, 128.96, 128.85, 128.61, 128.58, 128.54, 128.49, 128.27, 128.21, 128.01, 127.99, 127.93, 127.66, 127.63, 126.53, 126.36, 126.25, 126.10, 126.04, 126.01, 125.89, 125.81, 100.73, 100.69, 98.97, 98.35, 81.19, 81.14, 80.11, 77.84, 77.28, 77.25, 75.69, 75.51, 75.17, 75.04, 74.82, 74.62, 74.58, 74.19, 73.68, 73.43, 73.35, 72.23, 67.44, 66.47, 61.62, 60.04, 52.80, 52.61, 52.57, 52.08, 38.18, 29.25, 22.81, 22.68. HR-ESI-MS (*m/z*): $[M+2H]^{2+}$, calculated for $C_{98}H_{103}N_3O_{27}$, 1755.6935; found, 1755.6936.

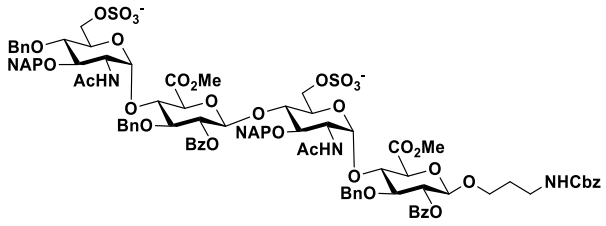
**_N_-benzyloxycarbonyl-3-aminopropyl-_O_-[methyl(2-acetamido-4-_O_-benzyl-6-_O_-_tert_-butyldiphenylsilyl-2-deoxy-_α_-D-glucopyranosyl)-(1→4)-_O_-(2-_O_-benzoyl-3-_O_-benzyl-_β_-D-glucopyranosyluronate)-(1→4)-_O_-(methyl(2-acetamido-6-_O_-_tert_-butyldiphenylsilyl-2-deoxy-3-_O_-(2-naphthylmethyl)-_α_-D-glucopyranosyl))]-(1→4)-_O_-2-_O_-benzoyl-3-_O_-benzyl-_β_-D-glucopyranosiduronate**




The NAP deprotection of compound **7** (0.22 mmol) was accomplished as described in the general procedure B, yielded 70% of **9**. $^1$H NMR (400 MHz, $CDCl_3$) δ 8.02 (d, *J* = 7.6 Hz, 2H), 7.83 (d, *J* = 7.5 Hz, 2H), 7.73 – 7.64 (m, 6H), 7.61 (d, *J* = 6.7 Hz, 2H), 7.55 (t, *J* = 7.2 Hz, 2H), 7.41 (m, 11H), 7.32 (dd, *J* = 7.1, 2.7 Hz, 14H), 7.22 (dt, *J* = 5.3, 2.4 Hz, 6H), 7.17 (d, *J* = 2.8 Hz, 1H), 7.14 (dd, *J* = 5.9, 3.2 Hz, 3H), 6.39 (d, *J* = 8.8 Hz, 1H), 5.92 (m, 1H), 5.48 – 5.38 (m, 1H), 5.29 (t, *J* = 7.8 Hz, 1H), 5.05 (d, *J* = 8.2 Hz, 4H), 4.97 (d, *J* = 3.2 Hz, 2H), 4.81 (d, *J* = 7.9 Hz, 1H), 4.76 (m, 1H), 4.68 (m, 1H), 4.61 (m, 3H), 4.54 (d, *J* = 7.0 Hz, 1H), 4.08 (t, *J* = 8.6 Hz, 4H), 4.00 (m, 1H), 3.95 (m, 1H), 3.87 (m, 3H), 3.80 (m, 4H), 3.74 – 3.61 (m, 6H), 3.44 (s, 3H), 3.32

(m, 1H), 3.28 (s, 3H), 3.16 – 3.09 (m, 2H), 3.06 (s, 1H), 2.95 (d, *J* = 3.6 Hz, 1H), 1.66 (d, *J* = 5.8 Hz, 2H), 1.50 (s, 3H), 1.36 (s, 3H), 1.09 (d, *J* = 3.8 Hz, 18H). $^{13}$C NMR (100 MHz, $CDCl_3$) δ 172.85, 170.97, 168.32, 167.75, 165.53, 165.26, 156.84, 139.03, 136.78, 136.33, 136.29, 136.12, 136.09, 134.30, 134.26, 134.06, 133.83, 133.47, 133.03, 130.46, 130.42, 130.24, 130.20, 130.14, 130.02, 129.64, 129.30, 129.22, 129.17, 129.10, 129.08, 129.02, 128.95, 128.90, 128.42, 128.36, 128.21, 128.14, 101.55, 100.82, 100.22, 99.30, 81.94, 81.59, 78.58, 78.52, 76.68, 75.86, 75.51, 75.37, 75.27, 74.93, 74.06, 73.51, 73.11, 71.96, 70.17, 67.77, 66.85, 62.80, 61.72, 55.19, 53.67, 53.47, 52.92, 38.36, 30.15, 29.79, 27.48, 27.40, 23.11, 22.58. HR-ESI-MS (*m/z*): $[M+2H]^{2+}$, calculated for $C_{108}H_{125}N_3O_{27}Si_2$, 1951.8039; found, 1951.8036.

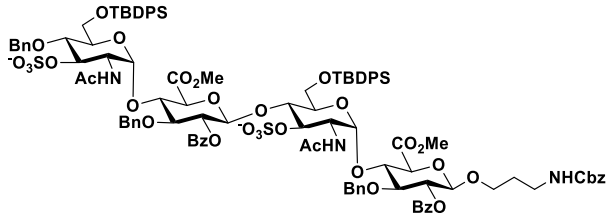
**_N_-benzyloxycarbonyl-3-aminopropyl-_O_-[methyl(2-acetamido-4-_O_-benzyl-2-deoxy-3-_O_-(2-naphthylmethyl)-6-_O_-sulfonato-_α_-D-glucopyranosyl))-(1→4)-_O_-(2-_O_-benzoyl-3-_O_-benzyl-_β_-D- glucopyranosyluronate)-(1→4)-_O_- (methyl (2-acetamido-3-_O_-(2-naphthylmethyl)-6-_O_-sulfonato-2-deoxy-_α_-D-glucopyranosyl))]-(1→4)-_O_-2-_O_-benzoyl-3-_O_-benzyl-_β_-D-glucopyranosiduronate**




The *O*-sulfation of compound **8** (0.17 mmol) was accomplished as described in the general procedure C, yielded 65% of **10**. $^1$H NMR (400 MHz, Methanol-$d_4$) δ 8.27 (d, *J* = 7.5 Hz, 2H), 7.99 (d, *J* = 7.7 Hz, 2H), 7.90 (d, *J* = 6.0 Hz, 1H), 7.83 – 7.79 (m, 4H), 7.77 (d, *J* = 6.6 Hz, 2H), 7.71 (s, 1H), 7.64 (t, *J* = 7.3 Hz, 1H), 7.56 (m, 3H), 7.48 – 7.37 (m, 8H), 7.31 (s, 7H), 7.26 (d, *J* = 7.5 Hz, 3H), 7.10 – 7.08 (m, 3H), 7.07 – 7.04 (m, 3H), 6.99 – 6.94 (m, 4H), 5.39 – 5.30 (m, 4H), 5.25 (m, 1H), 5.12 (m, 1H), 5.00 (s, 2H), 4.97 (s, 1H), 4.79 (m, 1H), 4.70 (m, 2H), 4.60 (d, *J* = 3.8 Hz, 2H), 4.50 (m, 3H), 4.39 (m, 1H), 4.34 – 4.21 (m, 5H), 4.15 (m, 1H), 4.12 – 3.97 (m, 5H), 3.78 (m, 2H), 3.70 (m, 1H), 3.67 – 3.59 (m, 5H), 3.47 (s, 4H), 3.37 (m, 1H), 3.17 (s, 3H), 3.01 (m, 2H), 1.83 (s, 3H), 1.80 (s, 3H), 1.63 – 1.56 (m, 2H). $^{13}$C NMR (100 MHz, Methanol-$d_4$) δ 172.69, 172.63, 170.29, 169.10, 165.37, 165.07, 157.31, 148.07, 138.61, 137.87, 137.31, 137.30, 137.03, 133.40, 133.25, 129.48, 129.45, 129.38, 129.34, 128.50, 128.31, 128.07, 127.84, 127.81, 127.74, 127.61, 127.55, 127.49, 127.33, 127.30, 127.19, 124.46, 100.77, 100.15, 96.93, 96.87, 82.15, 81.79, 78.08, 77.71, 76.02, 74.95, 74.82, 74.58, 74.51, 74.42, 74.39, 73.98, 73.55,

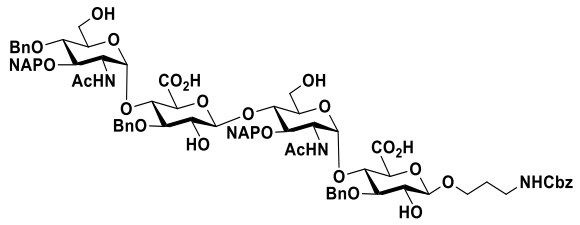
73.38, 72.66, 72.49, 67.03, 65.88, 60.34, 58.81, 53.68, 53.27, 52.67, 51.94, 37.17, 29.36, 21.66, 21.59. HR-ESI-MS (*m/z*): $[M]^+$, calculated for $C_{98}H_{101}N_3O_{33}S_2^{2-}$, 956.2902; found, 956.2906.

**_N_-benzyloxycarbonyl-3-aminopropyl-_O_-[methyl(2-acetamido-4-_O_-benzyl-6-_O_-_tert_-butyldiphenylsilyl-2-deoxy-3-_O_-sulfonato-_α_-D-glucopyranosyl)-(1→4)-_O_-(2-_O_-benzoyl-3-_O_-benzyl-_β_-D- glucopyranosyluronate)-(1→4)-_O_-(methyl(2-acetamido-6-_O_-_tert_-butyldiphenylsilyl-2-deoxy-3-_O_-sulfonato-_α_-D-glucopyranosyl))]-(1→4)-_O_-2-_O_-benzoyl-3-_O_-benzyl-_β_-D-glucopyranosiduronate**



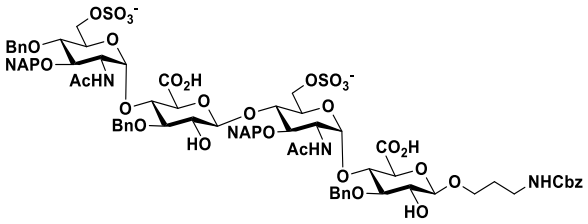

The *O*-sulfation of compound **9** (0.15 mmol) was accomplished as described in the general procedure C yielded 62% of **11**. $^1$H NMR (400 MHz, $CDCl_3$) δ 8.07 (d, *J* = 7.8 Hz, 2H), 7.89 (d, *J* = 7.5 Hz, 2H), 7.81 (d, *J* = 3.8 Hz, 2H), 7.74 (d, *J* = 6.9 Hz, 2H), 7.72 (s, 1H), 7.70 (s, 2H), 7.69 (s, 1H), 7.63 (d, *J* = 8.8 Hz, 2H), 7.57 (d, *J* = 4.1 Hz, 3H), 7.50 (s, 2H), 7.49 – 7.46 (m, 3H), 7.44 (d, *J* = 6.5 Hz, 3H), 7.40 (d, *J* = 7.6 Hz, 4H), 7.36 (d, *J* = 5.7 Hz, 5H), 7.36 – 7.27 (m, 7H), 7.23 – 7.20 (m, 2H), 7.15 (dd, *J* = 5.9, 2.4 Hz, 7H), 5.69 – 5.66 (m, 1H), 5.55 (d, *J* = 3.3 Hz, 1H), 5.43 (m, 2H), 5.18 (m, 1H), 5.04 (s, 2H), 4.98 – 4.92 (m, 1H), 4.83 (m, 1H), 4.78 (d, *J* = 7.4 Hz, 1H), 4.71 (d, *J* = 10.7 Hz, 1H), 4.64 (m, 2H), 4.57 (M, 1H), 4.54 – 4.48 (m, 1H), 4.18 (t, *J* = 9.1 Hz, 2H), 4.12 (m, 4H), 4.08 (s, 1H), 4.01 (m, 3H), 3.94 (m, 1H), 3.92 – 3.87 (m, 2H), 3.81 (m, 2H), 3.68 (s, 3H), 3.63 (s, 1H), 3.52 (m, 2H), 3.27 (m, 1H), 3.19 (s, 3H), 3.05 (q, *J* = 6.2 Hz, 2H), 1.94 (d, *J* = 3.7 Hz, 6H), 1.67 – 1.62 (m, 2H), 1.13 (s, 9H), 1.11 (s, 9H). $^{13}$C NMR (100 MHz, $CDCl_3$) δ 176.59, 176.41, 173.94, 173.92, 169.43, 168.89, 161.23, 142.85, 141.32, 141.27, 140.94, 139.67, 139.53, 139.31, 137.49, 137.25, 137.11, 136.65, 136.26, 134.13, 133.84, 133.52, 133.41, 133.34, 133.29, 132.93, 132.88, 132.44, 132.29, 132.00, 131.98, 131.84, 131.79, 131.68, 131.59, 131.52, 131.47, 131.43, 131.34, 131.25, 130.96, 104.61, 103.84, 100.75, 100.66, 86.23, 85.79, 81.15, 79.96, 78.66, 78.42, 78.35, 78.25, 77.91, 77.68, 77.62, 77.47, 76.92, 76.61, 76.15, 73.48, 70.94, 69.81, 68.95, 65.91, 64.71, 58.26, 57.20, 56.69, 55.68, 41.07, 36.56, 34.35, 33.28, 30.14, 29.98, 25.63, 25.61. HR-ESI-MS (*m/z*): [M], calculated for $C_{108}H_{121}N_3O_{33}S_2Si_2^{2-}$, 1054.3453; found, 1054.3454.

***N*-benzyloxycarbonyl-3-aminopropyl-*O*-[(2-acetamido-4-*O*-benzyl-2-deoxy-3-*O*-(2-naphthylmethyl)-*α*-D-glucopyranosyl)-(1→4)-*O*-(3-*O*-benzyl-*β*-D- glucopyranosyl)-(1→4)-*O*-(2-acetamido-3-*O*-(2-naphthylmethyl)-*α*-D-glucopyranosyl)]-(1→4)-*O*-3-*O*-benzyl-*β*-D-glucopyranosiduronate**



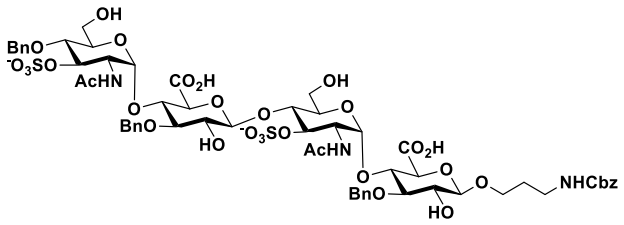

The saponification of compound **8** (0.03 mmol) was accomplished as described in the general procedure D, yielded 80% of **S5**. $^{1}$H NMR (400 MHz, Methanol-$d_4$) δ 8.01 (d, $J$ = 7.4 Hz, 1H), 7.85 (d, $J$ = 8.3 Hz, 1H), 7.80 (s, 2H), 7.77 (d, $J$ = 9.3 Hz, 3H), 7.67 (s, 1H), 7.47 – 7.41 (m, 5H), 7.37 – 7.31 (m, 5H), 7.30 – 7.21 (m, 16H), 5.48 – 5.41 (m, 2H), 5.19 (m, 1H), 5.09 (s, 1H), 5.03 (m, 3H), 4.92 (m, 1H), 4.77 (m, 4H), 4.56 (m, 3H), 4.29 (d, $J$ = 7.7 Hz, 1H), 4.21 (m, 2H), 4.04 – 3.83 (m, 12H), 3.75 (m, 2H), 3.65 (d, $J$ = 8.9 Hz, 1H), 3.62 – 3.53 (m, 2H), 3.47 (t, $J$ = 8.4 Hz, 1H), 3.41 (s, 1H), 3.27 – 3.18 (m, 2H), 1.81 (s, 3H), 1.75 (m, 5H). $^{13}$C NMR (151 MHz, Methanol-$d_4$) δ 171.71, 171.57, 157.56, 138.36, 138.31, 138.23, 137.01, 136.18, 133.43, 133.36, 133.00, 132.93, 128.07, 128.00, 127.96, 127.95, 127.67, 127.62, 127.60, 127.58, 127.51, 127.40, 127.34, 127.29, 127.27, 127.24, 127.22, 125.73, 125.69, 125.56, 125.50, 125.37, 125.31, 103.06, 97.34, 96.93, 84.96, 84.72, 80.76, 78.77, 77.36, 76.73, 75.41, 74.99, 74.64, 74.49, 74.15, 73.71, 71.54, 71.30, 66.83, 65.99, 61.21, 60.32, 53.05, 52.62, 37.36, 29.47, 21.69, 21.66. HR-ESI-MS (*m/z*): [M], calculated for $C_{82}H_{91}N_3O_{25}$, 1517.5942; found, 1516.5845.

***N*-benzyloxycarbonyl-3-aminopropyl-*O*-[(2-acetamido-4-*O*-benzyl-2-deoxy-3-*O*-(2-naphthylmethyl)- 6-*O*-sulfonato-*α*-D-glucopyranosyl)-(1→4)-*O*-(3-*O*-benzyl-*β*-D-glucopyranosyluronate)-4-*O*-(2-acetamido-2-deoxy-3-*O*-(2-naphthylmethyl)-6-*O*-sulfonato-*α*-D-glucopyranosyl)-(1→4)-*O*-3-*O*-benzyl-*β*-D-glucopyranosiduronate**



The saponification of compound **10** (0.04 mmol) was accomplished as described in the general procedure D, yielded 70% of **S6**. $^{1}$H NMR (400 MHz, $CDCl_3$) δ 7.78 (d, *J* = 7.8 Hz, 1H), 7.73 – 7.66 (m, 6H), 7.61 (s, 1H), 7.39 (d, *J* = 8.5 Hz, 1H), 7.36 – 7.27 (m, 5H), 7.23 (d, *J* = 6.1 Hz, 7H), 7.17 (d, *J* = 6.8 Hz, 7H), 7.15 – 7.09 (m, 6H), 5.34 (m, 2H), 5.15 (s, 1H), 5.04 (m, 1H), 4.96 (s, 2H), 4.92 (d, *J* = 10.5 Hz, 1H), 4.86 (s, 1H), 4.75 – 4.61 (m, 5H), 4.48 (m, 3H), 4.32 – 4.26 (m, 1H), 4.24 – 4.19 (m, 2H), 4.18 – 4.09 (m, 2H), 4.06 – 4.01 (m, 2H), 3.98 (m, 2H), 3.90 (d, *J* = 9.0 Hz, 1H), 3.82 (m, 5H), 3.73 (d, *J* = 9.4 Hz, 1H), 3.66 (m, 1H), 3.58 (m, 2H), 3.52 (m, 1H), 3.47 (s, 1H), 3.39 (m, 1H), 3.15 (m, 2H), 1.71 (s, 3H), 1.68 (s, 5H). $^{13}$C NMR (100 MHz, $CDCl_3$) δ 178.81, 178.67, 175.72, 175.45, 161.55, 142.55, 142.42, 142.21, 141.01, 140.96, 140.27, 137.37 (d, *J* = 5.6 Hz), 136.95, 136.87, 132.12, 132.02, 131.89, 131.75, 131.65, 131.51, 131.48, 131.36, 131.28, 131.23, 131.14, 131.06, 129.91, 129.79, 129.64, 129.54, 129.43, 129.39, 129.28, 129.17, 107.02, 106.15, 101.42, 100.69, 88.88, 88.45, 84.84, 81.97, 81.24, 80.75, 79.16, 78.86, 78.59, 78.42, 77.77, 77.65, 77.40, 73.87, 73.68, 70.73, 69.96, 56.99, 56.32, 41.27, 33.45, 25.61, 25.53. HR-ESI-MS (*m/z*): [M], calculated for $C_{82}H_{89}N_3O_{31}S_2^{2-}$, 837.7466; found, 837.7468.

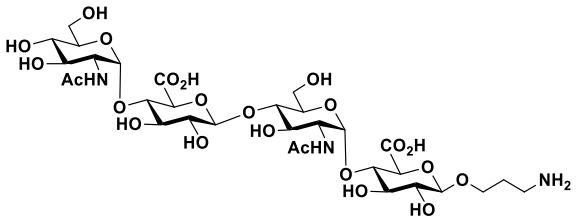
**_N_-benzyloxycarbonyl-3-aminopropyl-_O_-[(2-acetamido-4-_O_-benzyl-2-deoxy-3-_O_-sulfonato-_α_-D-glucopyranosyl)-(1→4)-_O_-(3-_O_-benzyl-_β_-D-glucopyranosyluronate)-(1→4)-_O_-(2-acetamido-3-2-deoxy- _O_-sulfonato-_α_-D-glucopyranosyl)-(1→4)-_O_-3-_O_-benzyl-_β_-D-glucopyranosiduronate (S7)**




The saponification and hydrogenolysis of compound **11** (0.49 mmol) was accomplished as described in the general procedure D and E, yielded 60% of **S7**. $^{1}$H NMR (400 MHz, Methanol-$d_4$) δ 7.40 (d, *J* = 7.4 Hz, 2H), 7.34 (d, *J* = 7.7 Hz, 2H), 7.32 – 7.30 (m, 4H), 7.28 (d, *J* = 7.9 Hz, 7H), 7.25 (s, 2H), 7.23 (d, *J* = 2.8 Hz, 1H), 7.20 (s, 2H), 5.45 – 5.40 (m, 2H), 5.11 (m, 1H), 5.03 (s, 2H), 4.99 – 4.94 (m, 2H), 4.72 (s, 1H), 4.70 – 4.65 (m, 2H), 4.60 (m, 2H), 4.49 (m, 1H), 4.35 (d, 1H), 4.31 – 4.24 (m, 1H), 4.06 (m, 2H), 4.00 (s, 1H), 3.90 (m, 6H), 3.80 (m, 2H), 3.73 (m, 2H), 3.60 (d, *J* = 1.8 Hz, 1H), 3.55 (s, 2H), 3.46 (m, 2H), 3.21 (d, *J* = 6.6 Hz, 2H), 1.94 – 1.90 (m, 3H), 1.86 (s, 3H), 1.74 (m, 2H). $^{13}$C NMR (100 MHz, Methanol-$d_4$) δ 174.74 (d, *J* = 4.9 Hz),

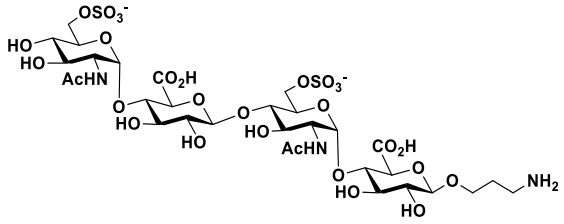
173.57 – 170.53 (m), 157.65, 138.57, 137.07, 128.78, 128.14, 127.96, 127.92, 127.77, 127.63, 127.47, 127.29, 127.13, 102.99, 102.83, 97.17, 97.09, 84.89, 83.94, 78.17, 77.05, 74.72, 74.55, 74.10, 71.78, 71.48, 66.71, 66.06, 53.81, 53.14, 53.00, 37.39, 29.52, 21.86. HR-ESI-MS (*m/z*): [M], calculated for $C_{60}H_{73}N_3O_{31}S_2^{2-}$, 697.6848; found, 697.6842.

**3-aminopropyl-*O*-[(2-acetamido-2-deoxy-*α*-D-glucopyranosyl)-(1→4)-*O*-(*β*-D-glucopyranosyluronate)-(1→4)-*O*-(2-acetamido-2-deoxy-*α*-D-glucopyranosyl)]-(1→4)-*O*-*β*-D-glucopyranosiduronate (G-0S)**



The hydrogenation of compound **S5** (0.017 mmol) was accomplished as described in the general procedure E, yielded 85% of **G-0S**. $^1$H NMR (400 MHz, $D_2O$) δ 5.29 (dd, *J* = 5.4, 3.8 Hz, 2H), 4.46 (m, 2H), 3.95 (m, 3H), 3.82 (m, 3H), 3.77 – 3.59 (m, 13H), 3.56 – 3.51 (m, 1H), 3.45 (d, *J* = 9.2 Hz, 1H), 3.32 – 3.23 (m, 2H), 3.06 (t, *J* = 6.9 Hz, 2H), 1.96 (d, *J* = 3.6 Hz, 5H), 1.91 (s, 2H). $^{13}$C NMR (100 MHz, $D_2O$) δ 176.90, 176.86, 104.72, 103.73, 100.24, 99.92, 82.14, 79.49, 79.31, 79.14, 78.63, 78.37, 75.86, 75.81, 75.66, 74.50, 74.02, 70.61, 70.47, 62.35, 61.89, 55.22, 54.73, 40.08, 29.21, 24.68, 24.61. HR-ESI-MS (*m/z*): $[M-H]^+$, calculated for $C_{31}H_{51}N_3O_{23}$, 833.2913; found, 833.2901.

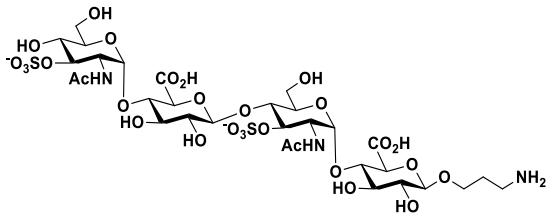
**3-aminopropyl-*O*-[(2-acetamido-2-deoxy-6-*O*-sulfonato-*α*-D-glucopyranosyl)-(1→4)-*O*-(*β*-D-glucopyranosyluronate)-(1→4)-*O*-(2-acetamido-2-deoxy-6-*O*-sulfonato-*α*-D-glucopyranosyl)]-(1→4)-*O*-*β*-D-glucopyranosiduronate (G-6S)**



The hydrogenation of compound **S6** (0.017 mmol) was accomplished as described in the general procedure E, yielded 75% of **G-6S**. $^1$H NMR (400 MHz, $D_2O$) δ 5.28 (t, *J* = 3.2 Hz, 2H), 4.55 (d, *J* = 7.9 Hz, 1H), 4.44 (d, *J* = 8.0 Hz, 1H), 4.35 (s, 1H), 4.24 (m, 1H), 4.11 (m, 2H), 3.98 (d, *J* =

9.5 Hz, 1H), 3.91 (d, *J* = 9.3 Hz, 1H), 3.87 (d, *J* = 5.5 Hz, 1H), 3.85 (d, *J* = 5.4 Hz, 2H), 3.76 (d, *J* = 9.7 Hz, 3H), 3.71 (m, 3H), 3.66 (d, *J* = 5.2 Hz, 2H), 3.62 (d, *J* = 9.6 Hz, 2H), 3.49 (m, 1H), 3.28 (q, *J* = 8.4 Hz, 2H), 3.07 (t, *J* = 6.8 Hz, 2H), 1.97 (s, 3H), 1.96 (s, 3H), 1.94 – 1.90 (m, 2H). $^{13}$C NMR (100 MHz, $D_2O$) δ 174.34, 173.02, 102.22, 101.92, 97.67, 97.33, 77.44, 76.74, 76.65, 76.03, 75.80, 74.99, 74.58, 73.26, 73.17, 70.40, 70.36, 69.05, 69.03, 68.79, 67.99, 66.34, 65.71, 53.41, 53.12, 37.56, 26.66, 21.92. HR-ESI-MS (*m/z*): [M], calculated for $C_{31}H_{49}N_3O_{29}S^{2-}$, 495.5952; found, 495.5948.

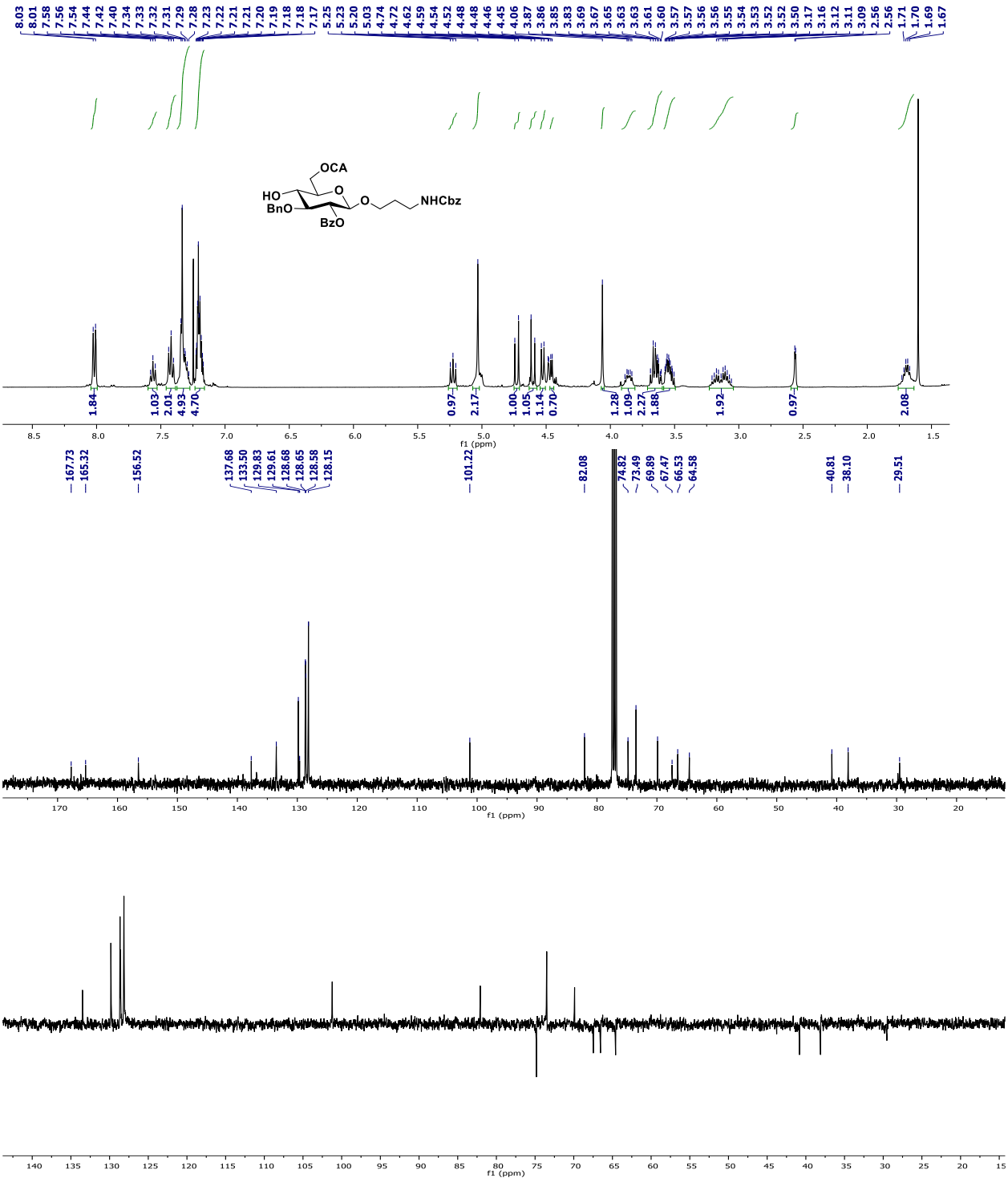
**3-aminopropyl-*O*-(2-acetamido-2-deoxy-3-*O*-sulfonato-*α*-D-glucopyranosyl)-(1→4)-*O*-(*β*-D-glucopyranosyluronate)-(1→4)-*O*-(2-acetamido-2-deoxy-3-*O*-sulfonato-*α*-D-glucopyranosyl)]-(1→4)-*O*-*β*-D-glucopyranosiduronate (G-3S)**



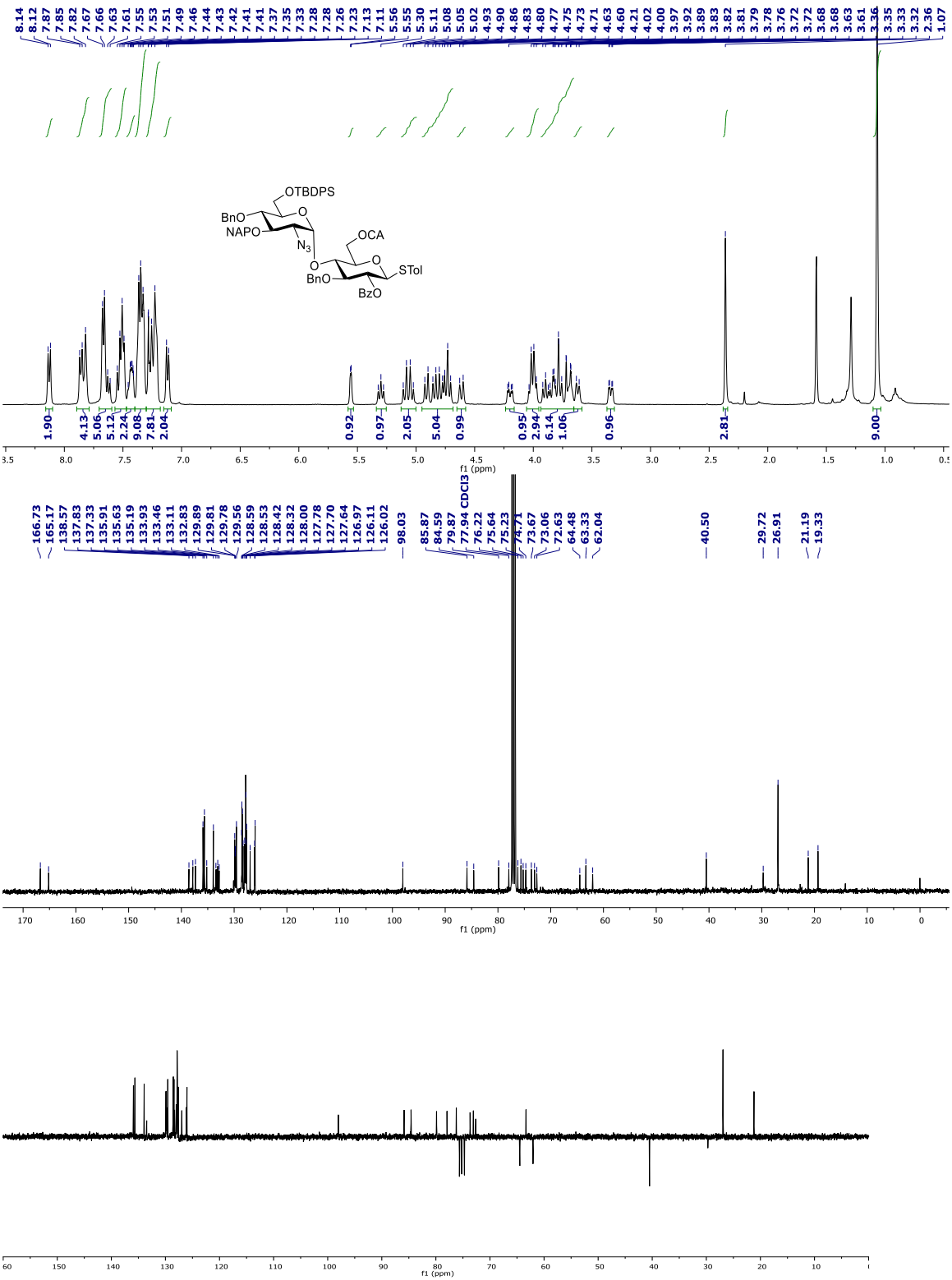

The hydrogenation of compound **S7** (0.023 mmol) was accomplished as described in the general procedure E, yielded 77% of **G-3S**. $^1$H NMR (400 MHz, $D_2O$) δ 5.39 (t, J = 4.1 Hz, 2H), 4.62 (d, J = 7.8 Hz, 1H), 4.56 (d, J = 9.7 Hz, 1H), 4.51 (m, 1H), 4.48 – 4.42 (m, 1H), 4.09 (m, 2H), 4.03 – 3.95 (m, 3H), 3.93 (d, J = 2.6 Hz, 1H), 3.89 – 3.80 (m, 7H), 3.75 (q, J = 7.6, 6.4 Hz, 4H), 3.69 (d, J = 8.9 Hz, 1H), 3.42 (t, J = 8.5 Hz, 1H), 3.33 (s, 1H), 3.16 (t, J = 6.6 Hz, 2H), 2.03 (s, 3H), 2.02 (s, 3H), 1.99 (d, J = 6.2 Hz, 2H). $^{13}$C NMR (100 MHz, $D_2O$) δ 176.90, 176.86, 104.72, 103.73, 100.24, 99.92, 82.14, 79.49, 79.31, 79.14, 78.63, 78.37, 75.86, 75.81, 75.66, 74.50, 74.02, 70.61, 70.47, 62.35, 61.89, 55.22, 54.73, 40.08, 29.21, 24.68, 24.61. HR-ESI-MS (*m/z*): [M], calculated for $C_{31}H_{49}N_3O_{29}S_2^{2-}$, 495.5952; found, 495.5959.

## 2.6 $^{1}H$, $^{13}C$, and DEPT NMR

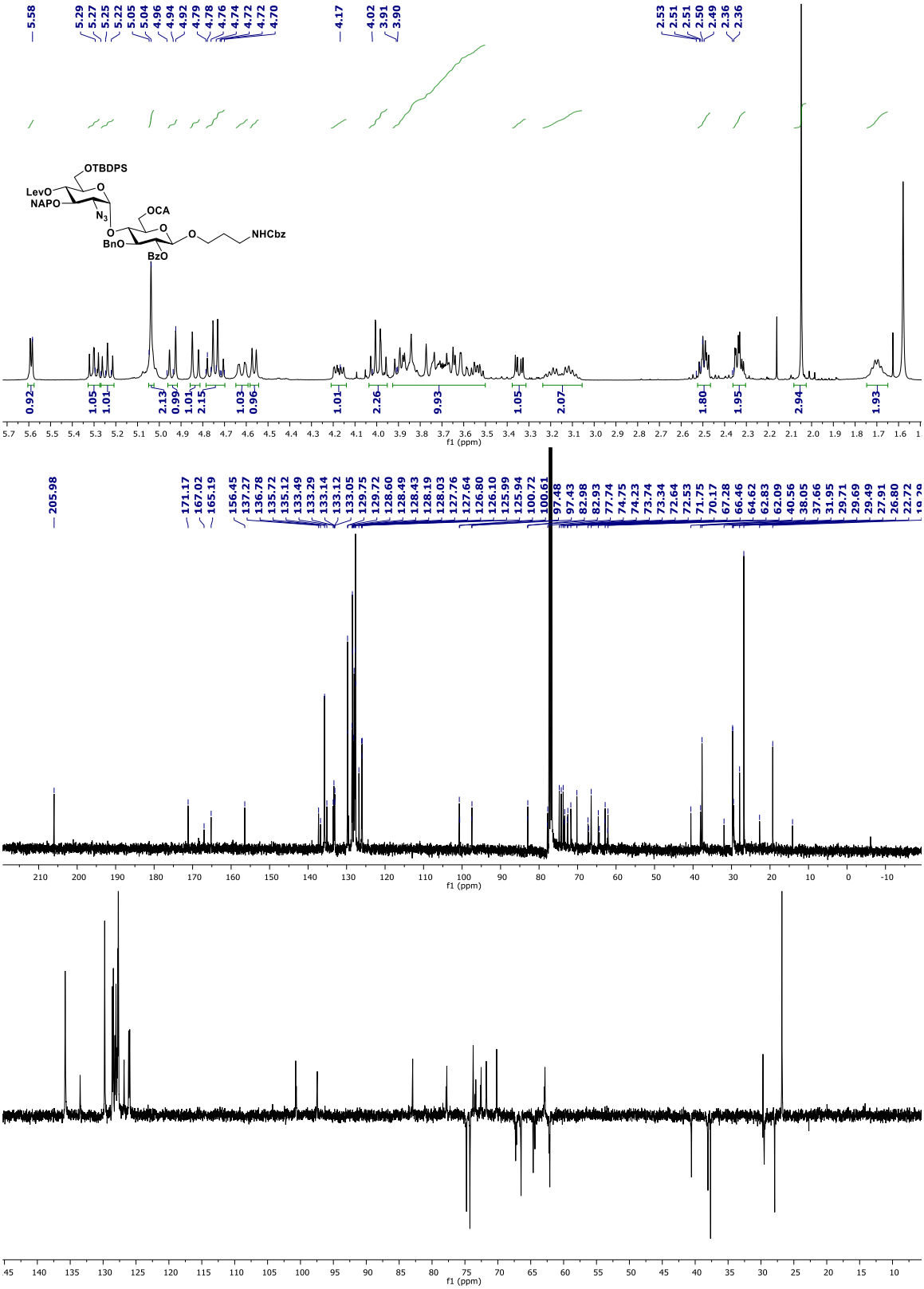
### $^{1}H$, $^{13}C$, and DEPT NMR spectrum of compound 4



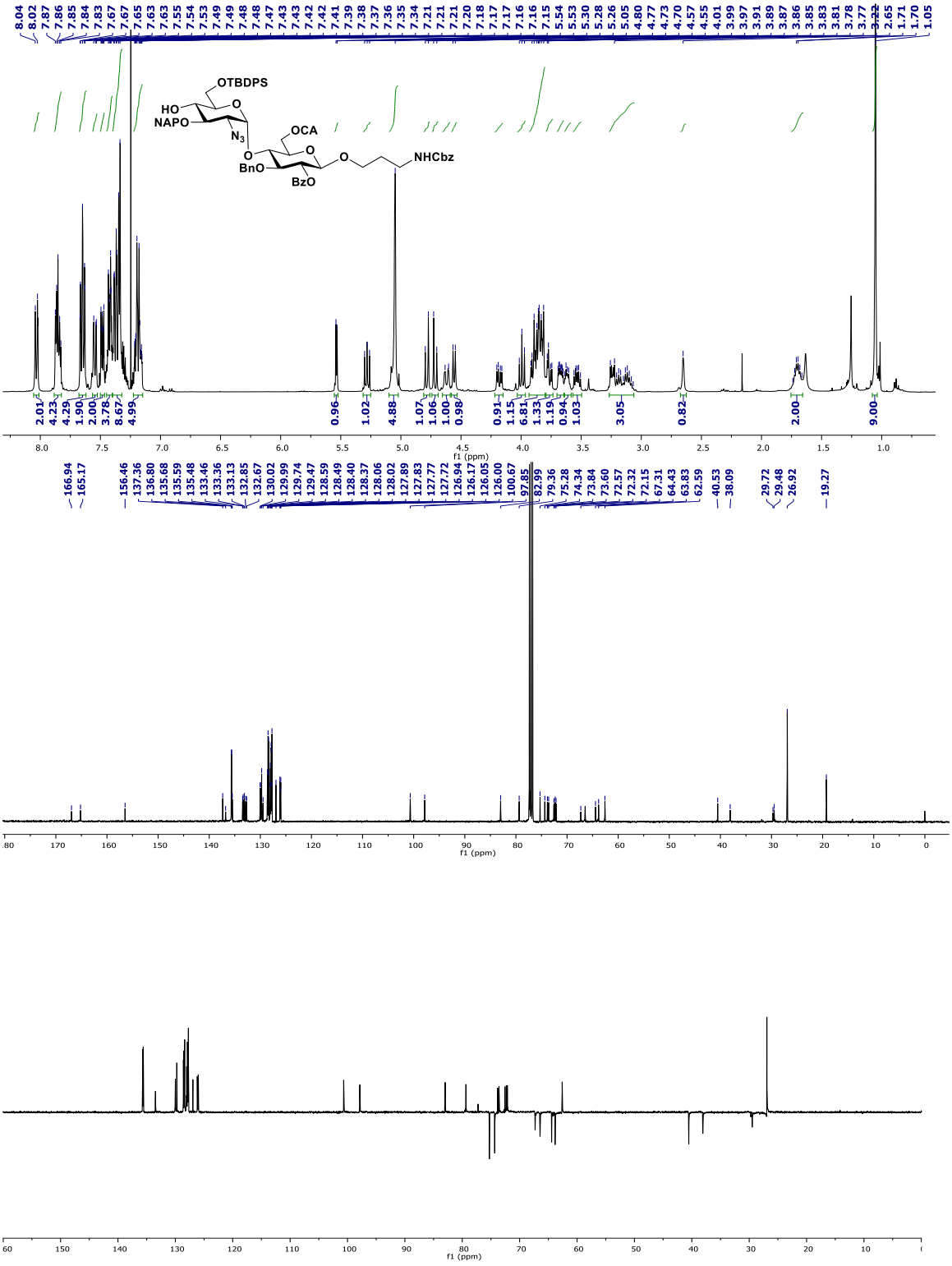
## $^{1}H$, $^{13}C$, and DEPT NMR spectrum of compound 5



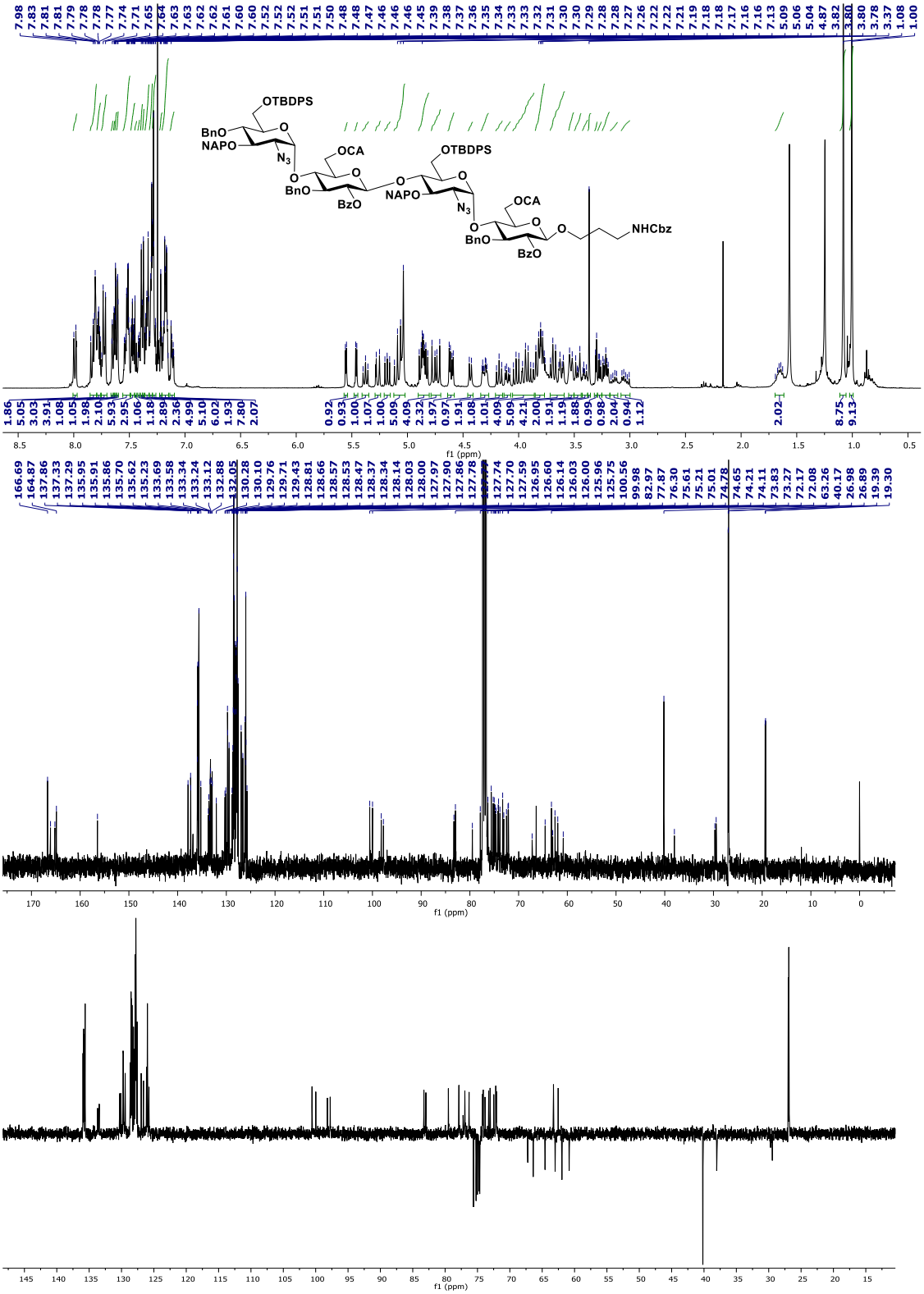
## $^{1}H$, $^{13}C$, and DEPT NMR spectrum of compound S1



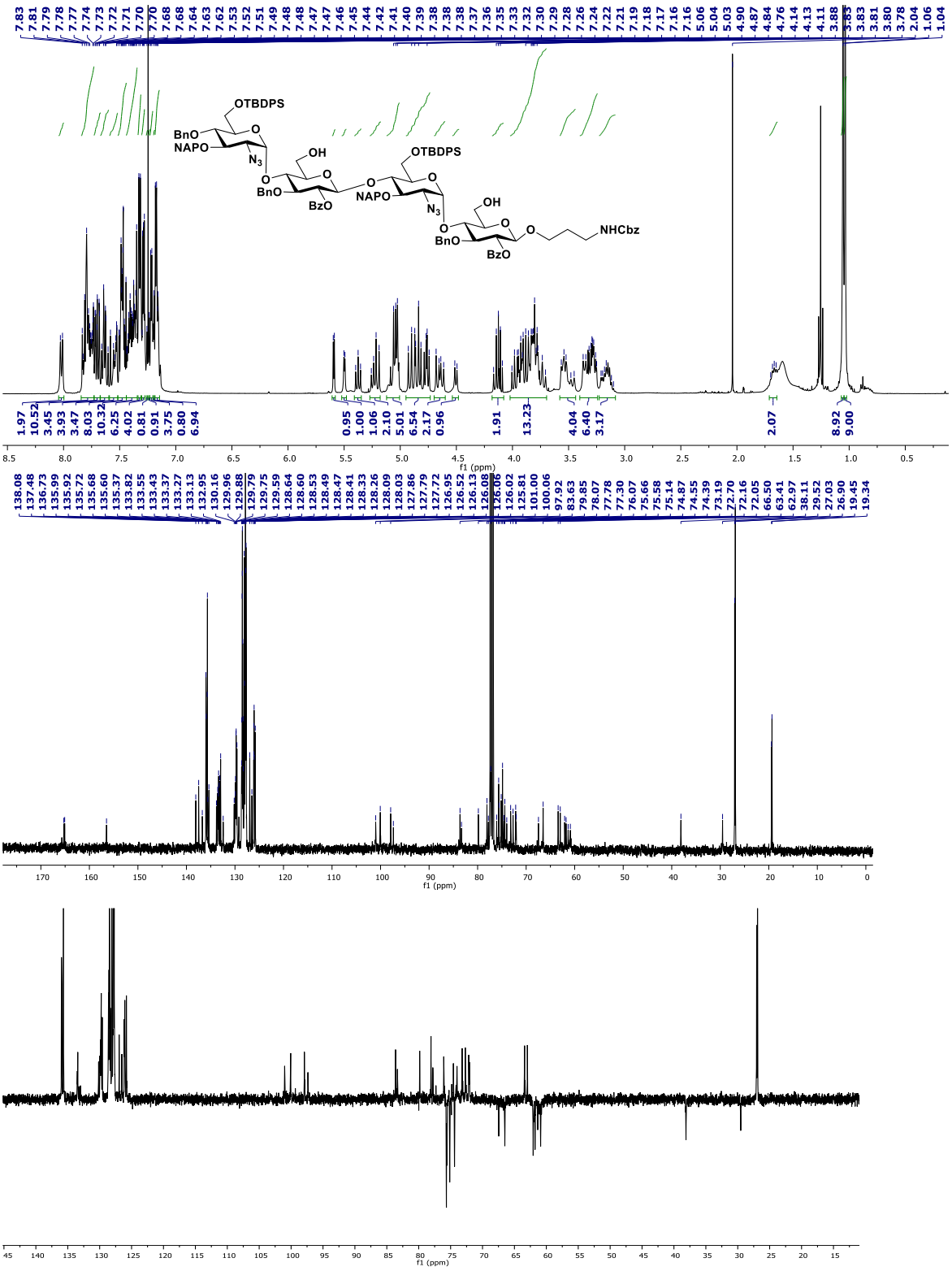
## $^{1}H$, $^{13}C$, and DEPT NMR spectrum of compound 6



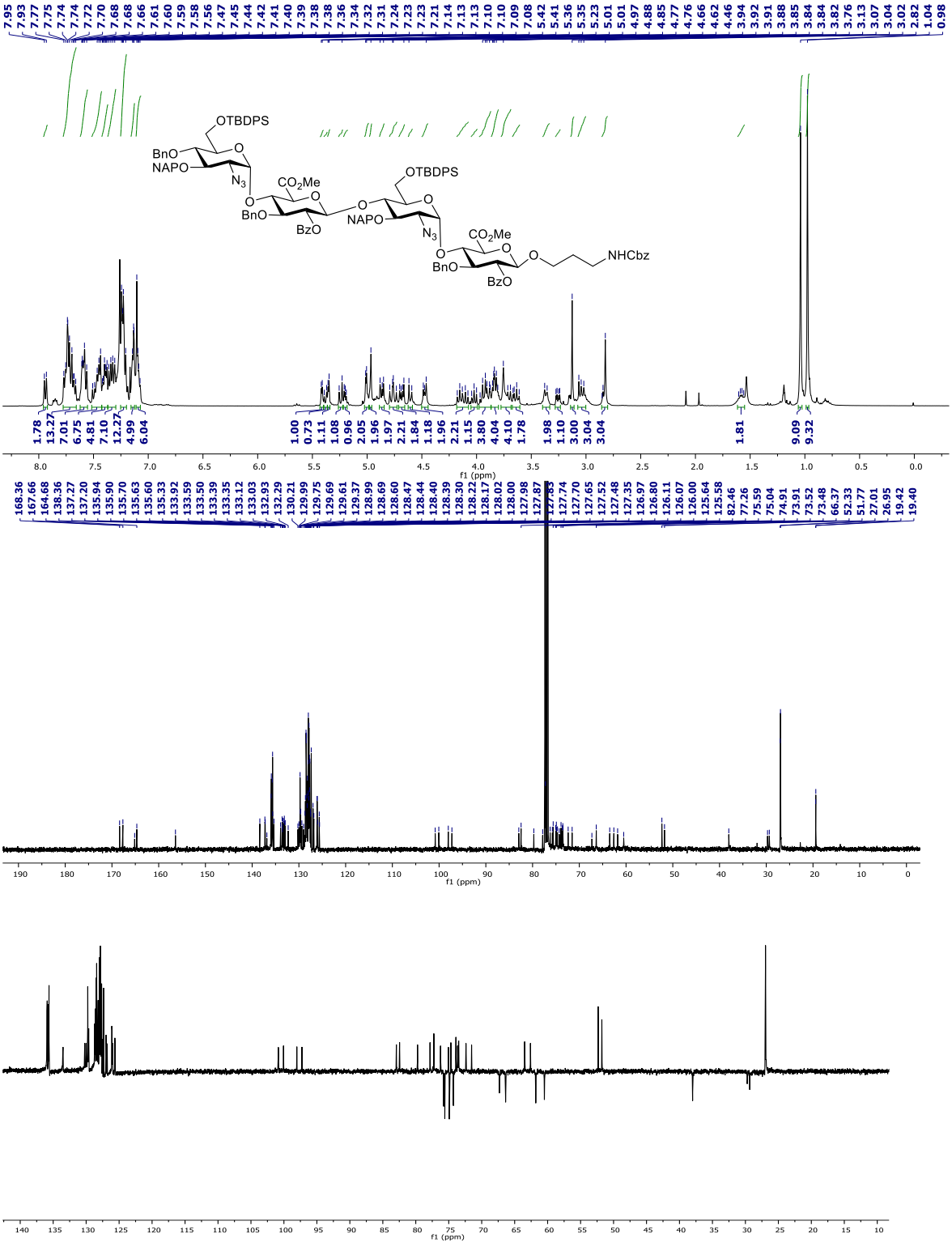
## $^{1}H$, $^{13}C$, and DEPT NMR spectrum of compound S2



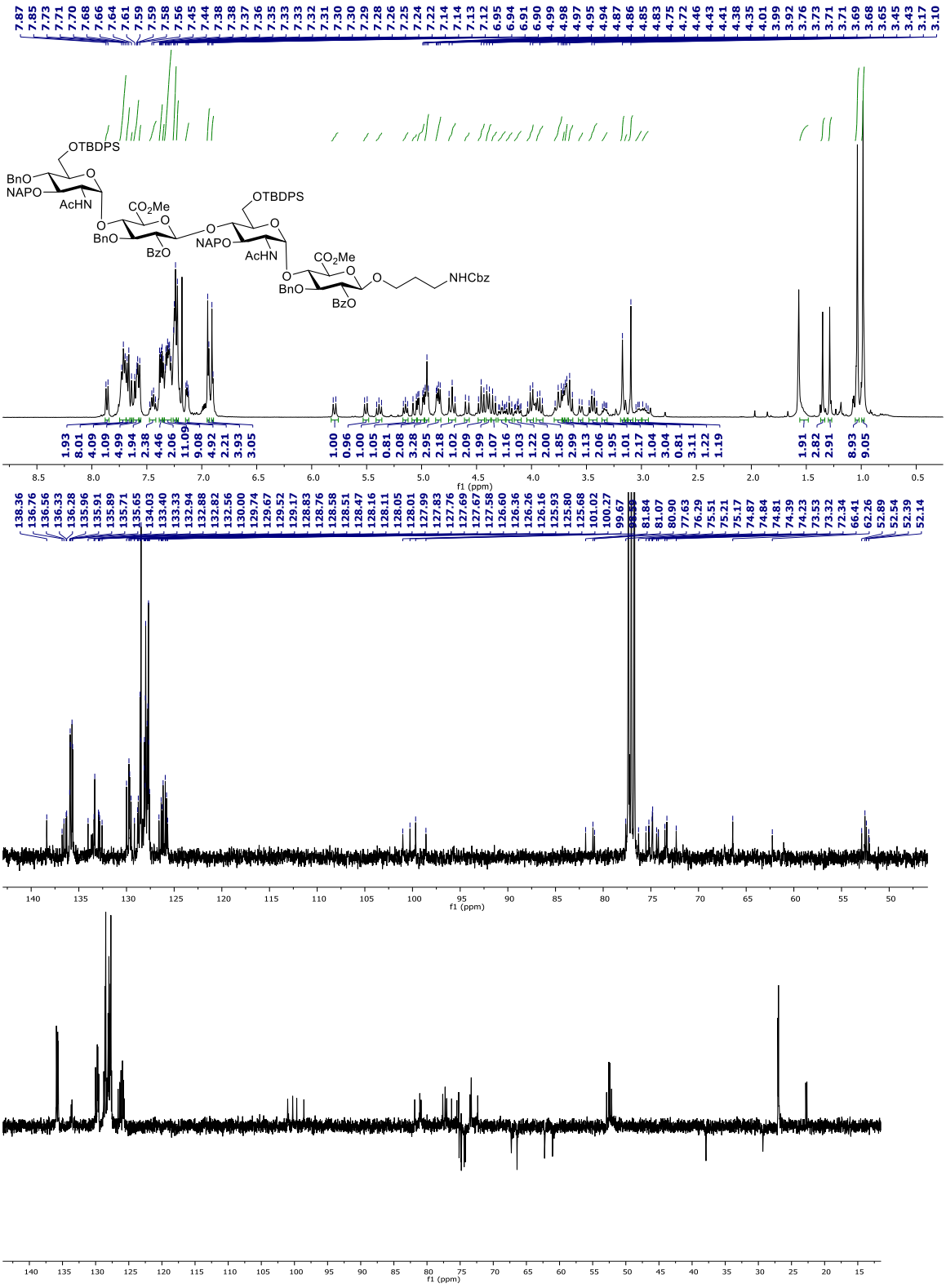
## $^{1}H$, $^{13}C$, and DEPT NMR spectrum of compound S3



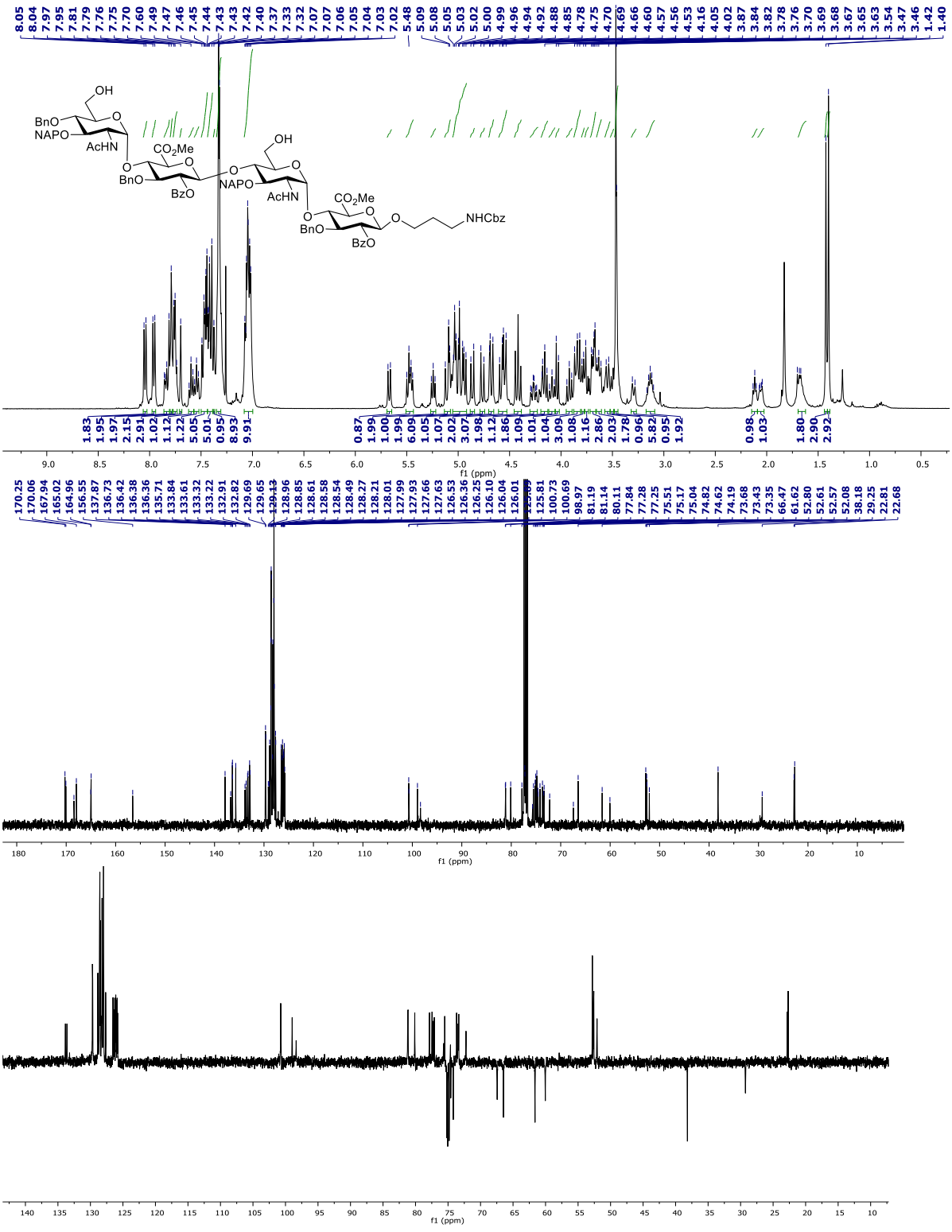
## $^{1}H$, $^{13}C$, and DEPT NMR spectrum of compound S4



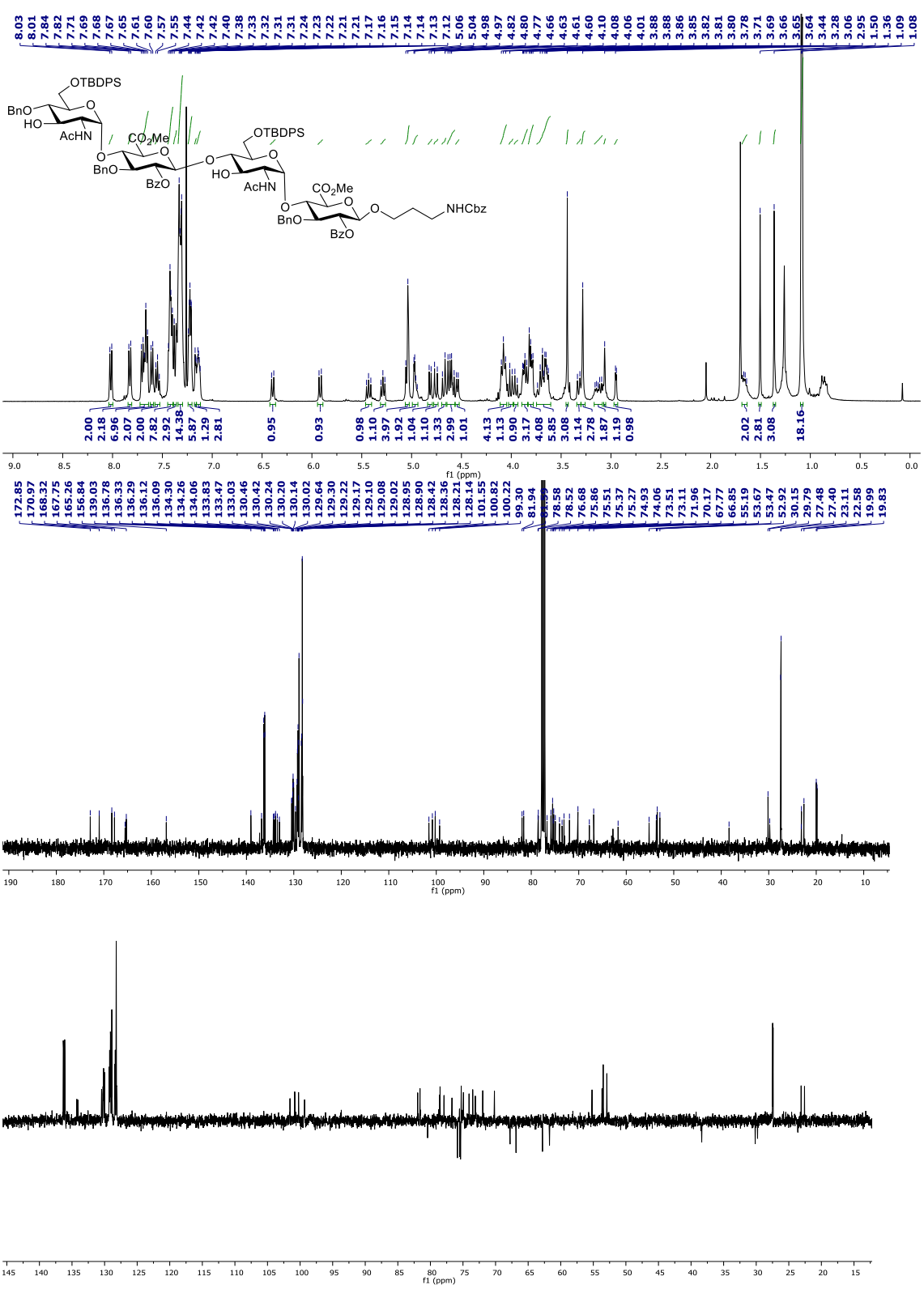
## $^{1}H$, $^{13}C$, and DEPT NMR spectrum of compound 7



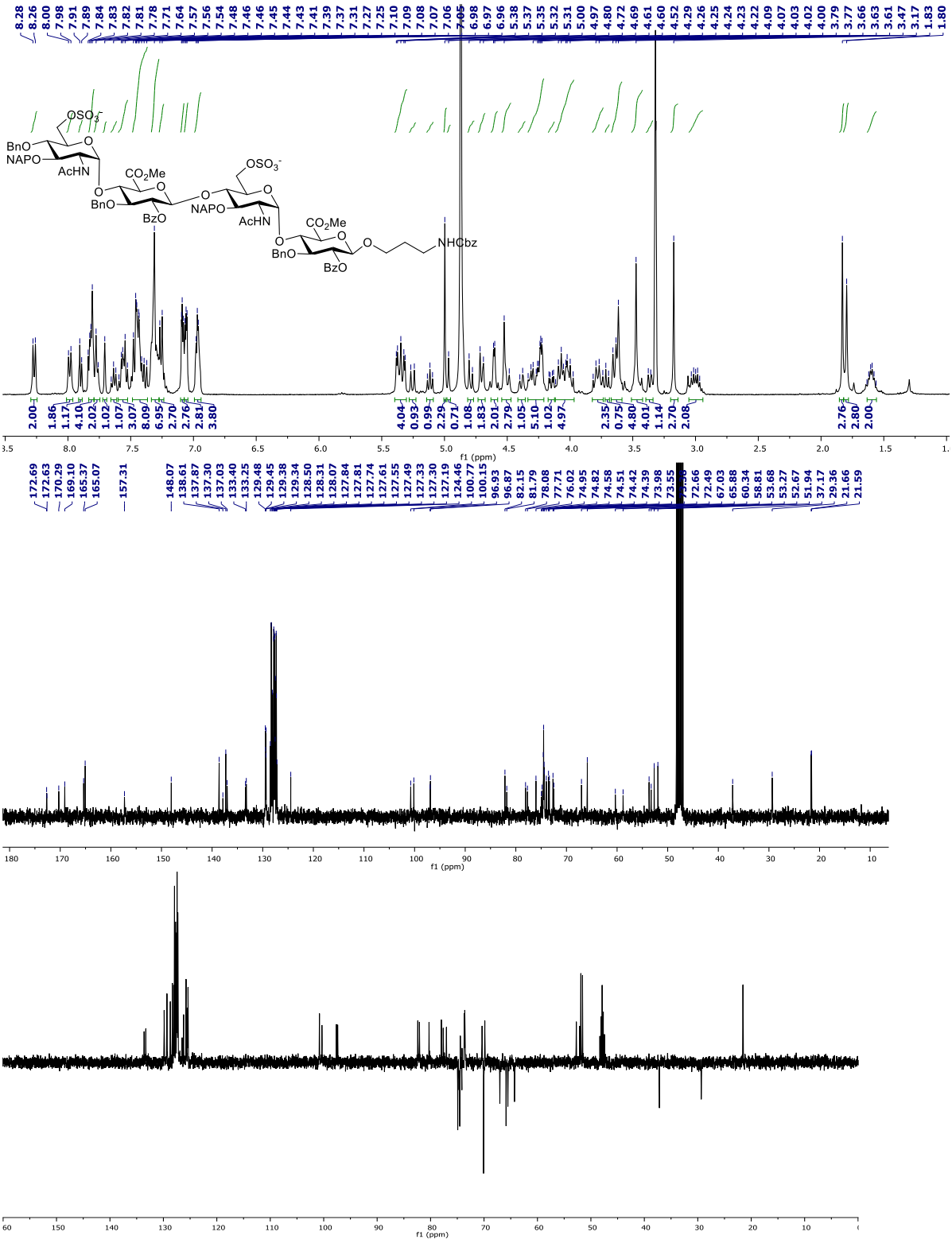
## $^{1}H$, $^{13}C$, and DEPT NMR spectrum of compound 8



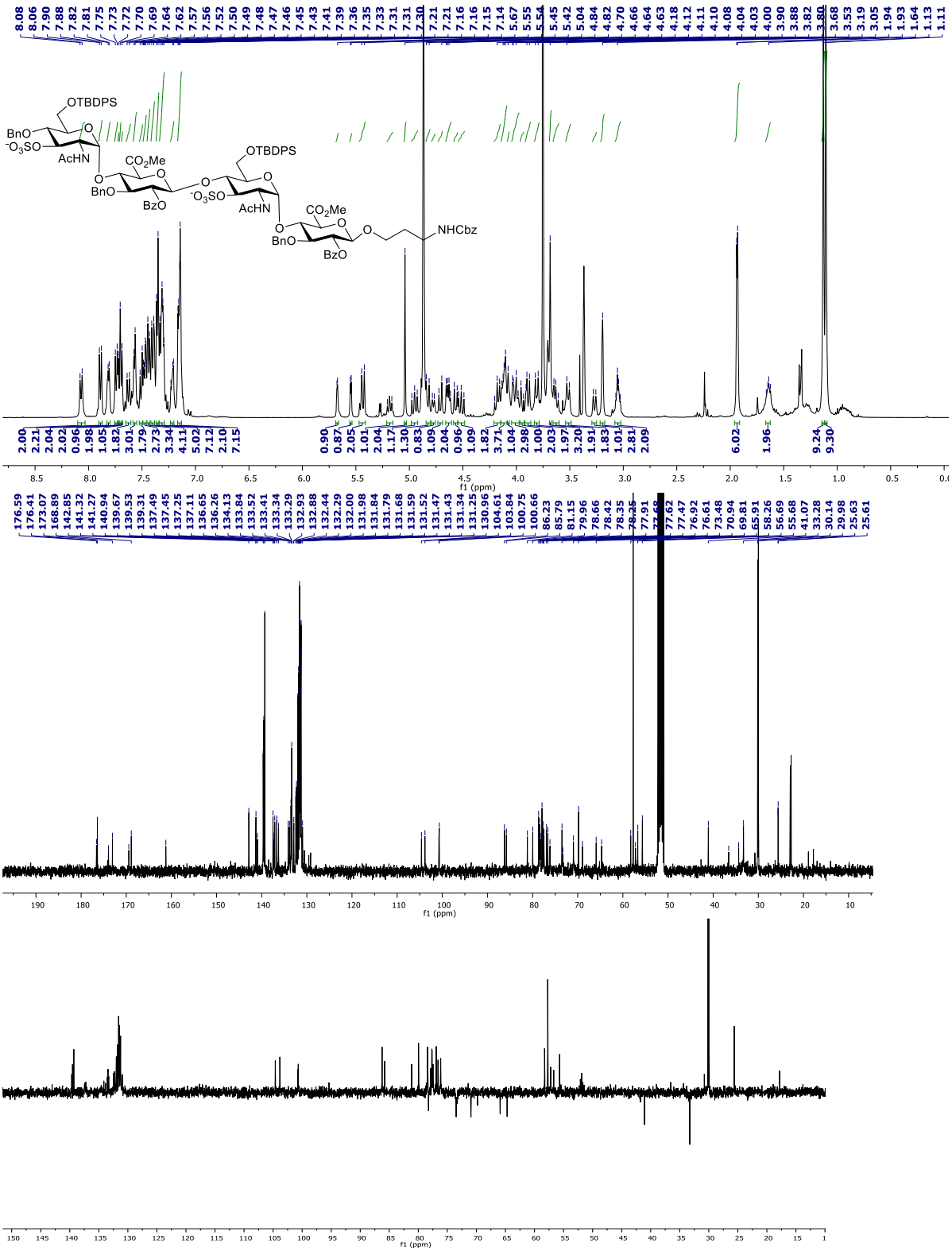
## $^{1}H$, $^{13}C$, and DEPT NMR spectrum of compound 9



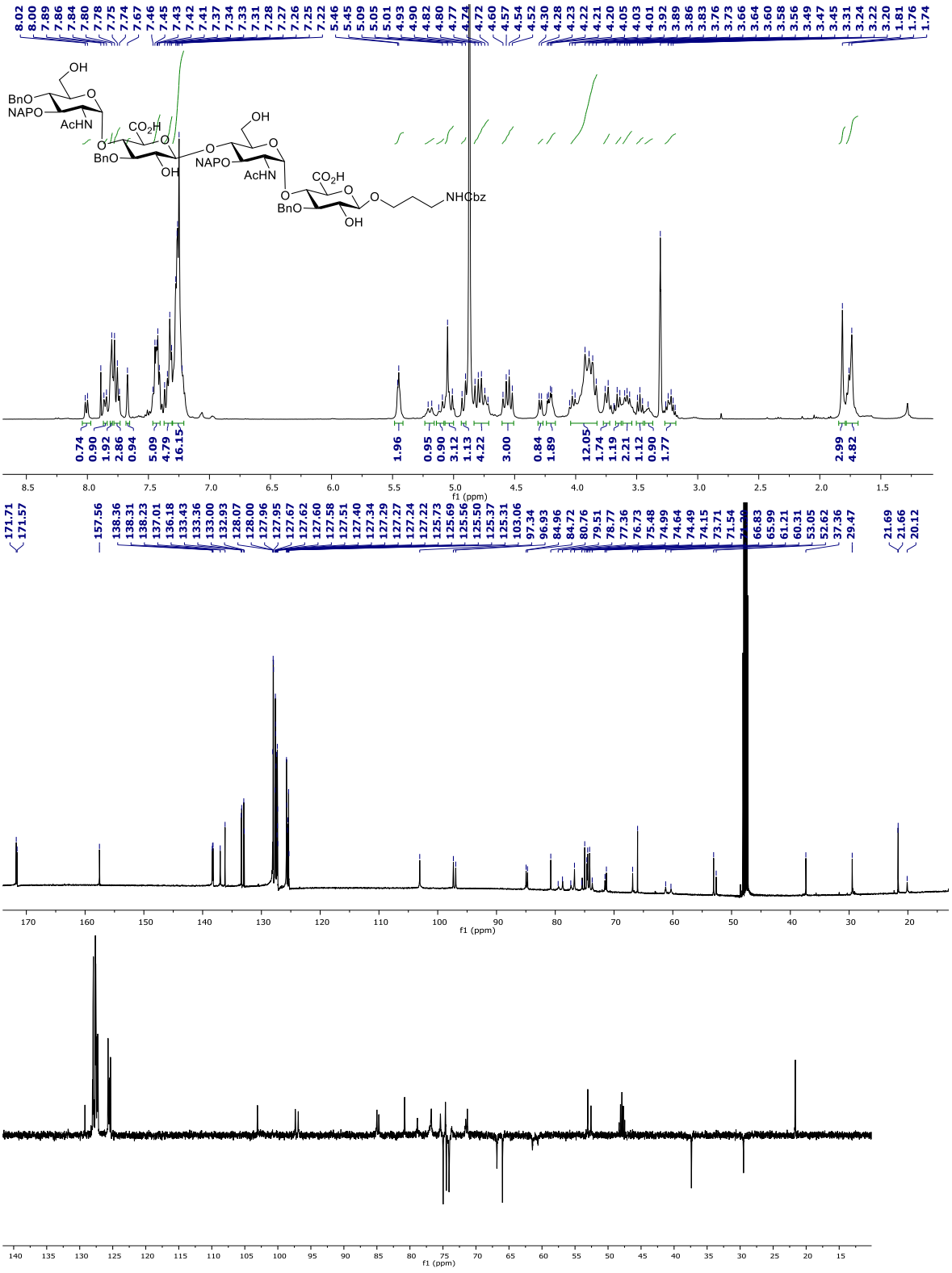
## $^{1}H$, $^{13}C$, and DEPT NMR spectrum of compound 10



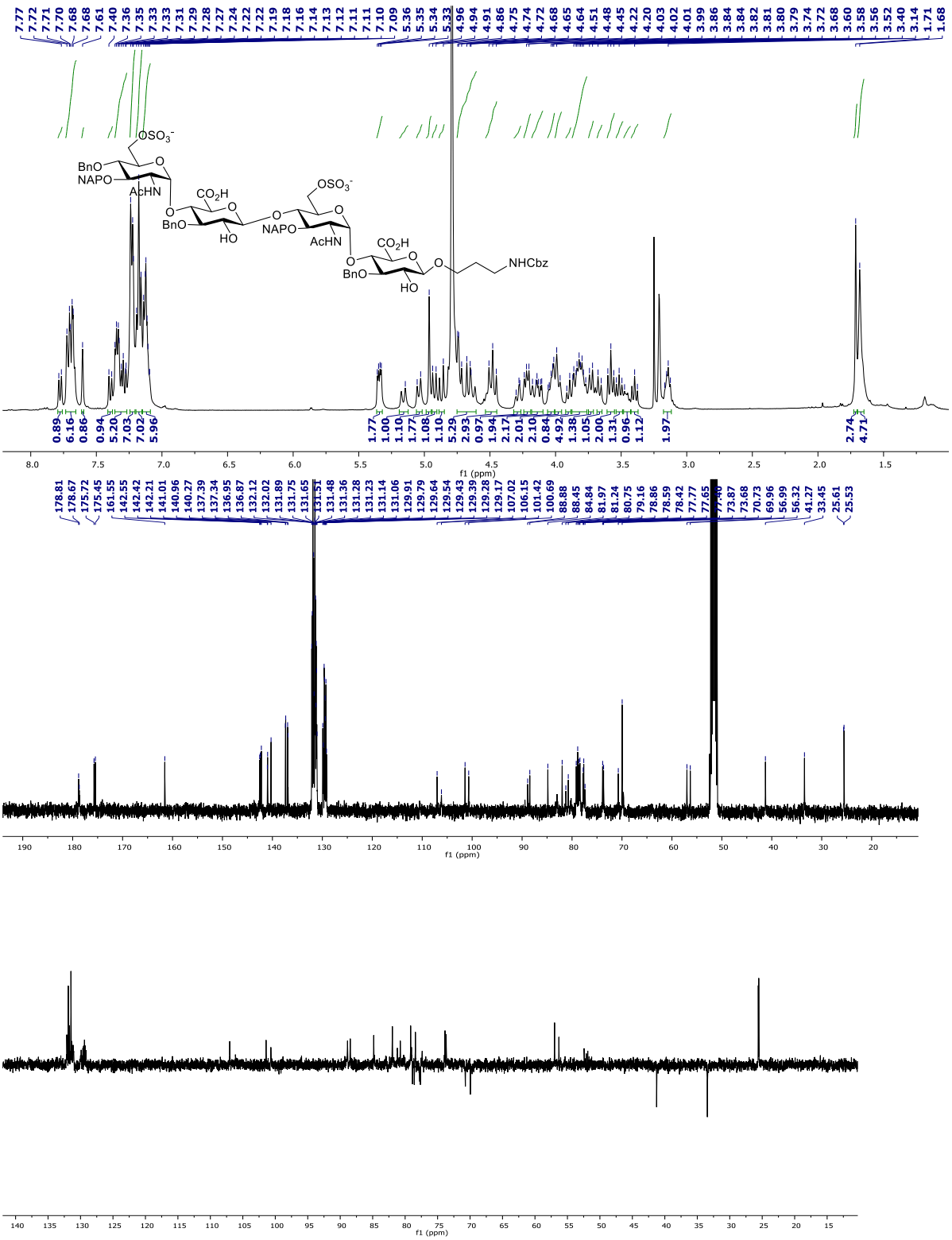
## $^{1}H$, $^{13}C$, and DEPT NMR spectrum of compound 11



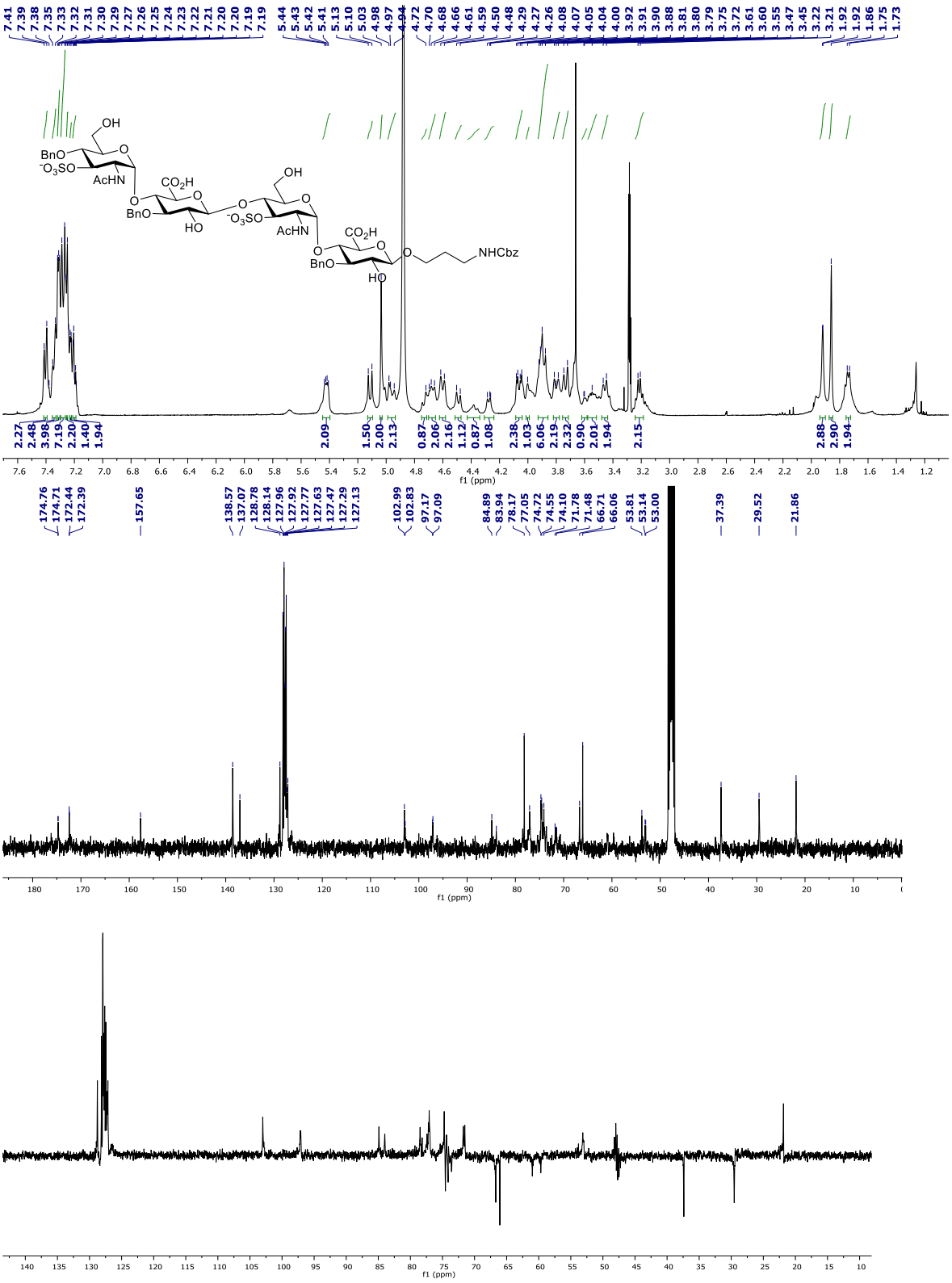
## $^{1}H$, $^{13}C$, and DEPT NMR spectrum of compound S5



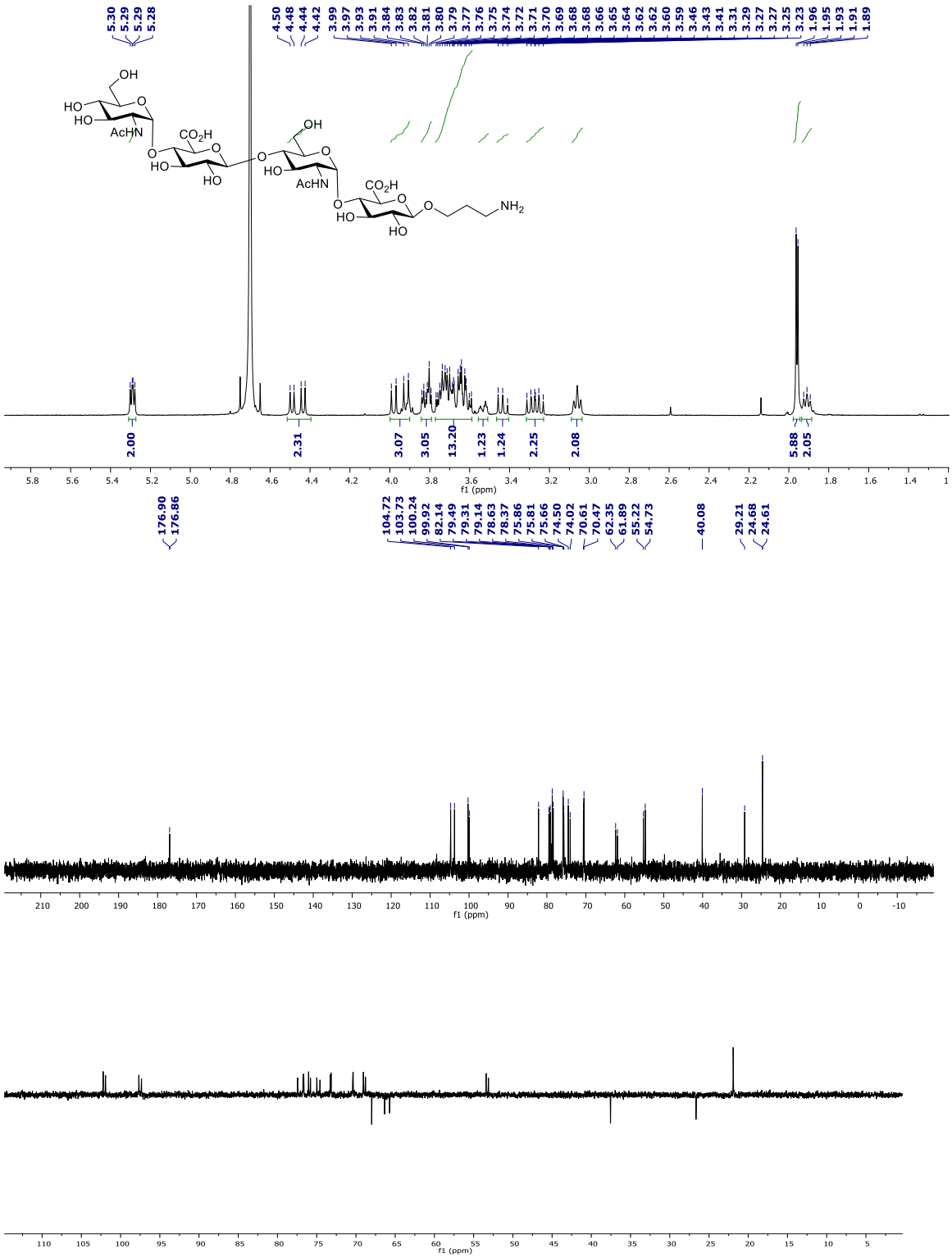
## $^{1}H$, $^{13}C$, and DEPT NMR spectrum of compound S6



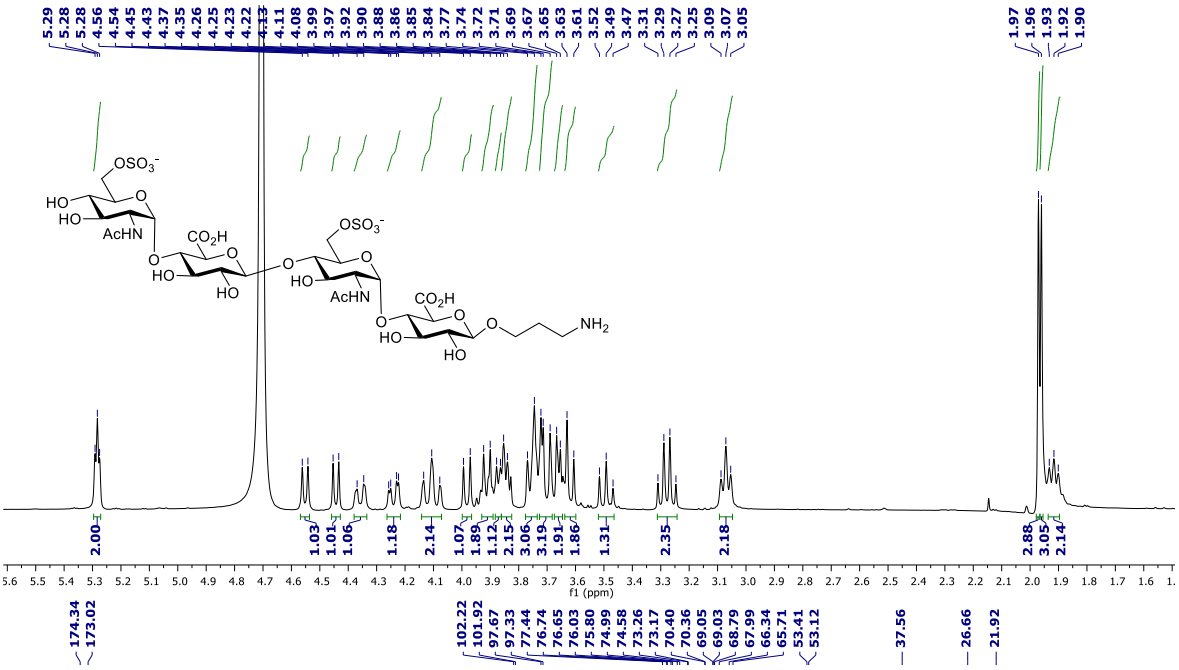
## $^{1}H$, $^{13}C$, and DEPT NMR spectrum of compound S7

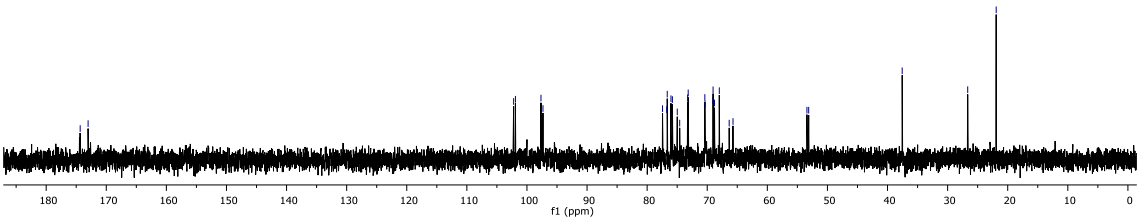


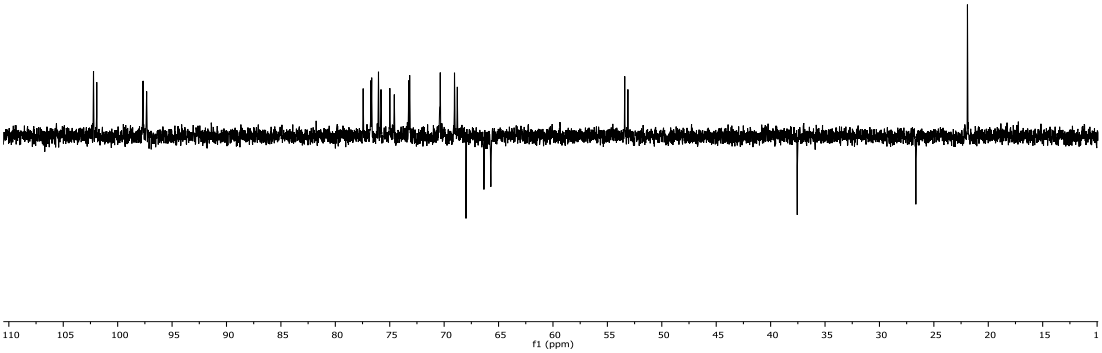
## $^{1}H$, $^{13}C$, and DEPT NMR spectrum of compound G-0S



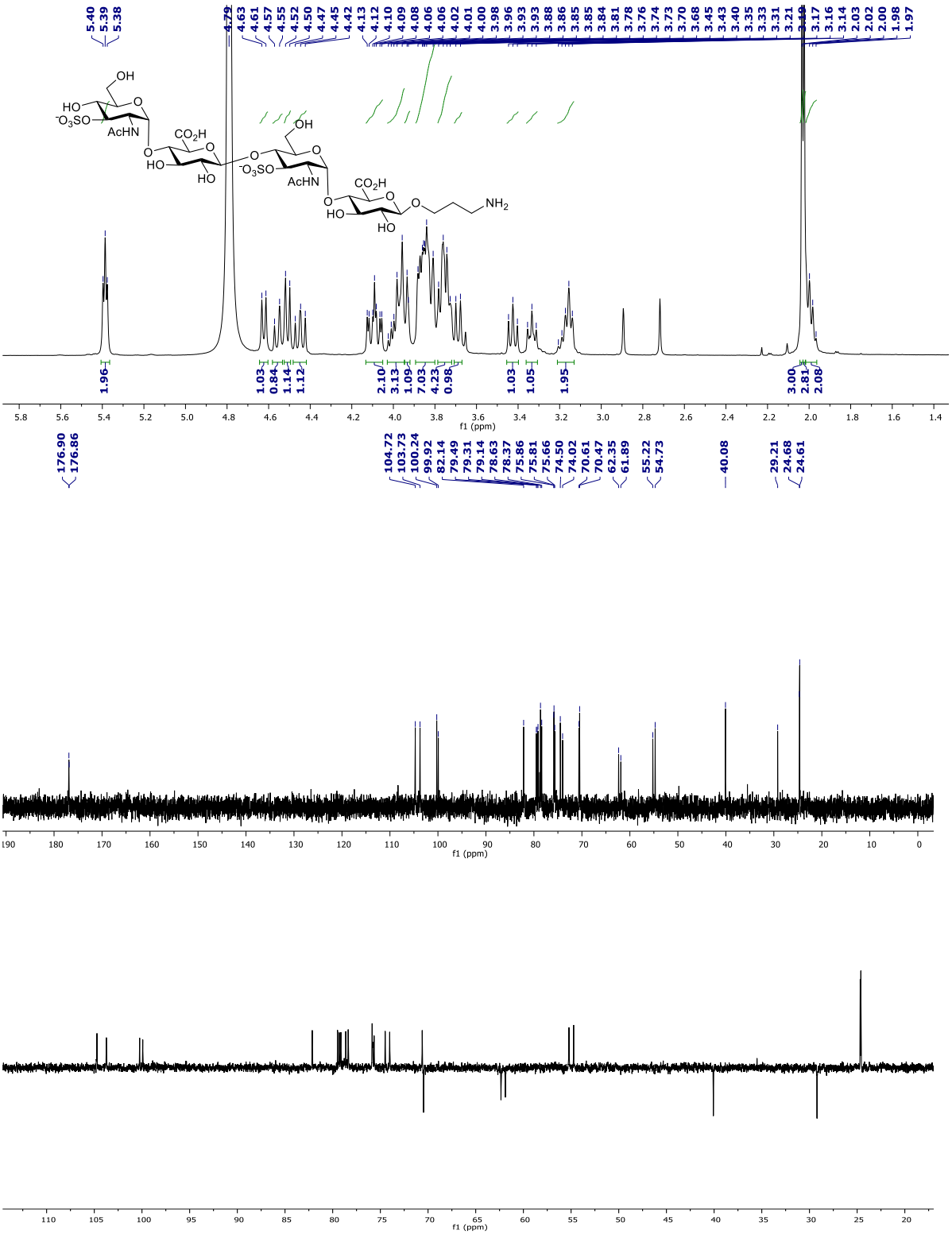
## $^{1}H$, $^{13}C$, and DEPT NMR spectrum of compound G-6S



## $^{1}H$, $^{13}C$, and DEPT NMR spectrum of compound G-3S



## 2.7 References:


1) S. K. Akiyama, K. Nagata, K. M. Yamada, *BBA - Rev. Biomembr.* **1990**, *1031*, 91–110.
2) C. Frantz, K. M. Stewart, V. M. Weaver, *J. Cell Sci.* **2010**, *123*, 4195–4200.
3) M. Mende, C. Bednarek, M. Wawryszyn, P. Sauter, M. B. Biskup, U. Schepers, S. Brase, *Chem. Rev.* **2016**, *116*, 8193–8255.
4) G. J. Sheng, Y. I. Oh, S. K. Chang, L. C. Hsieh-Wilson, *J. Am. Chem. Soc.* **2013**, *135*, 10898–10901.
5) C. Zong, A. Venot, X. Li, W. Lu, W. Xiao, J. S. L. Wilkes, C. L. Salanga, T. M. Handel, L. Wang, M. A. Wolfert, G. J. Boons, *J. Am. Chem. Soc.* **2017**, *139*, 9534–9543.
6) P. Jain, C. D. Shanthamurthy, S. Leviatan Ben-Arye, R. J. Woods, R. Kikkeri, V. Padler-Karavani, *Chem. Sci.* **2021**, *12*, 3674–3681.
7) C.-H. Chang, L. S. Lico, T.-Y. Huang, S.-Y. Lin, C.-L. Chang, S. D. Arco, S.-C. Hung, *Angew. Chemie* **2014**, *126*, 10034–10037.
8) X. Zhang, V. Pagadala, H. M. Jester, A. M. Lim, T. Q. Pham, A. M. P. Goulas, J. Liu, R. J. Linhardt, *Chem. Sci.* **2017**, *8*, 7932–7940.
9) Y. P. Hu, S. Y. Lin, C. Y. Huang, M. M. L. Zulueta, J. Y. Liu, W. Chang, S. C. Hung, *Nat. Chem.* **2011**, *3*, 557–563.
10) W. Lu, C. Zong, P. Chopra, L. E. Pepi, Y. Xu, I. J. Amster, J. Liu, G. J. Boons, *Angew. Chemie - Int. Ed.* **2018**, *57*, 5340–5344.
11) C. Noti, J. L. De Paz, L. Polito, P. H. Seeberger, *Chem. - A Eur. J.* **2006**, *12*, 8664–8686.
12) B. Wang, Y. Du, *Oxid. Med. Cell. Longev.* **2013**, DOI 10.1155/2013/898034.
13) M. Jaishankar, T. Tseten, N. Anbalagan, B. B. Mathew, K. N. Beeregowda, *Toxicology* **2014**, *7*, 60–72.
14) W. C. Lin, Z. Li, M. A. Burns, *Anal. Chem.* **2017**, *89*, 8748–8756.
15) O. Raize, Y. Argaman, S. Yannai, *Biotechnol. Bioeng.* **2004**, *87*, 451–458.
16) L. R. Andrade, R. N. Leal, M. Noseda, M. E. R. Duarte, M. S. Pereira, P. A. S. Mourão, M. Farina, G. M. Amado Filho, *Mar. Pollut. Bull.* **2010**, *60*, 1482–1488.
17) C. I. Gama, S. E. Tully, N. Sotogaku, P. M. Clark, M. Rawat, N. Vaidehi, W. A. G. Iii, A. Nishi, L. C. Hsieh-Wilson, *Nat. Chem. Biol.* **2006**, *2*, 467–473.

18) R. Tamilarasan, D. R. Mcmillin, **1986**, 2037–2040.

19) C. M. Che, S. W. Lai, *Coord. Chem. Rev.* **2005**, *249*, 1296–1309.

20) I. Alshanski, J. Blaszkiewicz, E. Mervinetsky, J. Rademann, S. Yitzchaik, M. Hurevich, *Chem. - A Eur. J.* **2019**, *25*, 12083–12090.

21) I. Alshanski, A. Shitrit, Y. Sukhran, C. Unverzagt, M. Hurevich, S. Yitzchaik, *Langmuir* **2022**, *38*, 849–855.

22) E. Mervinetsky, I. Alshanski, Y. Hamo, L. M. Sandonas, A. Dianat, J. Buchwald, R. Gutierrez, G. Cuniberti, M. Hurevich, S. Yitzchaik, *Sci. Rep.* **2017**, *7*, 1–7.

23) F. Brunori, D. K. Padhi, I. Alshanski, J. Freyse, J. N. Dürig, A. Penk, L. Vaccaro, M. Hurevich, J. Rademann, S. Yitzchaik, *ChemBioChem* **2022**, *23*, e202100552.

24) E. Mervinetsky, I. Alshanski, J. Buchwald, A. Dianat, I. Lončarić, P. Lazić, Ž. Crljen, R. Gutierrez, G. Cuniberti, M. Hurevich, S. Yitzchaik, *Langmuir* **2019**, *35*, 11114–11122.

25) B. Subramani, C. D. Shantamurthy, P. Maru, M. A. Belekar, S. Mardhekar, D. Shanmugam, R. Kikkeri, *Org. Biomol. Chem.* **2019**, *17*, 4535–4542.

26) S. Anand, S. Mardhekar, R. Raigawali, N. Mohanta, P. Jain, C. D. Shanthamurthy, B. Gnanaprakasam, R. Kikkeri, *Org. Lett.* **2020**, *22*, 3402–3406.

27) P. Jain, C. D. Shanthamurthy, P. M. Chaudhary, R. Kikkeri, *Chem. Sci.* **2021**, *12*, 4021–4027.

28) D. Bélanger, J. Pinson, *Chem. Soc. Rev.* **2011**, *40*, 3995–4048.

29) Y. H. Tang, H. C. Lin, C. L. Lai, P. Y. Chen, C. H. Lai, *Biosens. Bioelectron.* **2018**, *116*, 100–107.

30) D. A. Gorin, A. M. Yashchenok, A. O. Manturov, T. A. Kolesnikova, H. Möhwald, *Langmuir* **2009**, *25*, 12529–12534.

31) B. Yuan, C. Xu, D. Zhang, R. Zhang, H. Su, P. Guan, J. Nie, C. Fernandez, *Electrochem. commun.* **2017**, *81*, 18–23.

32) T. Nasir, L. Zhang, N. Vilà, G. Herzog, A. Walcarius, *Langmuir* **2016**, *32*, 4323–4332.

33) W. Bashir, B. Paull, *J. Chromatogr. A* **2002**, *942*, 73–82.

34) D. G. Kurth, M. Higuchi, *Soft Matter* **2006**, *2*, 915–927.

35) R. J. Sundberg, *Chem. Rev.* **1974**, *74*, 471–517.

36) J. Catalano, A. Murphy, Y. Yao, G. P. A. Yap, N. Zumbulyadis, S. A.Centeno, C. Dybowski, *Dalton Trans.* **2015**, *44*, 2340–2347.

37) E. Mervinetsky, I. Alshanski, S. Lenfant, D. Guerin, L. Medrano Sandonas,A. Dianat, R. Gutierrez, G. Cuniberti, M. Hurevich, S. Yitzchaik, D.Vuillaume, *J. Phys. Chem. C* **2019**, *123*, 9600–9608.

38) J. A. Cowan, *Chem. Rev.* **1998**, *98*, 1067–1087.

# CHAPTER- 3

## Glycosaminoglycan Nanoprobes Platform for Tuning Phenotypic Cellular Uptake

## 3.1 Abstract

Demystifying the sulfation code of glycosaminoglycans (GAGs) to induce precise homing of nanoparticles in tumor or neuron cells influences the development of a potential drug or gene delivery system. However, GAGs, particularly heparan sulfate (HS) and chondroitin sulfate (CS), are structurally highly heterogeneous, and synthesizing well-defined HS/CS composed nanoparticles is challenging. Here, we decipher how specific sulfation patterns on HS and CS regulate receptor-mediated homing of nanoprobes in primary and secondary cells. We discovered that aggressive cancer cells such as MDA-MB-231 displayed a strong uptake of GAG-nanoprobes compared to mild or moderate aggressive cancer cells. However, there was no selectivity towards the GAG sequences, indicating the presence of more than one receptors mediated uptake. Whereas U87 cells, olfactory bulb and hippocampal cells showed selective or preferential uptake of CS-E coated nanoprobes compared to other GAG-nanoprobes. Further, mechanistic studies revealed that 4,6-*O*-disulfated-CS nanoprobe utilized CD44 and caveolin-dependent endocytosis pathway for endocytosis. These results imply new opportunities to use GAG nanoprobes in nanomedicine.

## 3.2 Introduction

In recent years, carbohydrate-appended nanoparticles have provided a rich platform for designing diagnostic and cell imaging tools for biomedical applications.[1] Though relatively weak binding with protein, carbohydrates play a pivotal role in fine-tuning biological activities.[2] Hence, glyconanoparticles are a key construct to target lectins,[3] protein toxins,[4] cell surface receptors,[5] cell lines and tissues.[6] Of the plethora of nanostructural materials employed in designing glyconanoparticles, gold nanoparticles (AuNPs) are arguably one of the most common, as AuNPs are easy to synthesis with different sizes, shapes, and functionalizations.[7] Many successful glyco-goldnanoparticles contain scaffold features, including α-fucosylamine and α-mannose functionalized gold nanoparticles targeting DC-SIGN and viral infection.[8] Several lectins biosensors, and carbohydrate-carbohydrate interactions were established using gold nanoparticles.[9] However, the major challenge will be acquiring a pure form of carbohydrate ligands to synthesize glyconanoparticles, More specifically, the synthesis of glycosaminoglycans (GAGs) and sialic acid-based glyconanoparticles, which regulate major biological functions. Among various GAGs, heparan sulfate (HS) and chondroitin sulfate (CS) offers attractive scaffolds due to their structural diversity and ability to demonstrate wide biological applications.[10] For example, Wang et al, synthesized heparin-based magnetic nanoparticles to develop antimalarial drug delivery system.[11] Similarly, Samanta et al., synthesized heparin-based nanoprobes to target glioma in the murine model.[12] Hao et al., reported heparin-based nanocarrier to deliver siRNA to treat lung cancer.[13] Du et al., synthesized a heparin based nanocarrier for targeted delivery of doxorubicin.[14] Similarly, Sun et al., synthesized heparin-based nanoparticle targeting anti-metastasis of orthotopic breast cancer.[15] While, Li et al., reported the synthesis of CS-based product to target cancer metastasis.[16] Zhang et al. used CS-based liposomes for co-delivery of doxorubicin and retinoic acid to treat lung metastasis.[17] Similarly, Rojo et al. and Pashkuleva et al synthesized CS-based dendrimers and star-shaped microfibers to target growth factors.[18] Despite all this progress, there are no HS or CS-based nanomaterials in clinical trials. This is mainly due to the anticoagulation activity of native HS and strong binding affinity to more than one receptor. Therefore, it is better to synthesize well-defined HS and CS sequences and study their activity. Herein, we report the synthesis and characterization of a panel of HS tetrasaccharides and CS disaccharides appended to fluorescent nanoprobes to study selective cell targeting and homing. Although HS- and CS-based nanoprobes have been studied independently

as a cell targeting and drug-delivery system, to the best of our knowledge, comparative studies have never been explored with synthetic GAG-nanoprobes.

### 3.3 Results and Discussion

#### 3.3.1 Synthesis of HS and CS fluorescence conjugated nanoprobes

##### i) Synthesis of sugar appended tripods

HS and CS oligosaccharides can be synthesized with a wide range of sulfation patterns. Here, we chose four CS and three HS sequences predominantly found in GAGs in the hope of improving the selectivity and specificity of homing nanoprobes in phenotypic cells. At the structural level, CS is a heteropolysaccharide that comprises galactosamine-glucuronic acid (GluA) disaccharides repeating unit with different *O*-sulfation patterns.[19] Based on their sulfation codes, they are further classified as CS-A, C, D and E, respectively. In contrast, HS consists of disaccharide repeating units of glucosamine-uronic acid, with a wide range of sulfation patterns, including *N*-sulfation and *O*-sulfation.[20] Uronic acid may be in the form of L-iduronic acid (IdoA) or D-glucurnoic acid (GluA). Theoretically, there are 2,304 possible tetrasaccharides, which allow fine-tuning the carbohydrate-protein interactions. Hence, synthetic GAG-nanoprobes are extremely valuable scaffolds for constructing cell- and tissue-specific drug delivery probes. Recently, we reported the synthesis of a heparinoid-nanovehicle to target epidermal growth factor receptors (EGFR) overexpressed cancer cells in 2D and 3D co-culture models.[21] However, broadening the cell-specific homing of nanovehicles requires synthetic GAG nanoprobes of HS and CS epitopes. Therefore, we have used previousely synthesized HS and CS ligands predominantly found in GAGs to improve the selectivity and specificity of homing nanoprobes in phenotypic cells (Figure 1).

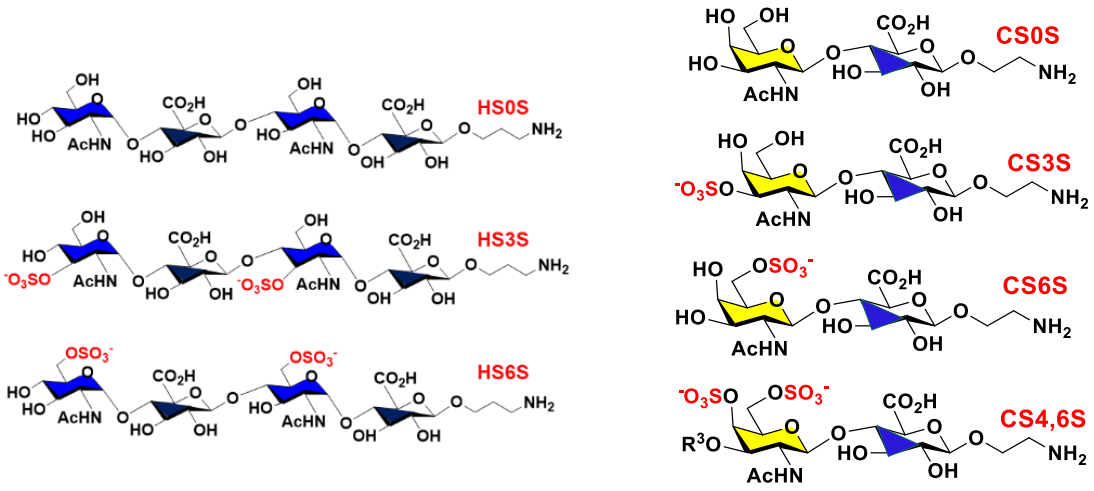
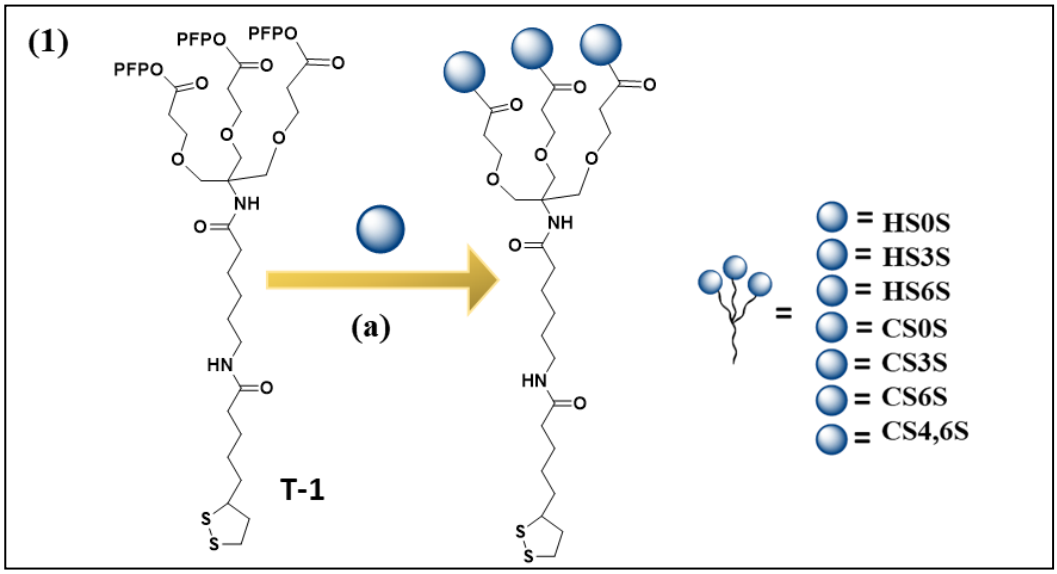



**Figure 1**. Amino-functionalized (a) HS tetrasaccharides (b) CS diasaccharides with different sulfation and carboxylation

These sythesised HS and CS GAG sequences were tethered on tripods (**T-1**), to achieve subsequent gold nanoparticle immobilization (Figure 1).

### 3.3.2 Surface functionalisation using tripodal sugars and fluorescence linker

Spherical gold nanoparticles 20nm in size are ideal for the designing of GAG nanoprobes as they are well-established for carbohydrate-mediated cell targeting studies.[25] The AuNPs were treated with GAG tripods (**27-33**) and a fluorescent linker **F-1** in a step-by-step method to obtain fluorescent GAG nanoprobes (**AuF@CS0S**, **AuF@CS3S**, **AuF@CS6S**, **AuF@CS46S**, **AuF@HS0S**, **AuF@HS6S,** and **AuF@HS3S**) (Figure 1).



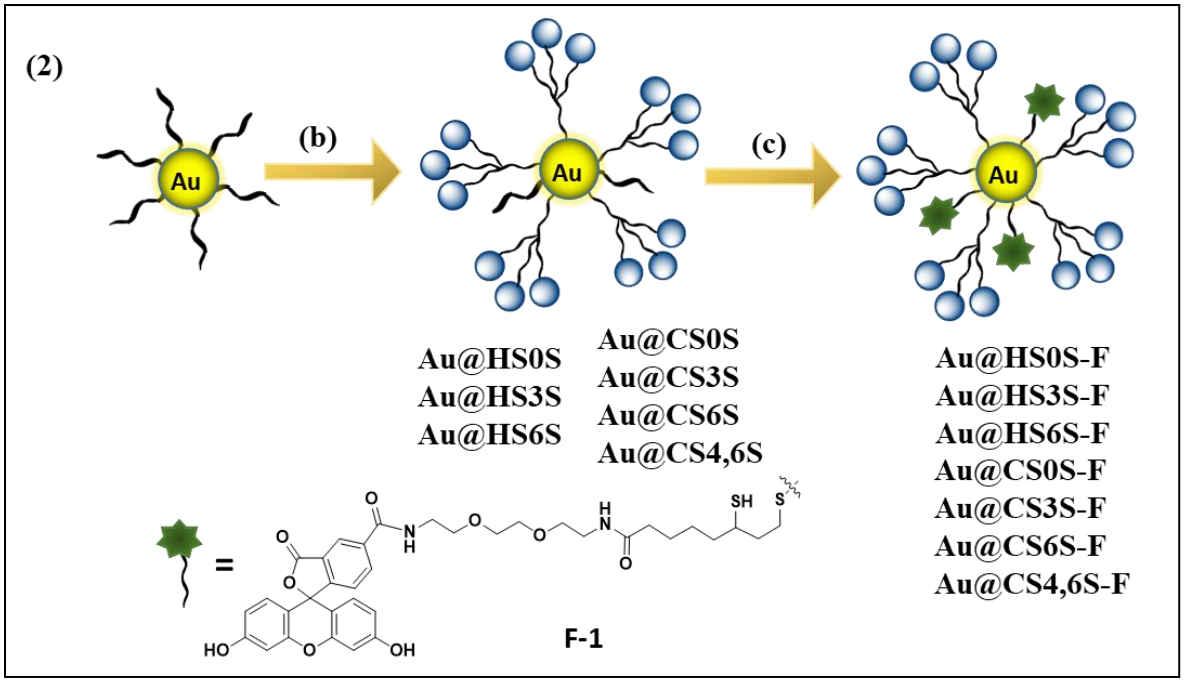



**Figure 2**. (1) CS and HS conjugation to tripod; (2) Schematic representation of HS and CS-tripod functionalized fluorescent AuNPs; Reagents and conditions. (a) DMF, $Et_3N$, RT, 5 h (b) **27- 33**, PBS buffer pH 7.4, 25 ºC, 24 h; (c) **F-1**, PBS buffer pH 7.4, 25 ºC, 12 h.

### 3.3.3 Physicochemical Characterization of HS and CS fluorescence conjugated nanoprobes

## i) SEM and UV-visible spectroscopy:

The size and shape of the nanostructure were confirmed by SEM and UV-visible spectroscopy (Figure 3).

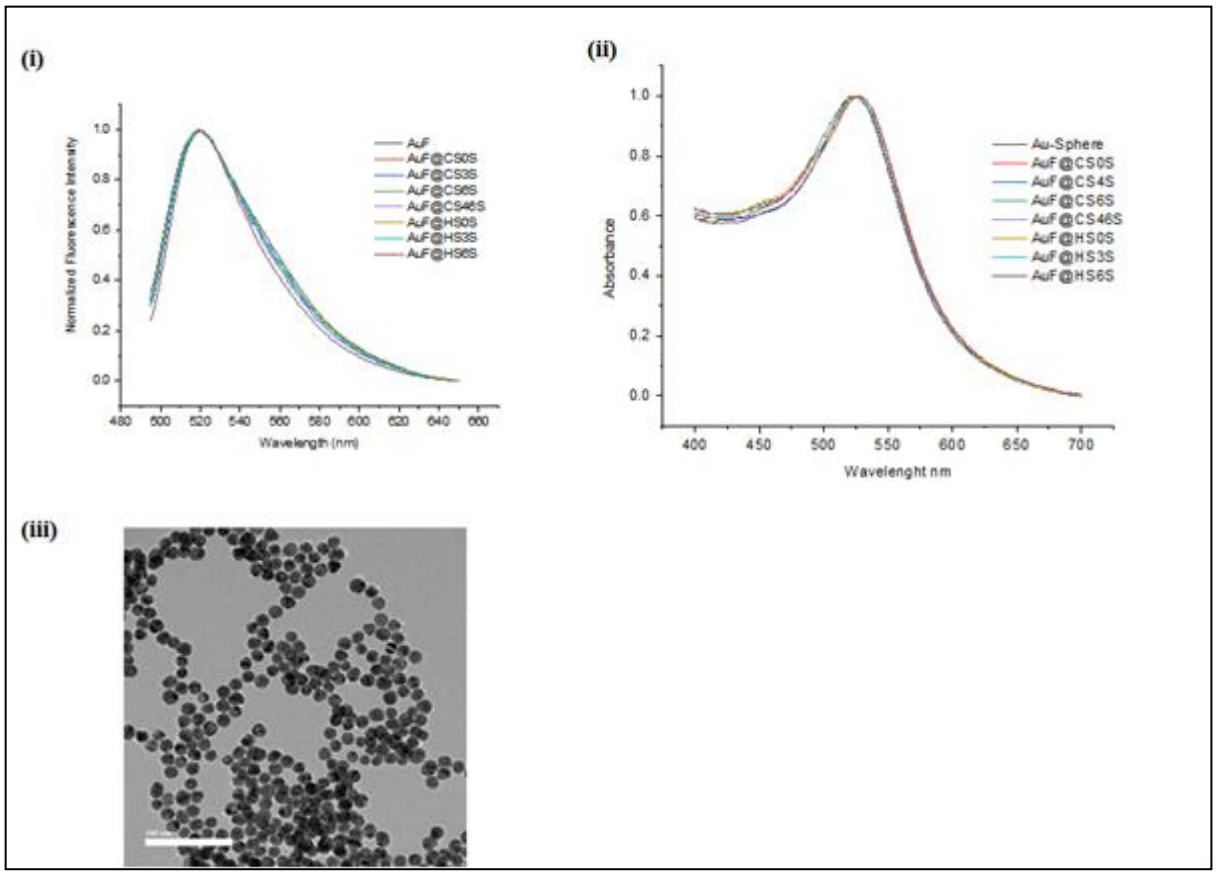



**Figure 3.** (i) UV-visible spectra of HS and CS-tripod functionalized fluorescent AuNPs; (ii) Fluorescence spectra of HS and CS-tripod functionalized fluorescent AuNPs; (iii) TEM image of AuNP.

### 3.3.4 Quantification of sugar concentration on nanoparticle surface

Finally, the amount of sugar immobilized on the nanostructure was confirmed by the thio-detection kit (Table 1).[26]

| Sr. No. | AuNP | Sugar Concentration (mg/mL) |
|---|---|---|
| 1 | AuF@CS0S | 0.3 |
| 2 | AuF@CS3S | 0.32 |
| 3. | AuF@CS6S | 0.35 |
| 4 | AuF@CS46S | 0.39 |
| 5 | AuF@HS0S | 0.31 |
| 6 | AuF@HS3S | 0.32 |
| 7 | AuF@HS6S | 0.29 |

**Table 1.** Qunatification of sugar concentration on nanoparticle surface

### 3.3.5 Cellular uptake assay

A cellular uptake assay was performed using the protocols reported in the literature.[28] In brief, cells A cellular uptake assay were seeded in an 8-well confocal imaging chamber and allowed to grow for 24 hours at 37°C in a 5% $CO_2$ incubator. GAG nanoprobes (5µg/ml) were added, and live images were recorded after 2 hours and 4 hours. To ensure consistency, we repeated all experiments in triplicate. We first used cancer cell lines MDA-MB-231, MDA-MB-468, T47D, MCF7, and SKBR3, which represent different aggression levels of breast cancer with a wide range of growth factor binding receptors.[29] After 4 hours of incubation, fluorescence was observed in the triple-negative cancer cells (MDA-MB-231, T47D, and MDA-MB-468). Among them, the MDA-MB-231 cell line showed intense fluorescence with all of the GAG nanoprobes, while MCF7 and SKBR3 did not bind to any uptake, confirming that cancer cells with different levels of aggression behave differently with GAG nanoprobes. Although triple-negative cancer cells showed strong uptake of the GAG nanoprobes, there was no specificity, which suggested that glucuronic acid-based HS or CS nanoprobes are not suitable probes to target cancer cells (Figure 4).

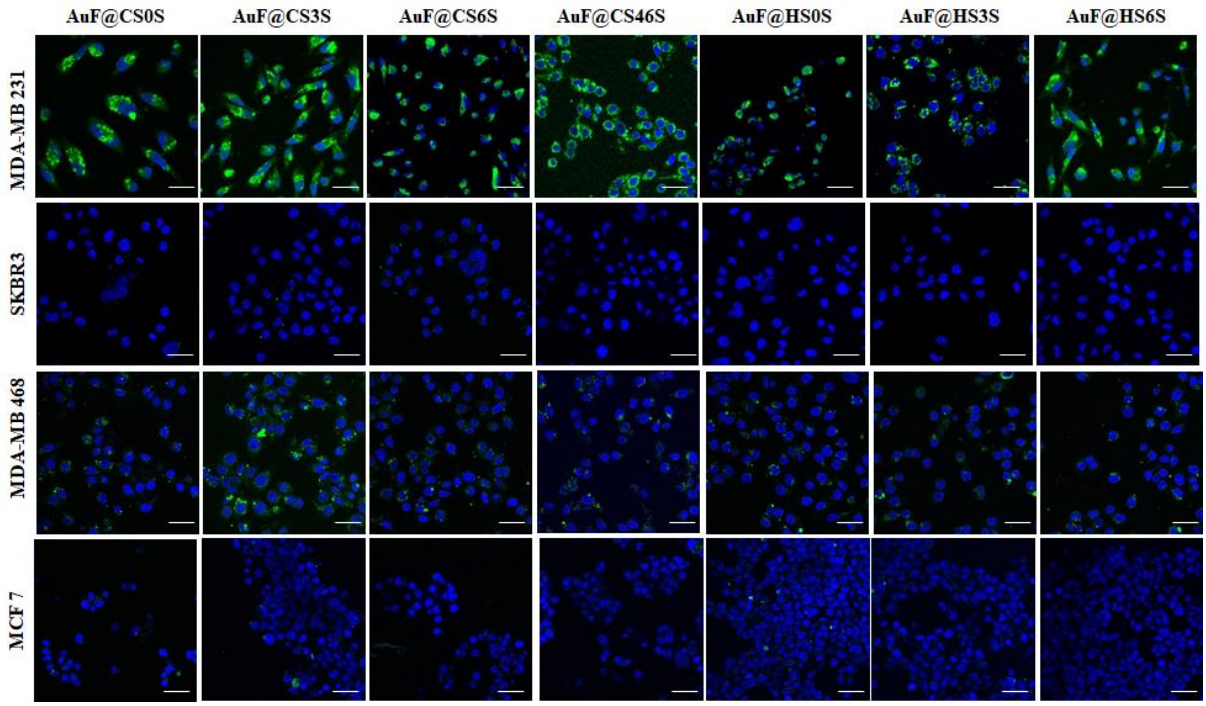



**Figure 4.** Confocal images of nanoparticle internalization by different cancer cell lines after 4 h (scale bar: 50 µm)

Next, we performed an in vitro assay with glial cells U87 and neuroblastoma cells SH-SY5Y, as these are widely used to probe the molecular and cellular mechanisms of brain disorders.

Interestingly, the U87 glial cells showed a pronounced uptake of **AuF@CS46S** as compared to the other GAG nanoprobes, while SH-SY5Y showed non-specific and poor uptake of the GAG nanoprobes (Figure 5). To further confirm the GAG nanoprobes' targeting of the neural cells, we used two primary neuronal cells isolated from the hippocampal and olfactory bulb regions of newborn mice. Fluorescent imaging studies of the olfactory bulbs showed increased uptake of two- to three-fold of **AuF@CS46S** as compared to the other ligands. While the hippocampal cells showed a similar trend with **AuF@CS46S** (Figure 5) however, uptake is less pronounced as compared to olfactory bulb cells. These findings indicate that glial cells and primary neurons might have a specific receptor for the **CS46S** ligand that mediated the receptor-mediated uptake (Figure 6).

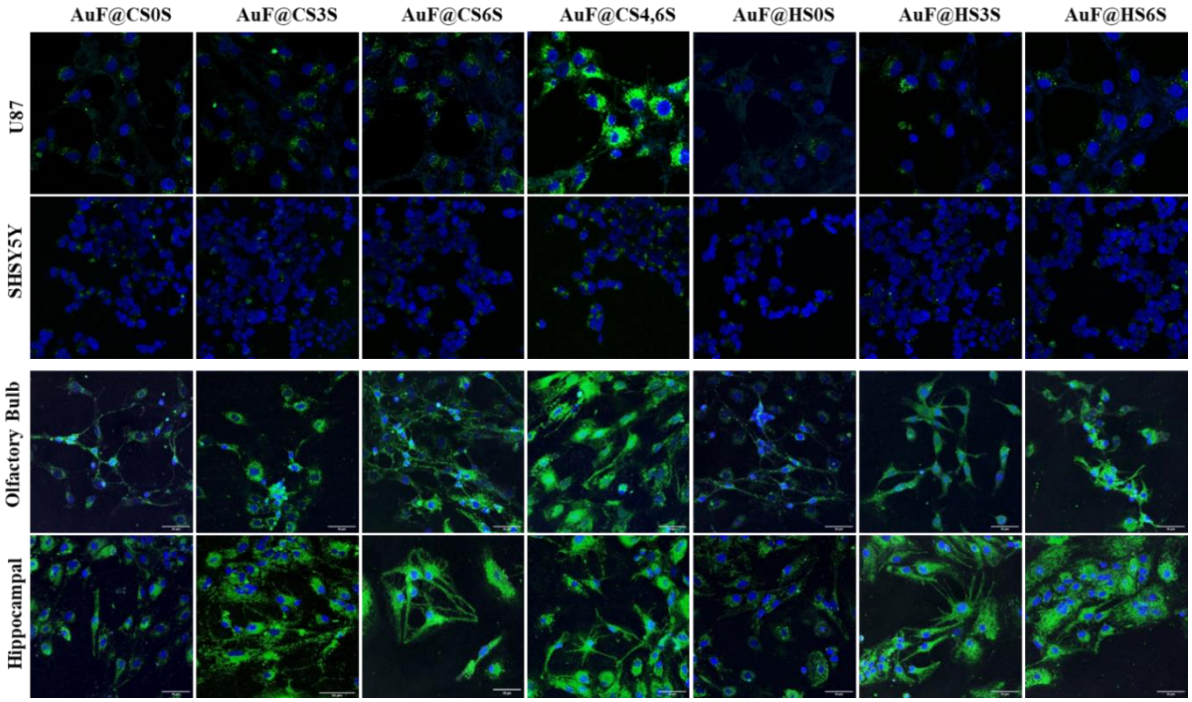



**Figure 5**: Plot for mean cellular uptake intensity (gray value) per neuron for HS and CS-tripod functionalized fluorescent AuNPs in olfactory bulb and hippocampus primary neural cells. Asterisks indicate statistically significant differences (**$p < 0.01$, *$p < 0.1$). Statistical analysis is between **Au@CS46S** Olfactory bulb and different AuNPs

### 3.3.6 A Flow cytometry assay

To show the rate of uptake of the GAG nanoprobes, a flow cytometry assay was performed. After 4 hours, **AuF@CS46S** showed 37% uptake by the U87 cell line compared to the other GAG nanoprobes (10-12%) (Figure 6). These findings suggest that **AuF@CS46S** binds to the cell surface receptors through specific carbohydrate-protein interaction and undergo endocytosis.

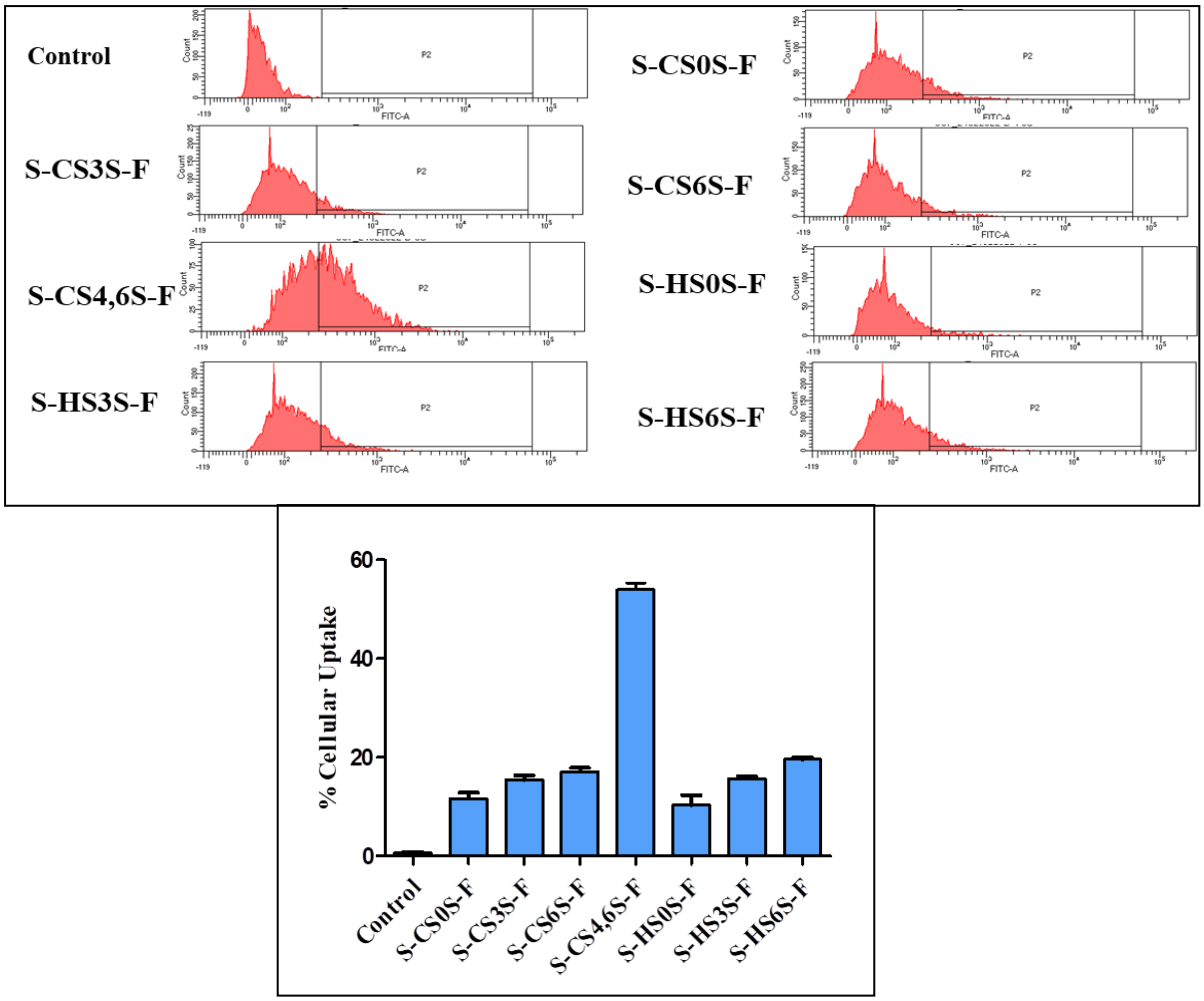



**Figure 6**: FACs analysis of uptake of HS and CS-tripod functionalized fluorescent AuNPs by U87 cells. Asterisks indicate statistically significant differences (**p < 0.001). Statistical analysis is between **Au@CS46S** and different AuNPs performed using a two-tailed Student t test.

### 3.3.7 Quantification of CD44 expression level

To understand the mechanism of endocytosis of **AuF@CS46S**, we first investigated different GAGs binding receptors expressed on these cell lines. The literature survey hypothesized that CD44 a transmembrane GAG binding receptor ubiquitously expressed on cancer and neural

cells, might be involved in this uptake mechanism. To validate CD44 mediated uptake of GAG-nanoprobes, we first investigated the expression level of CD44 on cancer and neuronal cell lines. All GAG-nanoprobes uptaking cells exhibited strong cell surface expression of CD44 receptors. In contrast, SH-SY5Y, MCF-7, and SKBR3 showed no staining of FITC-anti-CD44 protein, indicating that CD44 might be a potential receptor for GAG-nanoprobes uptake (Figure 7).

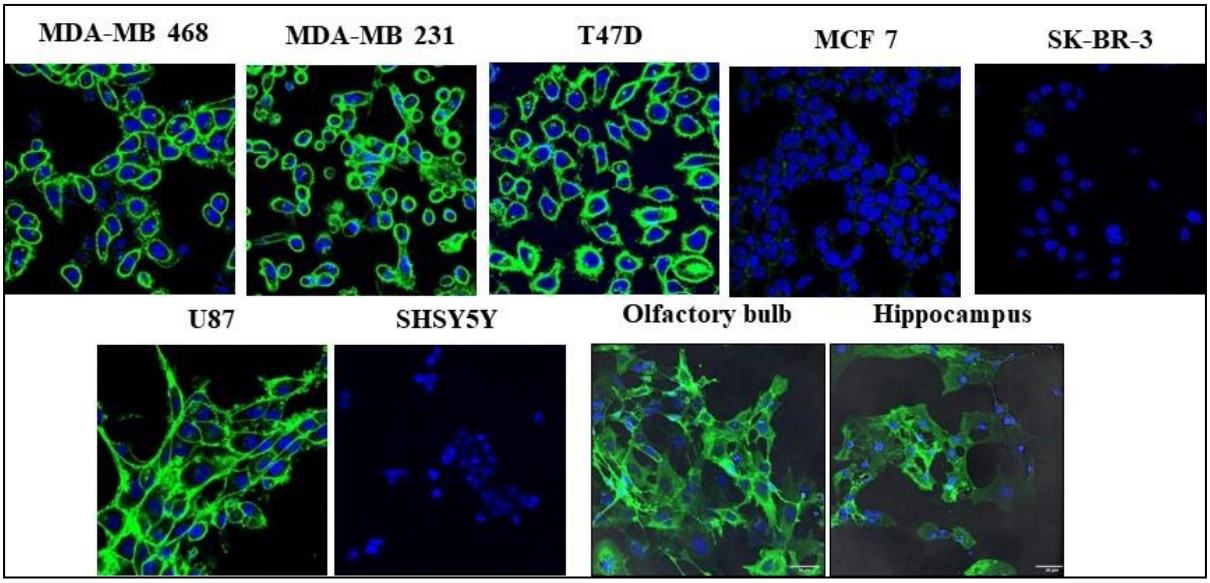



**Figure 7.** CD44 expression level by different cancer and neural cell lines

### 3.3.8 Homing of nanoprobes in cancerous cells as well as primary and secondary neural cells

## i) Uptake mechanism of nanoprobes

Next, we investigated receptor-mediated uptake of **AuF@CS46S** by the U87 cell line. To this end, we treated the cell lines with $NaN_3$ solution for 30 mins, followed by treating **AuF@CS46S** for 4 h. We observed a substantial decrease in the cellular uptake of **AuF@CS46S**, indicating a receptor-mediated endocytic pathway. Next, we confirmed whether the uptake is dynamin-dependent by adding dynasore hydrate inhibitor into the cell culture media. **AuF@CS46S** internalization was fully inhibited, revealing that the internalization mechanism follows either clathrin or caveolae-dependent pathway. Finally, we studied the effect of methyl-β-cyclodextrin (m-β-CD, inhibitor of caveolae-mediated endocytosis), chlorpromazine (inhibitor of clathrin-mediated endocytosis). As shown in Figure 8, cells pre-treated with the caveolae inhibitor showed a considerable reduction in internalization, whereas chlorpromazine

pre-treatment of cells exhibited a minor inhibition effect. These findings revealed that **AuF@CS46S** was uptaken *via* energy-dependent caveolae pathway. Similar studies with olfactory bulb and hippocampal cells showed the CD44 mediated encocytosis pathway (Figure 9). Although CD44 showed remarkable binding affinity to hyaluronic acid (HA) and CS ligands.[30] In our results, we have shown that CD44 overexpressed cell lines can be targeted by using simple GalNAc(4,6-*O*-disulfate)β(1-3)GlcA disaccharide ligand conjugated nanoprobes more effectively than other sulfated CS-di or HS-tetrasaccharide ligands. Further, we demonstrated that HS ligands are potential negative control ligand, for CD44 mediated nanoparticles uptake studies. Finally, we have demonstrated efficient targeting of primary neural cells using **AuF@CS46S** nanoprobe.

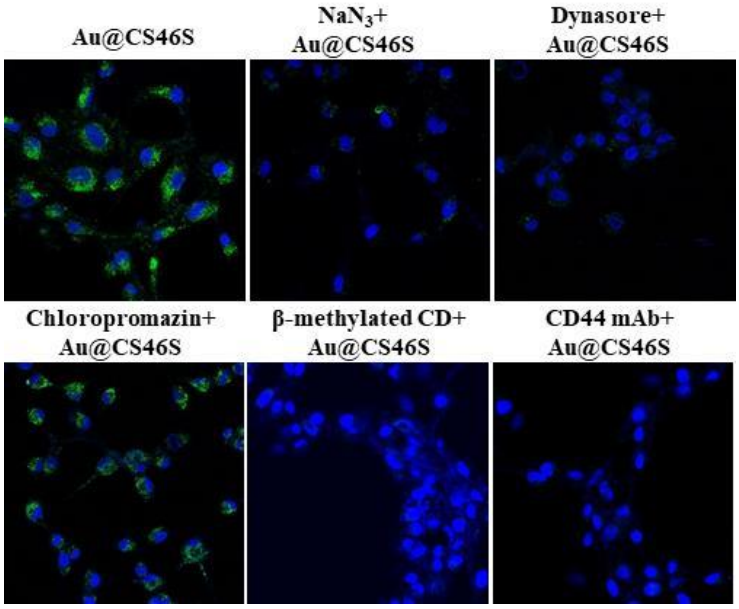



**Figure 8.** Confocal microscopy images of **AuF@CS46S** in the presence of different endocytotic pathway inhibitors ($n$ = 3) (scale bar: 50 μm)

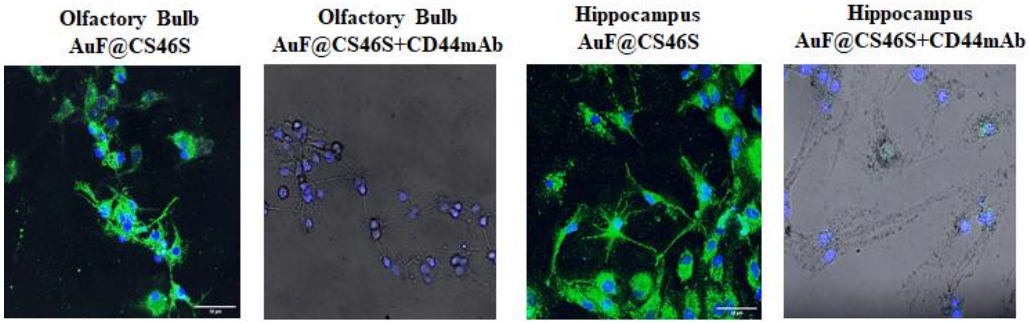


**Figure 9.** Confocal microscopy images of **AuF@CS46S** in the presence of CD44 monoclonal antibody in olfactory bulb and hippocampus primary neural cells ($n$ = 3) (scale bar: 50 μm).

Next, we investigated receptor-mediated uptake of **AuF@CS46S** by the U87 cell line. To this end, we treated the cell lines with $NaN_3$ solution for 30 mins, followed by treating **AuF@CS46S** for 4 h. We observed a substantial decrease in the cellular uptake of **AuF@CS46S**, indicating a receptor-mediated endocytic pathway. Next, we confirmed whether the uptake is dynamin-dependent by adding dynasore hydrate inhibitor into the cell culture media. **AuF@CS46S** internalization was fully inhibited, revealing that the internalization mechanism follows either clathrin or caveolae-dependent pathway. Finally, we studied the effect of methyl-β-cyclodextrin (m-β-CD, inhibitor of caveolae-mediated endocytosis), chlorpromazine (inhibitor of clathrin-mediated endocytosis). As shown in Figure 10, cells pre-treated with the caveolae inhibitor showed a considerable reduction in internalization, whereas chlorpromazine pre-treatment of cells exhibited a minor inhibition effect. These findings revealed that **AuF@CS46S** was uptaken *via* the energy-dependent caveolae pathway. Similar studies with olfactory bulb and hippocampal cells showed the same endocytic pathway.

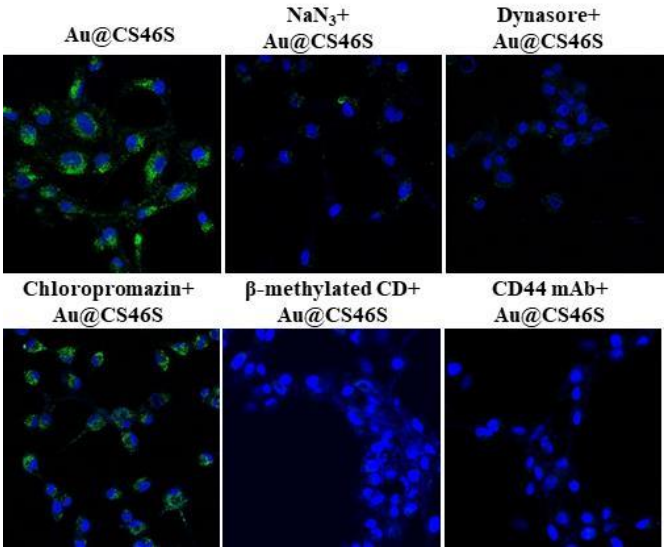



**Figure 10.** Confocal microscopy images of **AuF@CS46S** in the presence of different endocytotic pathway inhibitors ($n$ = 3).

## 3.4 Conclusion

In summary, we present a new set of GAG-nanoprobes composed of both HS and CS synthetic ligands that can give a broad picture of cell specific homing of nanoparticles and provide a novel

opportunity for nanotherapy. More specifically, we have shown that CS-E is a potential ligand to design nanoprobe to target CD44 overexpressed cancer cells and neurites.

## 3.5 Experimental Part

### a) General Information

All chemicals were reagent grade and used without further purification unless otherwise noted. Reactions were carried out in anhydrous solvents under a nitrogen atmosphere. Reaction progress was monitored by analytical thin-layer chromatography (TLC) on Merck silica gel 60 $F_{254}$. Spots on the TLC plate were visualized under UV light or dipping the TLC plate in CAM/ninhydrin solution followed by heating. Column chromatography was carried out using Fluka kieselgel 60 (230-400 mesh). $^{1}H$ and $^{13}C$ NMR spectra of compounds were measured with Bruker 400 MHz, Bruker 600 MHz and Jeol 400 MHz using residual solvents as an internal reference ($CDCl_3$ δH 7.26 ppm, δC 77.3 ppm, $CD_3OD$ δH 3.31 ppm, δC 49.0 ppm, and $D_2O$ δH 4.79 ppm). The chemical shifts (δ) are reported in ppm and coupling constants (J) in Hz. UV-visible measurements were performed with Evolution 300 UV-visible spectrophotometer (Thermo Fisher Scientific, USA). Fluorescence spectra were measured with FluoroMax-4 spectrofluorometer (Horiba Scientific, U.S.A.). CD44 (8E2) Mouse mAb and CD44 Monoclonal Antibody (IM7), FITC used for inihibition study and cell level expression study were purchased from cell signalling technology and biosciences respectively. All microscopy images were captured using Leica SP8 confocal microscope and processed using Image J software.

### ii) Synthesis of tripod GAG derivatives

Respective glycan (3.5 eq) and pentafluorophenol tripod **T-1** (1 eq) were dissolved in anhydrous DMF (400 µl) and triethylamine was added (3 eq per PFP active ester). The resulting mixture was stirred at room temperature. After 5 h the reaction mixture was concentrated and purified by bond elute column (water as eluent) followed by lyophilisation to afford corresponding glycan conjugated tripod.

**Synthesis of 31:** The general procedure for glycan conjugation on tripod was followed to afford **31** (1.2 mg, 56 %) as a white solid. $^{1}H$ NMR (400 MHz, $D_2O$) δ 5.34 – 5.29 (m, 2H), 4.52 (d, *J* = 7.7 Hz, 1H), 4.38 (d, *J* = 9.2 Hz, 2H), 4.27 (d, *J* = 8.9 Hz, 2H), 4.10 (t, *J* = 12.6 Hz, 3H), 3.91 (d,

*J* = 11.2 Hz, 1H), 3.88 – 3.75 (m, 7H), 3.73 – 3.57 (m, 14H), 3.54 – 3.46 (m, 2H), 3.29 – 3.06 (m, 9H), 2.40 (d, *J* = 11.5 Hz, 3H), 2.19 – 2.11 (m, 3H), 1.96 (d, *J* = 4.5 Hz, 6H), 1.93 – 1.89 (m, 1H), 1.77 – 1.64 (m, 4H), 1.60 – 1.39 (m, 6H), 1.37 – 1.31 (m, 2H), 1.29 – 1.22 (m, 2H). ). HRMS (ESI) m/z: calc'd for $[M]^{6-}$ $C_{120}H_{187}O_{95}N_{11}S_8^{6-}$: 593.1329; Found: 593.1338.

**Synthesis of 32:** The general procedure for glycan conjugation on tripod was followed to afford **32** (0.95 mg, 51 %) as a white solid.$^1$H NMR (600 MHz, $D_2O$) δ 5.37 (d, *J* = 11.1 Hz, 2H), 4.62 (d, *J* = 8.1 Hz, 1H), 4.55 – 4.48 (m, 1H), 4.46 – 4.40 (m, 1H), 4.21 – 4.12 (m, 1H), 4.11 – 3.98 (m, 4H), 3.97 – 3.74 (m, 15H), 3.68 (q, *J* = 13.7, 12.0 Hz, 9H), 3.44 – 3.38 (m, 1H), 3.28 (ddd, *J* = 37.7, 18.8, 10.3 Hz, 4H), 3.18 (dt, *J* = 14.0, 7.0 Hz, 3H), 2.66 – 2.60 (m, 2H), 2.51 – 2.45 (m, 3H), 2.28 – 2.19 (m, 3H), 2.02 (d, *J* = 6.8 Hz, 6H), 1.83 – 1.72 (m, 3H), 1.62 (dq, *J* = 19.3, 6.4, 5.6 Hz, 3H), 1.53 (dt, *J* = 29.4, 6.3 Hz, 4H), 1.45 – 1.37 (m, 2H), 1.35 – 1.28 (m, 2H). HRMS (ESI) m/z: calc'd for $[M]^{6-}$ $C_{120}H_{187}O_{95}N_{11}S_8^{6-}$: 593.1329; Found: 593.1335.

**Synthesis of 33:** The general procedure for glycan conjugation on tripod was followed to afford **33** (1.1 mg, 58 %) as a white solid.$^1$H NMR (400 MHz, $D_2O$) δ 5.31 (s, 1H), 5.28 (d, *J* = 3.6 Hz, 1H), 4.49 (d, *J* = 7.9 Hz, 1H), 4.41 (d, *J* = 7.9 Hz, 1H), 3.92 (dd, *J* = 15.3, 9.5 Hz, 2H), 3.82 (dt, *J* = 9.0, 5.1 Hz, 5H), 3.73 (dt, *J* = 20.7, 9.5 Hz, 9H), 3.67 – 3.61 (m, 8H), 3.61 – 3.53 (m, 6H), 3.46 – 3.40 (m, 2H), 3.33 – 3.08 (m, 9H), 2.40 (t, *J* = 5.7 Hz, 3H), 2.15 (dt, *J* = 11.5, 6.7 Hz, 2H), 1.97 (d, *J* = 2.7 Hz, 6H), 1.93 – 1.88 (m, 1H), 1.78 – 1.70 (m, 4H), 1.59 – 1.52 (m, 2H), 1.51 – 1.39 (m, 3H), 1.38 – 1.29 (m, 2H), 1.28 – 1.21 (m, 3H). HRMS (ESI) m/z: calc'd for $[M]^{6-}$ $C_{120}H_{194}O_{77}N_{11}S_2$: 3085.1044; Found: 3085.1037.

## iii) Synthesis of gold nanoparticles

Sphere shape gold nanoparticles were synthesized according to the previously reported procedure.[3] In detail, to the boiling solution of 300 µl of 1% chloroauric acid in 30 mL of distilled water added 300 µl of 1% citric acid was added to get 25 nm of sphere gold nanoparticles. Resulting solution was refluxed until the colour of the boiling solution changes from dark purple to the red vine. The nanoparticles solution was cooled, centrifuged, and the pellet was washed with distilled water. The nanoparticles were characterized by HRTEM and UV-vis spectrophotometry.

### iv) Synthesis of GAG-nanoprobes

Thiol-modified tripodal CS and HS saccharides were conjugated directly onto the surface of spherical AuNPs using a simple ligand exchange method under sterile condition. Briefly, Spherical AuNPs (1000 µg) were dispersed in PBS buffer pH 7.4 (1 mL, 0.1 M), to this tripod (**29-35** 500 µg) was added. The resulting solution was kept at 25 ºC for 24 h with constant shaking. Finally solution was centrifuged and pellet was washed three times with Mili Q water followed by purification using 3 KD cuttoff centrifugal filtration to get **Au@CS0S, Au@CS3S, Au@CS6S, Au@CS46S, Au@HS0S, Au@HS3S, Au@HS6S**. A change in zeta potential confirmed functionalization of the tripod on AuNP surface. Qunatification of antigen loading on AuNP surface was determined by a thiol detection kit (Cayman chemicals, USA).

Further **Au@CS0S, Au@CS3S, Au@CS6S, Au@CS46S, Au@HS0S, Au@HS3S, Au@HS6S** AuNPs were functionalized with fluorescent linker by adding fluorescent linker F-1 (15 µg) to solution of these AuNPs in PBS buffer pH 7.4 (1 mL, 0.1 M). The resulting solution was kept at 25 ºC for 12 h under constant shaking. Solution was centrifuged and pellet was washed three times with Mili Q water followed by purification using 3 KD cuttoff centrifugal filtration to get **AuF@CS0S, AuF@CS3S, AuF@CS6S, AuF@CS46S, AuF@HS0S, AuF@HS3S, AuF@HS6S**.

## b) Biological study of glyconanoprobes for targating caner and neural cells

### i) Secondary cell lines

| **Cell lines** | **Growth Media** |
|---|---|
| MDA-MB 231, MDA-MB-468, T-47D, MCF-7, SL-BR-3 SHSY-5Y and U87 | All cells were grown at 37 ºC in 5% CO2 in DMEM medium containing 10 % fetal bovine serum and 0.1 % streptomycin |

### ii) Isolation and characterisation of primary neural cells

**Primary Neuronal Culture**

Wild-type postnatal mice specimens (neonatal p0/p1, N = 36) were used to optimize and establish primary neuronal cultures of the murine olfactory bulb and hippocampus. All animal

care and procedures were in accordance with the Institutional Animal Ethics Committee (IAEC) at IISER Pune and the Committee for the Purpose of Control and Supervision of Experiments on Animals (CPCSEA), Government of India.

**Preparation**

The day prior to isolation, appropriately sized tissue culture plasticware was coated with a 1X poly-D-lysine solution for proper cell attachment to the plate. All dissection tools were sterilized prior to use and the tissue harvesting was performed under a stereomicroscope.

**Tissue Harvesting**

The pup was decapitated using scissors, the skin and cranium were opened from the back of the neck to the nose in order to completely remove the skull. The entire brain was removed and placed onto a sterile petri dish with HBSS. The olfactory bulb appears as two small lobes on the rostral end of the brain, protruding from the cerebral hemispheres. The OB was dissected from the brain, the tissue was minced and collected in HBSS.

The cerebellum was removed from the caudal side of the brain and the brain was separated into two hemispheres by making an incision down the midline. The midbrain, thalamus, and hypothalamus tissue were removed by placing each of the hemispheres with their medial side facing up, allowing us to visualize the hippocampus and the cortex. The hippocampus is a flat, curved structure that begins in the distal part of the hemisphere and curves towards the ventral side. It is free from attachment towards its concave (caudal) side; the hippocampal tissue was separated by cutting along the convex outer side which is attached to the cortex. Each of the brain hemispheres was utilized to harvest two hippocampi from one individual, and the tissue was minced on a spatula and collected in HBSS.

**Tissue Dissociation**

The OB and Hippocampal tissues were allowed to settle in the HBSS. The supernatant is removed and 1ml of 0.25% Trypsin is added for dissociation. The tissues were then placed in the incubator at 37°C and 5% CO2 for 15 minutes after trituration. Following the incubation, 3ml of serum enriched neurobasal complete media (10%, NB+FBS) at room temperature is added to each of the tubes containing the neuronal tissue. The neuronal cells were triturated and were

subjected to centrifugation at 4°C, 1000rpm for 10 minutes. After separating the supernatant media, 5ml of wash buffer (3.3% Hepes + 1% PenStrep in HBSS) was added to the cells and trituration was performed again. The cells were centrifuged at 4°C, 1000 rpm for additional 10 minutes before separating the supernatant from the pellet of cells.

**Cell Plating**

1ml of NB+FBS media is added to the cells, and trituration was performed to obtain a more homogeneous cellular suspension. The cells in the culture were counted using a hemocytometer and the cells were plated in the appropriate tissue culture plasticware, roughly 600,000-800,000 cells/ml of suspension. Proper recommendations were followed for the optimal cell count and the plating volume for different culture surfaces such as 24 well plates, 8 well plates, 35mm coverslips, etc. Both the OB and Hippocampal cells were plated in NB+FBS media and placed in the incubator for approximately 8 hours to allow for cellular attachment to the tissue culture surface. Following the attachment of cells, the appropriate volume (determined by the dimensions of the well) of NB+FBS media was added to the primary OB neuron culture and similarly, serum-free NB complete media was added to the primary hippocampal neuronal culture as CM. The serum enriched media was removed completely after a period of 24 hours and replaced with NB complete media. The primary cell culture was fed and maintained by replacing 50% of the NB media after every 96 hours.

## iii) Purity of primary cell culture

For ensuring the purity of the primary cultures and characterizing the cells, the following steps were performed:

**Using serum-controlled culture media**

By limiting the concentration of FBS in the plating and feeding media for the cell culture, we were able to inhibit the proliferation of glial cells in the culture. The optimal FBS concentration for culture media was determined after several iterations of testing and 2% FBS in Neurobasal complete media was found to be the most effective serum concentration for the growth of primary neurons in the culture without contamination by other cell types.

**Characterization using neuronal markers**

The primary neuronal cultures of the olfactory bulb and hippocampus were established using pre-established protocols that were developed and tested in the LNCB at IISER Pune. The cell cultures had already been characterized using neuronal markers. The neuronal cultures were grown on sterile coverslips and fixed using 4%PFA. After fixation of the neurons, the non-specific sites were blocked using a blocking buffer consisting of normal goat serum and triton-x. Anti-MAP-2 Antibody (1:1500, ab92434), a widely used neuronal cytoskeletal marker was added to the cells and kept overnight at 4°C. Goat anti-chicken Alexa Fluor 647 was used as the secondary antibody (1:500). This antibody staining was performed specifically to visualize the morphology of neurites and DAPI (4′,6-diamidino-2-phenylindole) staining was performed to visualize the cellular nuclei. (Figure 11)

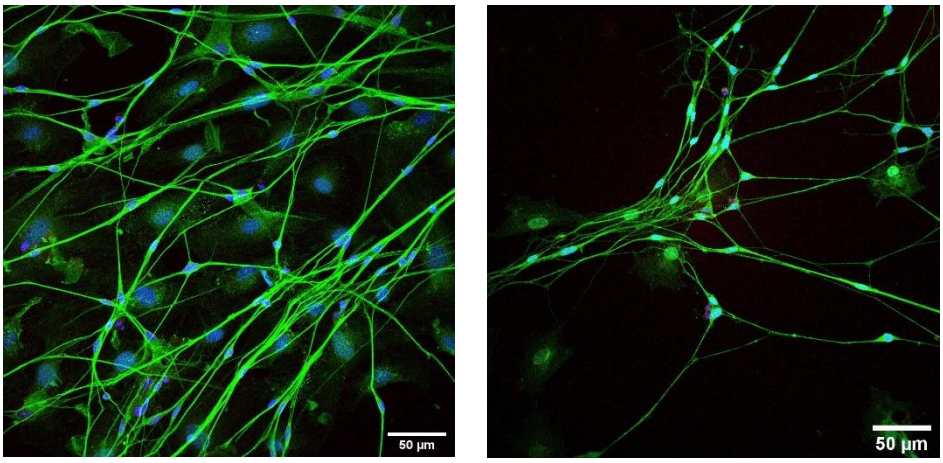



**Figure 11:** Olfactory bulb primary neuronal cultures stained with MAP2 antibody (green) and DAPI (blue)

## iv) Confocal Imaging

$2 \times 10^4$ cells were seeded on poly-D-lysine coated coverslip emersed in growth media and incubated at 37 ºC for overnight. The cells were incubated with CS/HS tripod functionalised AuNPs (10 µg/ml) for different time intervals 2 h and 4 h. Then the cells were washed with the cold PBS and fixed with 4% paraformaldehyde at room temperature for 10 min followed by 3X washings with PBS and water and mounted on a slide using mounting medium. The fluorescent images were taken using Leica sp8 microscope.

## v) FACS analysis

U87 cells ($2 \times 10^6$ cells) were seeded in 96 well plates in MEM media and incubated at 37 ºC for overnight. The cells were pulsed with CS/HS tripod functionalized AuNPs (10µg/ml) for 4 h. The cells were washed with PBS to remove noninternalized AuNPs, trypsinzed, and finally resuspended in FACS buffer and preceded for analysis. Quantification of uptake was done by using Flowjo software.

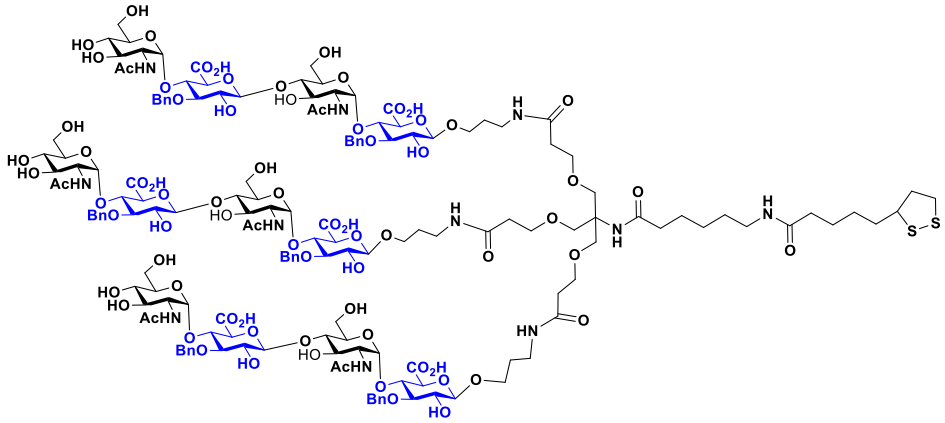
### vi) CD44 receptor expression level

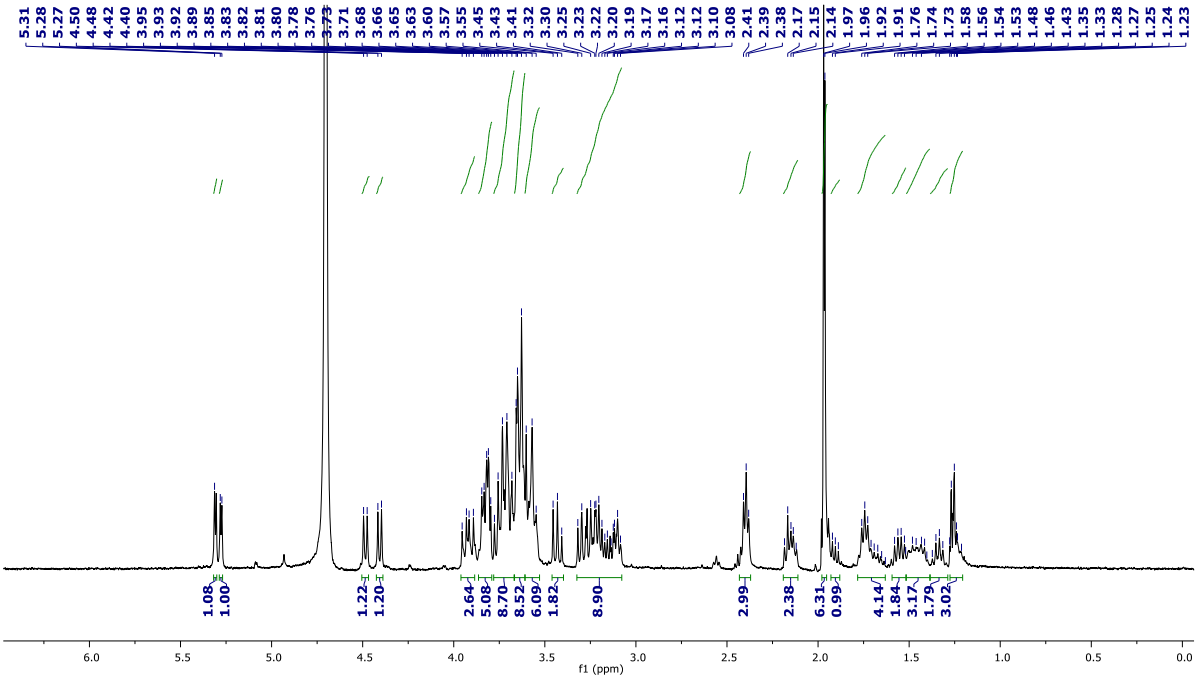
All cells ($2 \times 10^6$ cells) were seeded in 8 well plates in respective growth media and incubated at 37 ºC for overnight. The cells were pulsed with FITC-CD44 Monoclonal Antibody (IM7) for 4 h. Then cells were washed and nuclei were stained with Hoechst 33342 and taken for imaging.

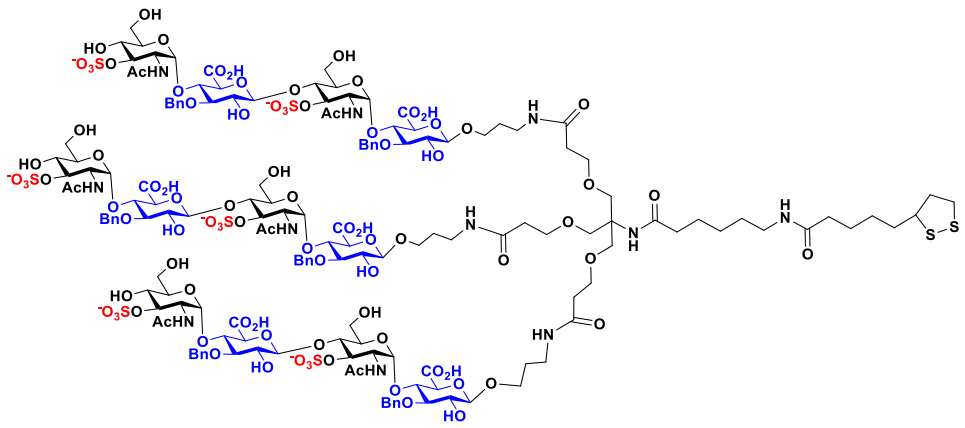
### vii) Cellular uptake mechanism studies

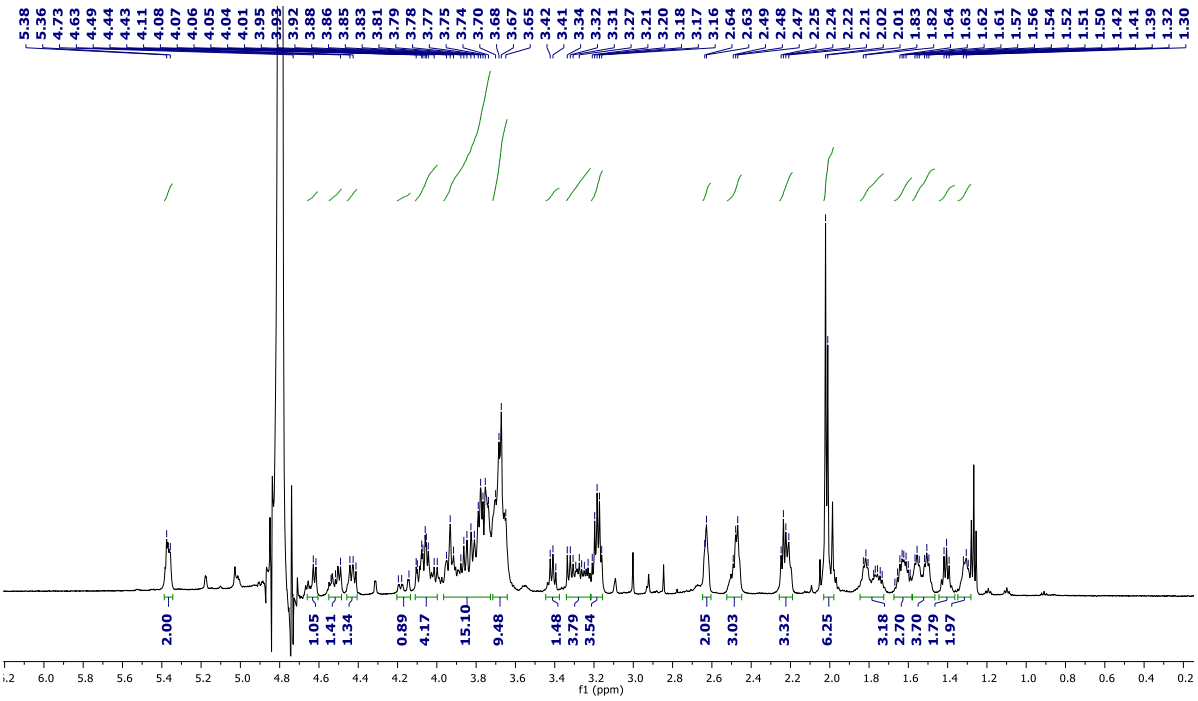
To study cellular internalization mechanism U87 cells were grown in an 8-well chamber cover glass ($1 \times 10^4$ cells per well) overnight and treated with the specific inhibitor for 30 min followed by treatment with **AuF@CS46S** (10µg/ml) for 4 h at 37 °C. For the energy dependent, dynamin-mediated, clathrin mediated, caveolae mediated study cells were incubated for 30 min with $NaN_3$ (50 mM), dynasore hydrate (50 µM), chlorpromazine (25 µM) and methylated-β-cyclodextrin (10 mM) respectively. After 4 h of treatment of **AuF@CS46S**, the cells were washed to remove unbound materials and taken for imaging.

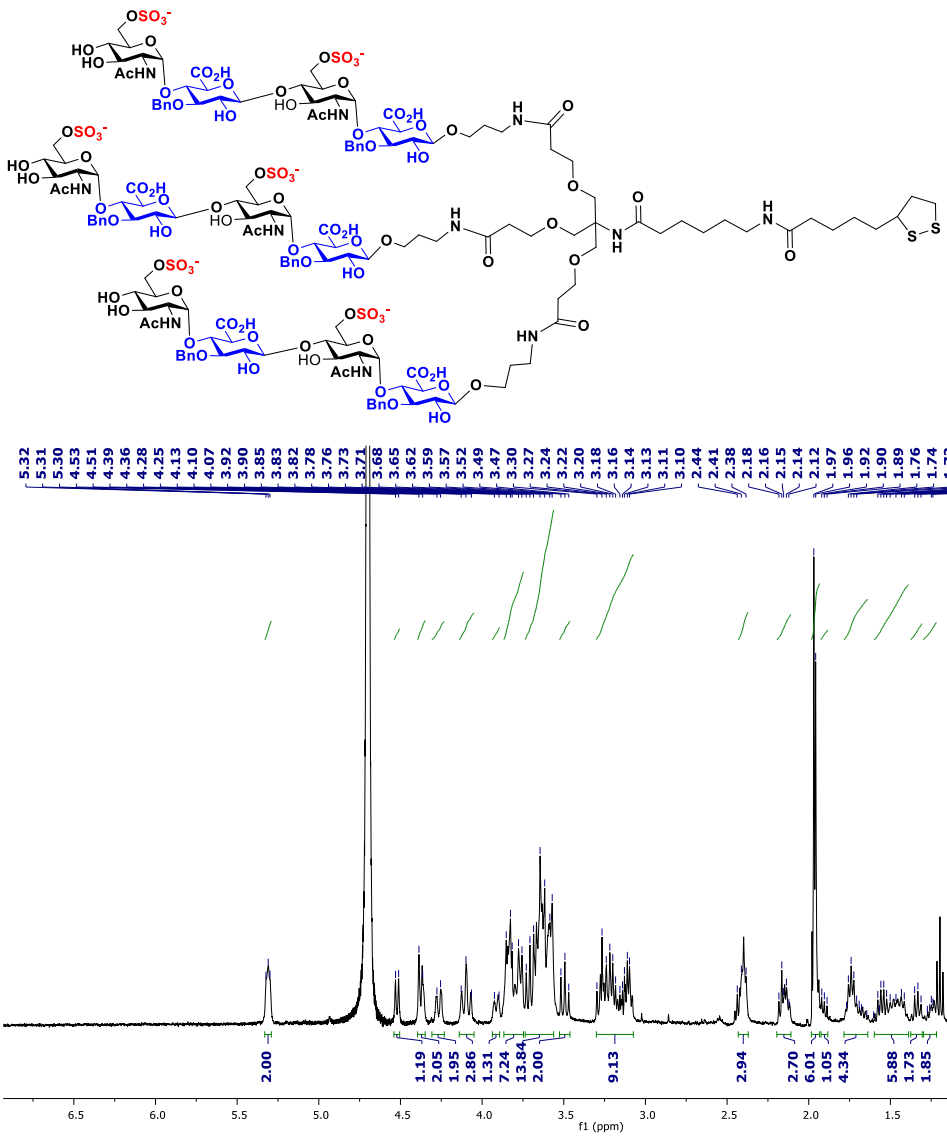
## 3.6 NMRs




5.31 5.28 5.27 4.50 4.48 4.42 4.40 3.95 3.93 3.92 3.89 3.85 3.83 3.82 3.81 3.80 3.78 3.76 3.73 3.71 3.68 3.66 3.65 3.63 3.60 3.57 3.55 3.45 3.43 3.41 3.32 3.30 3.25 3.23 3.22 3.20 3.19 3.17 3.16 3.12 3.12 3.10 3.08 2.41 2.39 2.38 2.17 2.15 2.14 1.97 1.96 1.92 1.91 1.76 1.74 1.73 1.58 1.56 1.54 1.53 1.48 1.46 1.43 1.35 1.33 1.28 1.27 1.25 1.24 1.23
1.08 1.00 1.22 1.20 2.64 5.08 8.70 8.52 6.09 1.82 8.90 2.99 2.38 6.31 0.99 4.14 1.84 3.17 1.79 3.02
6.0 5.5 5.0 4.5 4.0 3.5 3.0 2.5 2.0 1.5 1.0 0.5 0.0
f1 (ppm)




5.38 5.36 4.73 4.63 4.49 4.44 4.43 4.11 4.08 4.07 4.06 4.05 4.04 4.01 3.95 3.93 3.92 3.88 3.86 3.85 3.83 3.81 3.79 3.78 3.77 3.75 3.74 3.70 3.68 3.67 3.65 3.42 3.41 3.34 3.32 3.31 3.27 3.21 3.20 3.18 3.17 3.16 2.64 2.63 2.49 2.48 2.47 2.25 2.24 2.22 2.21 2.02 2.01 1.83 1.82 1.64 1.63 1.62 1.61 1.57 1.56 1.54 1.52 1.51 1.50 1.42 1.41 1.39 1.32 1.30
2.00 1.05 1.41 1.34 0.89 4.17 15.10 9.48 1.48 3.79 3.54 2.05 3.03 3.32 6.25 3.18 2.70 3.70 1.79 1.97
f1 (ppm)



## 3.7 References


[1] J. M. de la Fuente, A. G. Barrientos, T. C. Rojas, J. Rojo, J. Cañada, A. Fernández, S. Penadés. *Angew. Chem. Int. Ed Engl.* **2001,** *40*, 2257-2261.

[2] a) C. Fasting, C. A. Schalley, M. Weber, O. Seitz, S. Hecht, B. Koksch, J. Dernedde, C. Graf, E. W. Knapp, R. Haag. *Angew. Chem. Int. Ed. Engl*. **2012**, *51*, 10472-10498; b) Haag R. *J. Org. Chem.* **2015**, *11*, 848-849.

[3] a) W. Ma, HT. Liu, XP. He, Y. Zang, J. Li, GR. Chen, H. Tian, YT. Long. *Anal. Chem.* **2014**, *86*, 5502-5507; b) L. Wang, Y. Zhang, H. He, H. Yang, W. Wei. *Chem. Commun. (Camb)*. **2018**, *54*, 7754-7757.

[4] a) C. L. Schofield, R. A. Field, D. A. Russell. *Anal. Chem.* **2007**, *79*, 1356-1361; b) V. Poonthiyil, VB. Golovko, AJ. Fairbanks. *Org. Biomol. Chem.* **2015**, *13*, 5215-23; c) F. Y. Kuo, B. Y. Chang, C. Y. Wu, K. K. Mong, Y. C. Chen. *Anal. Chem*. **2015**, *87*, 10513-10520.

[5] a) D. Budhadev, E. Poole, I. Nehlmeier, Y. Liu, J. Hooper, E. Kalverda, U. S. Akshath, V. Hondow, W. B. Turnbull, S. Pöhlmann, Y. Guo, D. Zhou. *J. Am. Chem. Soc*. **2020**, *142*, 18022-18034; b) R. Kikkeri, B. Lepenies, A. Adibekian, P. Laurino, P. H. Seeberger. *J. Am. Chem. Soc.* **2009**, *131*, 2110-2112; c) A. J. Cagnoni, J. M. Pérez Sáez, G. A. Rabinovich, K. V. Mariño. *Front. Oncol*. **2016**, *6*, 109.

[6] a) C. L. Schofield, M. J. Marín, M. Rejzek, P. R. Crocker, R. A. Field, D. A. Russell, *Analyst.* **2016**, *141*, 5799-5809; b) C. H. Lai, J. Hütter, C. W. Hsu, H. Tanaka, S. Varela-Aramburu, L. De Cola, B. Lepenies, P. H. Seeberger. *Nano. Lett*. **2016**, *16*, 807-811; c) C. W. Hsu, D. Septiadi, C. H. Lai, P. Chen, P. H. Seeberger, L. De Cola. *Chempluschem.* **2017**, *82*, 660-667; d) H. Y. Li, H. C. Lin, B. J. Huang, A. Z. Kai Lo, S. Saidin, C. H. Lai. *Langmuir*. **2020**, *36*, 11374-11382; e) J. Ashree, Q. Wang, Y. Chao. *Front. Chem. Sci. Eng.* **2020**, *14*, 365–377.

[7] a) P. M. Chaudhary, S. Sangabathuni, R.V. Murthy, A. Paul, H. V. Thulasiram, R. Kikkeri. *Chem. Commun. (Camb).* **2015**, *51*, 15669-15672; b) S. Sangabathuni, R. Vasudeva Murthy, P. M. Chaudhary, M. Surve, A. Benerjee, R. Kikkeri. *Nanoscale*, **2016**, *25*, 12729-12735.

[8] a) D. Arosio, F. Chiodo, J. J. Reina, M. Marelli, S. Penadés, Y. Van Kooyk, J. J. Garcia-Vallejo, A. Bernardi. *Bioconjugate Chem*. **2014**, *25*, 2244-2251; b) Y. Guo, I. Nehlmeier, E. Poole, C. Sakonsinsiri, N. Hondow, A. Brown, Q. Li, S. Li, J. Whitworth, Z. Li, A. Yu, R.

Brydson, W. B. Turnbull, S. Pöhlmann, D. Zhouet. *J. Am. Chem. Soc*. **2017**, *139*, 11833-11844.

[9] a) M. Marradi, F. Chiodo, I. García, S. Penadés. *Chem. Soc. Rev.* **2013**, *42*, 4728–4745; b) F. Kveton, A. Blsakova, P. Kasak, J. Tkac. *Nanomaterials.* **2020**, *7*, 1406–1430; c) S. A. Torres-Pérez, C. E. Torres-Pérez, M. Pedraza-Escalona, S. M. Pérez-Tapia, E. Ramón-Gallegos. *Front. Oncol.* **2020**, *10*, 1–10.

[10] a) P. M. Chaudhary, S. Toraskar, R. Yadav, A. Hande, R. A. Yellin, R. Kikkeri. *Chem Asian J.* **2019**, *14*, 1344-1355; b) D. Ganesh, P. Jain, C. D. Shanthamurthy, S. Toraskar, R. Kikkeri. *Front Chem.* **2021**, *9*, 773027; c) M. del P. Rodriguez-Torres, L. S. Acosta-Torres, L. A. Diaz-Torres. *J. Nanomater.* **2018**, *8*, 1-8; d) M. M. Kemp, R. J. Linhardt. *Wiley Interdiscip Rev Nanomed Nanobiotechnol.* **2010**, *2*, 77-87; e) M. Nurunnabi, Z. Khatun, W. C. Moon, G. Lee, Y. K. Lee. *Quant. Imaging Med. Surg*. **2012**, *2*, 219-226.

[11] X. Wang, Y. Xie, N. Jiang, J. Wang, H. Liang, D. Liu, N. Yang, X. Sang, Y. Feng, R. Chen, Q. Chen. *ACS Appl. Mater. Interfaces*, **2021,** *1*, 287-297.

[12] S. Samanta, V. L. Joncour, O. Wegrzyniak, V. K. Rangasami, H. Ali-Löytty, T. Hong, Ram K. Selvaraju, O. Aberg, J. Hilborn, P. Laakkonen, O. P. Varghese, O. Eriksson, H. Cabral, O. P. Oommen. *Adv. Ther*. **2022,** *6*, 2200001.

[13] Y. Hao, Y. Gao, Y. Wu, C. An. *Int. J. Mol. Med.* **2019**, *2*, 861–867.

[14] H. Du, M. Liu, A. Yu, J. Ji, G. Zhai. *Int. J. Pharm.* **2017,** *1*, 427-438.

[15] H. Sun, D. Cao, Y. Liu, H. Wang, X. Ke, T. Ci. *Biomater Sci.* **2018,** *6*, 2172-2188.

[16] H. Li, P. Zhang, J. Luo, D. Hu, Y. Haung, Z-R. Zhang, Y. Fu, T. Gong. *ACS Nano.* **2019**, *13*, 9386–9396.

[17] Z. Zhang, L. Ma, J. Luo. *Pharmaceutics*. **2021**, *13*, 406.

[18] a) P. Domínguez-Rodríguez, J. J. Reina, S. Gil-Caballero, P. M. Eito, J. L. De Paz, J. Rojo. *Chem. Eur. J.* **2017**, 23, 11338-11345; b) R. Novoa-Carballal, A. Carretero, R. Pacheco, R. L. Reis, I. Pashkuleva. *Chem. Eur. J.* **2018,** 24, 14341-14345.

[19] U. Lindahl, M. Kusche-Gullberg, L. Kjellen. *J. Biol. Chem*. **1998,** *273*, 24979-24982.

[20] E. Bedini, A. Laezza, A. Iadonisi. *Eur. J. Org. Chem*. **2016**, *18*, 3018-3043.

[21] P. Jain, C. Shanthamurthy, P. M. Chaudhary, R. Kikkeri. *Chem. Sci*. **2021**, *12*, 4021-4027.

[22] a) M. Mende, C. Bednarek, M. Wawryszyn, P. Sauter, M. B. Biskup, U. Schepers, S. Bräse. *Chem. Rev.* **2016**, *116*, 8193–8255; b) W. Lu, C. Zong, P. Chopra, L. E. Pepi, Y. Xu, I. J. Amster, J. Liu, G. J. Boons. *Angew. Chem., Int. Ed.* **2018**, *57*, 5340–5344; c) S. U. Hansen, G. J. Miller, M. J. Cliff, G. C. Jayson, J. M. Gardiner. *Chem. Sci.* **2015**, *6*, 6158–6164; d) Y. P. Hu, S. Y. Lin, C. Y. Huang, M. M. L. Zulueta, J. Y. Liu, W. Chang, S. C. Hung. *Nat. Chem.* **2011**, *3*, 557–563; e) X. Zhang, V. Pagadala, H. M. Jester, A. M. Lim, T. Q. Pham, A. M. P. Goulas, J. Liu, R. Linhardt. *J. Chem. Sci.* **2017**, *8*, 7932–7940; f) C. Noti, J. L. de Paz, L. Polito, P. H. Seeberger. *Chem. Eur. J.* **2006**, *12*, 8664–8686; g) J. L. de Paz, C. Noti, P. H. Seeberger. *J. Am. Chem. Soc.* **2006**, *128*, 2766–2767; **h)** Y. P. Hu, Y.Q. Zhong, Z. G. Chen, C. Y.Chen, Z. Shi, M. M. L. Zulueta, C. C. Ku, P. Y. Lee, C. C. Wang, S. C. Hung. *J. Am. Chem. Soc.* **2012**, *134*, 20722–20727; i) N. J. Pawar, L. Wang, T. Higo, C. Bhattacharya, P. K. Kancharla, F. Zhang, K. Baryal, C. X. Huo, J. L. Jian, R. J. Linhardt, X. H. Xuefei, L. C. Hsieh-Wilson. *Angew. Chem., Int. Ed.* **2019**, *58*, 18577–18583; j) R. S. Boothello, A. Sarkar, V. M. Tran, T. K. Nguyen, N. V. Sankaranarayanan, A. Y. Mehta, A. Alabbas, S. Brown, A. Rossi, A. C. Joice, C. P. Mencio, M. V. Quintero, B. Kuberan, U. R. Desai. *ACS Chem. Biol.* **2015**, *10*, 1485–1494; k) N. V. Sankarayanarayanan, T. R. Strebel, R. S. Boothello, K. heerin, A. Raghuraman, F. Sallas, P. D. Mosier, N. D. Watermeyer, S. Oscarson, U. R. Desai. *Angew. Chem., Int. Ed.* **2017**, *56*, 2312–2317; l) L. Sun, P. Chopra, G. J. Boons. *J. Org. Chem.* **2020**, *85*, 16082–16098; m) S. Arungundram, K. Al-Mafraji, J. Asong, F. E. Leach III, I. J. Amster, A. Venot, J. E. Turnbull, G. J. Boons. *J. Am. Chem. Soc.* **2009**, *131*, 17394–17405; n) C. H. Chang, L. S. Lico, T. Y. Huang, S. Y. in, C. L. Chang, S. D. Arco, S. C. Hung. *Angew. Chem., Int. Ed.* **2014**, *126*, 10034–10037; o) T. N. Laremore, F. Zhang, J. S. Dordick, J. iu, R. Linhardt. J. *Curr. Opin. Chem. Biol.* **2009**, *13*, 633–640; p) S. B. Dulaney, X. Huang. *Adv. Carbohydr. Chem. Biochem.* **2012**, *67*, 95–136; q) S. U. Hansen, G. J. Miller, G. C. Jayson, J. M. Gardiner. *Org. Lett.* **2013**, *15*, 88–91; s) X. Zhang, H. Liu, W. Yao, X. Meng, Z. Li. *J. Org. Chem*. **2019**, *84*,7418-7425; t) Torres-Rico, M. Maza, S. De Paz, J. L. Neito, P. M. *Org. Biomol. Chem*. **2021**, 19, 5312-5326; u) Garcia-Jimenez, M.J. Gil-Caballero, S. Maz, S. Carzana, F. Juarez-Vicente, F. Miles, J. R. Skamoto, K. Kadomatsu, K. Garcia-Dominguez, M. De Paz, J. L. Neito, P. M. *Chem. Eur. J.* **2021**, 27, 12395-12409; v) Solera, C. Macchione, G. Maza, S. Kayser, M. M. Corzana, F. De Paz, J. L. Neito, P. M. *Chem. Eur. J.* **2016**, 22, 2356-2369; w) S. Kőhling, J. Blaszkiewicz, G. Ruiz-

Gómez, M. S. Fernández-Bachiller, K. Lemnitzer, N. Panitz, A. G. Beck-Sickinger, J. Schiller, M. T. Pisabarro, J. Rademann. *Chem. Sci.* **2019**, 10, 866-878.

[23] a) P. Jain, C. Shanthamurthy, S. Leviatan Ben-Arye, R. J. Woods, R. Kikkeri, V. Padler-Karavani, *Chem. Sci.* **2021**, *12*, 3674-3681; b) B. Subramani, C. D. Shantamurthy, P. Maru, M. A. Belekar, S. Mardhekar, D. Shanmugam, R. Kikkeri, *Org. Biomol. Chem*. **2019**, *17*, 4535-4542; c) S. Anand, S. Mardhekar, R. Raigawali, N. Mohanta, P. Jain, C. D. Shanthamurthy, B. Gnanaprakasam, R. Kikkeri, *Org. Lett*. **2020,** *22*, 3402-3406; d) C. D. Shanthamurthy, S. Leviatan Ben-Arye, N. V. Kumar, S. Yehuda, R. Amon, R. J. Woods, V. Padler-karavani, R. Kikkeri, *J. Med. Chem.* **2021**, 64, 3367-3380; e) C. D. Shanthamurthy, A. Gimeno, S. Leviatan Ben-Arye, N. V. Kumar, P. Jain, V. Padler-Karavani, J. Jimėnez-Barbero, R. Kikkeri. *ACS Chem Bio.* **2021**, 16, 2481-2489.

[24] L. Zhang, P. Xu, B. Liu, B. Yu, *J. Org. Chem***. 2020**, *85*, 15908-15919.

[25] F. Compostella, O. Pitirollo, A. Silvestri, L.. Polito. *Beilstein J Org Chem.* **2017**, *13*,1008-1021.

[26] S. Toraskar, P. M. Chaudhary, R. Kikkeri. *ACS Chem. Biol*. **2022**, *17*, 1122-1130.

[27] a) E. Mandarini, E. Tollapi, M. Zanchi, L. Depau, A. Pini, J. Brunetti, L. Bracci, C. Falciani, *Int. J. Mol. Sci*. **2020**, *21*, 8282; b) H. Park, M. Kim, H. J. Kim, Y. Lee, Y. Seo, C. D. Pham, J. Lee, S. J. Byun, M. H. Kwon, *Sci. Rep*. **2017**, *7*, 14373.

[28] S. Sangabathuni, R. V. Murthy P. M. Chaudhary, M. Surve, A. Banerjee, R. Kikkeri, *Nanoscale* **2016**, *8*, 12729-12735.

[29] G. E. Konecny, M. D. Pegram, N. Venkatesan, R. Finn, G. Yang, M. Rahmeh, M. Untch, D. W. Rusnak, G. Spehar, R. J. Mullin, B. Keith, T.M. Gilmer, M. Berger, K. C. Podratz, D. J. Slamon, *Cancer Res*. **2006**, *66*, 1630-1639.

[30] a) M. Li, J. Sun, W. Zhang, Y. Zhao, S. Zhang, S. Zhang. *Carbohydr Polym*. **2021**, *251*,117103; b) M. Zhang, Y. Ma, Z. Wang, Z. Han, W. Gao, Q. Zhou, Y. Gu. *ACS Appl. Mater. Interfaces*. **2019,** *11*, 5851-5861; c) P. Kesharwani, R. Chadar, A .Sheikh, W. Y. Rizg, A. Y. Safhi. *Front. Pharmacol*. **2022**, *12*, 800481

# CHAPTER- 4

## Synthesis of Carbohydrate Based Adjuvants

## 4.1 Abstract

Toll-like receptors (TLRs) are one of the well characterized pattern recognition receptors (PRRs) in innate immune system cells. TLRs recognize danger-associated molecular patterns (DAMPs)—for example, fragments of glycosaminoglycans (GAGs) (heparan sulfate, chondroitin sulfate, and hyaluronic acids) thereby triggering pro-inflammatory and effector cytokines which help direct adaptive immune responses. However, GAGs exhibit highly sulfated complex polydisperse structures. There has been significant research interest in the identification of unique GAG DAMPs that activate the innate/adaptive immune system to combat infections. Accordingly, we synthesized a combinatorial library of heparinoids proposal and examines their ability to activate specific TLRs to induce the nuclear translocation of transcription factors. Ultimately, these potent adjuvantic immunostimulants will be used in subunit vaccine constructs for flaviviruses.

## 4.2 Introduction

Innate immune system cells recognize a wide range of molecular patterns derived from various pathogens to induce immune responses. Toll-like receptors (TLRs) are among the most studied of these pattern recognizing receptors (PRRs), and there are 10 TLRs in the human genome.[1] These trans-membrane/endolysosomal proteins comprise unique ectodomains with leucine-rich repeats to recognize pathogen-associated molecular patterns (PAMPs) and cytoplasmic Toll/IL-1 receptor (TIR) domains to propagate downstream signaling pathways.[2] During infection, for example, TLRs recognize PAMPs recruiting TIR domains that contain adaptor proteins such as MyD88 and TRIF to initiate signal transduction pathways.[3] Bacterial lipopolysaccharide (LPS), capsular polysaccharides (CPSs), flagellin, and CpG motifs in bacterial DNA are common PAMPs recognized by TLR4, TLR2, TLR5, and TLR9, respectively.[4] Upon PAMPs-TLRs interaction, transcription factors such as AP-1 and NF-κB and interferon regulatory factors (IRFs) are activated, leading to inflammatory response in the form of cytokines, chemokines, and interferons which help direct and orchestrate downstream pathogen-specific adaptive immune responses.[5]

In addition to PAMPs, TLRs also recognize danger-associated molecular patterns (DAMPs) such as heat shock proteins and extracellular protein fragments.[6] DAMPs are generally released upon tissue injury and cellular stress. Emerging evidence has indicated that DAMPs also play a pivotal role in inducing inflammation diseases.[7] As a result, the identification of specific DAMPs and the characterization of their inflammation responses could result in the discovery and development of novel vaccine adjuvants. In particular, extracellular matrix (ECM) components such as proteoglycans, glycosaminoglycans, and glycoproteins (fibronectin, fibrinogen, and tenascin-C) are critical DAMP molecules capable of activating the TLRs.[8]

Previously, Hsieh et al. have demonstrated the interactions of proteoglycans biglycan and decorin with TLR2 and TLR4 and the generation of pro-inflammatory responses in macrophages.[9] Elsewhere, Lees et al. report that aggrecan protein activates chondrocytes, synovial fibroblasts, and macrophages in a TLR2-dependent manner and also activate nitric oxide synthase, IL-1a, and IL-6 cytokines.[10] On the other hand, most glycosaminoglycans bind to TLRs to activate the innate immune system. For example, hyaluronic acid, a non-sulfated

glycosaminoglycan, induced TLR2/4-mediated responses and activated NF-κB pathways. In addition, chondroitin-6-*O*-sulfate activates macrophages which displays an anti-inflammatory effect and suppresses NF-κB nuclear translocation.[11]

Heparan sulfate (HS) fragments of perlecan (basement membrane), syndecans, and glypicans bind to TLR4 and activate pro-inflammatory cytokines. Preliminary studies by Lie et al have shown that heparanase treatment of immune cells results activating of TLRs.[12] Recently studies further demonstrated that HS bind to specific TLRs extracellular domains.[13] For instance, HS binds to TLR1, TLR2, TLR4, and TLR6 via the HRARH, IRRLHA, RHIFWRR, and YHKLRA and HRARH domains.[14] These results illustrate that HS-TLR binding is governed by sulfation pattern, uronic acid composition, and oligosaccharide length. Nevertheless, the structure of HS is highly heterogeneous and so there is no information about the specific HS specific composition preferentially mediate specific TLR activations. Careful examination of combinatorial libraries of structurally defined HS oligosaccharides and its monosaccharide would therefore not only be instructive in determining the precise structural requirements for innate immune recognition but would also provide detailed mechanistic insights on HS-TLR interactions.

### 4.3 Results and Discussion

#### 4.3.1 1st generation HS tetrasaccharides

In the first-generation HS library, we primarily focused on the design and synthesis of rare N-unsubstituted and N-acetylated HS tetrasaccharides. Using a divergent synthetic strategy, we developed a combinatorial library of HS oligosaccharides in 24-28 steps (Figure 1). All compounds were well characterized by using NMR and Mass spectroscopy techniques. The purity of all final compound was quantified by using HPLC and LC-MS. Then we tested their TLR4 and TLR2 agonist activity.

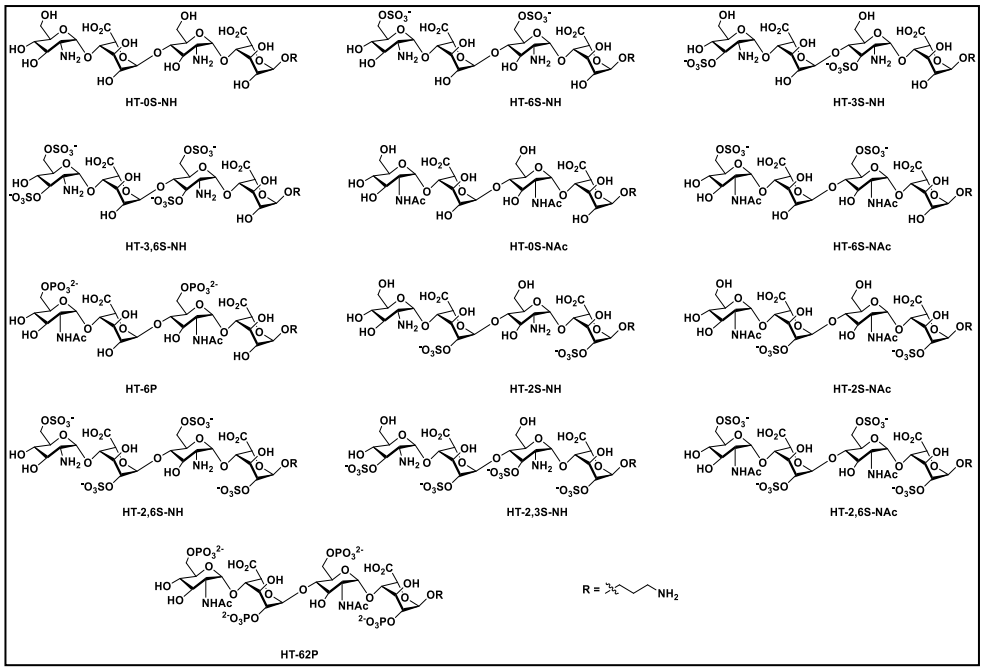



**Figure 1.** Structures of 1st generation heperinoids

### 4.3.2 TLR4 and TLR2 activity of HS oligosaccharides

The induction of NF-κB in a TLR2 and TLR4-specific reporter gene assay was quantified using HEK-Blue™ cells as previously described by Prof. Sunil David. HEK293 cells stably transfected with human TLR2 or TLR4 alkaline phosphatase (sAP) were obtained from InvivoGen (San Diego, CA), and were maintained in HEK-Blue™ Selection medium containing zeocin and normocin. Stable expression of secreted alkaline phosphatase (sAP) under control of NF-κB promoters is inducible by TLR2/4 agonists, and extracellular sAP in the supernatant is proportional to NF-κB induction. HEK-Blue cells were incubated at a density of ~105 cells/mL in a volume of 80 µL/well, in 384-well, flat-bottomed, cell culture-treated microtiter plates until confluency was achieved, and then stimulated with seriallydiluted aliquots of compounds (DMSO stock solutions) for 12 h. sAP was assayed spectrophotometrically using an alkaline phosphatase-specific chromogen (present in the HEKdetection medium as supplied by the vendor) at 620 nm. Our results showed that out all HS analogs only HS-3S-NH showed promising TLR4 agonist activity as compared to all other analogs (Figure 2). However, the activity is in millmolar range. To improve that we need to increase the oligosaccharide chain length and modify with $NH_2$ group with more positively charged substrates.

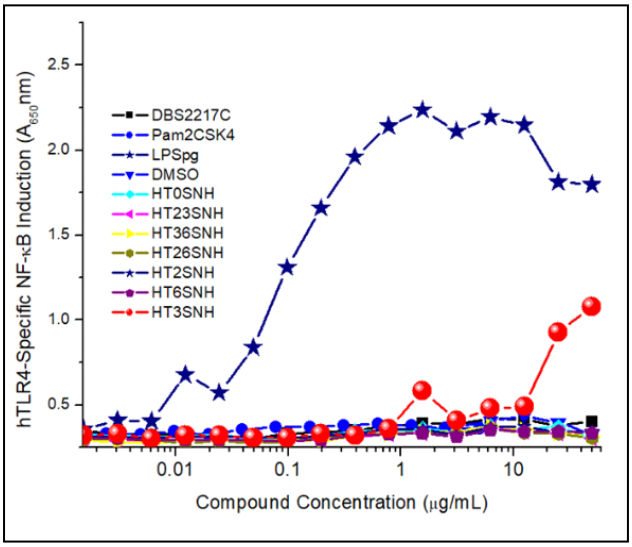



**Figure 2.** hTLR4 activity of 1st generation heparinoids.

### 4.3.3 Monosaccharide and disaccharide derivatives

Nucleotide-binding oligomerization-domain-containing protein 2 (NOD2) belongs to the intracellular NOD-like receptor family of PRRs, which sense bacterial cell wall peptidoglycan fragments that enter the cytosol. The minimal essential peptidoglycan substructure that can activate NOD2 is muramyl dipeptide (MDP), a glycopeptide in the cell wall of both Gram-positive and Gram-negative bacteria. MDP comprises N-acetylmuramic acid (MurNAc) and an L-alanine-D-isoglutamine dipeptide, which is attached to the MurNAc via a lactic acid spacer. Here, we integrate the MurNAc structure with glucosamine derivative with positive and negative charge species and check their TLR4/2 activity. A combinatorial library of glucosamine, glucose, galactose, glucuronic acid and iduronic acid derivatives were synthesized and tested their TLR4/2 activity (Figure 3).

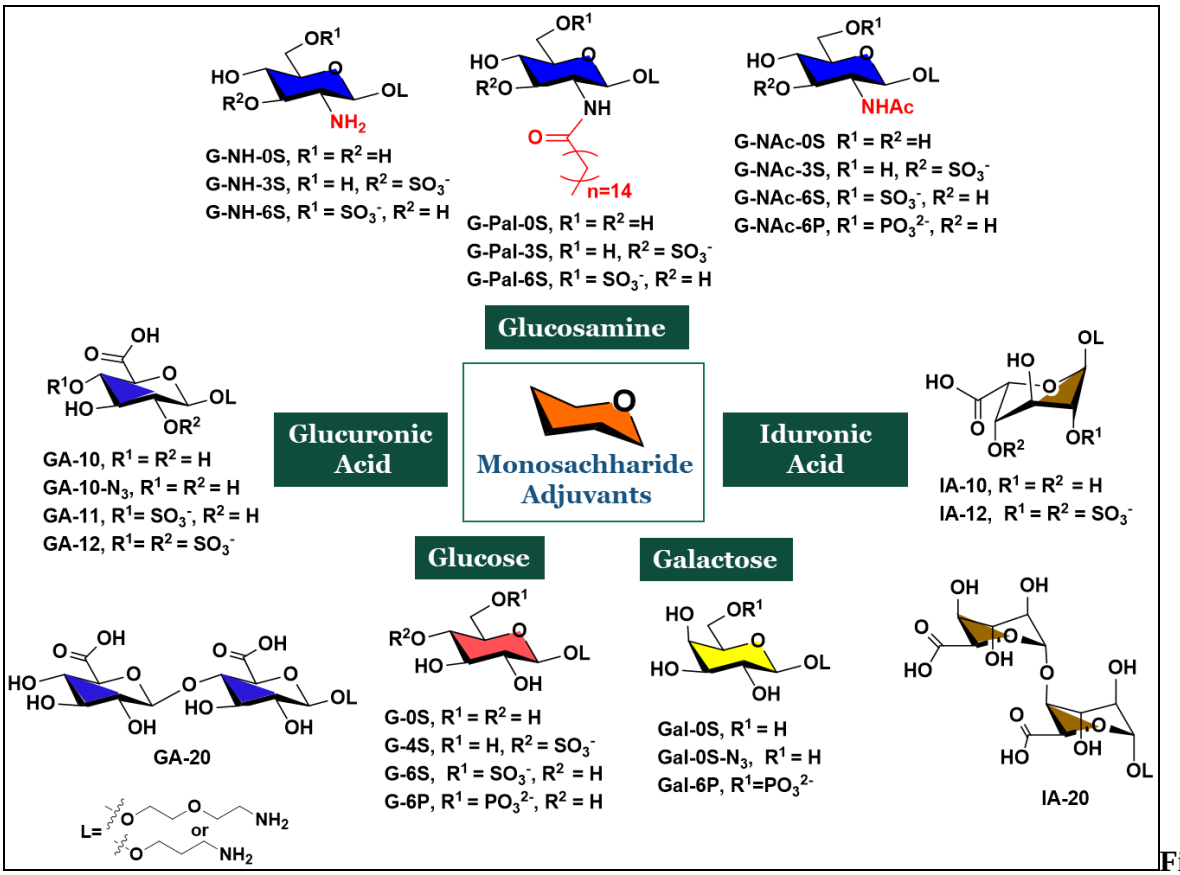
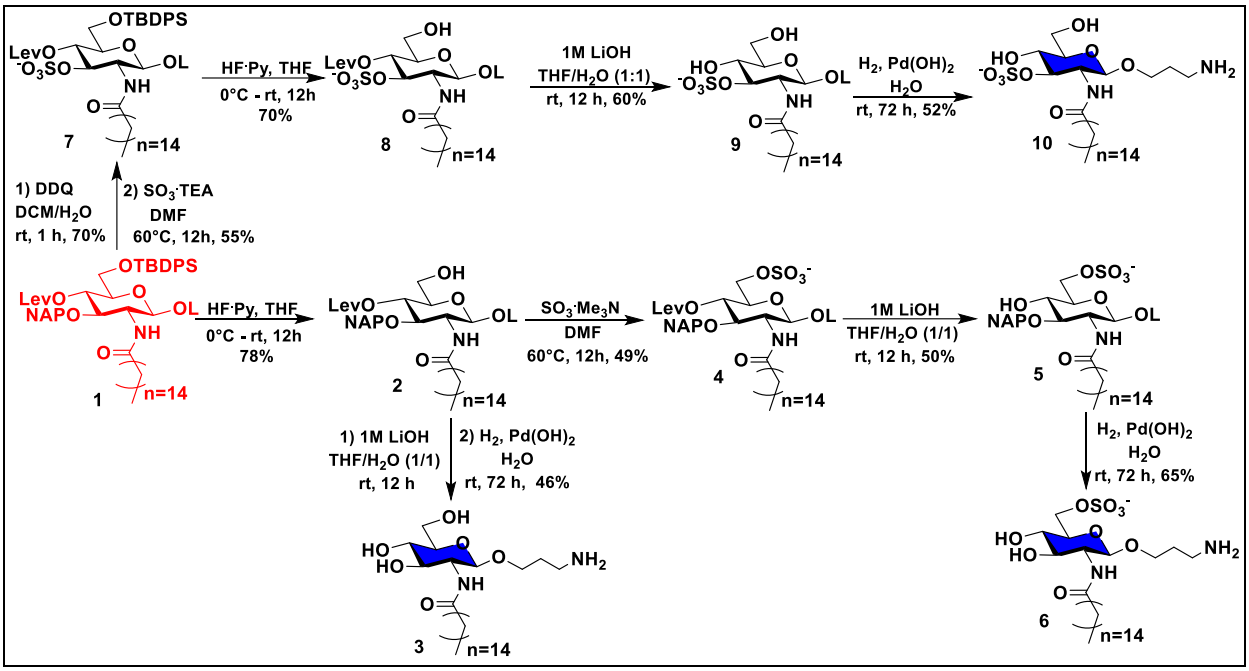



**Figure 3.** Structures of monosaccharide heparinoid derivatives

### 4.3.4 Synthesis of *N*-palmitic acid conjugated glucosamine derivatives

Palmitic acid conjugated glucosamine library with regioselective sulfation were obtained by fully protected precursor **1** (scheme 1). Next, silyl protecting group TBDPS was deprotected selectively using 70% HF.py to get the compound **2** next sulfation carried out by using $SO_3.Me_3N$ for 6-*O*-sufate derivative **4**, similarly, NAP was deprotected by using DDQ for 3-*O*-sulfate derivative **7**. Finally global deprotection of **4** by using 1M LiOH and $H_2$, $Pd(OH)_2$ yeilded desired derivative **6**. Whereas 3-*O*-sulfted compound 7 treated with HF-py for TBDPS protecting group followed by global deprotection to get the desired product **10**. Finally global deprotection of compound 2 yeilded non sulphated derivative **3**.

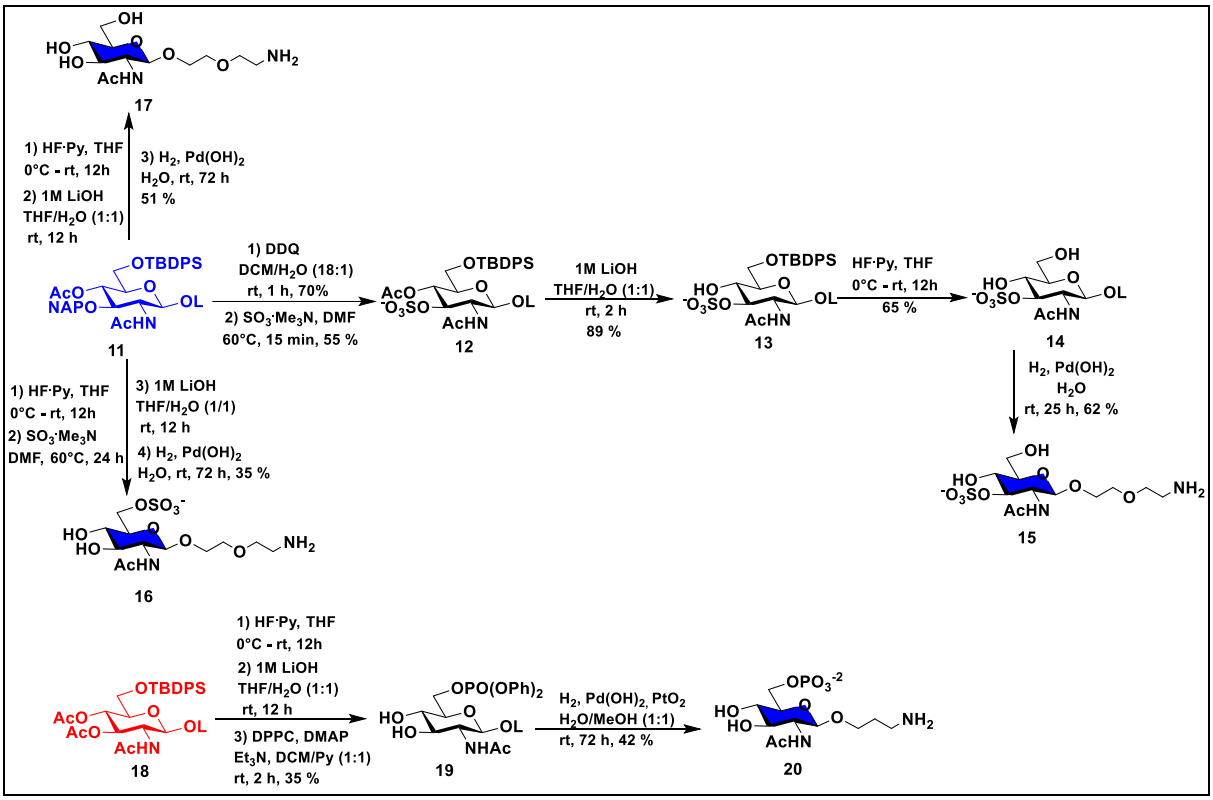



**Scheme 1:** Synthesis of palmitic acid conjugated glucosamine (G-Pal) derivatives.

### 4.3.3 Synthesis of *N*-acetate glucosamine derivatives:

In case of acetate conjugated glucosamine derivatives, glucosamine precursor **11** has treated with 70% HF.py, DDQ for TBDPS and NAP deprotection selectively followed by sulfation with $SO_3$.$Me_3N$ for selective sulfation, finally global deprotection of all sulfated and nonsulfated derivatives get the desired 3-*O*-sulphated **15**, 6-*O*-sulfated **16** and nonsulfated **17** acetate modified derivatives.

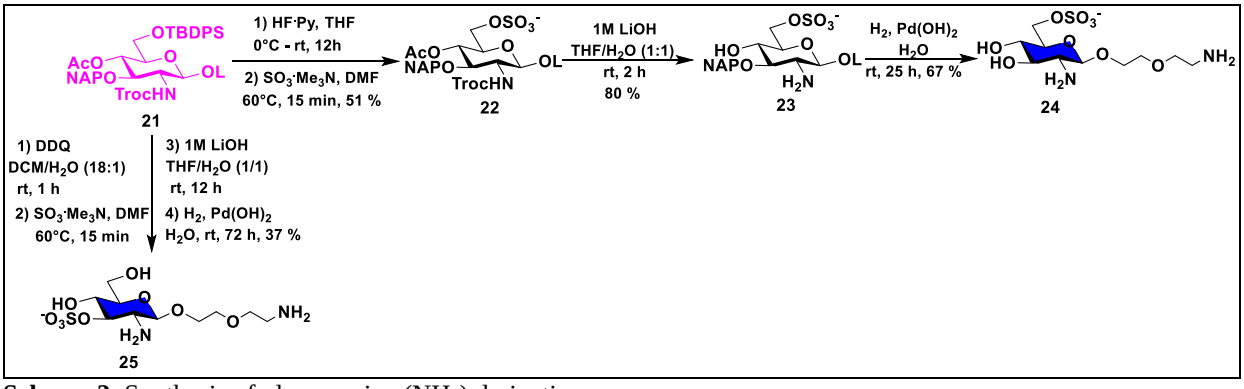
whereas for the phosphate derivative **20,** precursor **18** has tereated with 70% HF.py and 1M LiOH for TBDPS and acetate group deprotection respectively which further treated with diphenylphsphoryl chloride (DPPC) to get compound **19** finaly hydrogenation with $H_2$, $Pd(OH)_2$, $PtO_2$ yeilded 6-*O*-phophorylated acetate conjugated glucosamine derivative **20** in 42% yeild.




**Scheme 2:** Synthesis of acetate conjugated glucosamine (G-NH) derivatives.

### 4.3.4 Synthesis of *N*-unsubstituted glucosamine derivatives:

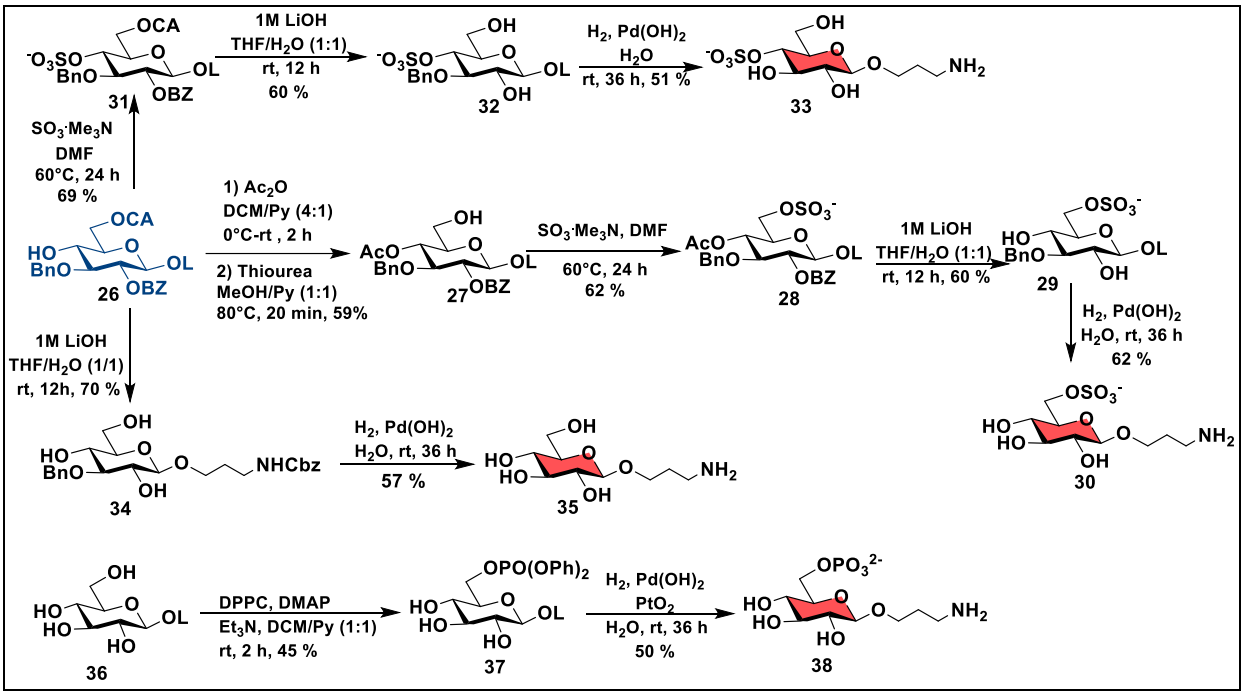
Next for glucosamine 3 and 6-*O*-sulfated derivatives precursor **21** treated with 70% HF.py, and DDQ for TBDPS and NAP deprotection respectively finally global deprotection yielded **24** with 67% yield and **25** with 37% yield over four steps.




**Scheme 3**: Synthesis of glucosamine ($NH_2$) derivatives.

### 4.3.5 Synthesis of glucose derivatives

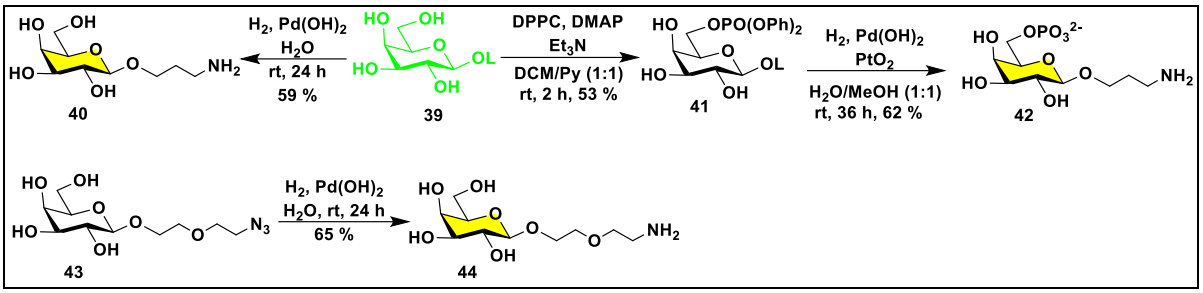
D-Glucose derivatives were synthesised from precursor **26**, for 6-*O*-sulftion compound **11** was treated with $Ac_2O$ for acetate protection and thenchloroacetate deprotection by uding thiourea to get compound **27** which was further sulfated and after global deprotection yielded **30** with 62% yeild. For another 3-*O*-sufated derivative **26** has treated with $SO_3.Me_3N$ followed by global deprotection yielded 3-*O*-sulfated D-glucose derivative **33** with 51% yeild. Similarly nonsulfated D-glucose derivative synthesised by same precursor after global deprotection yielded **35** with 57% yeild. Subsequently 6-*O*-phosphorylated compound synthesis by 36 using diphenylphsphoryl chloride (DPPC) to get compound **38** with 50% yield after hydrogenation by using $H_2$, $Pd(OH)_2$, $PtO_2$.




**Scheme 4:** Synthesis of glucose (Glu) derivatives.

### 4.3.6 Synthesis of galactose derivatives

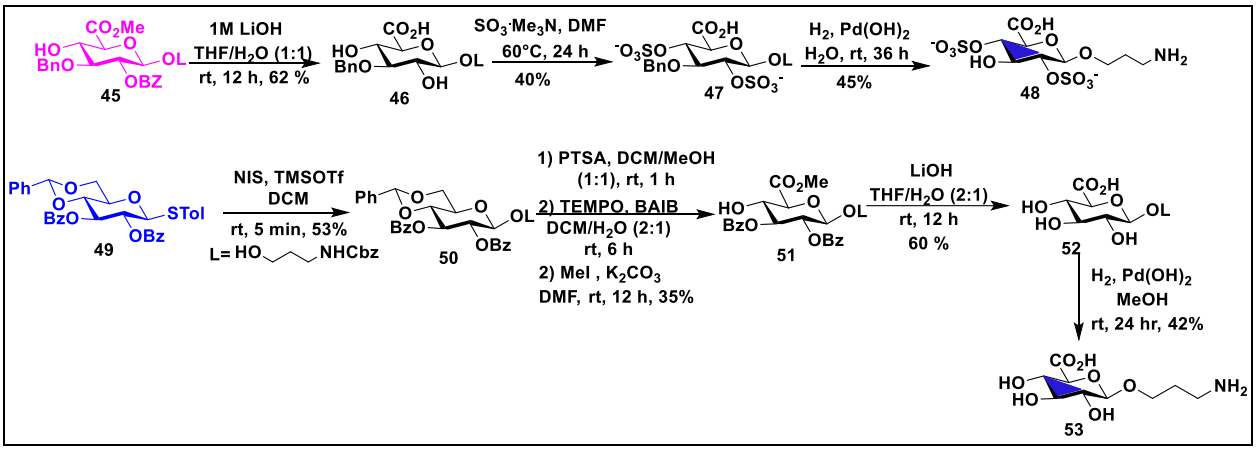
Similarly galactose 6-*O*-phosphorylated **42** with 62% yeild and nonsulfted **40** with 59% yeild derivatives synthesised by using compound **40.**



**Scheme 5:** Synthesis of galactose (Gal) derivatives.

### 4.3.7 Synthesis of glucuronic acid derivatives

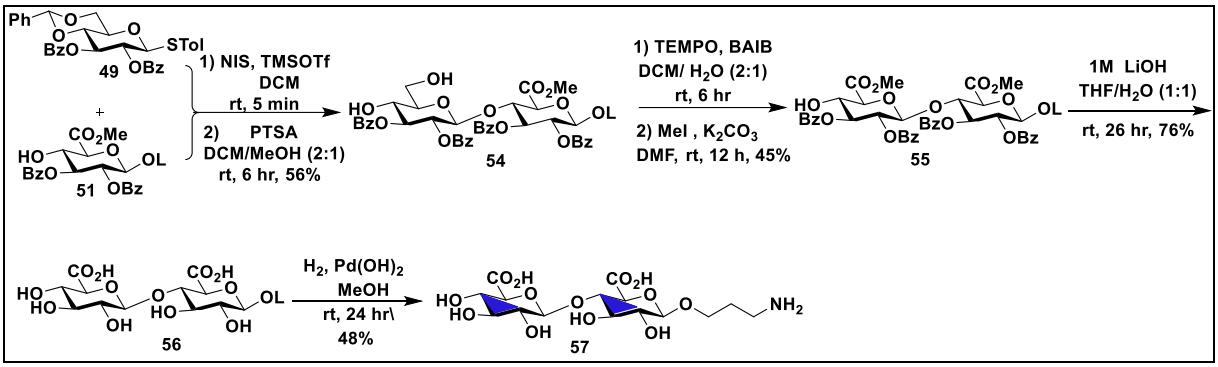
In case of glucuronic acid derivaties, started with comound **45** which was treated with 1M LiOH to get the compound **46** which followed by sulfation and hydrogenation to yeild **48** with 45%. For nonsulfated derivative compound **49** used as sarting glucose and then linker glycosylation by using NIS and TMSOTf followed by benzilidene deprotection and oxidation esterification which lead to compound **51**, finally global deprotection of **52** yeilds final nonsulfated compound **53** with 42% yield.



**Scheme 6:** Synthesis of glucuronic acid monosachharide (GA) derivatives.

### 4.3.8 Synthesis of glucuronic acid disachharide derivatives

Lastly, for disachharide derivtives compound **49** and **51** used ass a donor and acceptor for glycosylation further bezilidene deprotection leads to **54**. Next oxidation by using TEMPO BAIB and esterification by MeI, $K_2CO_3$ got **55** finally after global deprotection of compound **55** yields **57** nonsulfated glucuronic acid disaccharide derivative with 48% yeild.




**Scheme 5:** Synthesis of glucuronic acid disachharide (GA) derivatives.

Iduronic acid derivatives has synthised as previously reported.

### 4.3.9 TLR agonist activity of monosaccharide derivatives

Our results showed that iduronic acid monosaccharide with amine and 2nd amine linker showed promising TLR agonist activity. Further cytokine secretion studies and potential application of these molecule as adjuvant is under progress (Figure 4).

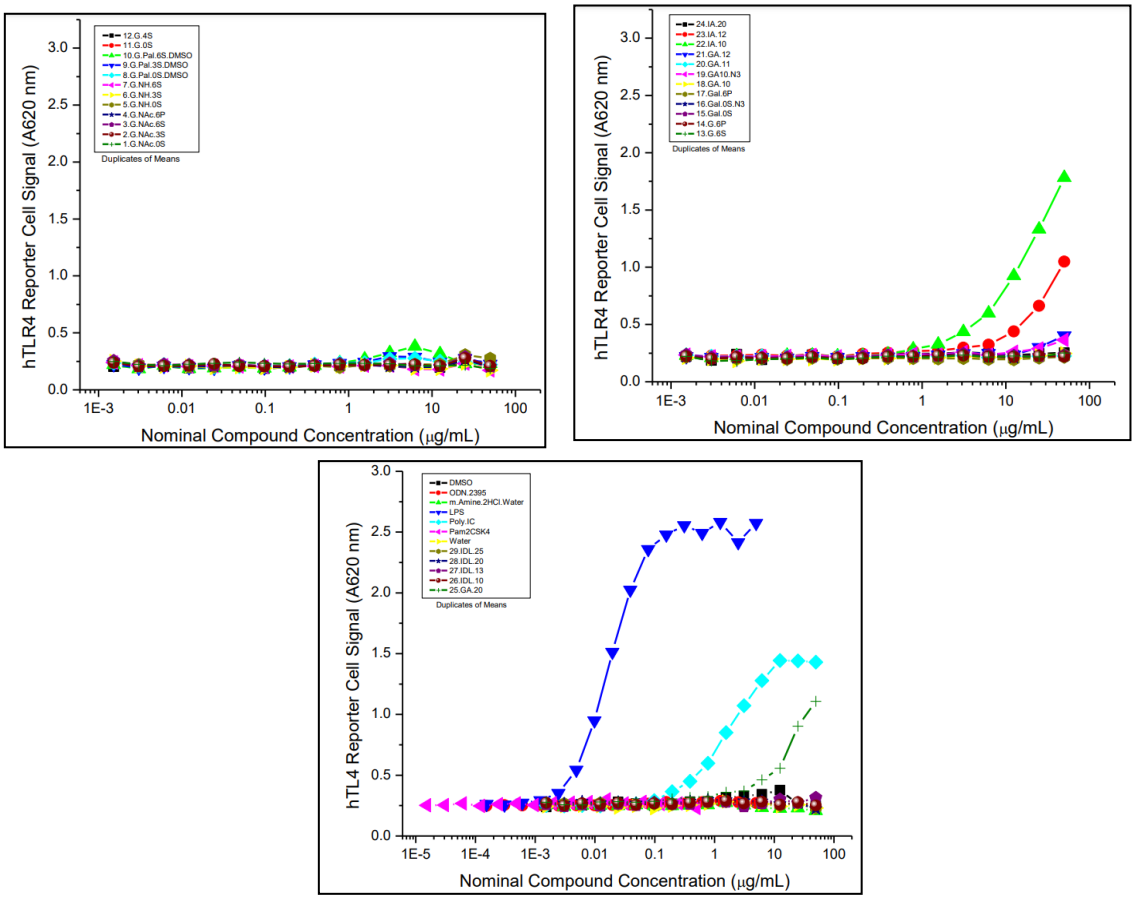



**Figure 4**. hTLR4 activity of monosaccharide derivatives.

## 4.4. Conclusion

We have successfully synthesised 25 carbohydrate based monosachharide dervatives Also we have checked its TLR4 agonist activity. Further cytokine secretion studies and potential application of these molecule as adjuvant is under progress.

## 4.5 Experimental part

### a) General Experimental Procedures

#### i) General Procedure A

A solution of starting material (1 mmol) in DCM/pyridine (4:1, 4 mL) was stirred at ice cold temperature under $N_2$ atmosphere then $Ac_2O$ (1 mmol) was added drop wise and reaction mixture was stirred for 2 h. Upon completion, the mixture was extracted with ethyl acetate and washed with 1 N HCl and brine. The combined organic layer was dried over $Na_2SO_4$, filtered, concentrated and purified through silica gel column chromatography (Ethyl Acetate/Hexane) to obtain desired compound.

#### ii) General Procedure B

A solution of donor (1.30 mmol) and acceptor **18** (0.41 mmol) in DCM (15 mL) was stirred under $N_2$ atmosphere in round bottom flask containing freshly dried 4 Å molecular sieves for 2 h. The mixture solution was cooled down to -10 $^{o}$ C followed by the addition of NIS (1.18 mmol) and TMSOTf (0.39 mmol). After 15 minutes reaction completion was monitored by TLC and quenched using few drops of $Et_3N$. Molecular sieves were filtered using celite and organic layer was washed with aqueous $Na_2S_2O_3$ and brine. The collected organic layer was dried over $Na_2SO_4$, filtered, concentrated and purified through silica gel column chromatography (Ethyl Acetate/Hexane) to obtain desired compound**.**

#### iii) General Procedure C

To a solution of starting material (0.34 mmol) in DCM/$H_2O$ (2:1, 12 mL) was added 2,2,6,6-tetramethyl-1-piperidinyloxyl free radical (TEMPO) (0.07 mmol), and [Bis(acetoxy)iodo] benzene (BAIB) (5.2 mmol) and stirred at RT for 6 h. The organic layer was washed with saturated $NH_4Cl$ solution and concentrated. Then, the crude product was dissolved in DMF (10

mL) and mixed with $K_2CO_3$ (0.001 mmol), MeI (0.001 mmol), and stirred overnight at rt. On completion of reaction, reaction mixture extracted with EtOAc and brine. The organic layer was concentrated and purified through silica gel column chromatography (Ethyl Acetate/Hexane) to obtain desired compound

**iv) General Procedure D**

The vacuum dried compound **4** (2.78 mmol) was dissolved in dry DCM and stirred at room temperatue. Then catalytic amount of PTSA (5.56 mmol) were added in to the reaction mixture and stirred it in nitrogen atmosphere for 6h. The reaction was monitored using TLC. After completion of reaction PTSA was neutralized using $Et_3N$. Evaporated the ACN using rota evaporation and the reaction mixture was dissolved in EtOAc and extracted with water and brine. The organic layer was collected and dried using anhydrous $Na_2SO_4$ and evaporated using rota evaporator. The reaction mixture was further purified by silica gel column chromatography (Ethyl Acetate/Hexane) to obtain desired compound.

**v) General Procedure E**

A solution of starting material (1 mmol) in methanol/ pyridine (1:1, 5 mL) was stirred at 80 º C under $N_2$ atmosphere then thiourea (1 mmol) was added and reaction mixture was stirred for 2 h. Upon completion, the mixture was extracted with ethyl acetate and washed with 1 N HCl and brine. The combined organic layer was dried over $Na_2SO_4$, filtered, concentrated and purified through silica gel column chromatography (Ethyl Acetate/ Hexane) to obtain desired compound.

**vi) General Procedure F**

To a solution of starting material (1 mmol) in DCM (6 mL) and $H_2O$ (340 µL) was added DDQ (5 mmol) portion wise over the interval of 20 min. After 1 h, the reaction mixture was quenched using $NaHCO_3$, extracted with DCM and washed with brine. The collected organic layer was dried over $Na_2SO_4$, filtered, concentrated and purified through silica gel column chromatography (Ethyl Acetate/Hexane) to obtain final compound.

**vii) General Procedure G**

A solution of starting material (1 mmol) in pyridine (1 mL) was stirred at ice cold temperature under $N_2$ atmosphere. After 15 minutes, 70% HF.py complex (5 mmol) was added drop wise and reaction mixture was stirred for 12 h. Upon completion, the mixture was extracted with ethyl acetate and washed with 1 N HCl and brine. The combined organic layer was dried over $Na_2SO_4$, filtered, concentrated and purified through silica gel column chromatography (Hexane/Ethyl Acetate) to obtain final and desired compound.

**viii) General Procedure H**

To a solution of starting material (1 mmol) in pyridine (1 mL) was added 70% HF.py (5 mmol) at ice cold temperature. After stirring for 12 h the reaction mixture was quenched with Amberlite-18 $H^+$ resin, after filtration the volatiles were evaporated and the residue was purified using Sephadex LH 20 column using MeOH as an eluent to get the desired compound.

**ix) General Procedure I**

To a solution of starting material (1 mmol) in DCM (1 mL) and pyridine (1 mL) was added $NEt_3$ (10 mmol), DMAP (0.3 mmol) and Diphenyl phosphoryl chloride (5 mmol) at 0 ° C. After 12 h, the reaction mixture was diluted with DCM and extracted with 1 N HCl and brine. The combined organic layer was dried over $Na_2SO_4$, further concentrated and purified through silica gel column chromatography (Ethyl Acetate/Hexane) to get the desired compound.

**x) General Procedure J**

To a solution of starting material (1 mmol) in DMF (2 mL) was added $SO_3.NMe_3$ complex (10 mmol per -OH) under $N_2$ atmosphere and stirred at 60 ° C for 3 days. Upon completion of reaction, aqueous $NaHCO_3$ (20 mmol) was added to reaction mixture and stirred for another 16 h. Next, the reaction mixture was concentrated under reduced pressure and the resulting residue and the crude product was purified by column chromatography (MeOH/DCM).

**xi) General Procedure K**

To a solution of starting material (1 mmol) in THF (1 mL) and $H_2O$ (1 mL) was added 1M LiOH (10 mmol) and stirred at room temperature for 10 h. Upon completion, the reaction mixture was

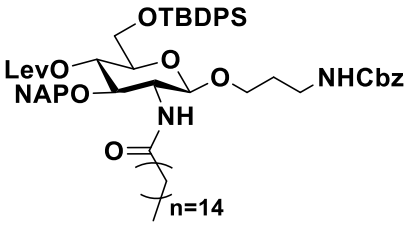
diluted with MeOH and quenched using Dowex 50WX8 H+ resin. The mixture was filtered, concentrated and eluted through Bond Elute C-18 column ($H_2O$/ACN).

### xii) General procedure L

The reaction mixture along with $Pd(OH)_2$ was stirred under $H_2$ atm. After 36 h, the mixture was filtered, concentrated and eluted through Bond Elute C-18 column using $H_2O$ as eluent. The combined $H_2O$ fraction were lyophilized to yield fully deprotected *O*-sulfated compound. For phosphorylated compound after $Pd(OH)_2$ hydrogenolysis the obtained product was again kept for hydrogenolysis using $PtO_2$ as a catalyst under $H_2$ atm for 24 h. Finally, the reaction mixture was filtered, concentrated under reduced pressure and eluted through Bond Elute C-18 column using $H_2O$ as eluent. The combined $H_2O$ fraction lyophilized to yield fully deprotected phosphorylated and sulfated compound.

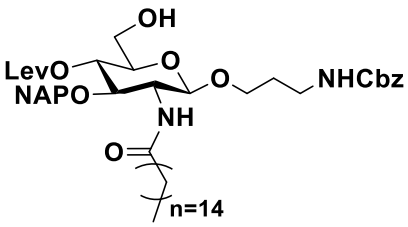
## b) Synthesis of 1st generation heparonoids

**Compound 1**




1H), 4.10 – 4.02 (m, 1H), 3.98 (m, 1H), 3.88 (dd, *J* = 12.5, 2.3 Hz, 1H), 3.80 – 3.72 (m, 1H), 3.70 – 3.62 (m, 2H), 3.53 (m, 1H), 3.30 (dd, *J* = 9.5, 8.0 Hz, 1H), 3.09 (t, *J* = 6.9 Hz, 2H), 1.93 (m, 2H). $^{13}$C NMR (101 MHz, Deuterium Oxide) δ 102.07, 76.65, 74.33, 72.85, 67.87, 60.47, 37.58, 26.65.

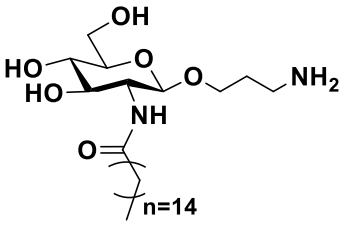
**Compound 2**




The TBDPS deprotection of compound **1** was accomplished as described in the general procedure **G** yielded 78% of **2**. $^1$H NMR (400 MHz, Chloroform-*d*) δ 7.75 – 7.62 (m, 4H), 7.42 – 7.35 (m, 2H), 7.33 – 7.20 (m, 6H), 6.03 (d, *J* = 7.4 Hz, 1H), 5.22 (t, *J* = 5.7 Hz, 1H), 5.00 (s, 2H), 4.93 (t, *J* = 9.4 Hz, 1H), 4.83 (d, *J* = 8.2 Hz, 1H), 4.75 – 4.67 (m, 2H), 4.22 (s, 1H), 3.85 (m, 1H), 3.63 (d, *J* = 11.8 Hz, 1H), 3.57 – 3.43 (m, 2H), 3.39 – 3.25 (m, 2H), 3.19 – 3.09 (m, 1H), 2.53 (d, *J* = 7.9 Hz, 1H), 2.46 – 2.34 (m, 2H), 2.25 – 2.14 (m, 1H), 2.00 (s, 3H), 1.97 – 1.89 (m, 2H), 1.71 – 1.60 (m, 2H), 1.44 (s, 2H), 1.15 (d, *J* = 22.3 Hz, 23H), 0.81 (t, *J* = 6.9 Hz, 3H). $^{13}$C NMR (101 MHz,

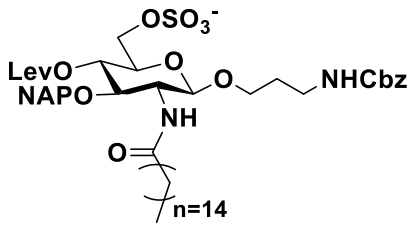
Chloroform-*d*) δ 206.44, 174.12, 172.61, 156.56, 136.69, 135.85, 133.26, 132.92, 128.54, 128.12, 128.10, 127.90, 127.65, 126.33, 126.19, 125.98, 125.76, 78.54, 74.24, 74.13, 71.55, 67.25, 66.61, 61.34, 57.37, 37.95, 37.67, 36.72, 31.94, 29.71, 29.68, 29.64, 29.56, 29.42, 29.37, 29.34, 27.85, 25.56, 22.70.

**Compound 3 (G-Pal-0S)**



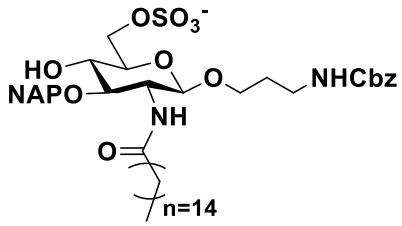

The saponificationa and hydrogenation of compound **2** was accomplished as described in the general procedure **E**, yielded 46 % of **3**. $^{1}$H NMR (400 MHz, Methanol-*d*$_4$) δ 4.42 (d, *J* = 8.4 Hz, 1H), 4.06 – 3.98 (m, 1H), 3.91 (dd, *J* = 11.8, 1.9 Hz, 1H), 3.76 – 3.63 (m, 5H), 3.49 – 3.43 (m, 1H), 3.12 (t, *J* = 5.1 Hz, 2H), 2.24 (td, *J* = 7.3, 1.8 Hz, 2H), 1.63 (d, *J* = 7.2 Hz, 2H), 1.30 (s, 27H), 0.95 – 0.88 (m, 3H). $^{13}$C NMR (101 MHz, Methanol-*d*$_4$) δ 175.66, 101.99, 76.67, 74.33, 70.70, 69.86, 68.89, 66.52, 61.09, 55.66, 39.34, 36.21, 31.74, 29.46, 29.37, 29.23, 29.14, 28.97, 25.80, 22.40, 13.09.

**Compound 4**



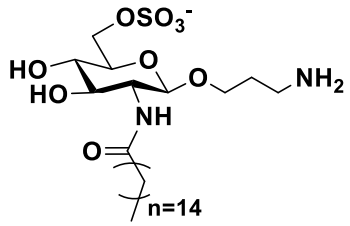

The *O*-sulfation of compound **3** was accomplished as described in the general procedure **J** yielded 62 % of **4**. $^{1}$H NMR (400 MHz, Methanol-*d*$_4$) δ 7.81 – 7.72 (m, 4H), 7.46 – 7.21 (m, 7H), 5.03 (s, 1H), 4.98 – 4.89 (m, 1H), 4.74 (m, 1H), 4.45 (d, *J* = 8.2 Hz, 1H), 4.09 – 3.94 (m, 2H), 3.92 – 3.69 (m, 3H), 3.51 (m, 1H), 3.16 (m, 2H), 2.71 – 2.47 (m, 3H), 2.05 (s, 4H), 1.70 (q, *J* = 6.4 Hz, 2H), 1.52 – 1.43 (m, 2H), 1.30 – 1.07 (m, 24H), 0.89 – 0.84 (m, 3H). $^{13}$C NMR (101 MHz, Methanol-*d*$_4$) δ 207.92, 175.19, 172.31, 157.54, 136.55, 133.41, 133.09, 128.18, 127.69, 127.63, 127.41, 127.38, 126.17, 125.76, 125.59, 101.25, 80.22, 78.25, 77.93, 77.60, 73.75, 72.21, 71.50, 66.91, 66.03, 54.92, 37.48, 37.23, 36.28, 31.76, 29.54, 29.45, 29.27, 29.17, 29.05, 28.38, 27.75, 25.63, 22.43, 13.19.

**Compound 5**



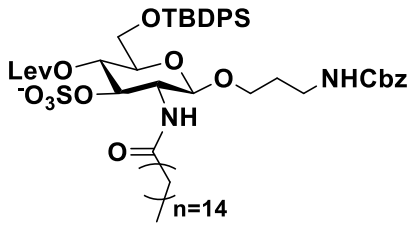

The Lev deprotection of compound **4** was accomplished as described in the general procedure **E**, yielded 65 % of **5**. $^{1}$H NMR (400 MHz, Methanol-$d_4$) δ 7.85 – 7.75 (m, 4H), 7.48 – 7.40 (m, 3H), 7.34 (d, *J* = 4.5 Hz, 5H), 5.11 – 5.03 (m, 3H), 4.84 (d, *J* = 12.1 Hz, 1H), 4.46 – 4.35 (m, 2H), 4.21 (d, *J* = 5.6 Hz, 1H), 3.91 – 3.83 (m, 2H), 3.66 – 3.46 (m, 4H), 3.27 – 3.09 (m,2H), 2.09 (t, *J* = 7.5 Hz, 2H), 1.73 (dt, *J* = 12.0, 4.0 Hz, 2H), 1.47 (q, *J* = 7.5 Hz, 2H), 1.32 – 1.08 (m, 25H), 0.93 – 0.87 (m, 3H). $^{13}$C NMR (101 MHz, Methanol-$d_4$) δ 175.17, 157.53, 137.16, 136.44, 133.46, 133.07, 128.15, 127.63, 127.49, 127.40, 127.34, 125.87, 125.67, 125.64, 125.45, 101.38, 82.60, 74.64, 74.35, 70.73, 66.97, 66.73, 66.00, 54.73, 37.52, 36.33, 31.76, 29.57, 29.46, 29.41, 29.24, 29.17, 29.05, 25.68, 22.43, 13.16.

**Compound 6 (G-Pal-6S)**




The hydrogenation of compound **5** was accomplished as described in the general procedure **L**, yielded 65 % of **6**. $^{1}$H NMR (400 MHz, Methanol-$d_4$) δ 4.49 (s, 4H), 4.30 – 4.24 (m, 1H), 4.04 (ddd, *J* = 11.2, 6.4, 2.1 Hz, 1H), 3.83 – 3.70 (m, 2H), 3.65 – 3.58 (m, 1H), 3.41 (ddd, *J* = 9.8, 6.3, 2.2 Hz, 1H), 3.33 (dd, *J* = 10.3, 8.7 Hz, 1H), 3.28 – 3.23 (m, 1H), 3.01 (td, *J* = 6.1, 1.8 Hz, 1H), 2.13 (tt, *J* = 7.3, 1.8 Hz, 2H), 1.97 – 1.85 (m, 1H), 1.81 – 1.72 (m, 1H), 1.53 (t, *J* = 7.3 Hz, 2H), 1.19 (s, 11H), 0.84 – 0.77 (m, 3H).$^{13}$C NMR (101 MHz, Methanol-$d_4$) δ 175.82, 102.50, 102.28, 74.41, 73.97, 70.60, 68.30, 55.41, 38.22, 36.07, 33.01, 31.67, 29.40, 29.36, 29.31, 29.14, 29.07, 28.84, 27.13, 25.70, 22.33, 13.04.

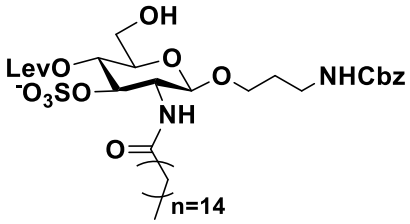
**Compound 7**




The NAP deprotection followed by *O*-sulfation of compound **1** was accomplished as described in the general procedure **F** and **J**, yielded 55 % of **7**. $^{1}$H NMR (400 MHz, Methanol-$d_4$) δ 7.74 (m, 4H), 7.45 – 7.27 (m, 11H), 5.15 (t, *J* = 9.6 Hz, 1H), 5.08 (s, 2H), 4.54 (d, *J* = 8.6 Hz, 2H), 3.95 – 3.75 (m, 4H), 3.54 (s, 2H), 3.25 (s, 2H), 2.77 (m, 2H), 2.59 (d, *J* = 6.3 Hz, 2H), 2.25 (t, *J* = 7.6 Hz, 2H), 2.15 (s, 3H), 1.78 (m, 2H), 1.64 (m, 2H), 1.29 (s, 24H), 1.04 (s, 9H), 0.94 – 0.89 (m, 3H).$^{13}$C NMR (101

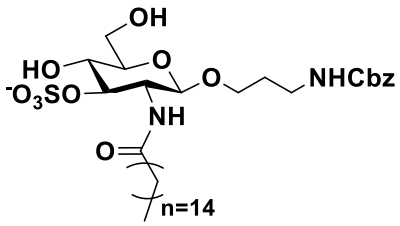
MHz, Methanol-$d_4$) δ 208.07, 175.51, 172.06, 157.44, 137.07, 135.52, 135.43, 133.29, 133.16, 129.39, 128.08, 127.53, 127.38, 127.30, 101.13, 78.02, 74.33, 69.01, 66.60, 65.95, 62.40, 54.67, 37.56, 37.33, 36.27, 31.68, 29.54, 29.42, 29.38, 29.31, 29.16, 29.08, 28.31, 27.94, 25.87, 25.31, 22.34, 18.74, 13.05.

**Compound 8**



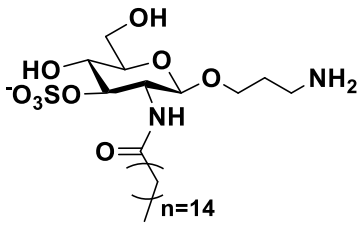

The desylilation post *O*-sulfation of compound **7** was accomplished as described in the general procedure **H** yielded 70 % of **8**. $^1$H NMR (400 MHz, Methanol-$d_4$) δ 7.37 – 7.20 (m, 4H), 5.04 (s, 2H), 4.56 – 4.48 (m, 2H), 3.91 – 3.64 (m, 3H), 3.54 – 3.47 (m, 2H), 3.18 (m, 2H), 2.88 – 2.71 (m, 2H), 2.58 (t, *J* = 6.4 Hz, 2H), 2.20 (td, *J* = 7.3, 3.1 Hz, 3H), 1.74 – 1.67 (m, 2H), 1.65 – 1.55 (m, 2H), 1.24 (s, 25H), 0.91 – 0.84 (m, 3H). $^{13}$C NMR (101 MHz, Methanol-$d_4$) δ 208.76, 175.48, 172.66, 157.47, 137.08, 128.09, 127.55, 127.38, 101.17, 77.90, 74.19, 69.55, 66.76, 65.94, 60.68, 54.56, 37.37, 36.24, 31.69, 29.51, 29.43, 29.38, 29.33, 29.18, 29.09, 28.28, 27.91, 25.30, 22.35, 13.08.

**Compound 9**




The Lev deprotection of compound **8** was accomplished as described in the general procedure **E** yielded 60 % of **9**. $^1$H NMR (400 MHz, Methanol-$d_4$) δ 7.41 – 7.26 (m, 5H), 5.09 (s, 2H), 4.52 (d, *J* = 8.4 Hz, 1H), 4.48 – 4.33 (m, 1H), 3.97 – 3.85 (m, 2H), 3.82 – 3.65 (m, 2H), 3.59 – 3.51 (m, 2H), 3.23 (m, 2H), 2.25 (td, *J* = 7.4, 2.0 Hz, 2H), 1.80 – 1.55 (m, 4H), 1.29 (s, 25H), 0.99 – 0.72 (m, 3H). $^{13}$C NMR (101 MHz, Methanol-$d_4$) δ 175.80, 157.57, 137.16, 128.16, 127.65, 127.42, 101.35, 76.60, 74.98, 70.89, 66.47, 66.02, 61.43, 55.93, 37.40, 36.12, 31.76, 29.64, 29.49, 29.36, 29.23, 29.17, 29.00, 25.76, 22.42, 13.14.

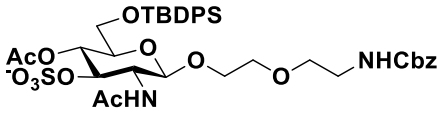
**Compound 10 (G-Pal-3S)**




The hydrogenation of compound **9** was accomplished as described in the general procedure **L** yielded 52 % of **10**. $^1$H NMR (400

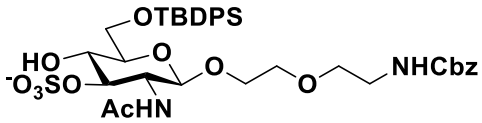
MHz, Methanol-$d_4$) δ 4.25 (d, $J$ = 8.4 Hz, 1H), 3.92 (m, 1H), 3.81 (m, 1H), 3.64 – 3.55 (m, 3H), 3.37 – 3.31 (m, 1H), 2.97 (t, $J$ = 6.1 Hz, 2H), 2.15 (t, $J$ = 7.3 Hz, 2H), 1.82 (m, 2H), 1.58 – 1.49 (m, 2H), 1.19 (s, 27H), 0.83 – 0.78 (m, 3H). $^{13}$C NMR (101 MHz, Methanol-$d_4$) δ 175.97, 101.76, 76.54, 74.02, 70.69, 67.30, 61.09, 55.54, 38.19, 36.11, 31.67, 29.40, 29.36, 29.32, 29.13, 29.07, 28.94, 26.88, 25.71, 22.33, 13.04.

**Compound 12**



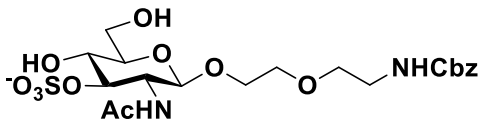

The NAP deprotection followed by *O*-sulfation of compound **11** was accomplished as described in the general procedure **F** and **J** yielded 55 % of **12**. $^1$H NMR (400 MHz, Methanol-$d_4$) δ 7.58 (m, 4H), 7.28 (q, $J$ = 7.8, 6.3 Hz, 6H), 7.24 – 7.14 (m, 5H), 5.04 (t, $J$ = 9.6 Hz, 1H), 4.95 (s, 2H), 4.58 (d, $J$ = 8.4 Hz, 1H), 4.48 – 4.41 (m, 1H), 3.83 (m, 1H), 3.76 (m, 1H), 3.65 – 3.57 (m, 3H), 3.54 – 3.48 (m, 3H), 3.43 (td, $J$ = 5.9, 5.3, 2.9 Hz, 2H), 3.18 (d, $J$ = 5.4 Hz, 1H), 1.88 (s, 3H), 1.86 (s, 3H), 0.91 (s, 9H). $^{13}$C NMR (101 MHz, Methanol-$d_4$) δ 172.71, 170.60, 157.53, 136.94, 135.47, 135.33, 133.09, 132.94, 129.57, 129.54, 128.10, 127.59, 127.48, 127.42, 101.06, 78.23, 74.14, 69.79, 69.01, 68.59, 66.08, 62.44, 54.83, 40.44, 25.91, 21.96, 19.98, 18.68.

**Compound 13**



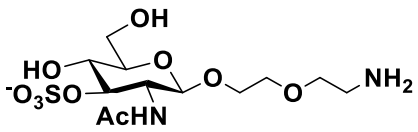

The acetate deprotection of compound **12** was accomplished as described in the general procedure **K**, yielded 89 % of **13**. $^1$H NMR (400 MHz, Methanol-$d_4$) δ 7.70 (dq, $J$ = 6.0, 1.9 Hz, 4H), 7.41 – 7.20 (m, 11H), 5.02 (s, 2H), 4.58 (d, $J$ = 8.4 Hz, 1H), 4.44 – 4.31 (m, 1H), 3.98 – 3.82 (m, 3H), 3.76 (t, $J$ = 8.3 Hz, 1H), 3.69 – 3.56 (m, 4H), 3.50 (dt, $J$ = 8.9, 4.8 Hz, 2H), 3.40 (m, 1H), 3.28 – 3.23 (m, 2H), 1.95 (s, 3H), 1.01 (s, 9H). $^{13}$C NMR (101 MHz, Methanol-$d_4$) δ 172.65, 157.58, 136.98, 135.52, 135.44, 133.50, 133.33, 129.51, 129.47, 128.16, 127.66, 127.56, 127.43, 101.07, 81.20, 76.40, 69.86, 69.75, 69.64, 68.54, 66.14, 62.99, 54.24, 40.49, 25.98, 21.86, 18.83.

**Compound 14**



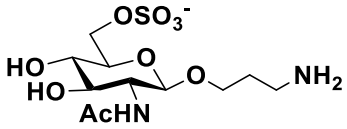
The desilylation post *O*-sulfation of compound **13** was accomplished as described in the general procedure **H**, yielded 65 % of **14**. $^{1}$H NMR (400 MHz, Deuterium Oxide) δ 7.36 (s, 5H), 5.05 (s, 2H), 4.58 (d, *J* = 8.5 Hz, 1H), 4.29 (m, 1H), 3.93 – 3.80 (m, 2H), 3.70 (ddd, *J* = 20.8, 11.3, 7.1 Hz, 3H), 3.58 (s, 2H), 3.54 – 3.47 (m, 3H), 3.46 – 3.39 (m, 1H), 3.23 (t, *J* = 5.1 Hz, 2H), 1.91 (s, 3H). $^{13}$C NMR (101 MHz, Deuterium Oxide) δ 174.56, 158.47, 128.83, 128.41, 127.74, 100.51, 81.49, 75.39, 69.41, 69.06, 68.78, 66.94, 60.65, 54.17, 40.14, 22.29.

**Compound 15 (G-NAc-3S)**



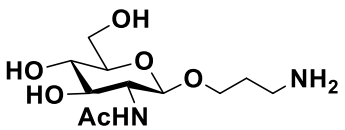
The hydrogenation of compound **14** was accomplished as described in the general procedure **L** yielded 62 % of **15**. $^{1}$H NMR (400 MHz, Deuterium Oxide) δ 4.70 (d, *J* = 8.6 Hz, 1H), 4.38 (m, 1H), 4.04 (s, 1H), 3.95 (m, 1H), 3.87 – 3.71 (m, 3H), 3.67 – 3.60 (m, 2H), 3.55 (m, 2H), 3.21 (t, *J* = 5.1 Hz, 3H), 2.03 (s, 2H). $^{13}$C NMR (151 MHz, Deuterium Oxide) δ 174.58, 100.63, 81.41, 75.36, 66.39, 60.51, 39.08, 22.24.

**Compound 16 (G-NAc-6S)**



The desilylation pre *O*-sulfation, *O*-sulfation, acetate deprotecton and finally hydrogenation of compound **15** (0.017 mmol) was accomplished as described in the general procedure G, J, K and L yielded 35 % of **16**. $^{1}$H NMR (400 MHz, Deuterium Oxide) δ 4.44 (d, *J* = 8.5 Hz, 1H), 4.28 (m, 1H), 4.15 (m, 1H), 3.96 – 3.85 (m, 1H), 3.72 – 3.55 (m, 3H), 3.51 – 3.38 (m, 2H), 3.02 (t, *J* = 6.7 Hz, 2H), 1.96 (s, 3H), 1.91 – 1.83 (m, 2H). $^{13}$C NMR (101 MHz, Deuterium Oxide) δ 174.80, 101.42, 73.63, 73.48, 69.53, 68.23, 67.02, 55.43, 37.73, 26.70, 22.13.

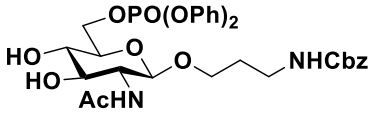
**Compound 18 (G-NAc-0S)**



The desilylation pre *O*-sulfation, acetate deprotection and hydrogenation of compound **17** was accomplished as described in the general procedure G, K and L, yielded 51 % of **18**.[1] H NMR

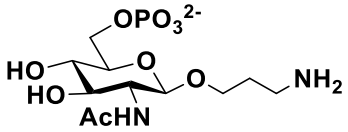
(400 MHz, Deuterium Oxide) δ 4.56 (d, *J* = 8.5 Hz, 1H), 4.07 – 4.01 (m, 1H), 3.93 (d, *J* = 13.3 Hz, 1H), 3.76 (d, *J* = 5.5 Hz, 7H), 3.72 (dd, *J* = 7.4, 2.7 Hz, 1H), 3.66 (t, *J* = 4.4 Hz, 2H), 3.58 – 3.52 (m, 2H), 3.47 – 3.43 (m, 2H), 3.20 (t, *J* = 4.8 Hz, 25H), 2.04 (s, 3H). $^{13}$C NMR (101 MHz, Deuterium Oxide) δ 101.23, 75.86, 73.77, 69.83, 69.64, 69.17, 66.40, 60.64, 55.48, 39.09, 22.14.

**Compound 19**



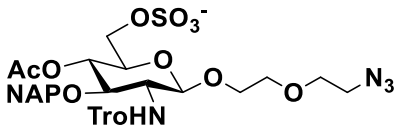

The desilylation pre *O*-sulfation, acetate deprotection and phosphorylation of compound **18** was accomplished as described in the general procedure **G, J** and **I** yielded 35 % of compound **19**. $^{1}$H NMR (400 MHz, Methanol-$d_4$) δ 7.34 – 7.09 (m, 15H), 4.96 (d, *J* = 3.2 Hz, 2H), 4.54 – 4.45 (m, 2H), 4.32 (m, 1H), 4.24 (d, *J* = 8.4 Hz, 1H), 3.68 (m, 1H), 3.54 (m, 1H), 3.39 – 3.28 (m, 3H), 3.25 (s, 1H), 3.05 (m, 2H), 1.88 (s, 3H), 1.62 – 1.52 (m, 2H). $^{13}$C NMR (101 MHz, Methanol-$d_4$) δ 172.59, 157.51, 150.46, 137.13, 129.69, 128.09, 127.59, 127.39, 125.46, 119.83, 119.81, 119.78, 119.76, 101.23, 74.64, 74.48, 74.42, 70.05, 68.41, 68.35, 66.50, 65.95, 55.90, 37.28, 29.44, 21.56.

**Compound 20 (G-NAc-6P)**




The hydrogenation of compound **19** was accomplished as described in the general procedure **L**, yielded 42 % of **20**. $^{1}$H NMR (400 MHz, Deuterium Oxide) δ 4.44 (d, *J* = 8.5 Hz, 1H), 4.07 (dd, *J* = 5.5, 1.6 Hz, 1H), 4.04 – 3.88 (m, 2H), 3.67 (m, 2H), 3.54 – 3.43 (m, 3H), 3.01 (t, *J* = 6.8 Hz, 2H), 1.96 (s, 3H), 1.87 (dt, *J* = 6.7, 4.6 Hz, 2H). $^{13}$C NMR (101 MHz, Deuterium Oxide) δ 174.74, 101.40, 74.60, 73.39, 69.37, 68.22, 63.86, 55.49, 37.65, 26.68, 22.14.

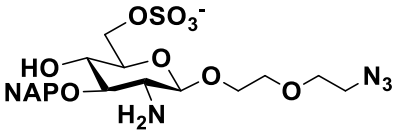
**Compound 22**




The desilylation pre *O*-sulfation and *O*-sulfation of compound **21** was accomplished as described in the general procedure **G** and **J**, yielded 51 % of compound **22.** $^{1}$H NMR (400 MHz, Methanol-$d_4$) δ 7.82 – 7.75 (m, 3H), 7.71 (s, 1H), 7.48 – 7.39 (m, 2H), 7.35 (dd, *J* = 8.4, 1.6 Hz,

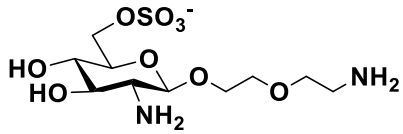
1H), 4.92 (d, *J* = 9.9 Hz, 1H), 4.79 (s, 2H), 4.69 – 4.53 (m, 3H), 4.07 – 3.89 (m, 3H), 3.87 – 3.79 (m, 1H), 3.74 (tt, *J* = 11.3, 6.0 Hz, 2H), 3.63 (tt, *J* = 9.1, 4.1 Hz, 5H), 3.35 (t, *J* = 5.0 Hz, 5H), 1.94 (s, 1H). $^{13}$C NMR (101 MHz, Methanol-$d_4$) δ 170.58, 155.39, 135.74, 133.38, 133.13, 127.72, 127.64, 127.37, 126.17, 125.85, 125.68, 125.64, 101.41, 95.82, 80.16, 74.31, 74.10, 72.23, 71.04, 69.98, 69.82, 69.17, 66.71, 57.30, 50.52, 19.67.

**Compound 23**



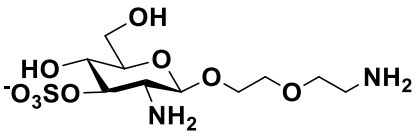

The acetate and Troc deprotection of compound **22** was accomplished as described in the general procedure **K**, yielded 80 % of compound **23.** $^{1}$H NMR (400 MHz, Deuterium Oxide) δ 7.90 (dd, *J* = 8.9, 4.7 Hz, 4H), 7.52 (td, *J* = 7.4, 6.8, 2.5 Hz, 3H), 5.03 (d, *J* = 11.1 Hz, 1H), 4.85 (d, *J* = 11.1 Hz, 1H), 4.36 – 4.24 (m, 2H), 4.16 (dd, *J* = 11.1, 3.9 Hz, 1H), 3.99 – 3.89 (m, 1H), 3.80 – 3.55 (m, 7H), 3.42 (dd, *J* = 9.8, 4.3 Hz, 3H), 2.65 (dd, *J* = 9.8, 8.2 Hz, 1H). $^{13}$C NMR (101 MHz, Deuterium Oxide) δ 135.00, 132.96, 132.89, 128.48, 128.01, 127.84 – 127.55 (m), 126.72, 126.62, 102.95, 83.55, 74.80, 73.83, 69.54, 69.47, 69.13, 68.77, 66.93, 55.55, 50.15.

**Compound 24 (G-NH-6S)**




The hydrogenation of compound **23** was accomplished as described in the general procedure **L**, yielded 67 % of **24**. $^{1}$H NMR (400 MHz, Deuterium Oxide) δ 4.22 (m, 1H), 4.11 (m, 1H), 3.94 (m, 1H), 3.80 (m, 1H), 3.71 – 3.51 (m, 6H), 3.41 (dd, *J* = 9.9, 8.9 Hz, 1H), 3.11 – 3.05 (m, 2H), 2.94 (dd, *J* = 10.6, 8.5 Hz, 1H). $^{13}$C NMR (101 MHz, Deuterium Oxide) δ 99.30, 73.89, 72.06, 69.54, 69.41, 69.30, 66.65, 66.29, 55.67, 39.10.

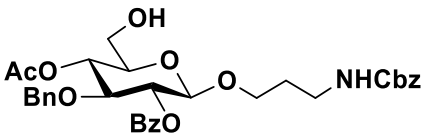
**Compound 25 (G-NH-3S)**




The NAP deprotection, followed by *O*-sulfation next acetate deprotectiona and Troc deprotection finally hydrogenation of compound **24** (0.017 mmol) was accomplished as described in the general procedure F, J, K and L yielded 37 % of compound **25.** $^{1}$H NMR (400 MHz, Methanol-$d_4$) δ 4.54 – 4.46 (m, 1H), 4.25 (m, 1H), 4.14 (m, 1H), 3.99 – 3.94 (m, 1H), 3.79 (m, 1H), 3.74 – 3.66 (m, 1H), 3.65 – 3.62 (m, 3H), 3.61 – 3.57 (m, 2H), 3.51 – 3.43 (m, 1H), 3.35 –

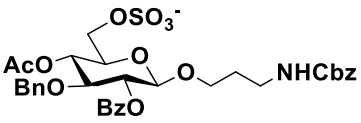
3.28 (m, 3H), 2.90 (m, 1H). $^{13}$C NMR (101 MHz, Methanol-$d_4$) δ 100.19, 80.23, 76.53, 69.73, 69.53, 68.82, 68.45, 60.78, 55.39, 50.37.

**Compound 27**



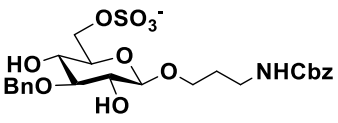

The acetate protection and chloroacetate deprotection of compound **26** was accomplished as described in the general procedure **A** and **F** yielded 59 % of **27**. $^{1}$H NMR (400 MHz, Chloroform-*d*) δ 8.00 (d, *J* = 7.5 Hz, 1H), 7.56 (t, *J* = 7.4 Hz, 1H), 7.42 (t, *J* = 7.7 Hz, 1H), 7.35 – 7.28 (m, 2H), 7.20 – 7.08 (m, 3H), 5.29 (dd, *J* = 9.4, 7.9 Hz, 0H), 5.18 – 5.02 (m, 2H), 4.63 – 4.53 (m, 2H), 3.88 (t, *J* = 9.2 Hz, 1H), 3.73 – 3.44 (m, 1H), 3.23 – 3.12 (m, 1H), 2.75 (s, 0H), 1.99 (s, 1H), 1.77 – 1.65 (m, 2H). $^{13}$C NMR (101 MHz, Chloroform-*d*) δ 170.39, 165.17, 156.58, 137.67, 136.77, 133.44, 129.86, 129.67, 128.60, 128.41, 128.14, 127.93, 127.85, 101.15, 79.80, 74.72, 74.07, 73.37, 70.46, 67.35, 66.59, 61.60, 38.02, 29.59, 20.91.

**Compound 28**




The *O*-sulfation of compound **27** was accomplished as described in the general procedure **J** yielded 62 % of **28.** $^{1}$H NMR (400 MHz, Methanol-$d_4$) δ 8.05 (d, *J* = 7.5 Hz, 2H), 7.63 (t, *J* = 7.4 Hz, 1H), 7.49 (t, *J* = 7.8 Hz, 2H), 7.38 – 7.28 (m, 5H), 7.20 – 7.07 (m, 5H), 5.16 (m, 1H), 5.03 (d, *J* = 6.8 Hz, 3H), 4.75 (d, *J* = 8.0 Hz, 1H), 4.66 – 4.54 (m, 2H), 4.10 (m, 3H), 3.91 (m, 2H), 3.58 (m, 1H), 3.07 (td, *J* = 6.7, 3.8 Hz, 2H), 2.06 (s, 3H), 1.68 (q, *J* = 6.6 Hz, 2H). $^{13}$C NMR (101 MHz, Chloroform-*d*) δ 168.49, 163.68, 155.55, 135.98, 135.29, 131.43, 127.82, 127.63, 126.55, 126.28, 126.11, 125.85, 125.74, 125.60, 125.57, 98.97, 78.23, 76.31, 72.48, 71.80, 70.43, 68.80, 65.39, 64.64, 64.07, 42.41, 35.56, 27.69, 17.82.

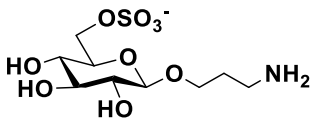
**Compound 29**




The saponification of compound **28** was accomplished as described in the general procedure **K**, yielded 60 % of **29.** $^{1}$H NMR (400 MHz, Deuterium Oxide) δ 7.33 – 7.20 (m, 10H), 4.93 (s, 2H), 4.23 (m, 1H), 4.13 (s, 1H), 4.03 (m, 1H), 3.75 (m, 1H), 3.56 – 3.27 (m, 4H), 3.25 – 3.13 (m, 1H), 3.13 – 3.01 (m, 2H), 1.63 (t, *J* = 6.4 Hz, 2H). $^{13}$C NMR (101 MHz, Deuterium Oxide) δ 158.42, 137.48,

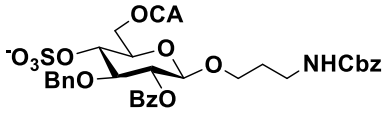
136.62, 128.80, 128.78, 128.66, 128.37, 127.66, 102.30, 83.61, 74.85, 73.62, 72.80, 68.91, 67.96, 66.88, 37.41, 28.79.

**Compound 30 (G-6S)**



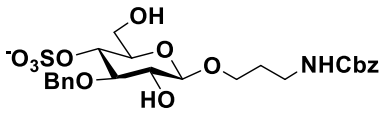

The hydrogenation of compound **29** (0.014 mmol) was accomplished as described in the general procedure **L**, yielded 62 % of **30.** $^{1}$H NMR (400 MHz, Deuterium Oxide) δ 4.42 (d, *J* = 8.0 Hz, 1H), 4.26 (m, 1H), 4.13 (m, 1H), 3.94 (m, 1H), 3.78 (m, 1H), 3.67 – 3.51 (m, 1H), 3.40 (m, 2H), 3.22 (m, 1H), 3.08 (t, *J* = 7.3 Hz, 2H), 2.00 – 1.88 (m, 2H). $^{13}$C NMR (101 MHz, Deuterium Oxide) δ 102.44, 75.54, 73.65, 72.95, 69.18, 68.13, 66.97, 37.64, 26.77.

**Compound 31**



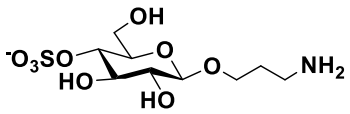

The *O*-sulfation of compound **30** was accomplished as described in the general procedure **J** yielded 69 % of **31.** $^{1}$H NMR (400 MHz, Chloroform-*d*) δ 7.93 (dd, *J* = 8.3, 1.2 Hz, 2H), 7.55 (t, *J* = 7.4 Hz, 1H), 7.39 (t, *J* = 7.7 Hz, 2H), 7.31 (d, *J* = 5.0 Hz, 5H), 7.16 (dd, *J* = 7.5, 1.8 Hz, 2H), 7.02 (d, *J* = 7.3 Hz, 3H), 5.19 (dd, *J* = 9.6, 8.1 Hz, 1H), 5.07 – 4.96 (m, 4H), 4.65 – 4.45 (m, 5H), 4.20 – 4.06 (m, 2H), 3.84 (t, *J* = 9.3 Hz, 2H), 3.78 – 3.69 (m, 1H), 3.53 (dt, *J* = 11.6, 5.8 Hz, 1H), 3.21 – 3.02 (m, 2H), 1.79 – 1.55 (m, 2H). $^{13}$C NMR (101 MHz, Chloroform-*d*) δ 167.94, 165.45, 156.52, 137.95, 136.86, 133.38, 129.85, 129.66, 128.85, 128.57, 128.22, 128.11, 128.08, 127.68, 101.00, 80.25, 76.07, 74.97, 72.88, 72.75, 67.48, 66.48, 64.96, 41.23, 38.03, 29.56.

**Compound 32**



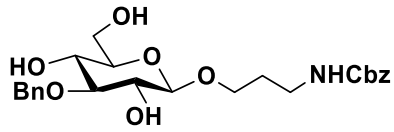

The saponification of compound **31** was accomplished as described in the general procedure **K** yielded 60 % of **32**. $^{1}$H NMR (400 MHz, Deuterium Oxide) δ 7.47 – 7.29 (m, 10H), 5.02 (s, 2H), 4.90 (m, 1H), 4.65 (m, 1H), 4.31 (d, *J* = 7.9 Hz, 1H), 4.15 (m, 1H), 3.87 (m, 2H), 3.73 – 3.52 (m, 3H), 3.51 – 3.40 (m, 1H), 3.29 (t, *J* = 8.7 Hz, 1H), 3.19 – 3.12 (m, 2H), 1.77 – 1.64 (m, 2H). $^{13}$C NMR (101 MHz, Deuterium Oxide) δ 158.45, 137.42, 136.62, 131.27, 129.09, 128.83, 128.55, 128.41, 128.31, 127.69, 102.14, 81.81, 76.32, 75.00, 74.54, 72.83, 67.85, 66.83, 60.58, 37.37, 28.78.

**Compound 33 (G-4S)**



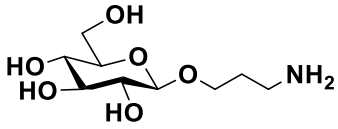
The hydrogenation of compound **32** was accomplished as described in the general procedure **L**, yielded 51 % of **33.** $^{1}$H NMR (400 MHz, Deuterium Oxide) δ 4.42 (d, *J* = 8.0 Hz, 1H), 4.26 (m, 1H), 4.13 (m, 1H), 3.94 (m, 1H), 3.78 (m, 1H), 3.67 – 3.51 (m, 1H), 3.40 (m, 2H), 3.22 (t, *J* = 8.5 Hz, 1H), 3.08 (t, *J* = 7.3 Hz, 2H), 2.00 – 1.88 (m, 2H). $^{13}$C NMR (101 MHz, Deuterium Oxide) δ 102.44, 75.54, 73.65, 72.95, 69.18, 68.13, 66.97, 37.64, 26.77.

**Compound 34**



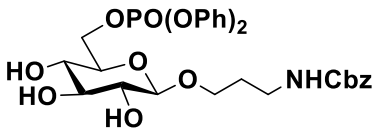
The saponification and hydrogenolysis of compound **33** was accomplished as described in the general procedure **K** and **L**, yielded 70 % of **34**. $^{1}$H NMR (400 MHz, Deuterium Oxide) δ 7.47 – 7.29 (m, 10H), 5.02 (s, 2H), 4.90 (m, 1H), 4.65 (m, 1H), 4.31 (d, *J* = 7.9 Hz, 1H), 4.15 (t, *J* = 9.5 Hz, 1H), 3.87 (m, 2H), 3.73 – 3.52 (m, 3H), 3.51 – 3.40 (m, 1H), 3.29 (t, *J* = 8.7 Hz, 1H), 3.19 – 3.12 (m, 2H), 1.77 – 1.64 (m, 2H). $^{13}$C NMR (101 MHz, Deuterium Oxide) δ 158.45, 137.42, 136.62, 131.27, 129.09, 128.83, 128.55, 128.41, 128.31, 127.69, 102.14, 81.81, 76.32, 75.00, 74.54, 72.83, 67.85, 66.83, 60.58, 37.37, 28.78.

**Compound 35 (G-0S)**



The hydrogenation of compound **34** was accomplished as described in the general procedure **L**, yielded 57 % of **35.** $^{1}$H NMR (400 MHz, Deuterium Oxide) δ 4.28 (d, *J* = 7.9 Hz, 1H), 3.95 – 3.88 (m, 1H), 3.78 (dd, *J* = 3.4, 0.8 Hz, 1H), 3.72 – 3.54 (m, 5H), 3.51 (m, 1H), 3.38 (m, 1H), 3.03 (t, *J* = 7.2 Hz, 2H), 1.87 (ddd, *J* = 7.4, 5.1, 2.5 Hz, 2H). $^{13}$C NMR (101 MHz, Deuterium Oxide) δ 102.85, 75.22, 72.71, 70.76, 68.64, 67.87, 61.04, 37.70, 26.69.

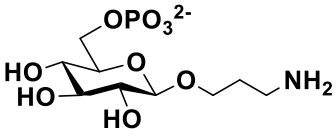
**Compound 37**



The phosphorylation of compound **36** was accomplished as described in the general procedure **I**, yielded 45 % of **37.** $^{1}$H

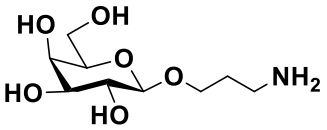
NMR (400 MHz, Chloroform-*d*) δ 7.30 – 7.21 (m, 9H), 7.19 – 7.11 (m, 6H), 5.02 (s, 1H), 4.50 – 4.28 (m, 2H), 4.10 (d, *J* = 7.7 Hz, 4H), 3.79 (s, 2H), 3.72 – 3.55 (m, 2H), 3.53 – 3.36 (m, 2H), 3.33 – 3.08 (m, 2H), 1.67 (dd, *J* = 11.8, 6.2 Hz, 2H). $^{13}$C NMR (101 MHz, Chloroform-*d*) δ 156.95, 150.48, 150.41, 136.77, 129.95, 129.66, 128.57, 128.12, 125.64, 120.17, 120.13, 120.09, 103.10, 73.32, 73.23, 71.13, 68.34, 67.87, 67.07, 66.63, 37.82, 29.79, 29.55.

**Compound 38 (G-6P)**



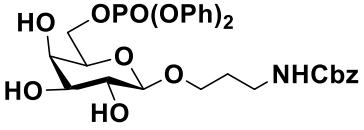

The hydrogenation of compound **37** was accomplished as described in the general procedure **L**, yielded 50 % of **38.** $^{1}$H NMR (400 MHz, Deuterium Oxide) δ 4.41 (d, *J* = 7.9 Hz, 1H), 4.01 – 3.93 (m, 4H), 3.89 – 3.81 (m, 2H), 3.64 (m, 3.5 Hz, 1H), 3.49 (m, 1H), 3.13 (qd, *J* = 6.7, 4.6 Hz, 2H), 1.98 (qd, *J* = 6.8, 5.8 Hz, 2H). $^{13}$C NMR (101 MHz, Deuterium Oxide) δ 103.03, 73.79, 72.57, 70.70, 68.28, 64.04, 37.64, 26.77.

**Compound 40 (Gal-0S)**




The hydrogenation of compound **39** was accomplished as described in the general procedure **L**, yielded 59 % of **40.** $^{1}$H NMR (400 MHz, Deuterium Oxide) δ 4.39 (d, *J* = 8.0 Hz, 1H), 3.96 (m, 1H), 3.84 (m, 1H), 3.72 (m, 1H), 3.63 (dd, *J* = 12.3, 6.0 Hz, 1H), 3.44 – 3.35 (m, 2H), 3.32 – 3.25 (m, 1H), 3.19 (dd, *J* = 9.3, 8.0 Hz, 1H), 3.07 (t, *J* = 7.0 Hz, 2H), 1.92 (m, 2H). $^{13}$C NMR (101 MHz, Deuterium Oxide) δ 102.26, 75.97, 75.70, 73.07, 69.64, 67.82, 60.69, 37.57, 30.25, 26.71.

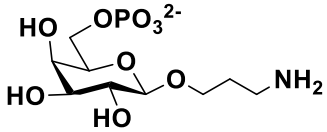
**Compound 41**




The phosphorylation of compound **39** was accomplished as described in the general procedure **I**, yielded 53 % of **41.** $^{1}$H NMR (400 MHz, Methanol-$d_4$) δ 7.25 (d, *J* = 16.5 Hz, 9H), 7.13 (d, *J* = 8.2 Hz, 6H), 4.94 (s, 2H), 4.58 – 4.42 (m, 1H), 4.36 – 4.25 (m, 1H), 4.14 (d, *J* = 7.8 Hz, 1H), 3.71 (d, *J* = 9.9 Hz, 1H), 3.39 (dd, *J* = 15.9, 6.1 Hz, 2H), 3.29 – 3.02 (m, 6H), 1.63 (d, *J* = 6.3 Hz, 2H). $^{13}$C NMR (101 MHz, Methanol-$d_4$) δ 157.51, 150.47, 150.39, 137.07, 129.68,

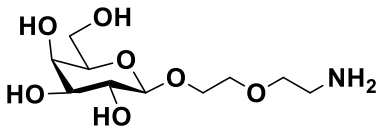
128.08, 127.57, 127.43, 125.45, 119.83, 119.78, 102.94, 76.43, 74.45, 74.39, 73.54, 69.56, 68.45, 68.39, 66.77, 65.96, 37.45, 29.48.

**Compound 42 (Gal-6P)**



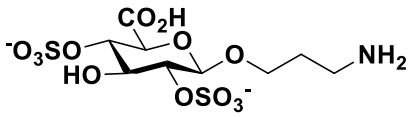
The hydrogenation of compound **41** was accomplished as described in the general procedure **L**, yielded 62 % of **42.** $^{1}$H NMR (400 MHz, Deuterium Oxide) δ 4.47 (d, *J* = 8.0 Hz, 1H), 4.13 (m, 1H), 4.08 – 3.95 (m, 2H), 3.83 (m, 1H), 3.55 (ddd, *J* = 5.5, 4.4, 2.7 Hz, 1H), 3.47 (dd, *J* = 5.4, 3.5 Hz, 2H), 3.32 – 3.24 (m, 1H), 3.13 (t, *J* = 6.6 Hz, 2H), 1.98 (p, *J* = 6.0 Hz, 2H). $^{13}$C NMR (101 MHz, Deuterium Oxide) δ 102.50, 75.49, 74.69, 74.61, 73.05, 69.04, 68.20, 63.87, 63.83, 37.63, 26.76.

**Compound 44 (Gal-0S-$N_3$)**



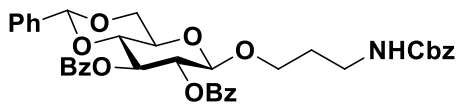
The hydrogenation of compound **43** was accomplished as described in the general procedure **L**, yielded 65 % of **44**. $^{1}$H NMR (400 MHz, Deuterium Oxide) δ 4.36 (d, *J* = 7.8 Hz, 1H), 4.01 (m, 1H), 3.84 (dd, *J* = 3.5, 1.0 Hz, 1H), 3.81 – 3.65 (m, 7H), 3.64 – 3.55 (m, 2H), 3.45 (dd, *J* = 9.9, 7.9 Hz, 1H), 3.14 – 3.09 (m, 2H). $^{13}$C NMR (101 MHz, Deuterium Oxide) δ 102.86, 75.23, 72.77, 70.76, 69.67, 68.90, 68.65, 66.51, 61.02, 39.12.

**Compound 48 (GA-12)**



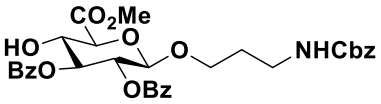
The hydrogenation of compound **47** was accomplished as described in the general procedure **J**, yielded % of **48.** $^{1}$H NMR (400 MHz, Deuterium Oxide) δ 4.40 (d, *J* = 8.0 Hz, 1H), 4.00 – 3.90 (m, 1H), 3.83 – 3.73 (m, 1H), 3.69 – 3.61 (m, 1H), 3.48 – 3.38 (m, 2H), 3.30 – 3.20 (m, 1H), 3.08 (td, *J* = 6.8, 2.8 Hz, 2H), 2.02 – 1.85 (m, 2H). $^{13}$C NMR (101 MHz, Deuterium Oxide) δ 181.49, 175.80, 102.08, 75.84, 75.49, 72.85, 71.73, 67.74, 37.45, 26.75, 23.24.

**Compound 50**



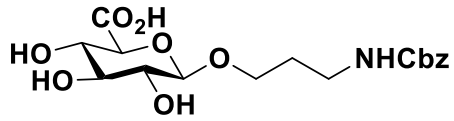

The linker glycosilation of compound **49** was accomplished as described in the general procedure **B**, yielded 53 % of **50.** $^{1}$H NMR (400 MHz, Chloroform-*d*) δ 7.99 (d, *J* = 8.1 Hz, 4H), 7.52 (t, *J* = 7.3 Hz, 2H), 7.46 (dd, *J* = 6.5, 2.9 Hz, 2H), 7.43 – 7.32 (m, 12H), 5.84 (t, *J* = 9.5 Hz, 1H), 5.57 (s, 1H), 5.54 – 5.47 (m, 1H), 5.10 (s, 2H), 5.04 (s, 1H), 4.81 (d, *J* = 7.8 Hz, 1H), 4.46 (m, 1H), 4.03 – 3.85 (m, 3H), 3.78 – 3.59 (m, 2H), 3.20 (m, 2H), 1.78 (m, 2H). $^{13}$C NMR (101 MHz, Chloroform-*d*) δ 165.62, 165.38, 156.44, 136.76, 133.38, 133.17, 129.83, 129.79, 129.38, 129.15, 129.08, 128.52, 128.49, 128.34, 128.23, 128.05, 126.14, 101.62 (d, *J* = 23.3 Hz), 78.80, 72.52, 71.96, 68.61, 68.05, 66.69, 66.49, 38.18, 29.73, 29.53.

**Compound 51**



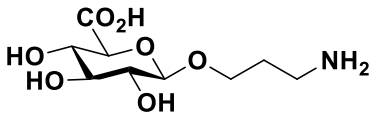

The benzilidene deprotection oxidation and followed by esterification of compound **50** was accomplished as described in the general procedure **D** and **C**, yielded 35 % of **51.** $^{1}$H NMR (400 MHz, Chloroform-*d*) δ 7.97 – 7.89 (m, 4H), 7.51 – 7.44 (m, 2H), 7.39 – 7.25 (m, 9H), 5.56 (t, *J* = 9.4 Hz, 1H), 5.43 – 5.36 (m, 1H), 5.20 (t, *J* = 5.7 Hz, 1H), 5.09 – 4.99 (m, 2H), 4.73 (d, *J* = 7.7 Hz, 1H), 4.22 – 4.13 (m, 1H), 4.09 (d, *J* = 9.7 Hz, 1H), 3.93 (ddd, *J* = 9.6, 7.6, 5.0 Hz, 1H), 3.77 (s, 2H), 3.63 (m, 1H), 3.57 (s, 1H), 3.29 – 3.19 (m, 1H), 3.13 (m, 1H), 1.72 (m, 2H). $^{13}$C NMR (101 MHz, Chloroform-*d*) δ 169.37, 166.55, 165.38, 156.60, 136.81, 133.51, 133.46, 130.00, 129.84, 129.17, 129.09, 128.57, 128.54, 128.49, 128.15, 128.12, 101.29, 74.79, 74.55, 71.35, 70.57, 67.57, 66.56, 53.09, 37.73, 29.41.

**Compound 52**



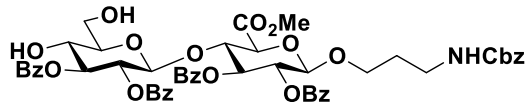

The saponification of compound **51** was accomplished as described in the general procedure **K** yielded 60 % of **52.** $^{1}$H NMR (400 MHz, Deuterium Oxide) δ 7.28 (m, 5H), 4.94 (s, 2H), 4.28 (d, *J* = 7.8 Hz, 1H), 3.73 (d, *J* = 8.8 Hz, 2H), 3.49 (m, 1H), 3.38 (m, 2H), 3.16 (t, *J* = 8.4 Hz, 1H), 3.07 (h, *J* = 7.2 Hz, 2H), 1.64 (p, *J* = 6.4 Hz, 2H). $^{13}$C NMR (101 MHz, Deuterium Oxide) δ 173.30, 158.41, 136.61, 128.80, 128.37, 127.65, 102.22, 75.35, 74.91, 72.79, 71.43, 67.79, 66.82, 37.25, 28.84.

**Compound 53 (GA-10)**



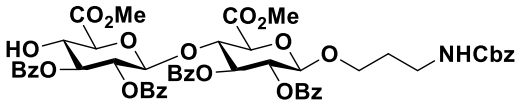
The hydrogenation of compound **52** was accomplished as described in the general procedure **L**, yielded 42% of **53**. $^{1}$H NMR (400 MHz, Deuterium Oxide) δ 4.40 (d, *J* = 8.0 Hz, 1H), 3.99 – 3.90 (m, 1H), 3.81 – 3.71 (m, 1H), 3.69 – 3.62 (m, 1H), 3.42 (dd, *J* = 5.9, 3.9 Hz, 2H), 3.28 – 3.21 (m, 1H), 3.08 (td, *J* = 6.8, 2.8 Hz, 2H), 1.99 – 1.88 (m, 2H). $^{13}$C NMR (101 MHz, Deuterium Oxide) δ 175.80, 102.08, 75.84, 75.49, 72.85, 71.73, 67.74, 37.45, 26.75, 23.24.

**Compound 54**



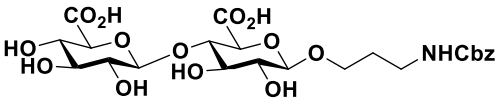
The linker glycosylation and bezilidene deprotection of compound **49 and 51** was accomplished as described in the general procedure **B** and **D** yielded 53 % of **54.** $^{1}$H NMR (400 MHz, Chloroform-*d*) δ 8.00 (s, 2H), 7.89 (s, 6H), 7.54 (d, *J* = 6.2 Hz, 1H), 7.51 – 7.44 (m, 3H), 7.40 (s, 2H), 7.34 (s, 11H), 5.68 (d, *J* = 9.5 Hz, 1H), 5.32 (s, 2H), 5.27 – 5.20 (m, 1H), 5.02 (s, 3H), 4.91 (s, 1H), 4.69 (d, *J* = 7.4 Hz, 1H), 4.42 – 4.34 (m, 1H), 4.01 (d, *J* = 9.8 Hz, 1H), 3.89 – 3.79 (m, 1H), 3.68 (s, 1H), 3.59 – 3.48 (m, 1H), 3.34 (s, 5H), 3.22 (m, 2H), 3.11 (d, *J* = 15.2 Hz, 2H), 1.69 (s, 2H). $^{13}$C NMR (101 MHz, Chloroform-*d*) δ 168.00, 167.27, 165.36, 165.20, 156.50, 136.78, 133.96, 133.12, 130.20, 129.37, 129.20, 127.85, 101.23, 100.81, 76.59, 75.96, 74.11, 72.48, 71.74, 71.65, 69.28, 67.75, 66.55, 61.63, 52.68, 37.89, 29.79, 29.40.

**Compound 55**



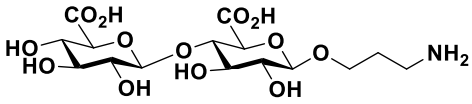
The oxidation and esterification of compound **54** was accomplished as described in the general procedure **C** yielded 45 % of **55.** $^{1}$H NMR (400 MHz, Chloroform-*d*) δ 8.07 – 7.87 (m, 8H), 7.57 – 7.47 (m, 4H), 7.44 – 7.33 (m, 13H), 5.71 (t, *J* = 8.8 Hz, 1H), 5.48 (t, *J* = 9.5 Hz, 1H), 5.39 – 5.28 (m, 2H), 5.06 (d, *J* = 2.8 Hz, 2H), 5.03 – 4.99 (m, 1H), 4.71 (d, *J* = 7.2 Hz, 1H), 4.51 (t, *J* = 8.9 Hz, 1H), 4.05 (d, *J* = 9.1 Hz, 1H), 3.98 (m, 1H), 3.93 – 3.83 (m, 2H), 3.56 (m, 1H), 3.40 (s, 6H), 3.26 – 3.11 (m, 3H), 1.70 (s, 3H). $^{13}$C NMR (101 MHz, Chloroform-*d*) δ 168.13 , 168.01 , 166.43 , 165.29 , 165.03 , 156.44 , 136.74 , 133.12 (d, *J* = 25.0 Hz), 130.11 – 129.50 (m), 129.46 – 128.82 (m), 128.40 (dd, *J* = 9.3, 3.9 Hz), 128.01 , 101.04 , 100.99 , 76.48 , 74.81 , 74.57 , 73.96 , 72.56 , 71.86 , 71.44 , 70.20 , 67.58 , 66.45 , 52.61 , 52.47 , 37.83 , 29.30 .

**Compound 56**



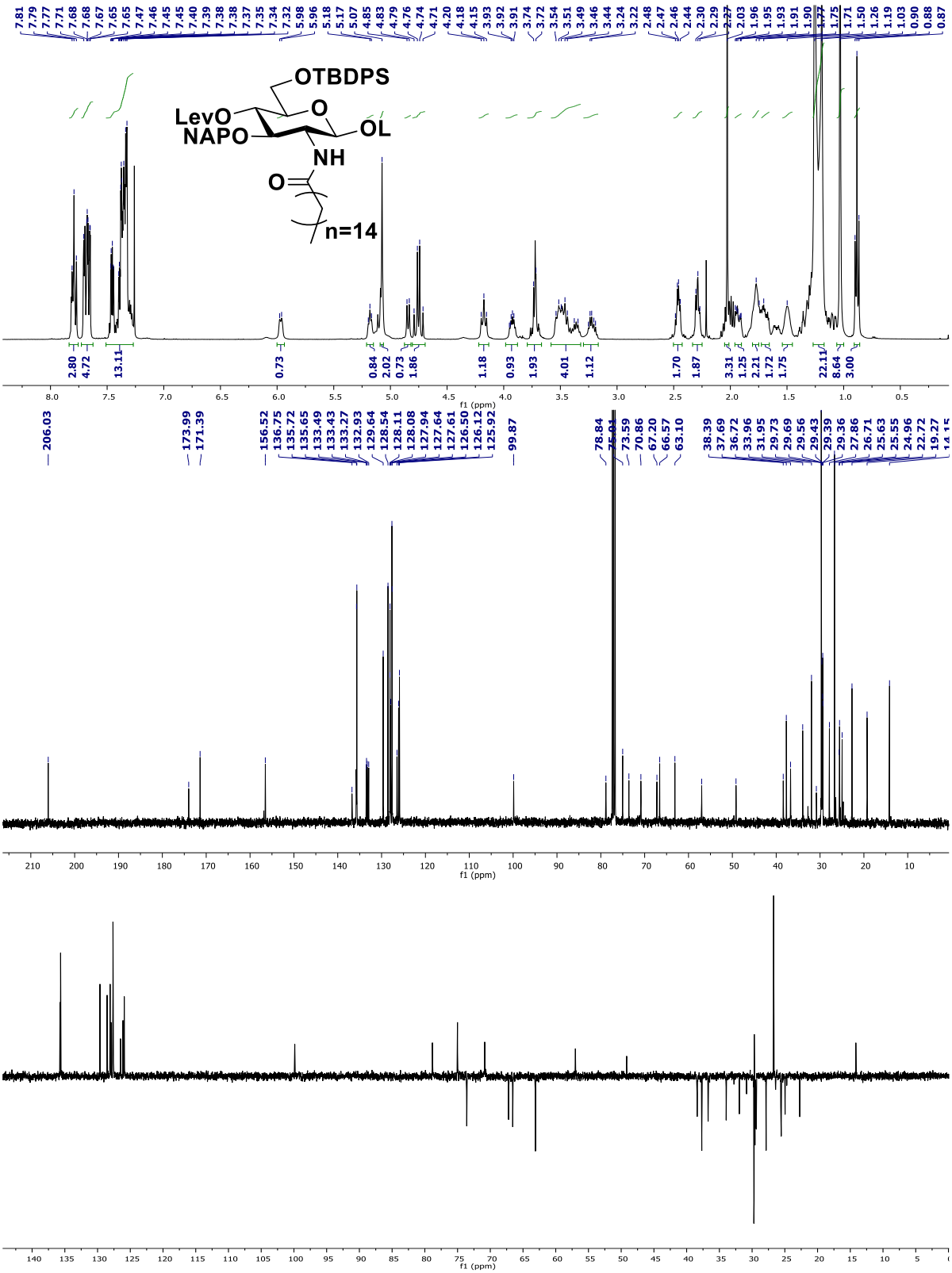

The saponification of compound **55** was accomplished as described in the general procedure **K**, yielded 76 % of **56**. $^{1}$H NMR (400 MHz, Deuterium Oxide) δ 7.27 (m, 5H), 4.95 (s, 2H), 4.35 (d, 1H), 4.28 (d, 1H), 3.79-3.74 (m, 1H), 3.66 (d, 1H), 3.64 – 3.57 (m, 1H), 3.55-3.44 (m, 3H), 3.40-3.32 (d, *J* = 6.7 Hz, 2H), 3.21-3.16 (m, 2H), 3.11-3.01 (m, 2H), 1.67 – 1.63 (q, 2H). $^{13}$C NMR (101 MHz, Deuterium Oxide) δ 177.19 , 176.67 , 160.02 , 130.38 , 129.93 , 129.21 , 104.03 , 103.53 , 82.68 , 77.44 , 77.16 , 76.86 , 76.04 , 74.69 , 74.19 , 73.25 , 69.26 , 68.39 , 38.84 , 30.38 .

**Compound 57 (GA-20)**

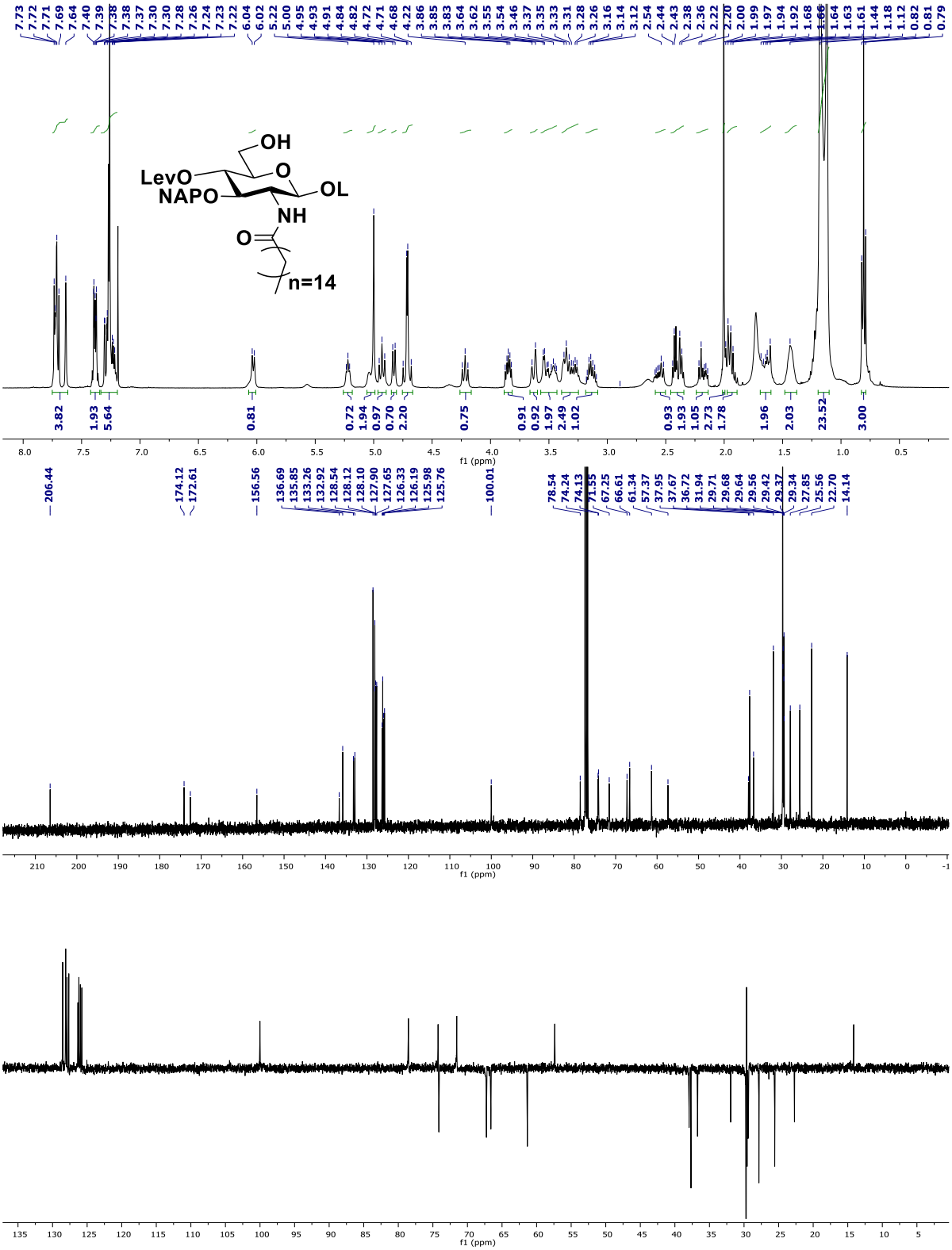



The hydrogenation of compound **56** was accomplished as described in the general procedure **L**, yielded 48% of **57**. $^{1}$H NMR (400 MHz, Deuterium Oxide) δ 4.42 (dd, *J* = 7.9, 4.2 Hz, 2H), 3.93 (m, 1H), 3.80 – 3.71 (m, 2H), 3.69 – 3.64 (m, 1H), 3.58 (m, 2H), 3.47 – 3.37 (m, 2H), 3.33 – 3.20 (m, 2H), 3.07 (td, *J* = 6.8, 1.7 Hz, 2H), 1.97 – 1.87 (m, 2H). $^{13}$C NMR (101 MHz, Deuterium Oxide) δ 181.20 , 175.59 , 175.09 , 102.34 , 101.98 , 80.85 , 75.84 , 75.45 , 75.26 , 74.38 , 73.07 , 72.55 , 71.62 , 67.90 , 48.86 , 37.55 .

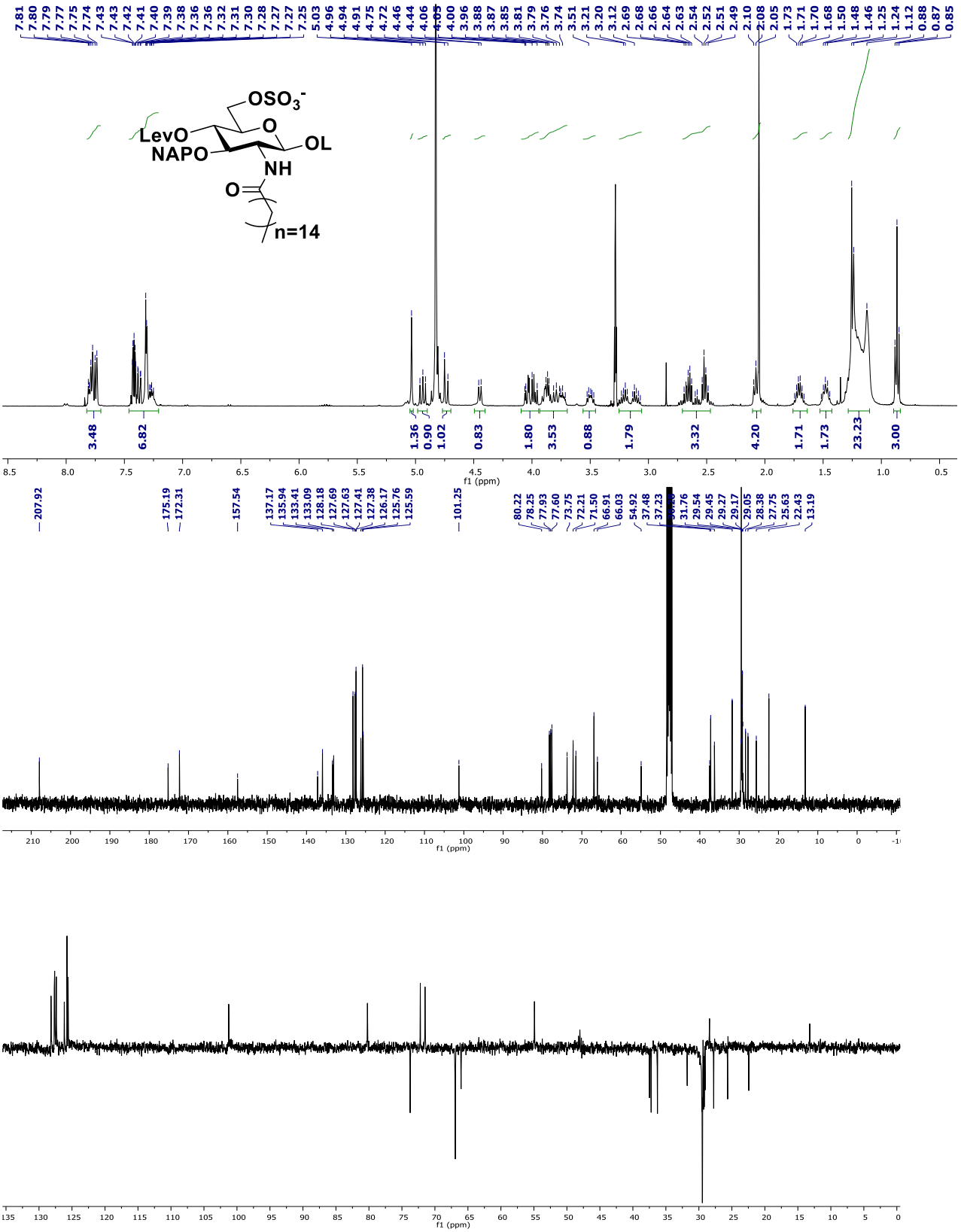
## 4.6. NMRs: $^{1}H$, $^{13}C$, and DEPT NMR spectrum of compound 1



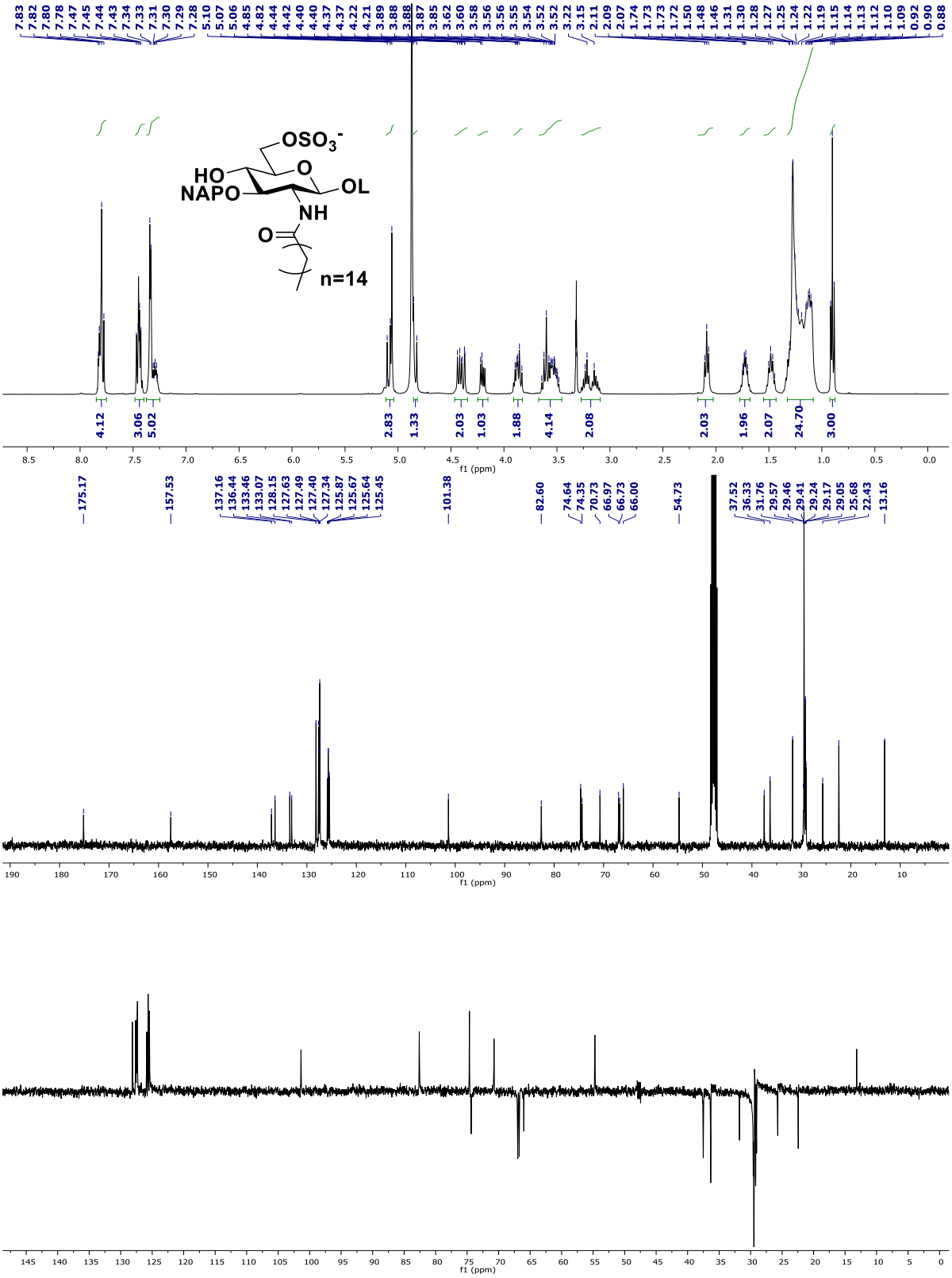
## $^{1}H$, $^{13}C$, and DEPT NMR spectrum of compound 2



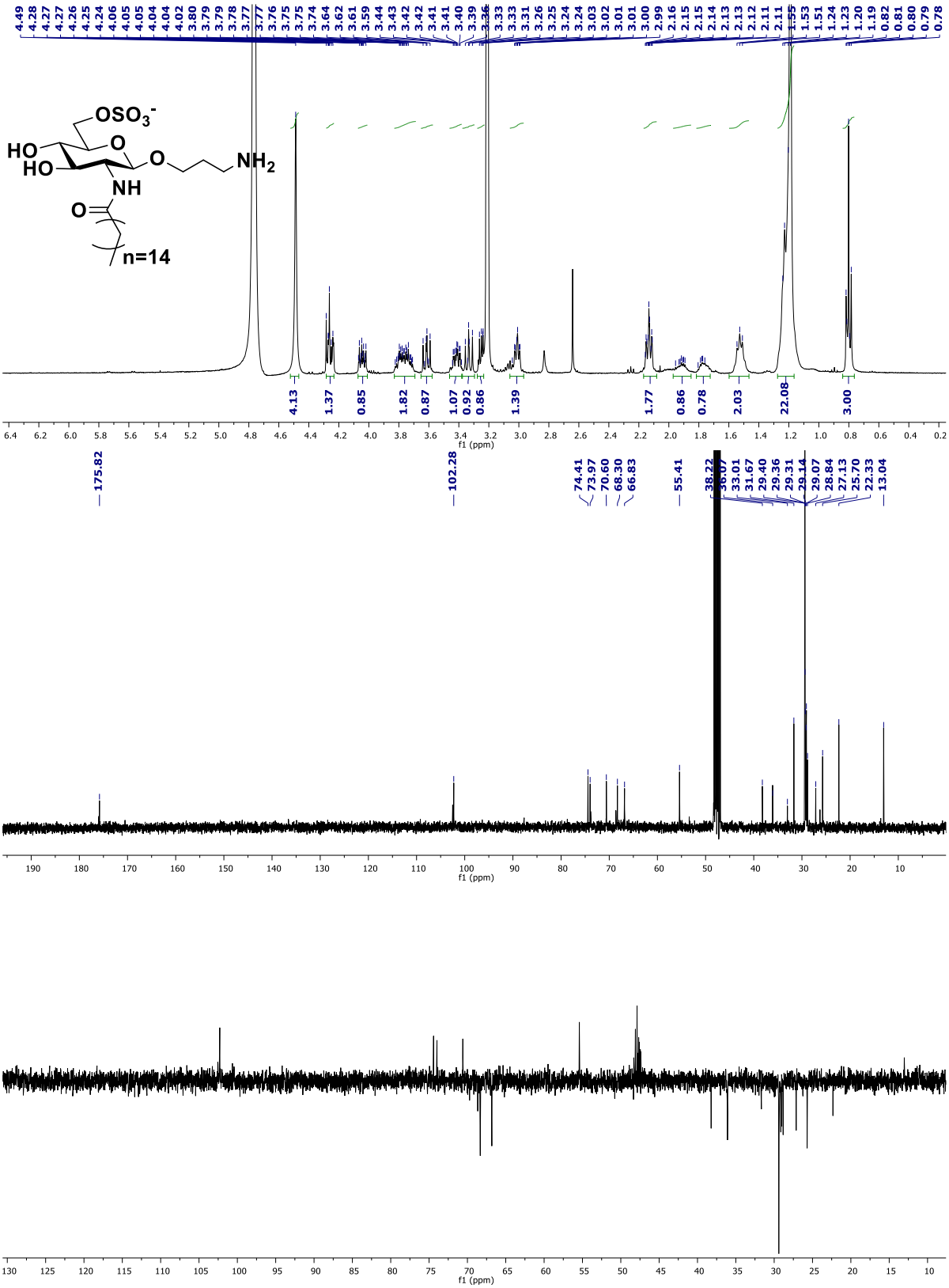
## $^{1}H$, $^{13}C$, and DEPT NMR spectrum of compound 4



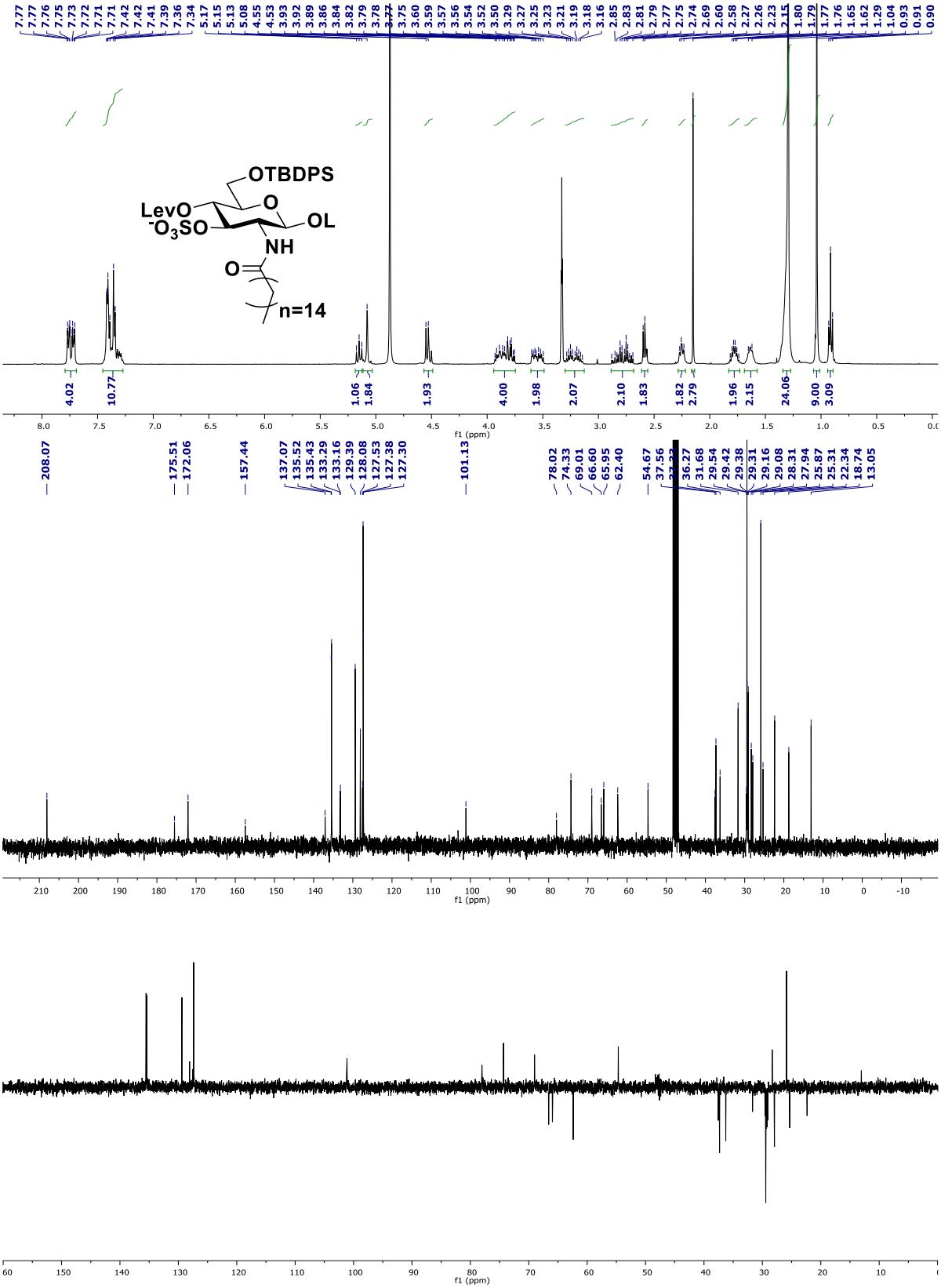
## $^{1}H$, $^{13}C$, and DEPT NMR spectrum of compound 5



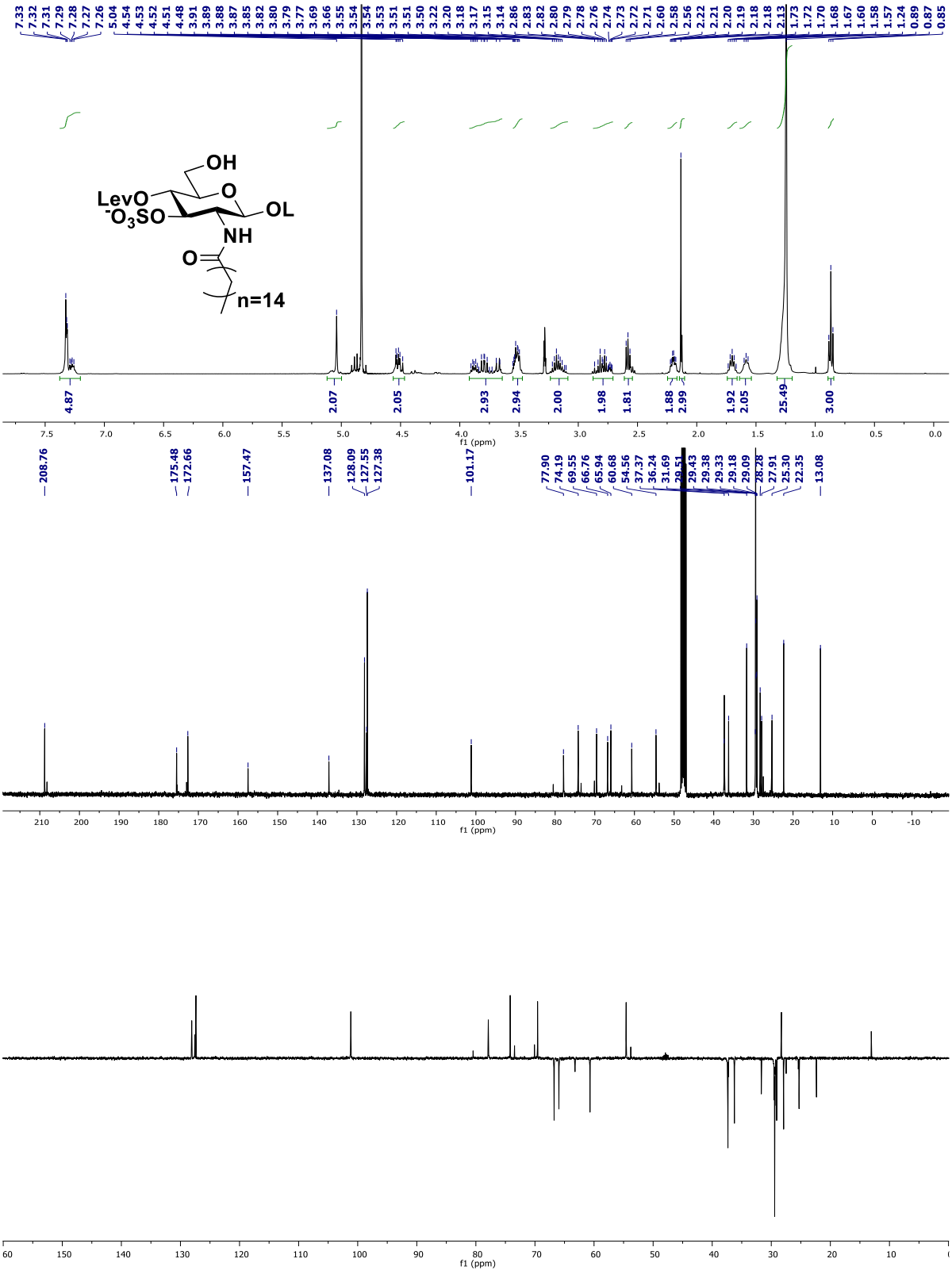
## $^{1}H$, $^{13}C$, and DEPT NMR spectrum of compound 6

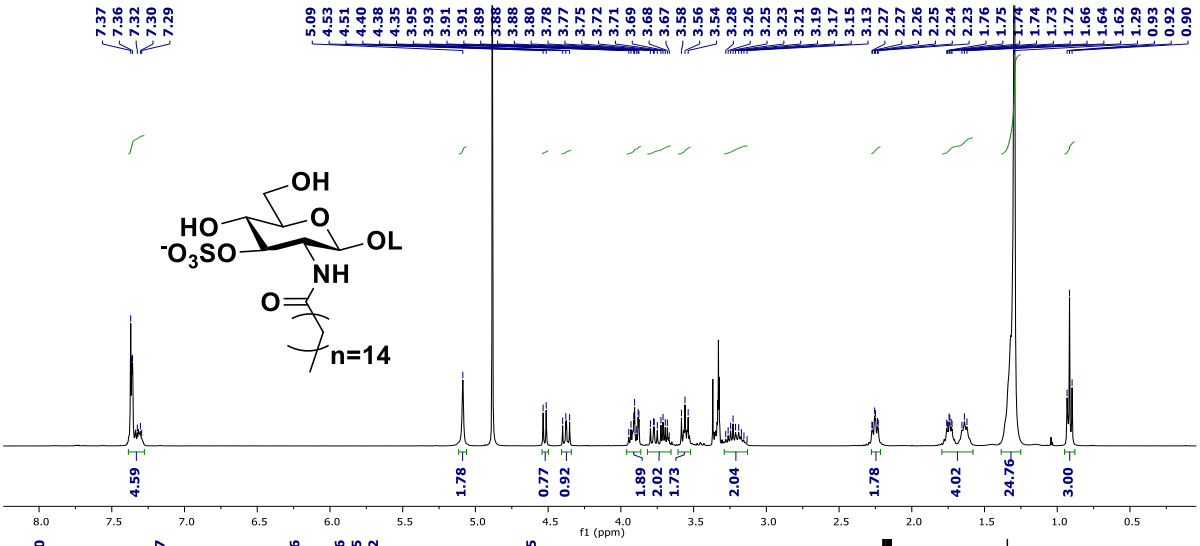


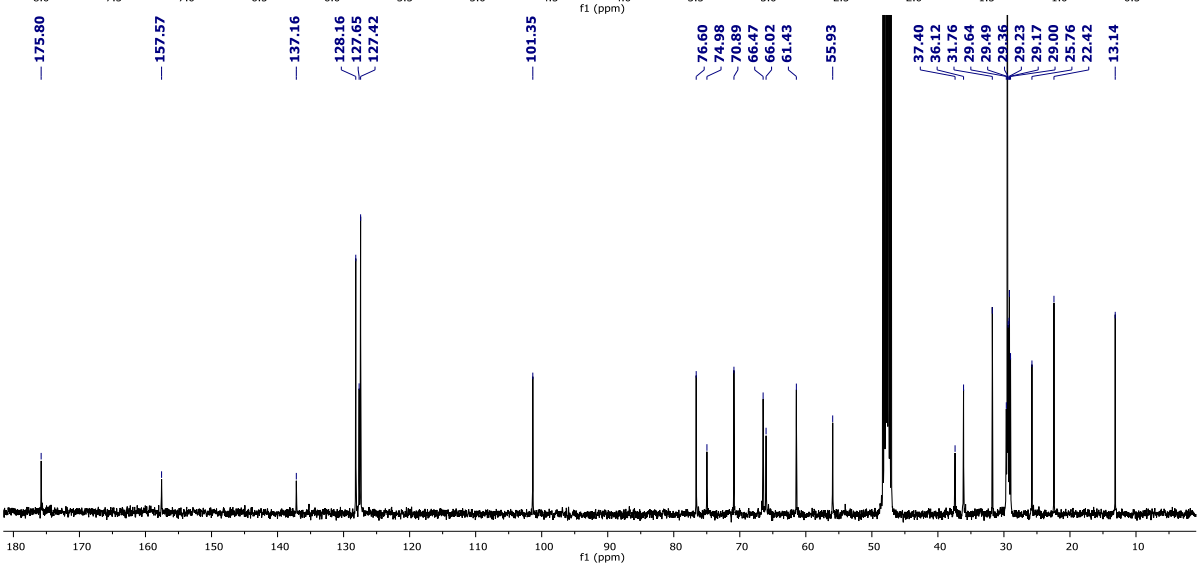
## $^{1}H$, $^{13}C$, and DEPT NMR spectrum of compound 7

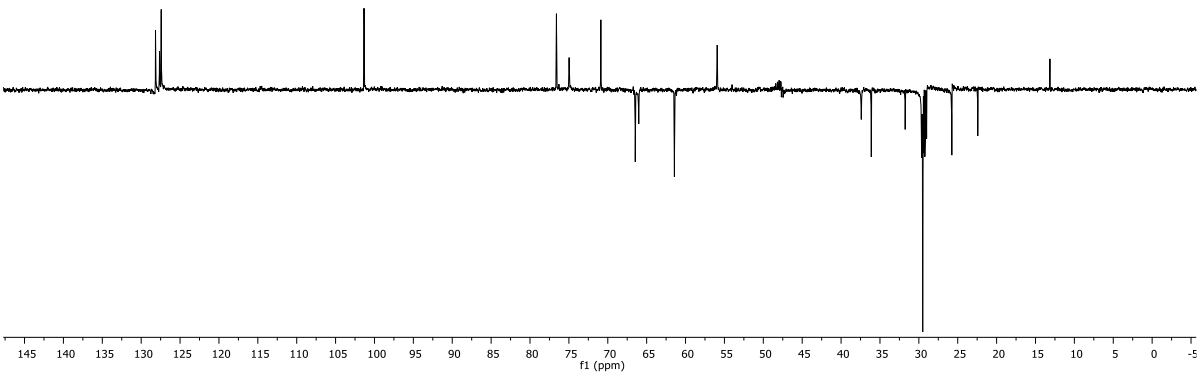


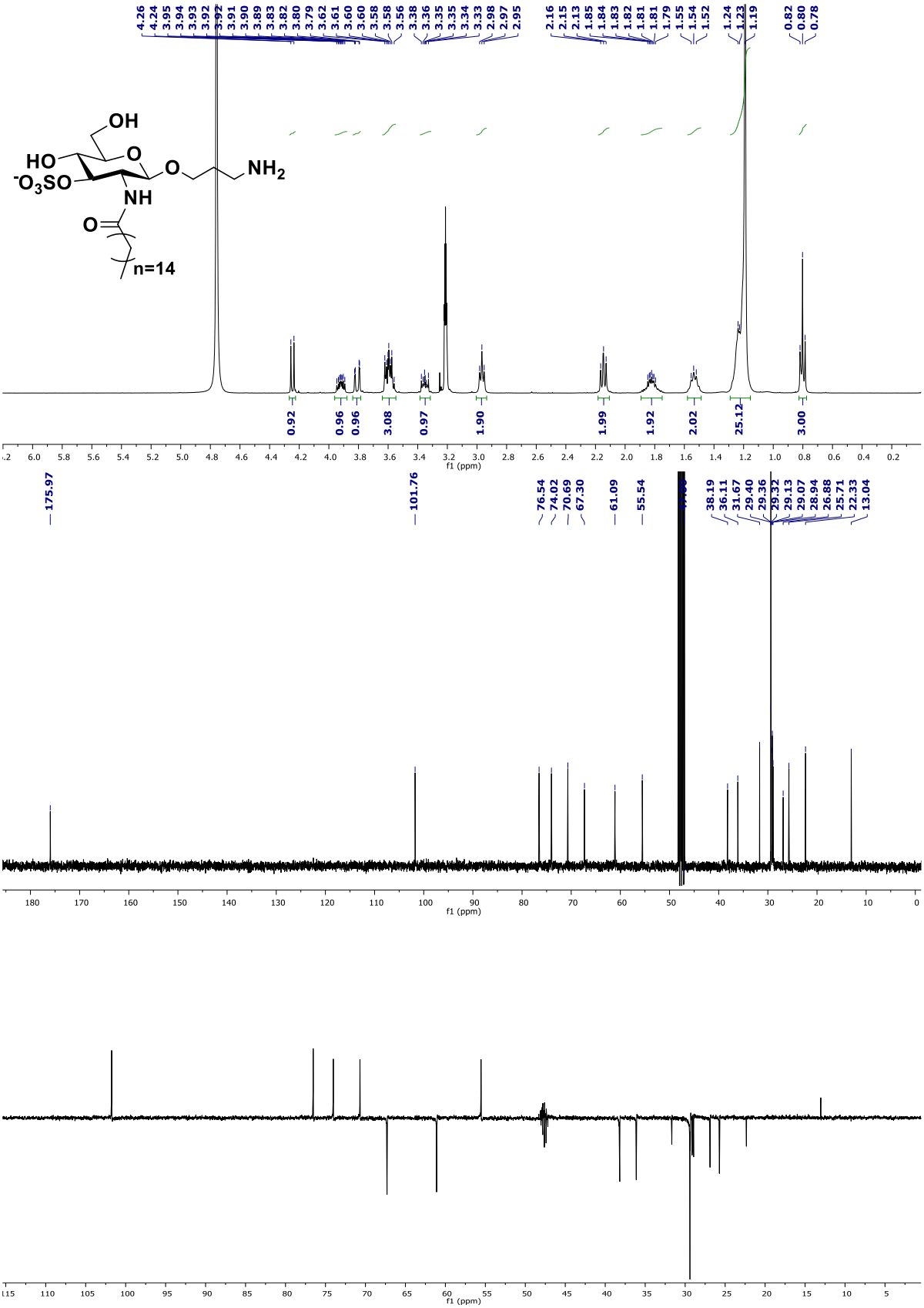
## $^{1}H$, $^{13}C$, and DEPT NMR spectrum of compound 8



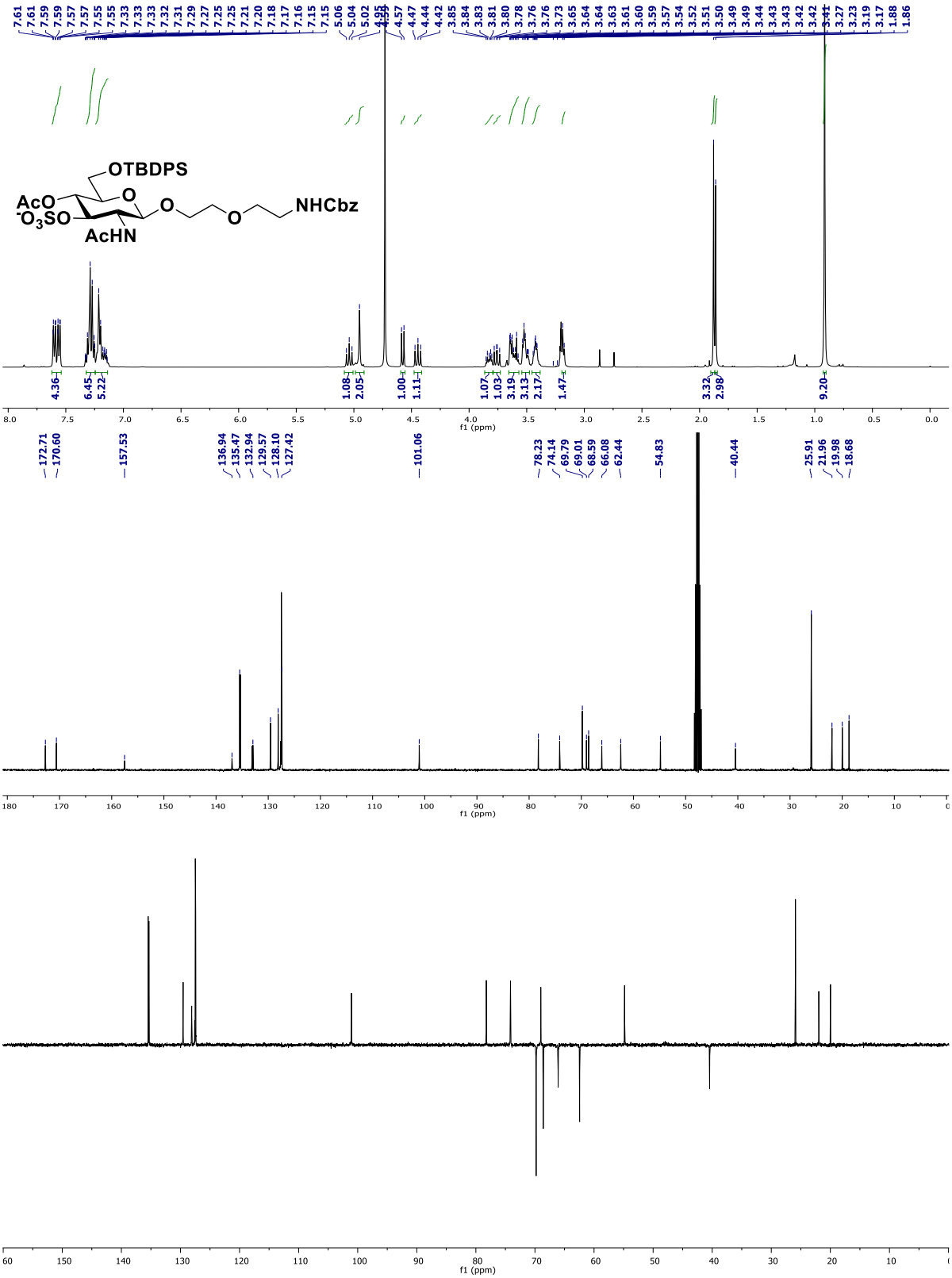

7.37 7.36 7.32 7.30 7.29
5.09 4.53 4.51 4.40 4.38 4.35 3.95 3.93 3.91 3.91 3.89 3.88 3.88 3.80 3.78 3.77 3.75 3.72 3.71 3.69 3.68 3.67 3.58 3.56 3.54 3.28 3.26 3.25 3.23 3.21 3.19 3.17 3.15 3.13 2.27 2.27 2.26 2.25 2.24 2.23 1.76 1.75 1.74 1.74 1.73 1.72 1.66 1.64 1.62 1.29 0.93 0.92 0.90
OH
HO
O
OL
-O3SO
NH
O
n=14
4.59 1.78 0.77 0.92 1.89 2.02 1.73 2.04 1.78 4.02 24.76 3.00
f1 (ppm)


175.80 157.57 137.16 128.16 127.65 127.42 101.35 76.60 74.98 70.89 66.47 66.02 61.43 55.93 37.40 36.12 31.76 29.64 29.49 29.36 29.23 29.17 29.00 25.76 22.42 13.14
f1 (ppm)

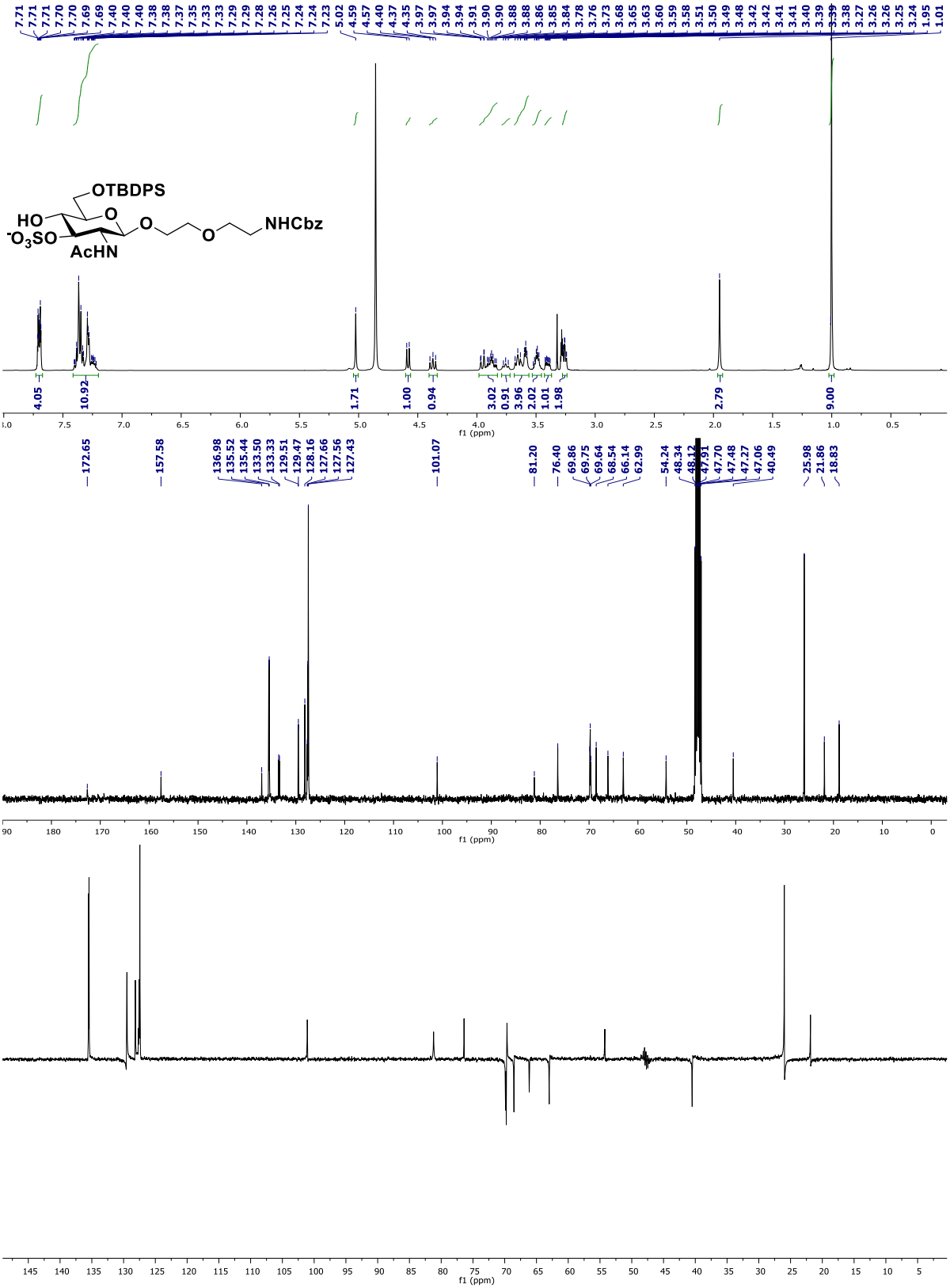

f1 (ppm)


OH
HO
O
O
NH2
-O3SO
NH
O
n=14
f1 (ppm)

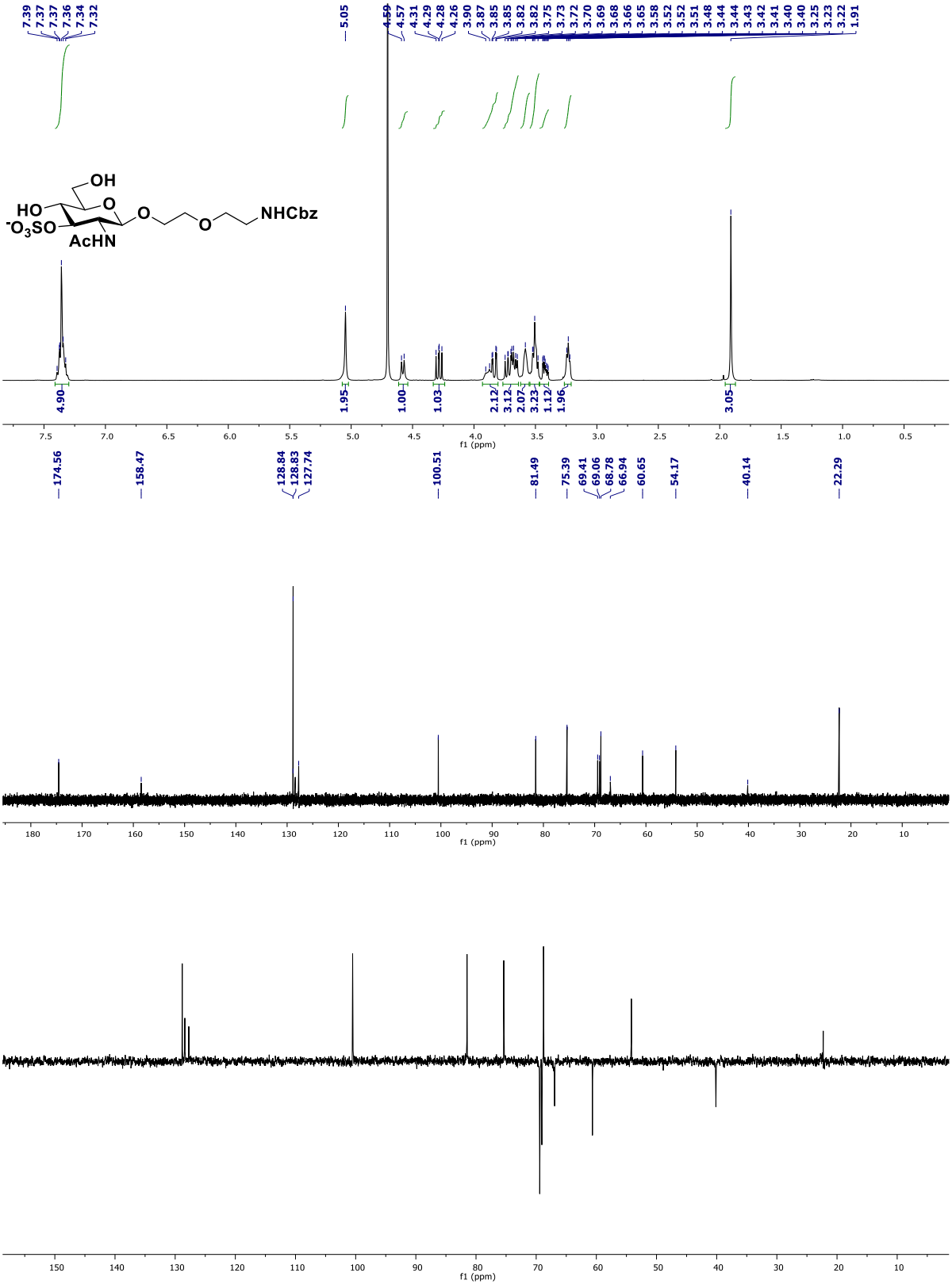
## $^{1}H$, $^{13}C$, and DEPT NMR spectrum of compound 12



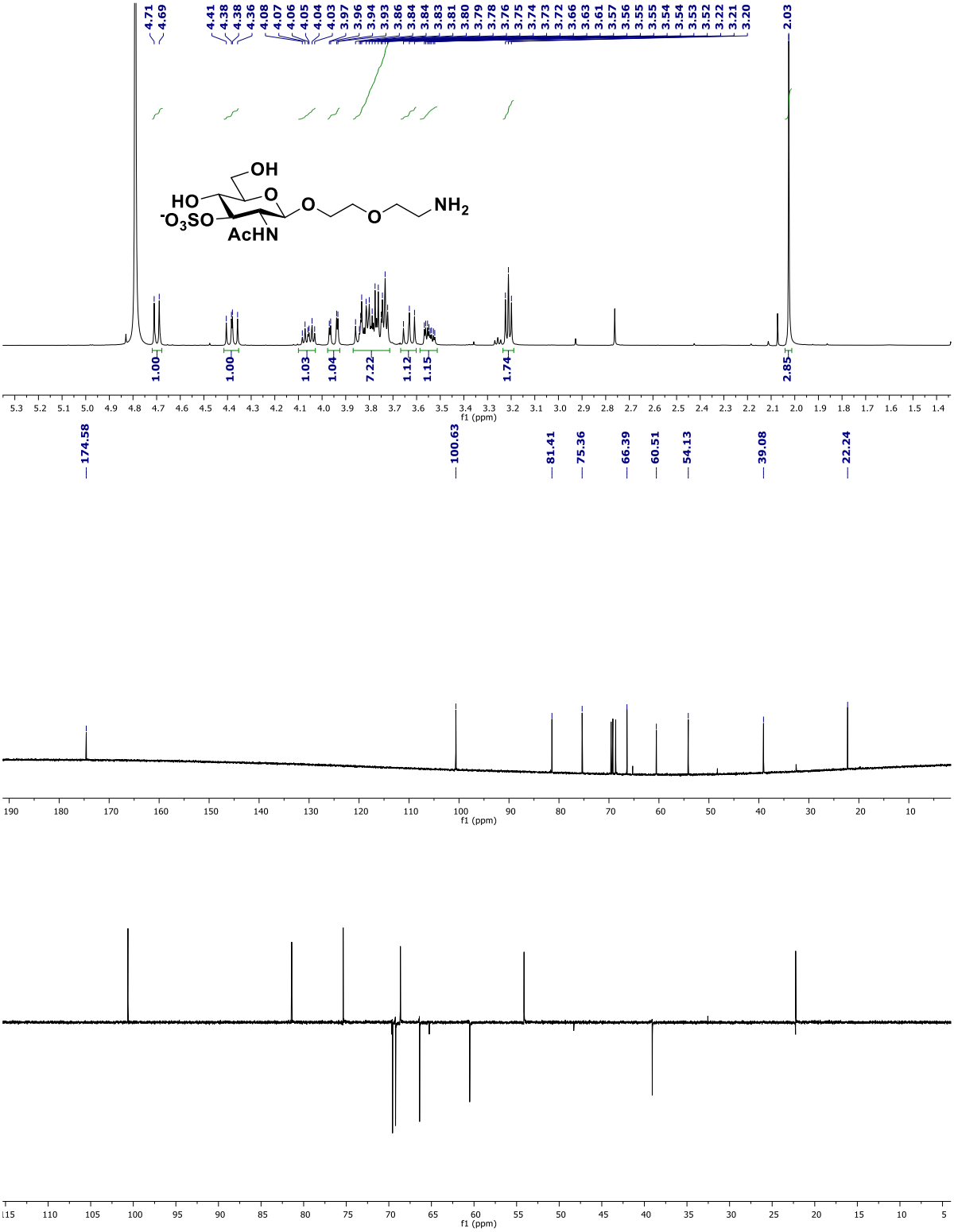
## $^{1}H$, $^{13}C$, and DEPT NMR spectrum of compound 13



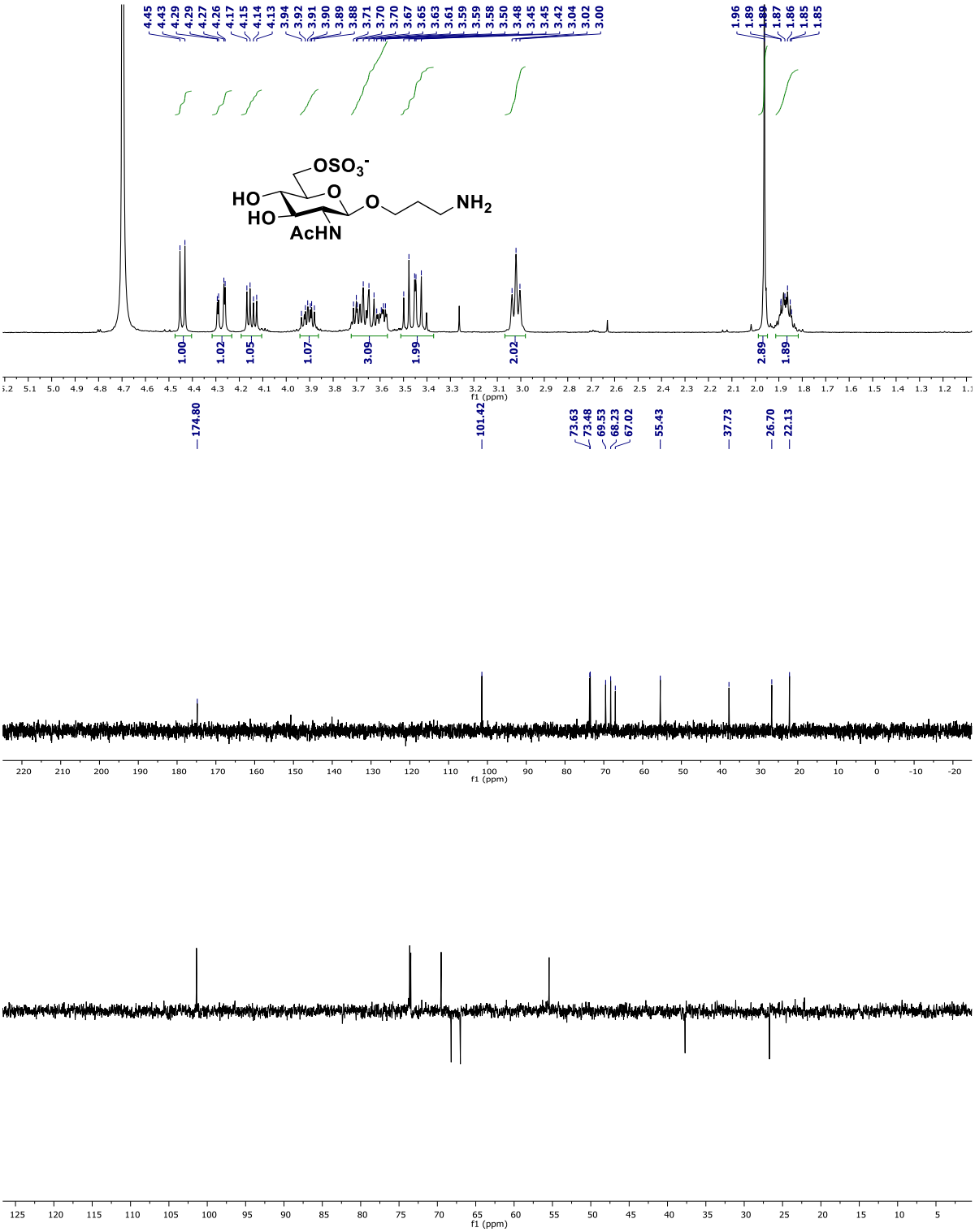
## $^{1}H$, $^{13}C$, and DEPT NMR spectrum of compound 14



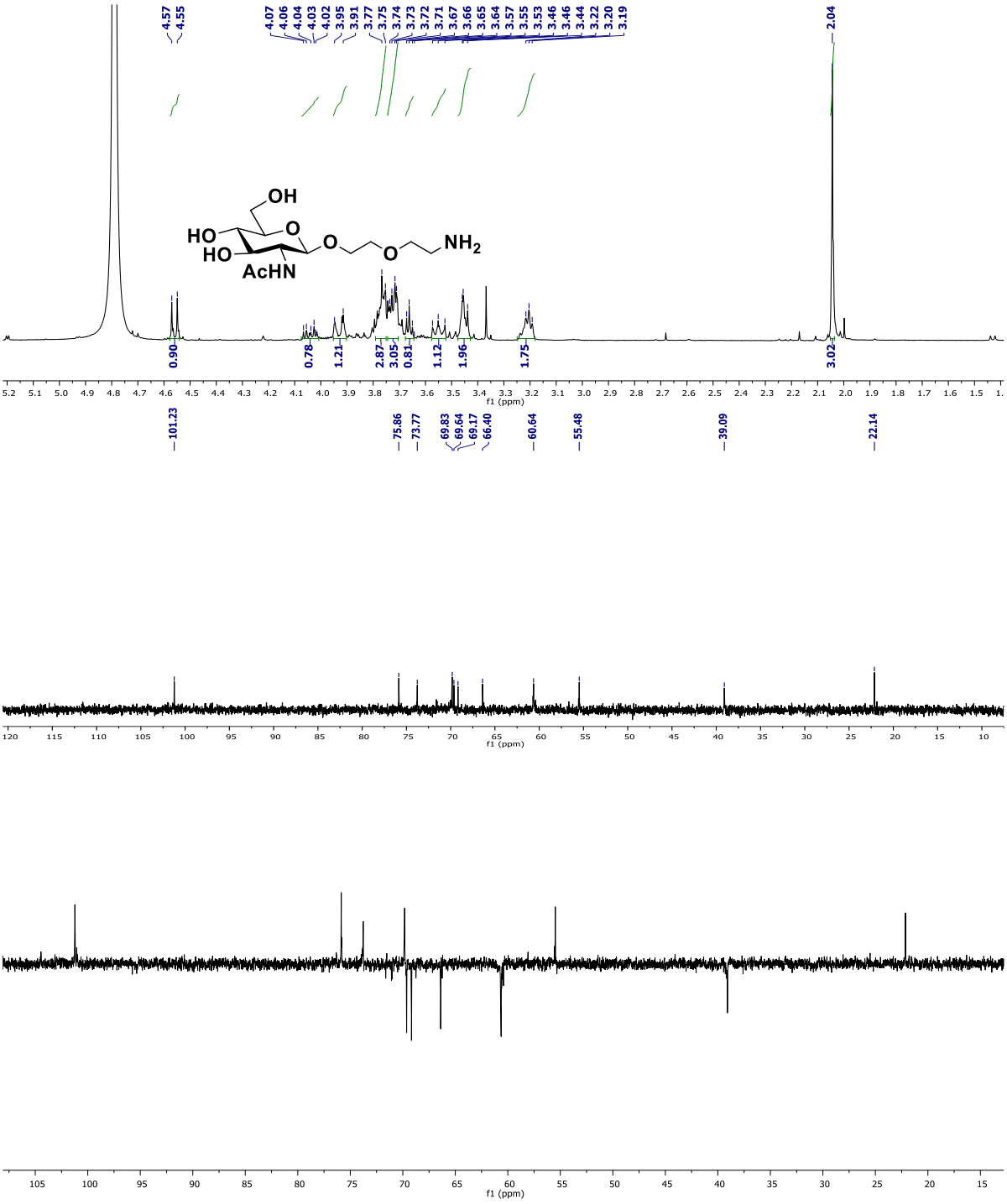
## $^{1}H$, $^{13}C$, and DEPT NMR spectrum of compound 15



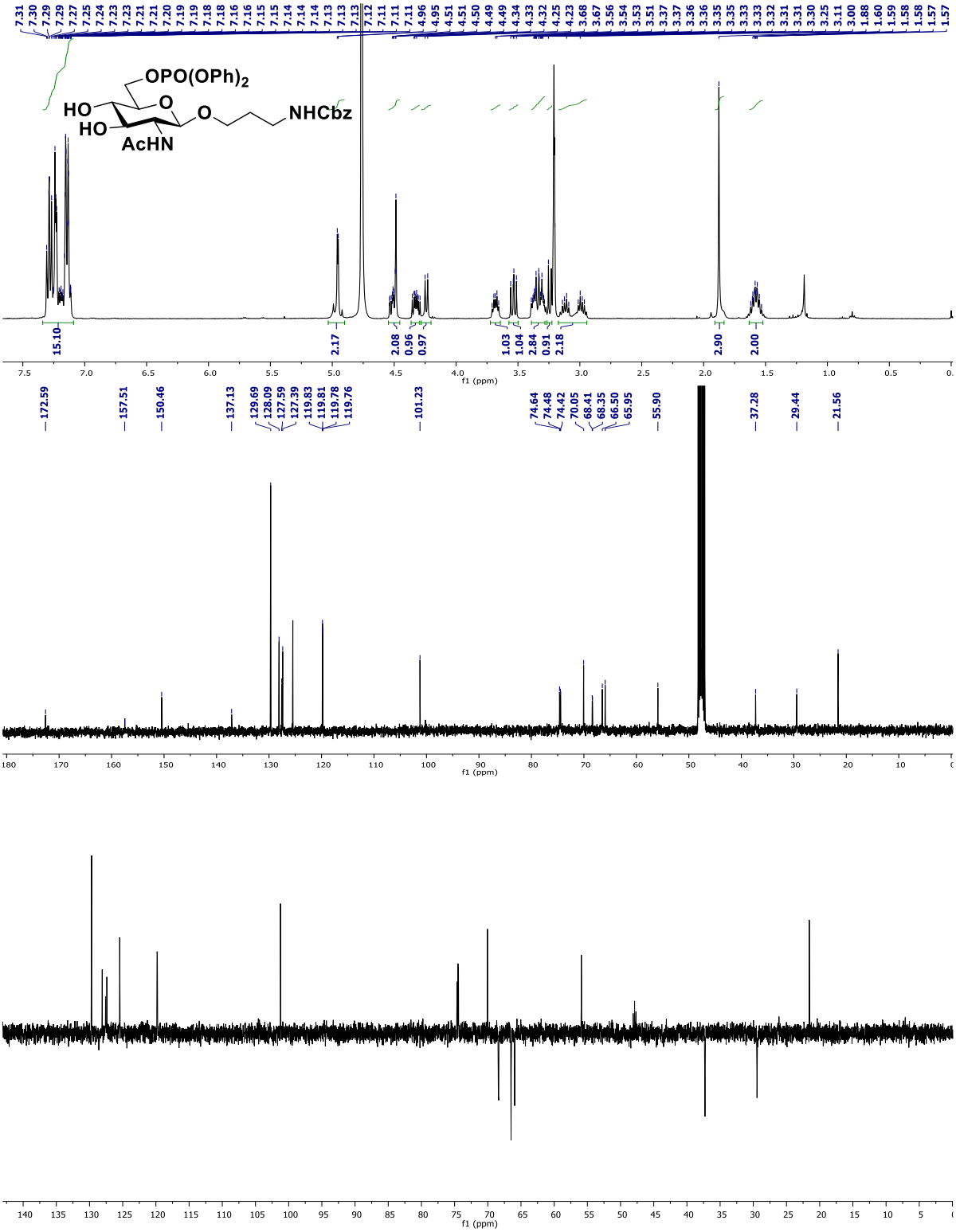
## $^{1}H$, $^{13}C$, and DEPT NMR spectrum of compound 16



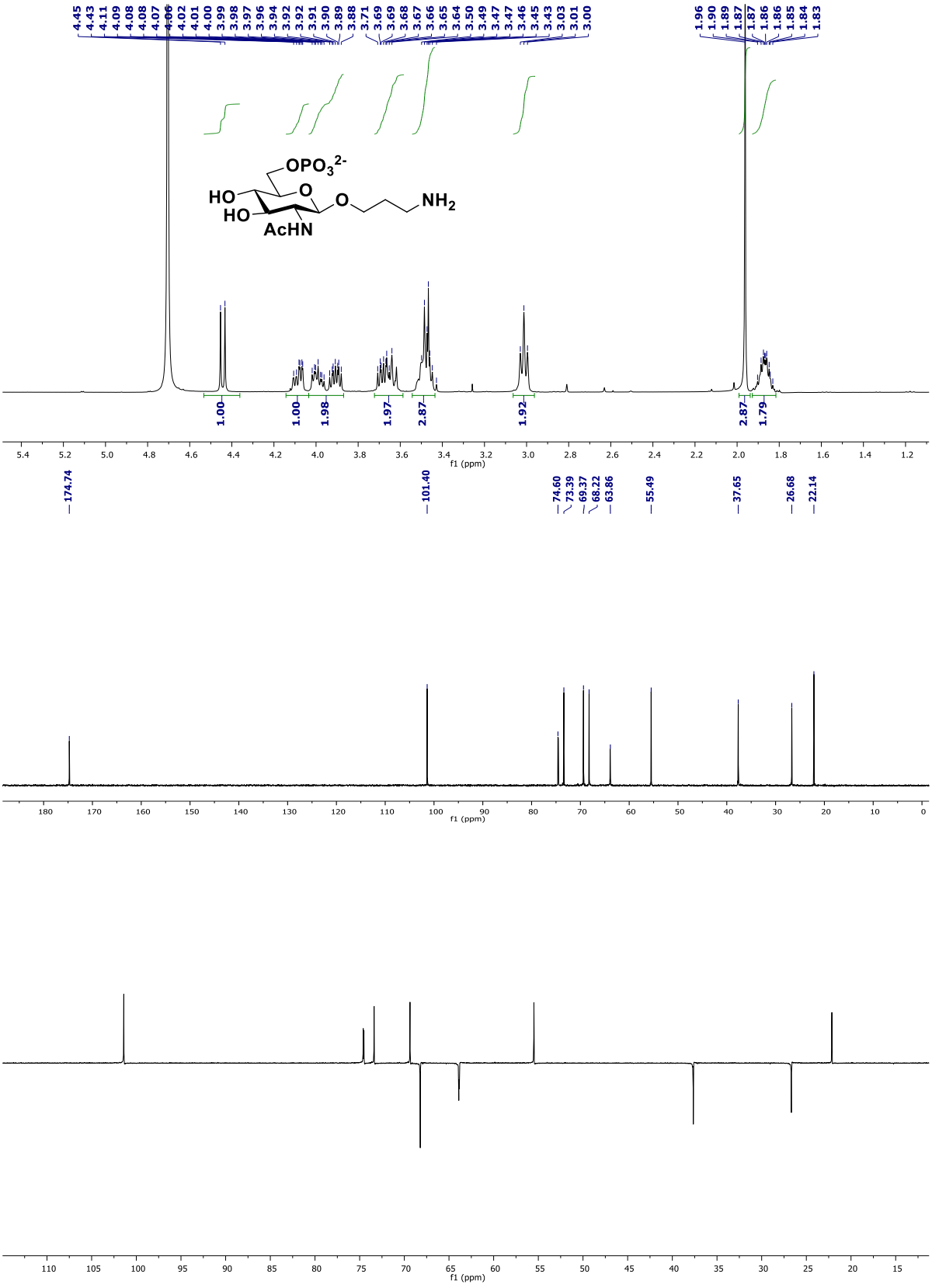
## $^{1}H$, $^{13}C$, and DEPT NMR spectrum of compound 17



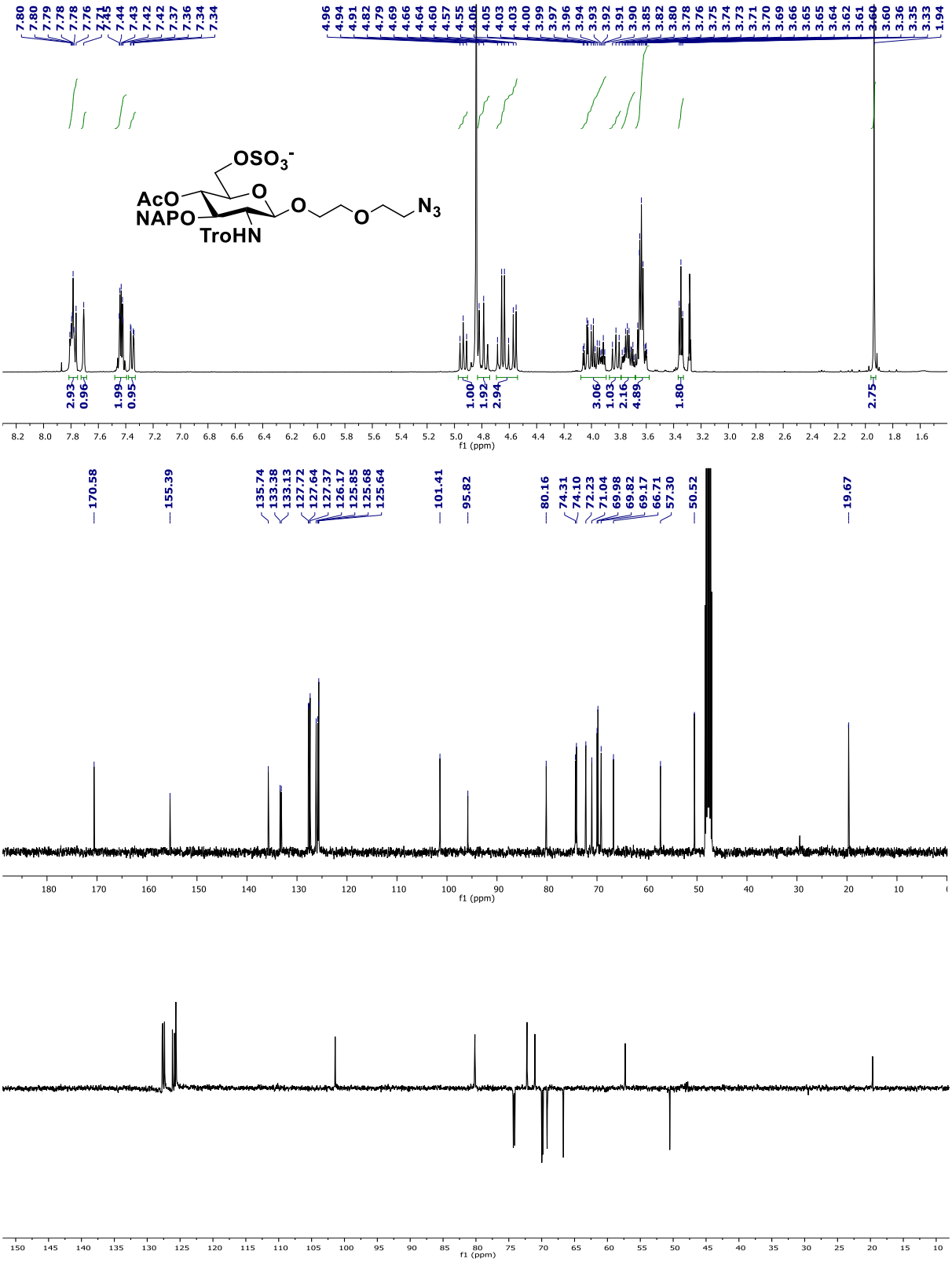
## $^{1}H$, $^{13}C$, and DEPT NMR spectrum of compound 19



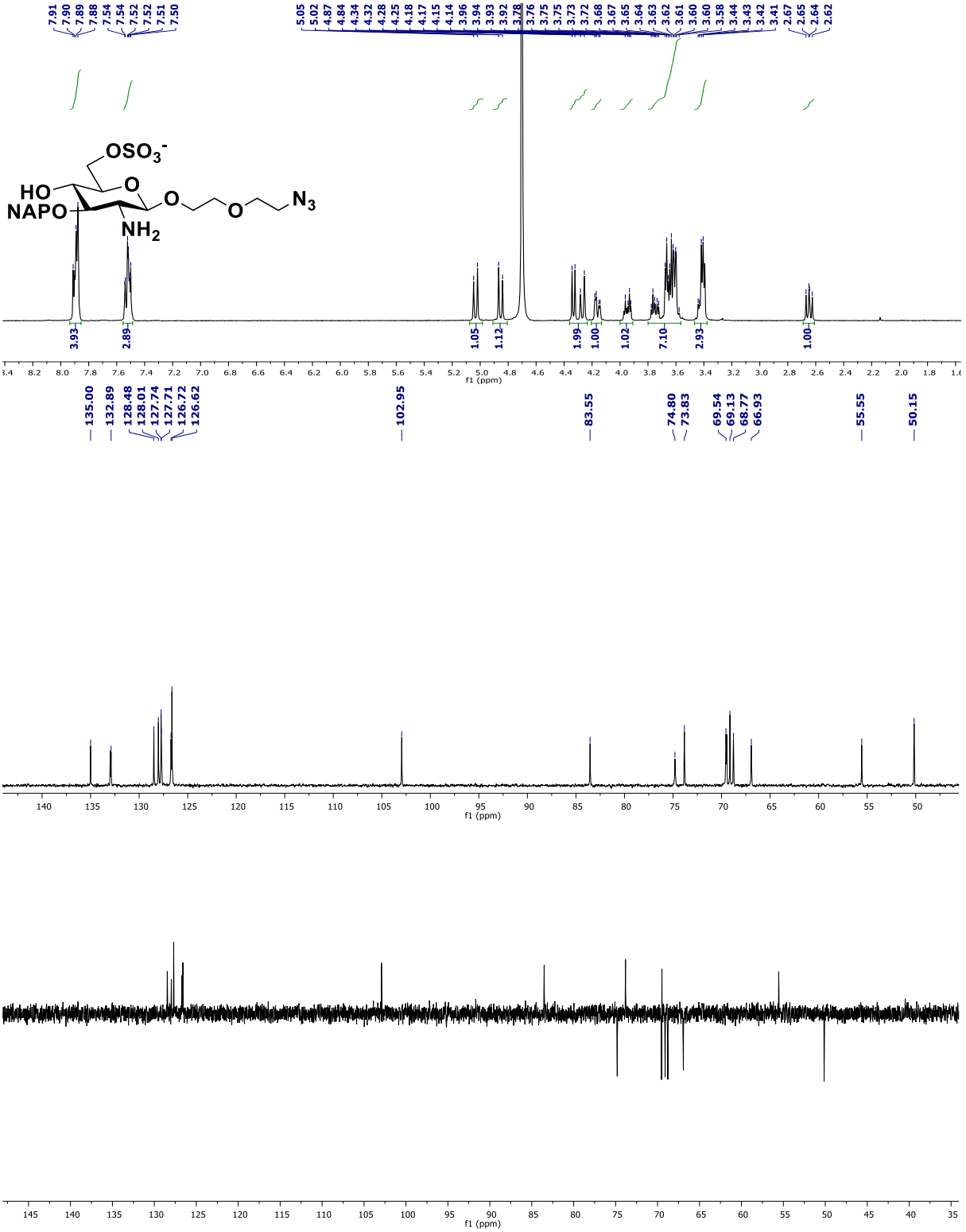
## $^{1}H$, $^{13}C$, and DEPT NMR spectrum of compound 20



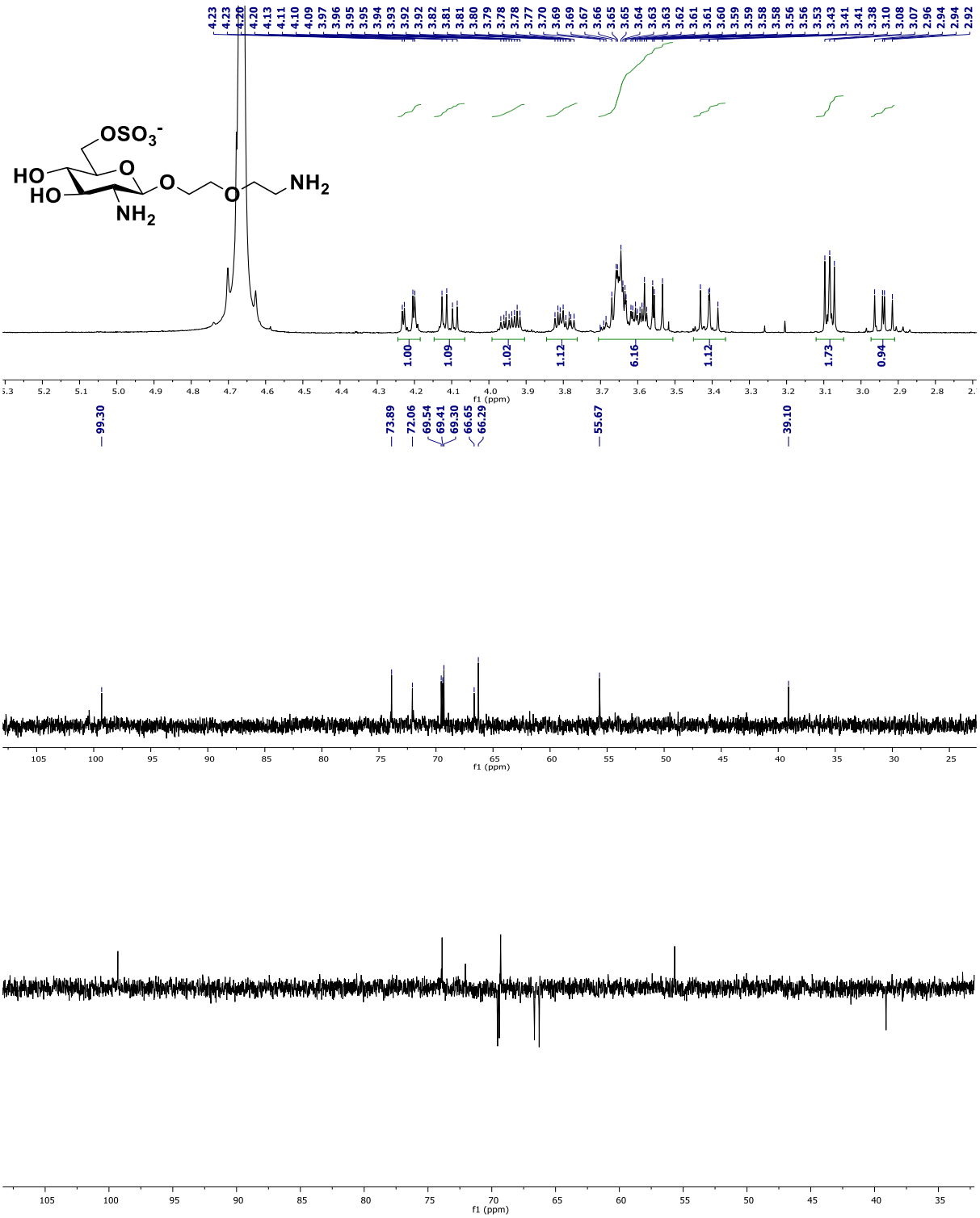
## $^{1}H$, $^{13}C$, and DEPT NMR spectrum of compound 22



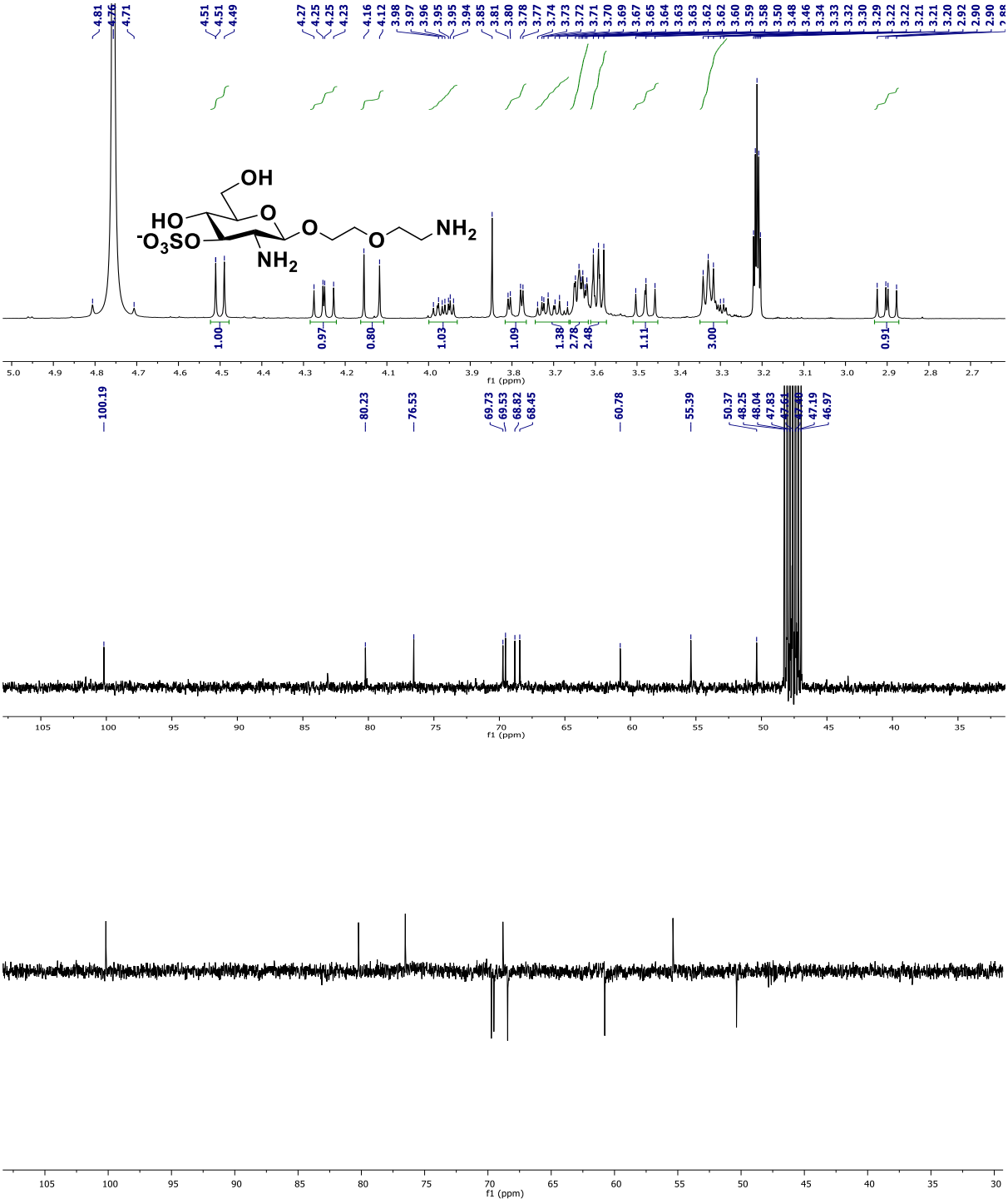
## $^{1}H$, $^{13}C$, and DEPT NMR spectrum of compound 23



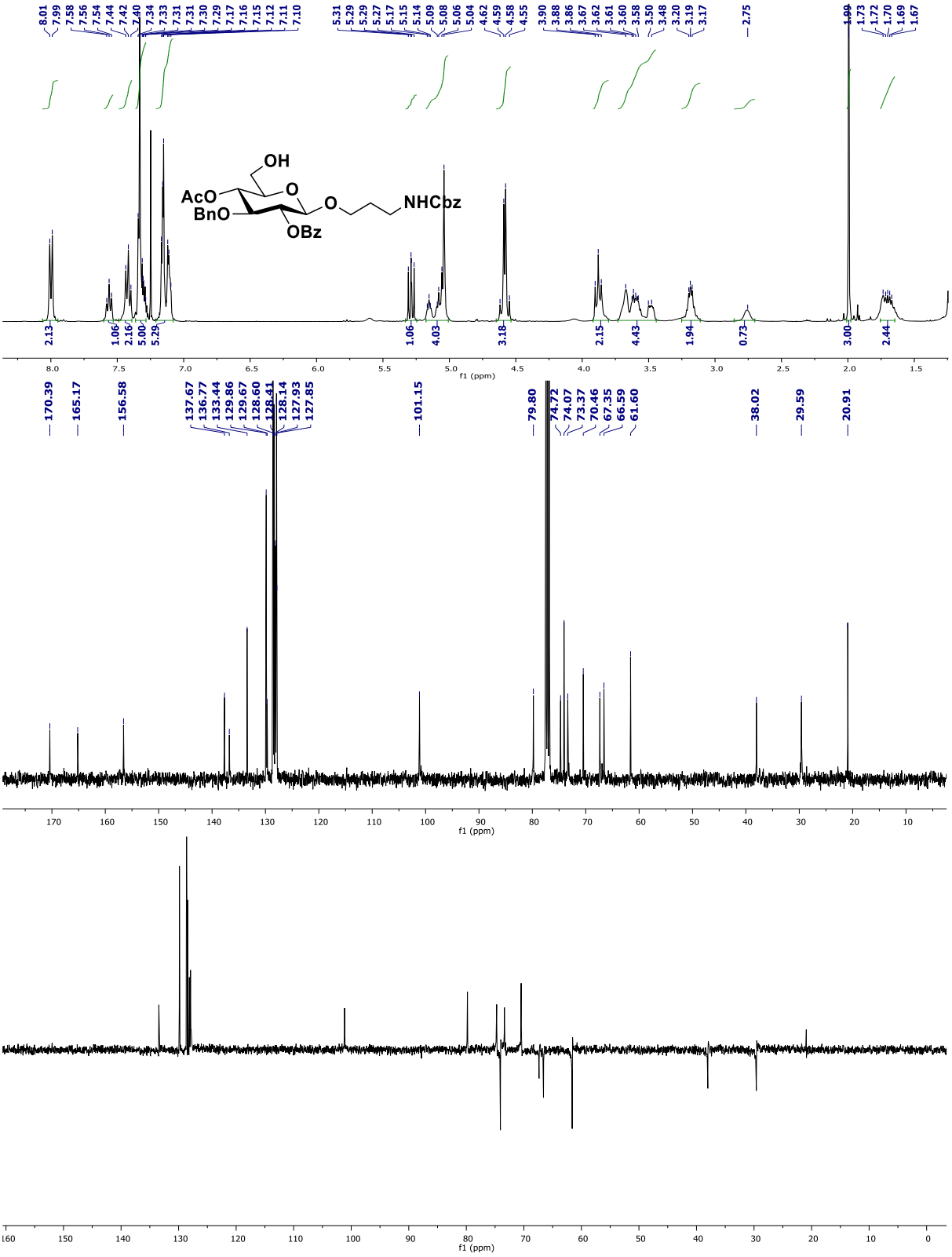
## $^{1}H$, $^{13}C$, and DEPT NMR spectrum of compound 24



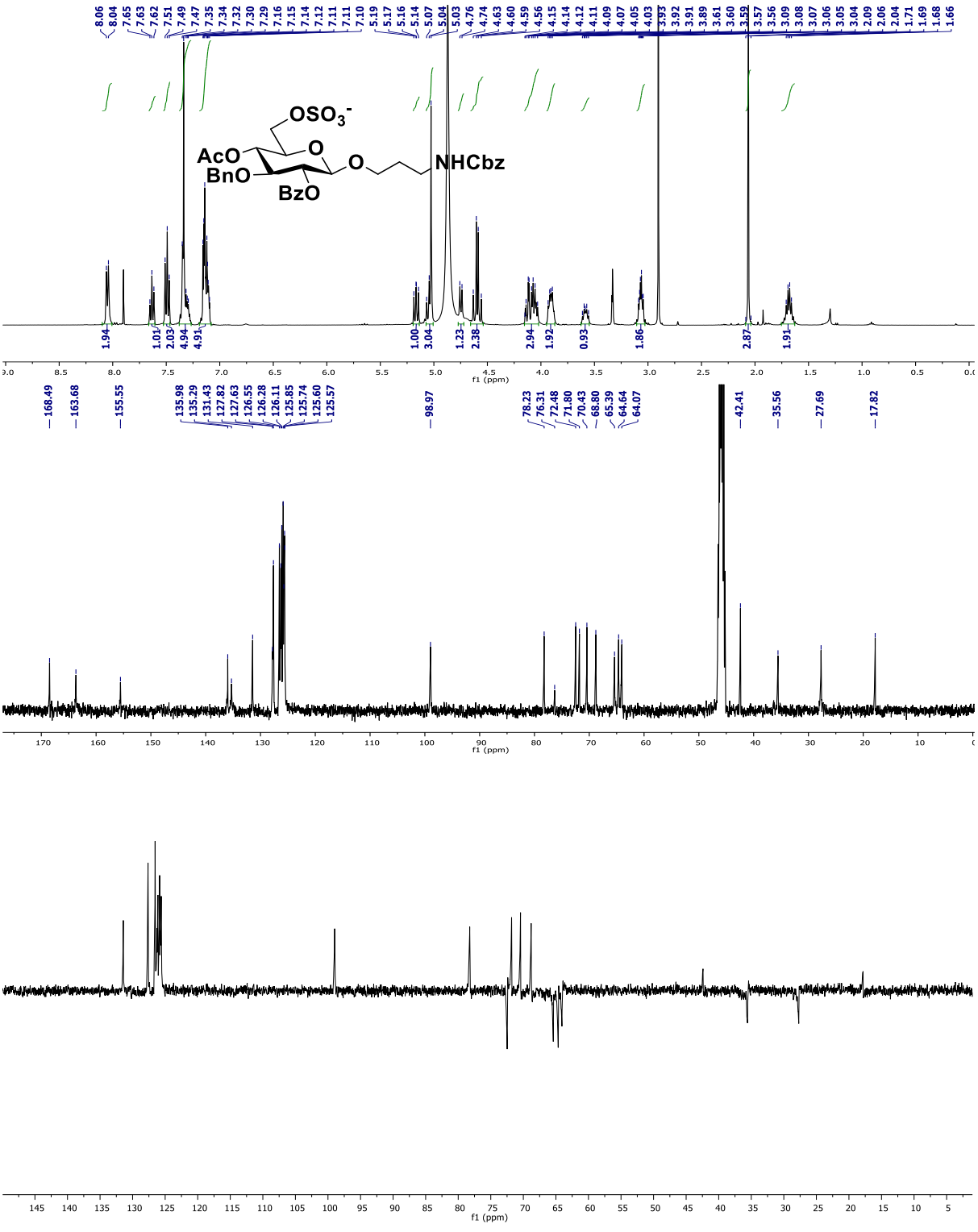
## $^{1}H$, $^{13}C$, and DEPT NMR spectrum of compound 25



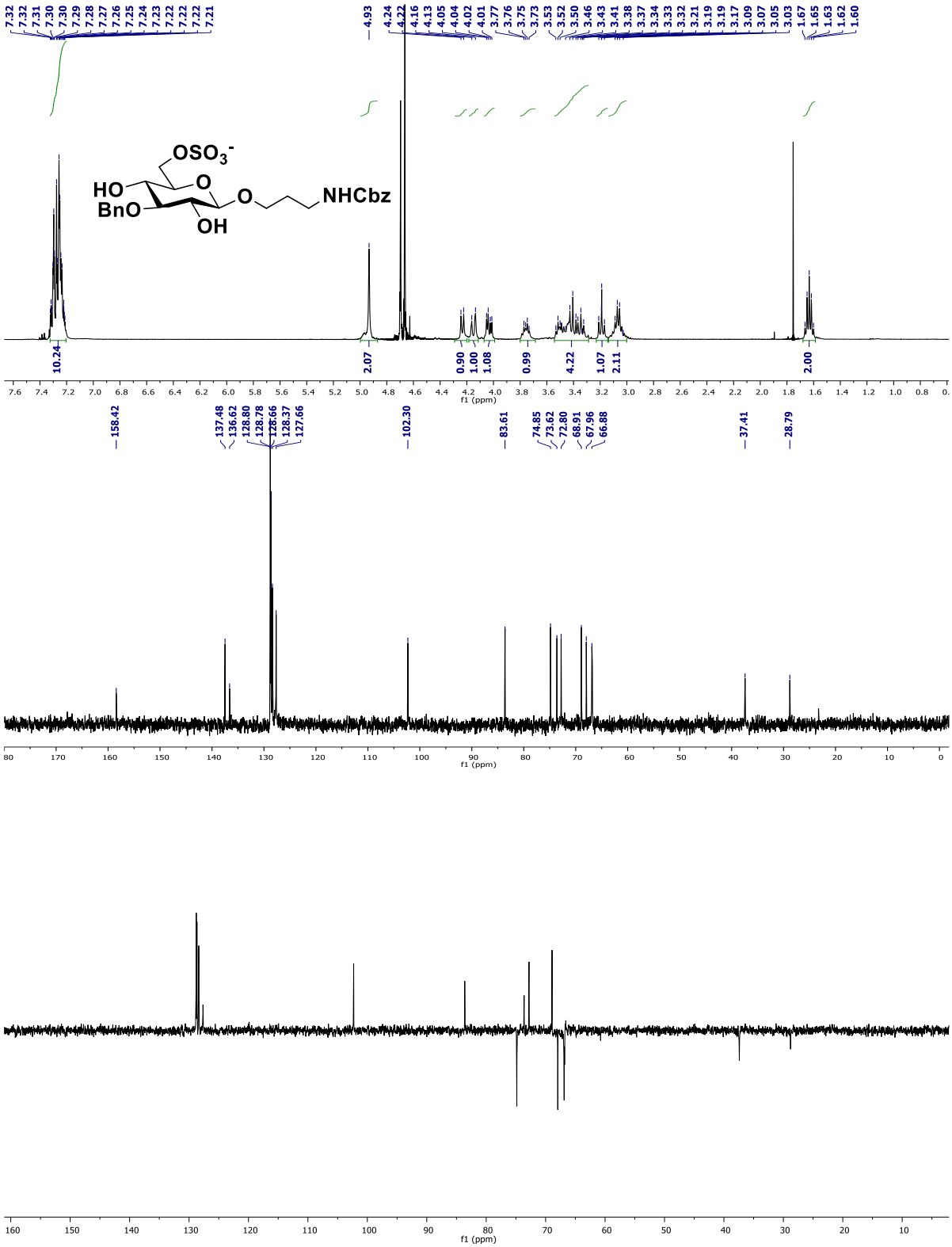
## $^{1}H$, $^{13}C$, and DEPT NMR spectrum of compound 27



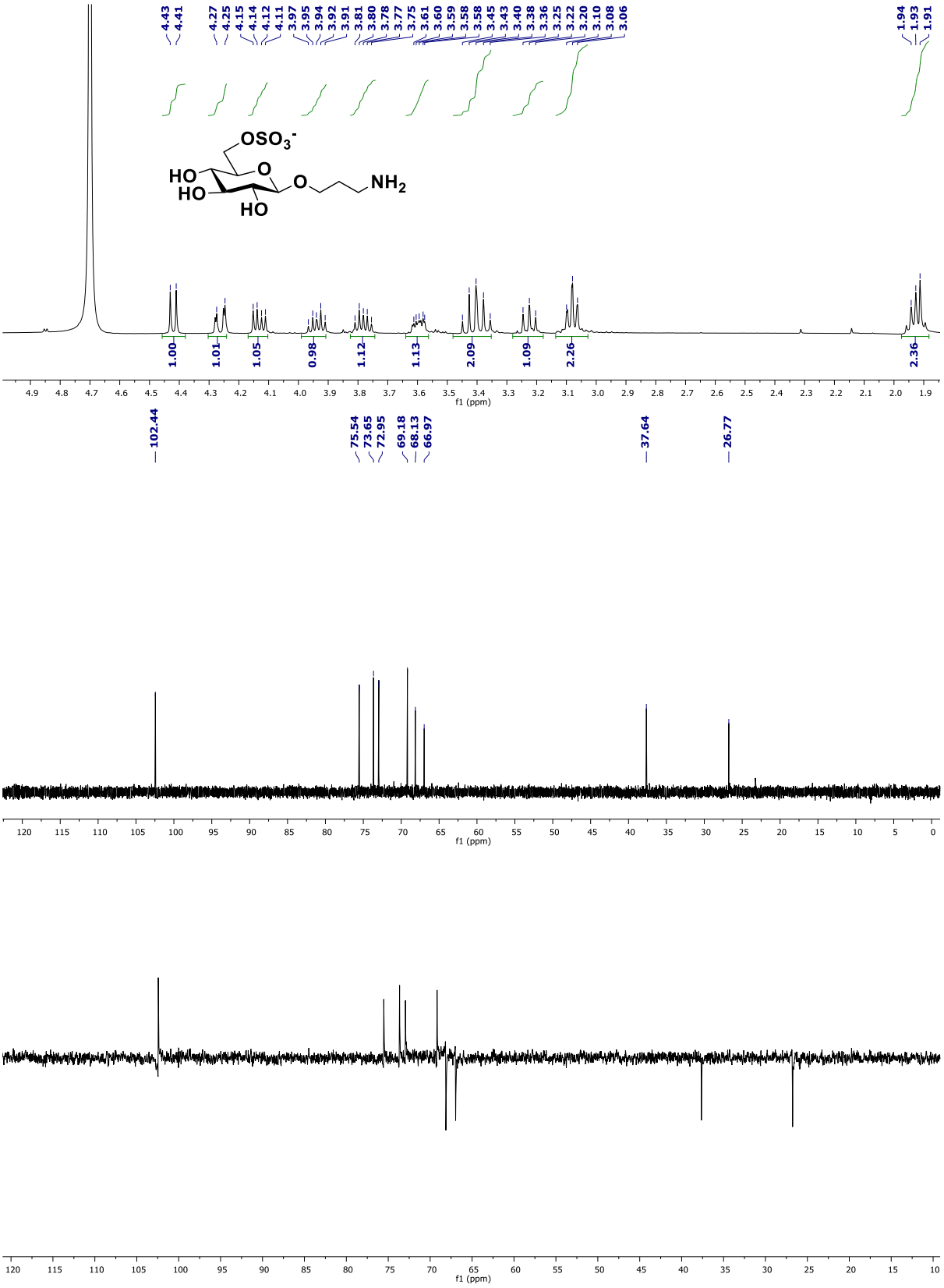
## $^{1}H$, $^{13}C$, and DEPT NMR spectrum of compound 28



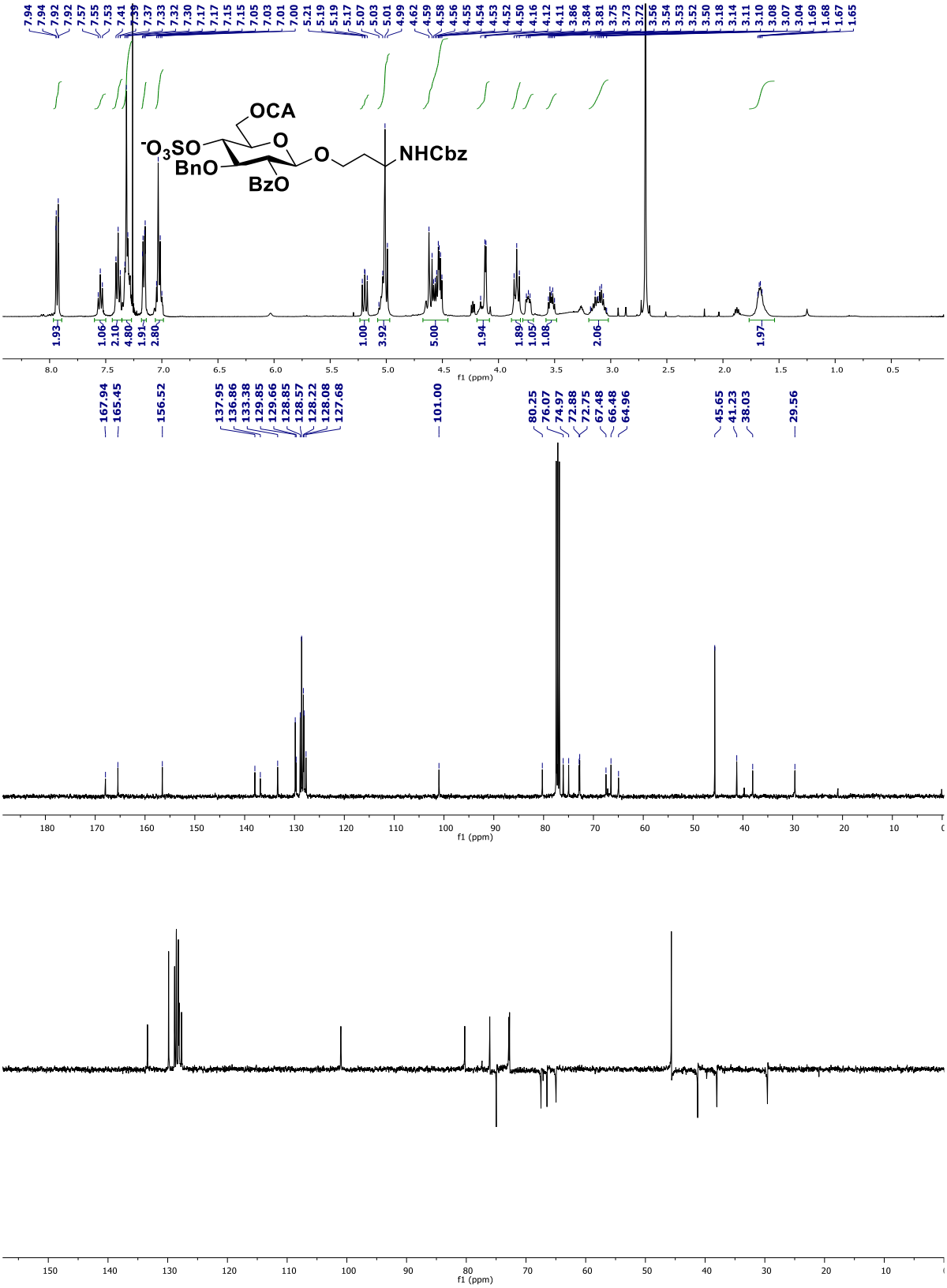
## $^{1}H$, $^{13}C$, and DEPT NMR spectrum of compound 29



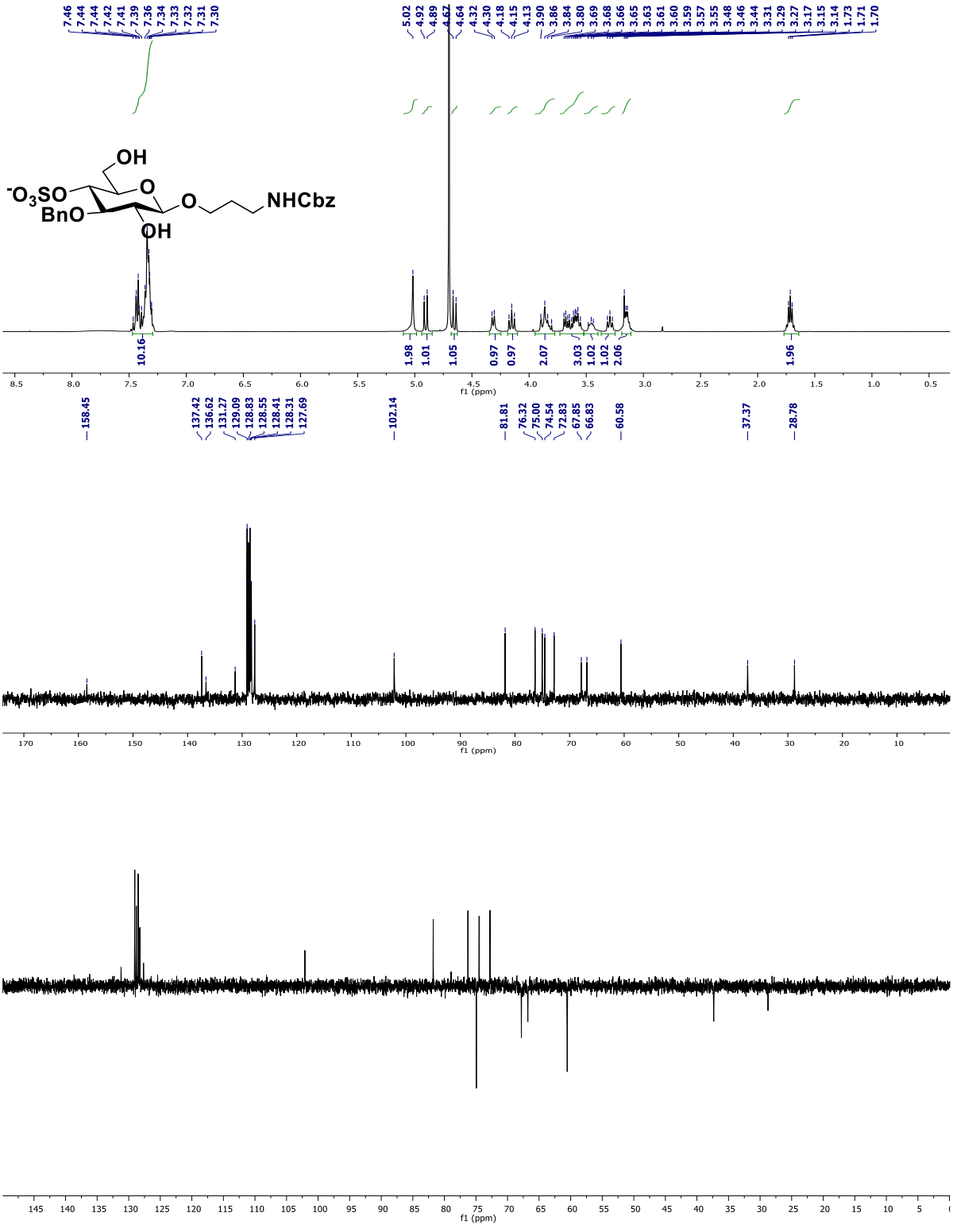
## $^{1}H$, $^{13}C$, and DEPT NMR spectrum of compound 30



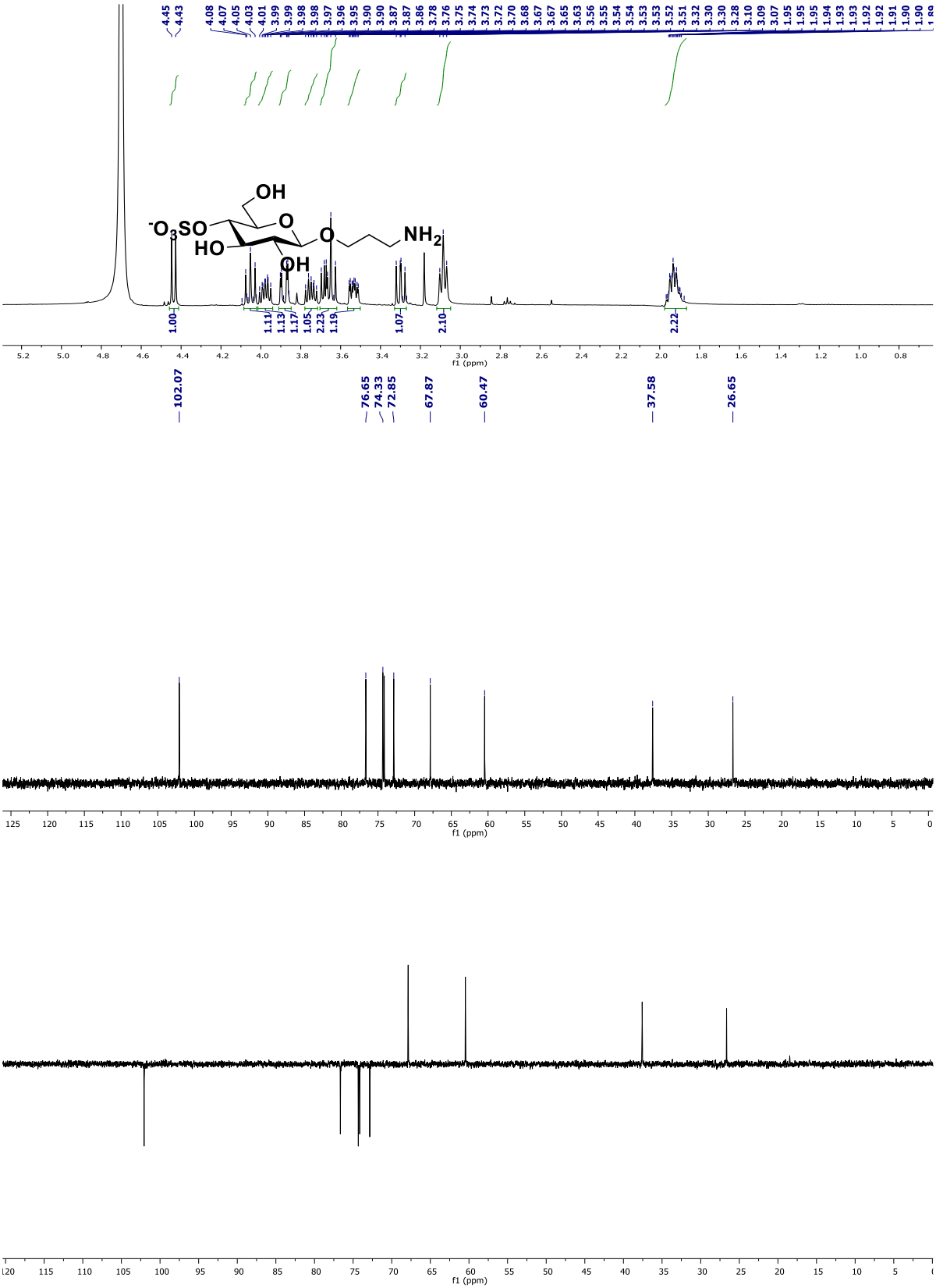
## $^{1}H$, $^{13}C$, and DEPT NMR spectrum of compound 31



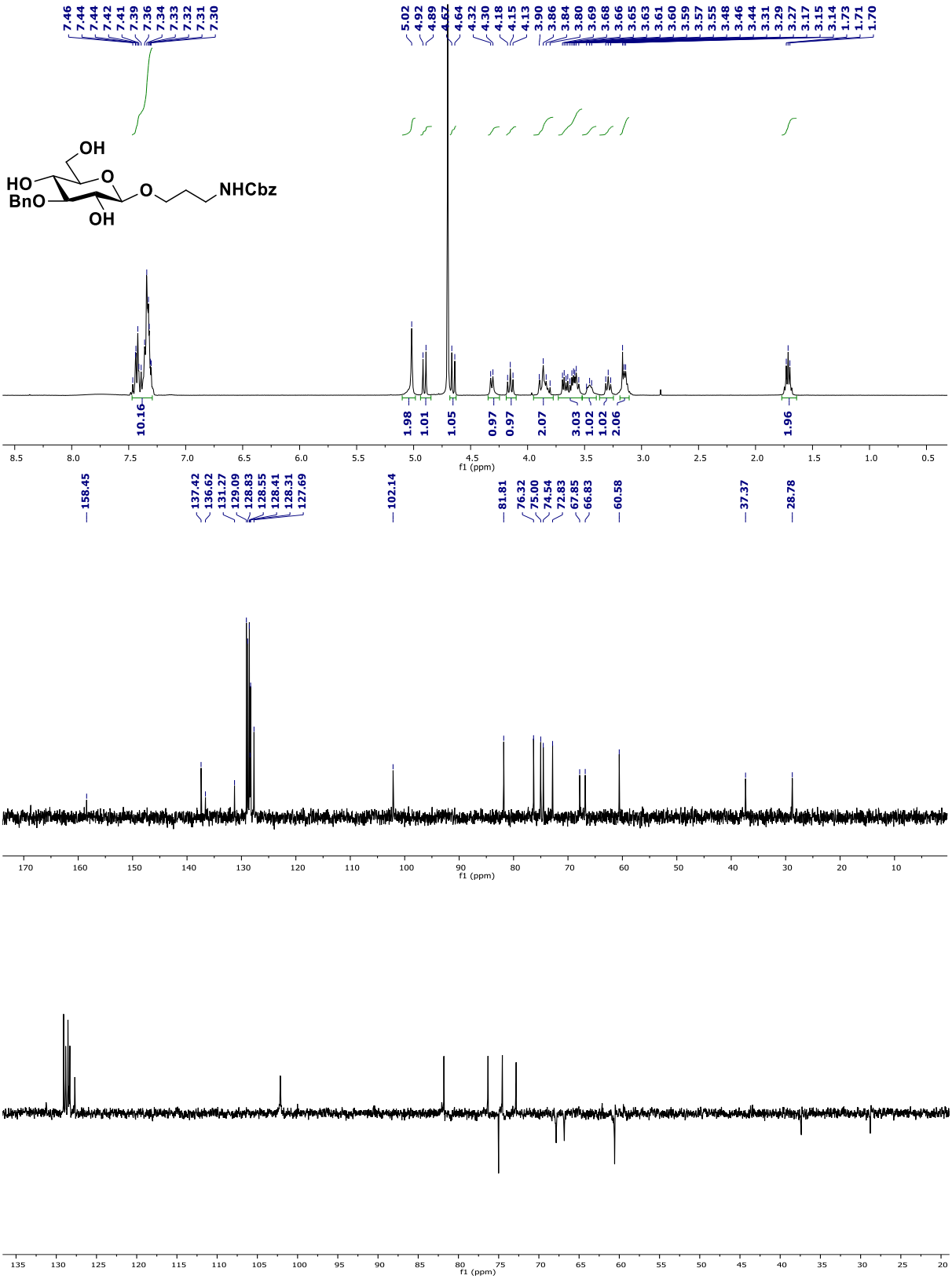
## $^{1}H$, $^{13}C$, and DEPT NMR spectrum of compound 32



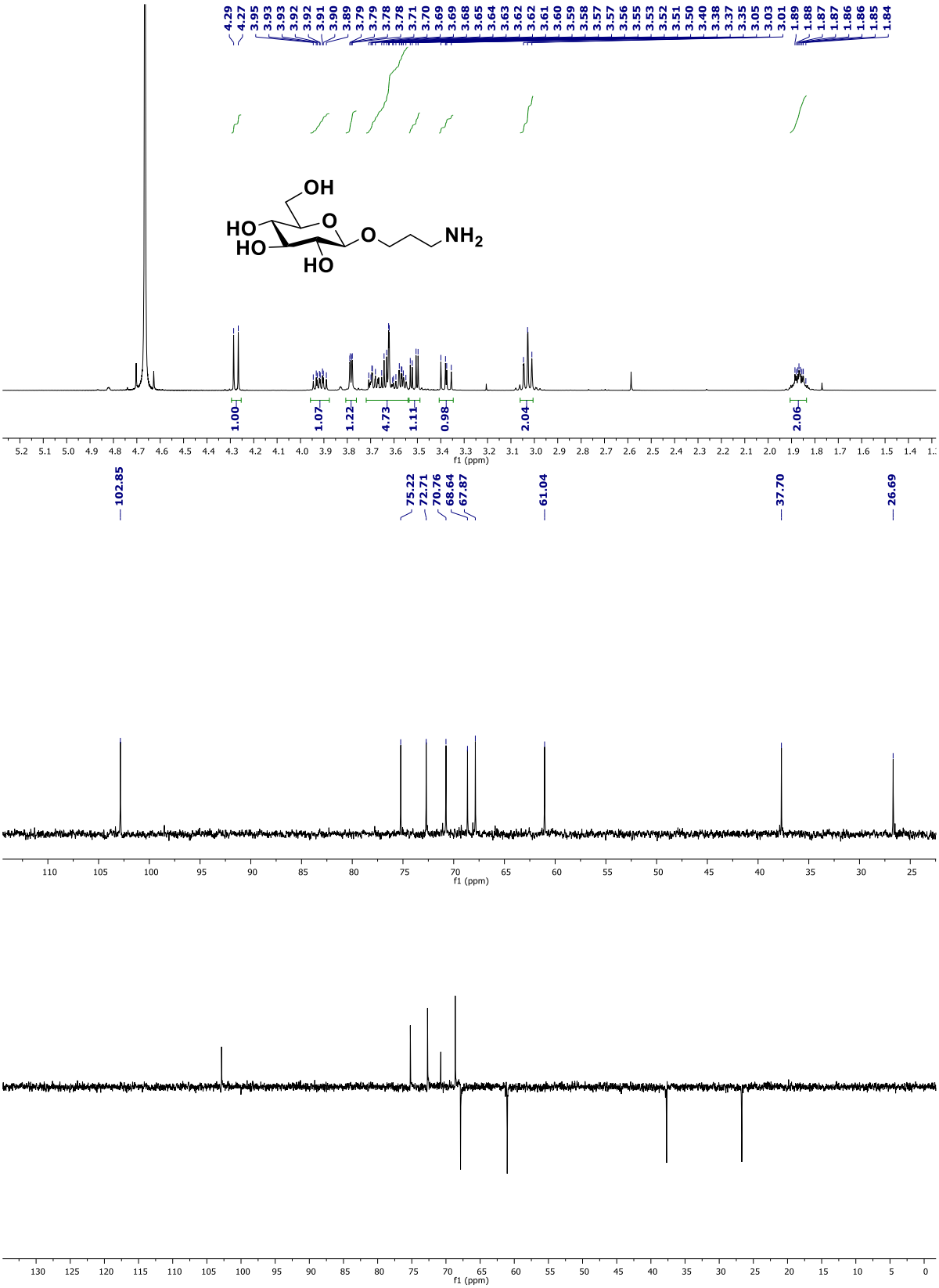
## $^{1}H$, $^{13}C$, and DEPT NMR spectrum of compound 33



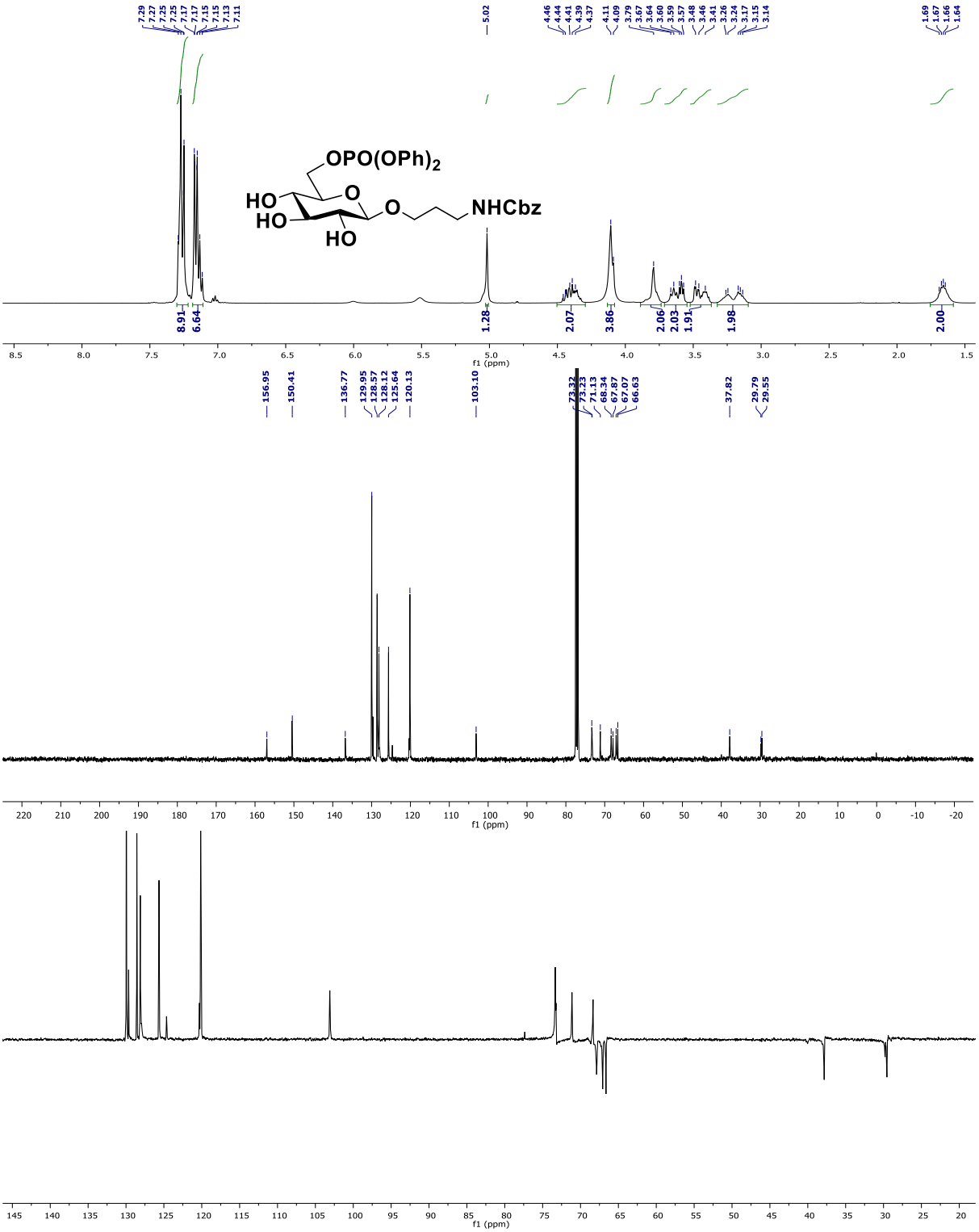
## $^{1}H$, $^{13}C$, and DEPT NMR spectrum of compound 34



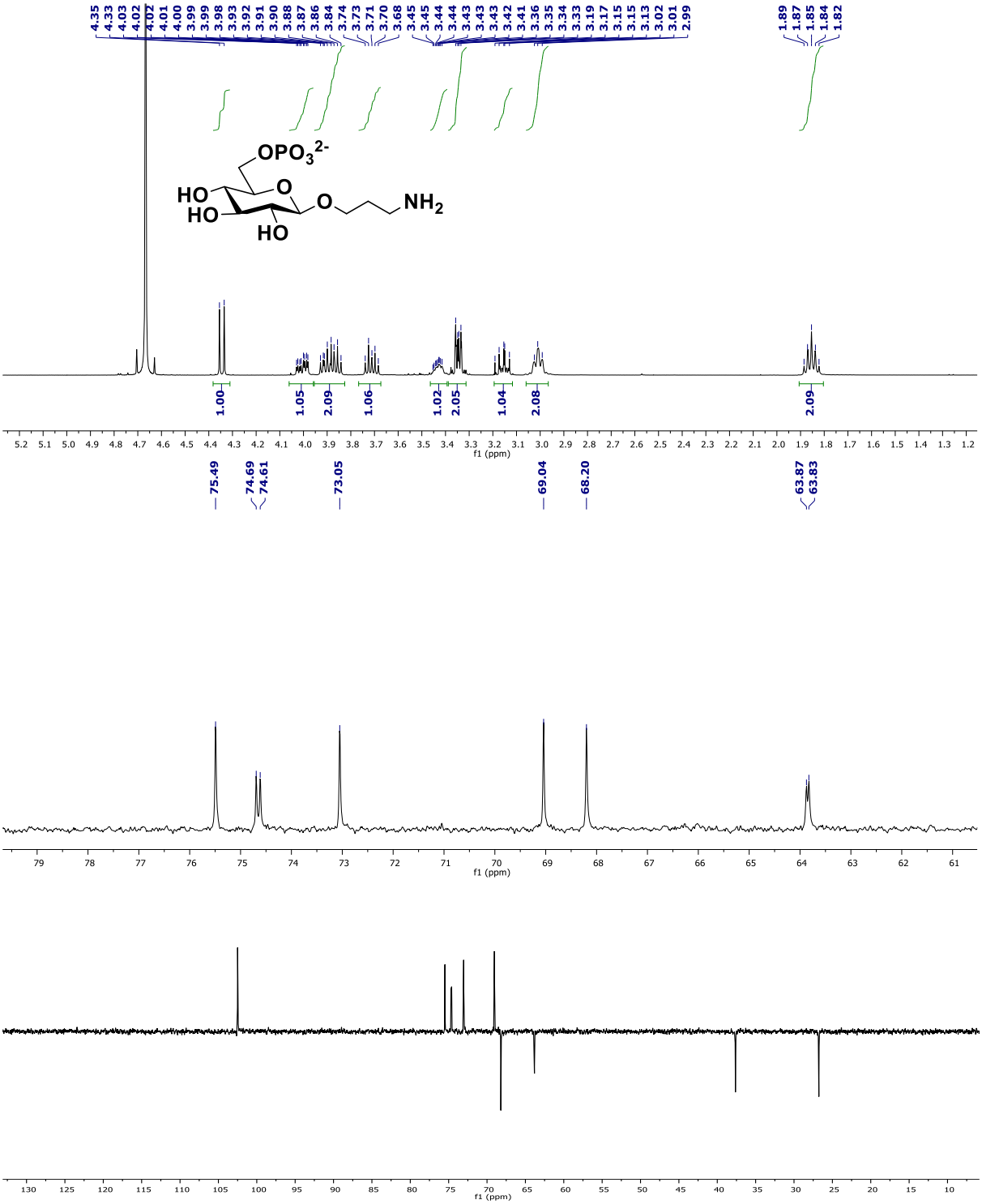
## $^{1}H$, $^{13}C$, and DEPT NMR spectrum of compound 35



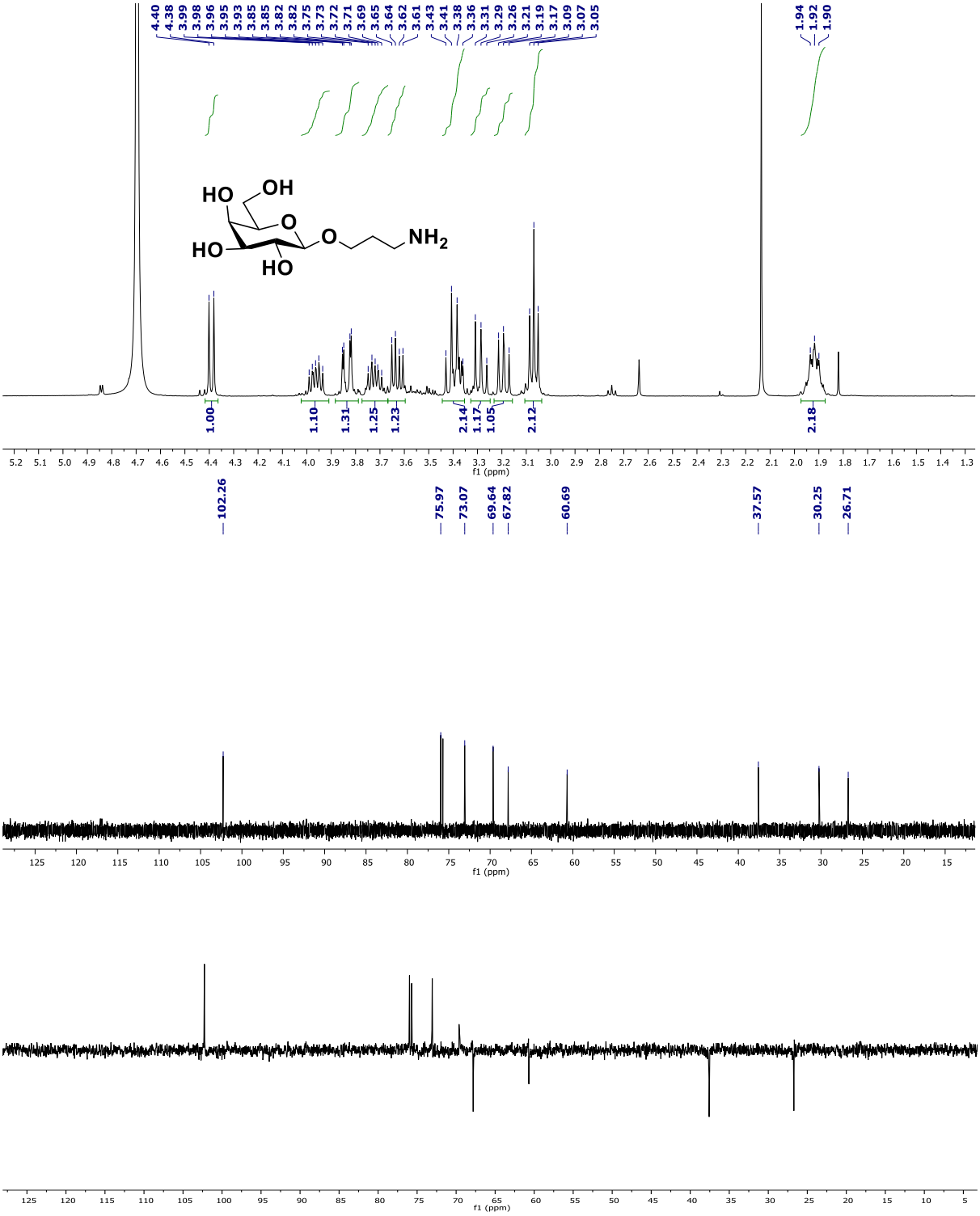
## $^{1}H$, $^{13}C$, and DEPT NMR spectrum of compound 37



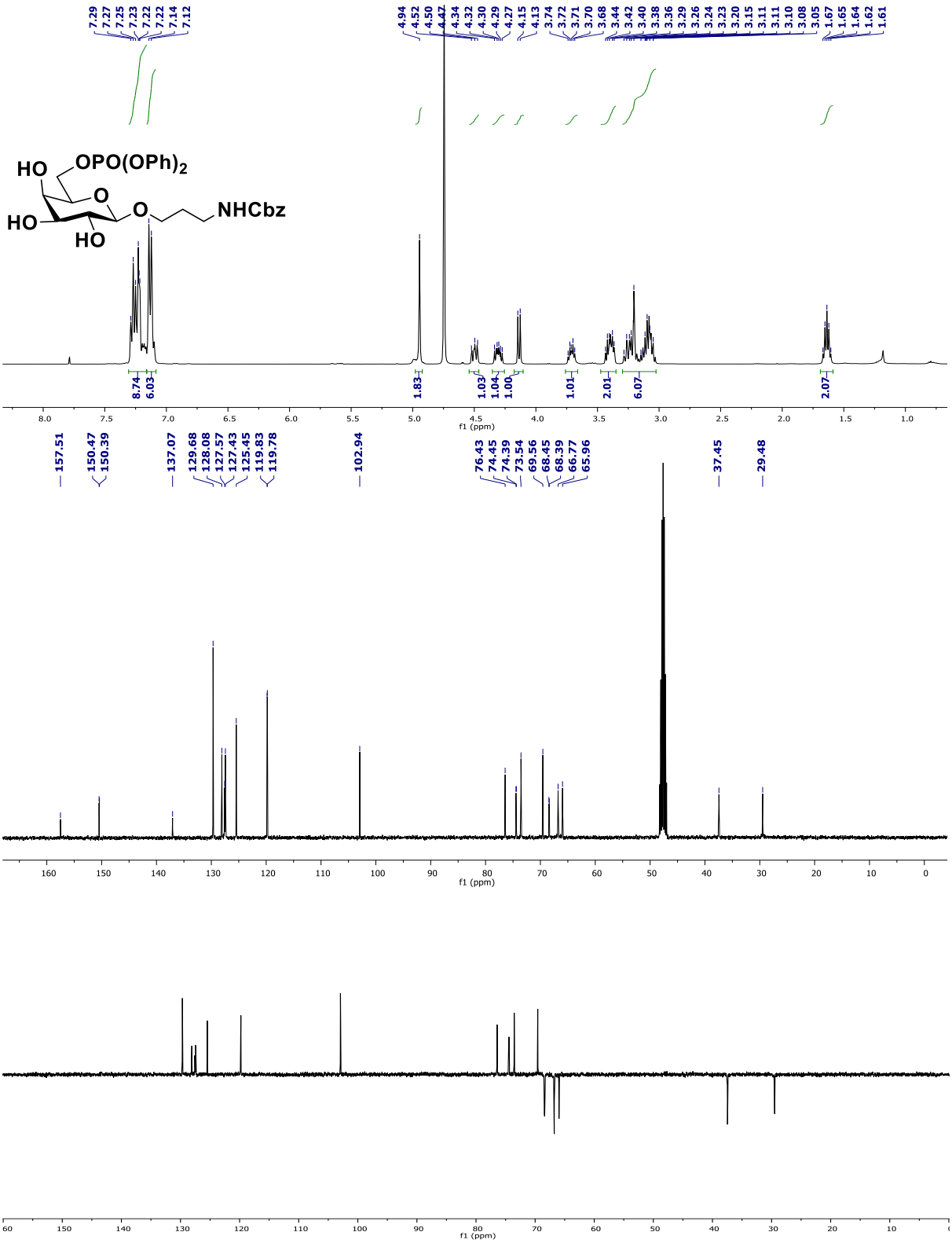
## $^{1}H$, $^{13}C$, and DEPT NMR spectrum of compound 38



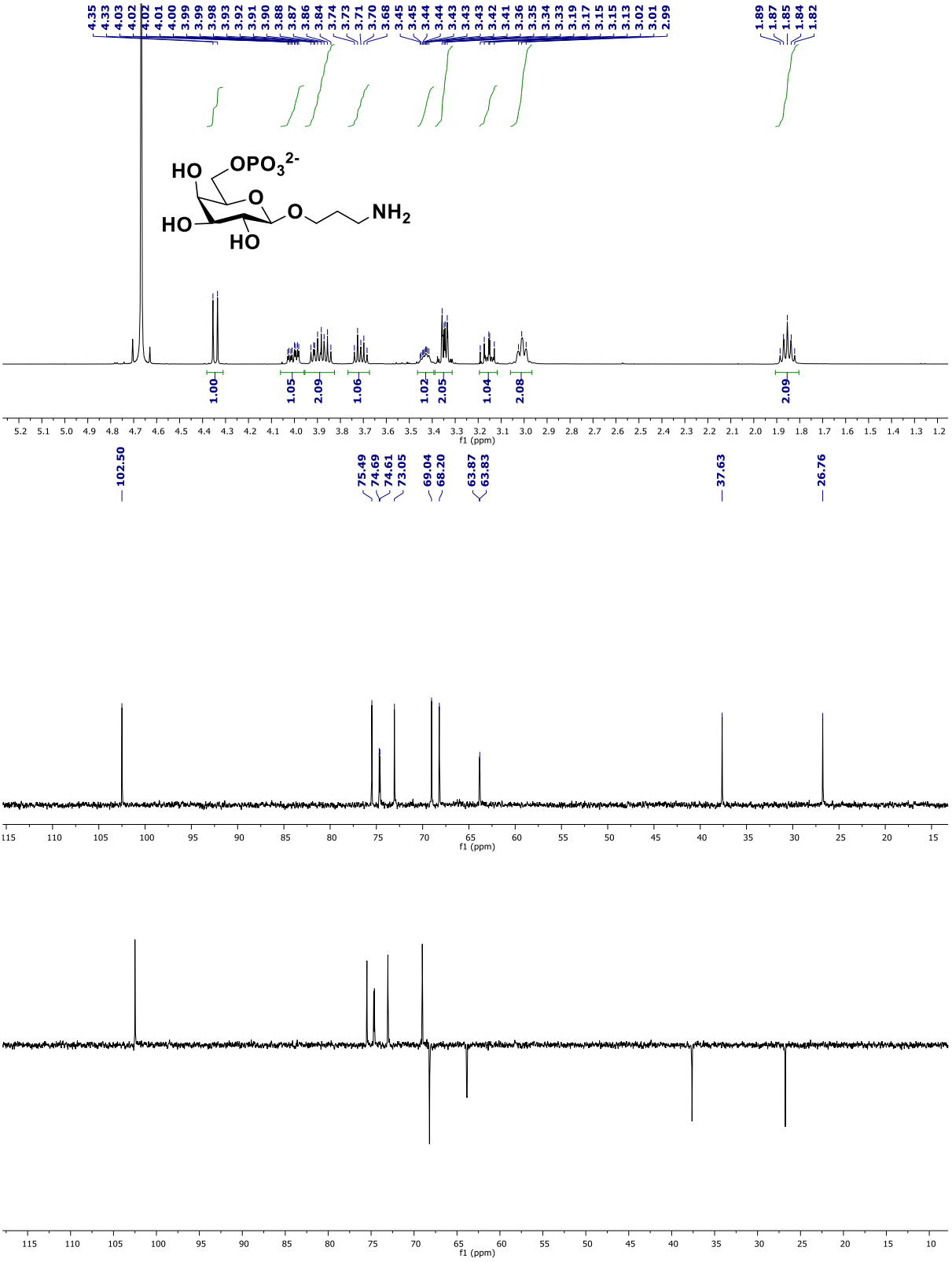
## $^{1}H$, $^{13}C$, and DEPT NMR spectrum of compound 40



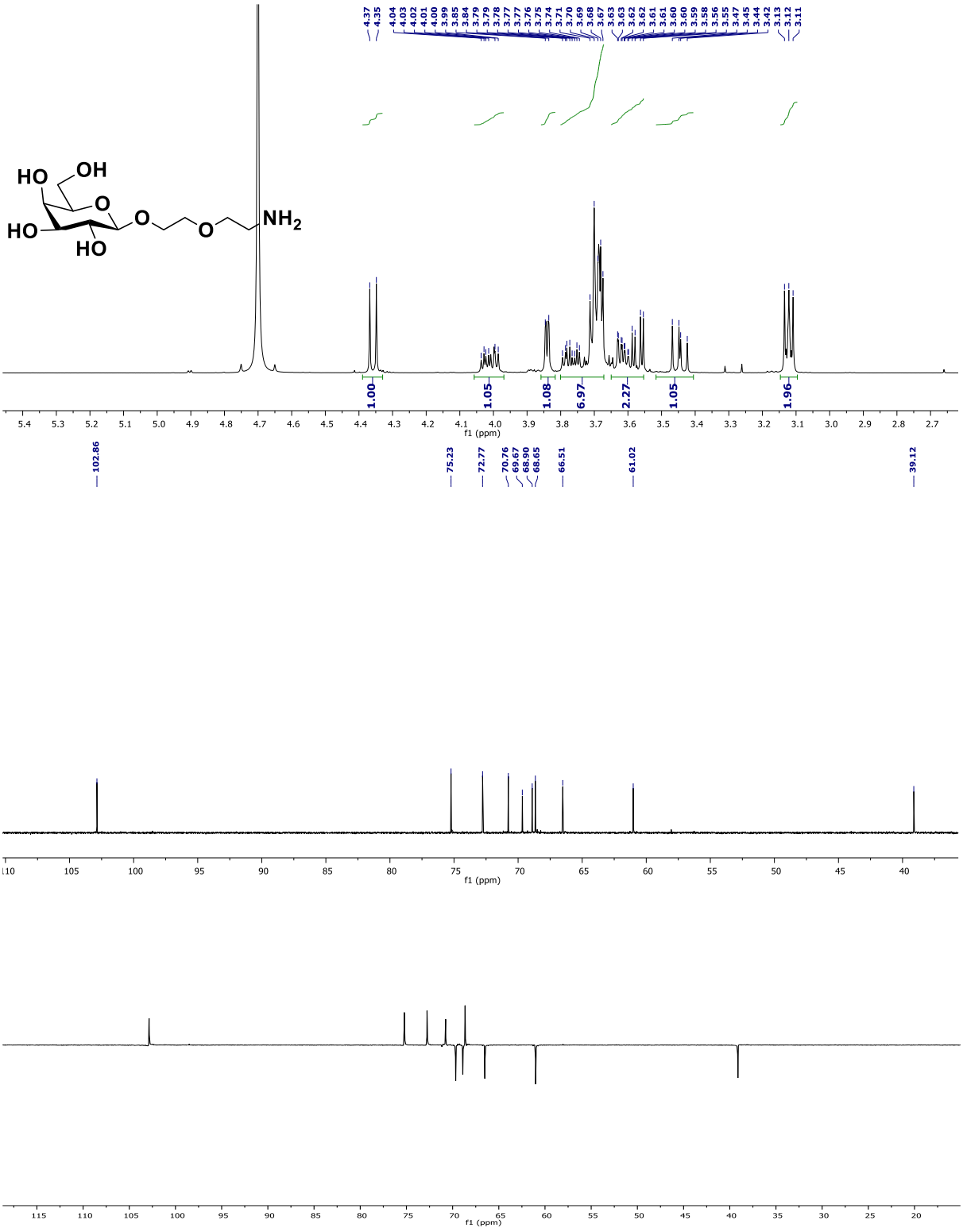
## $^{1}H$, $^{13}C$, and DEPT NMR spectrum of compound 41



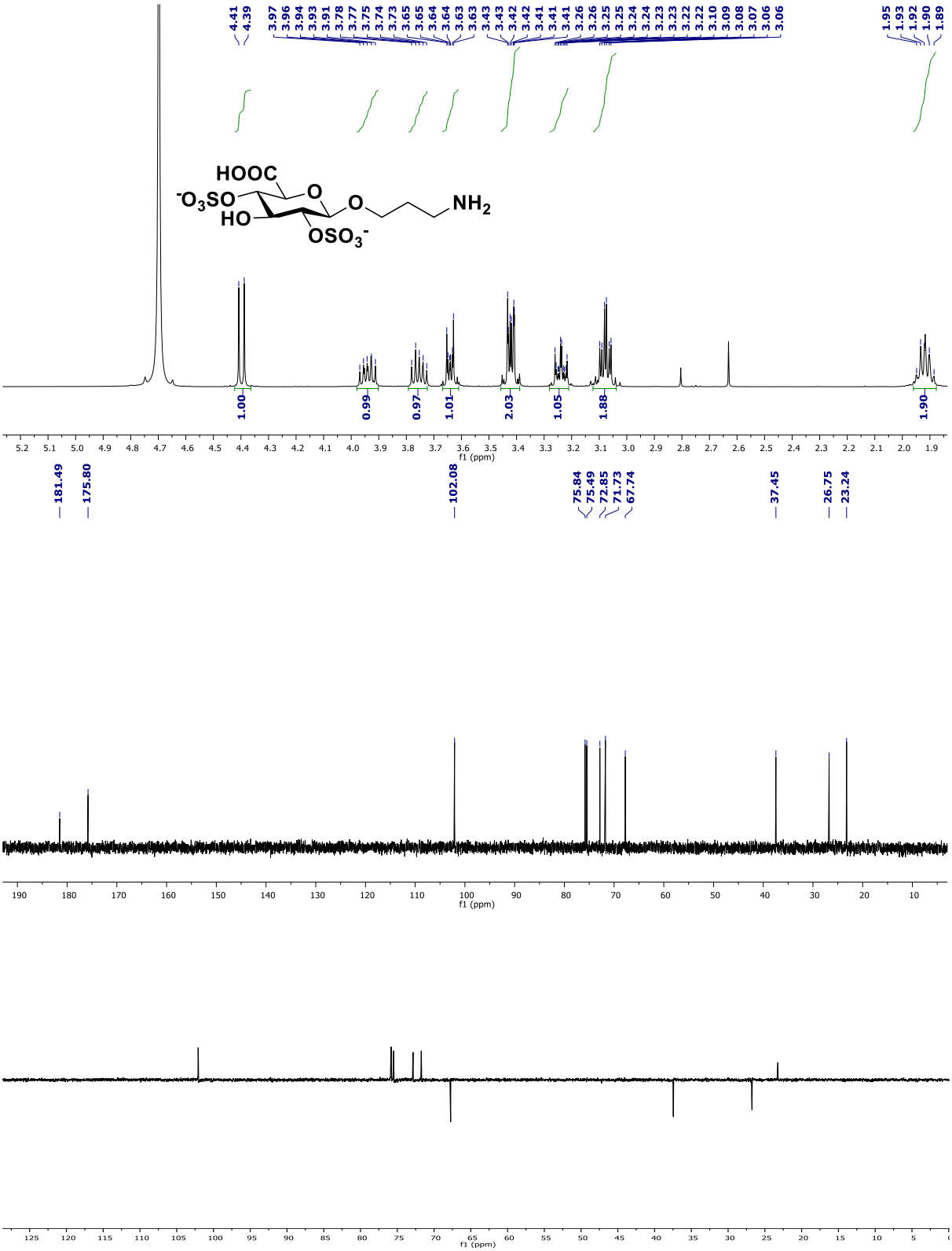
## $^{1}H$, $^{13}C$, and DEPT NMR spectrum of compound 42



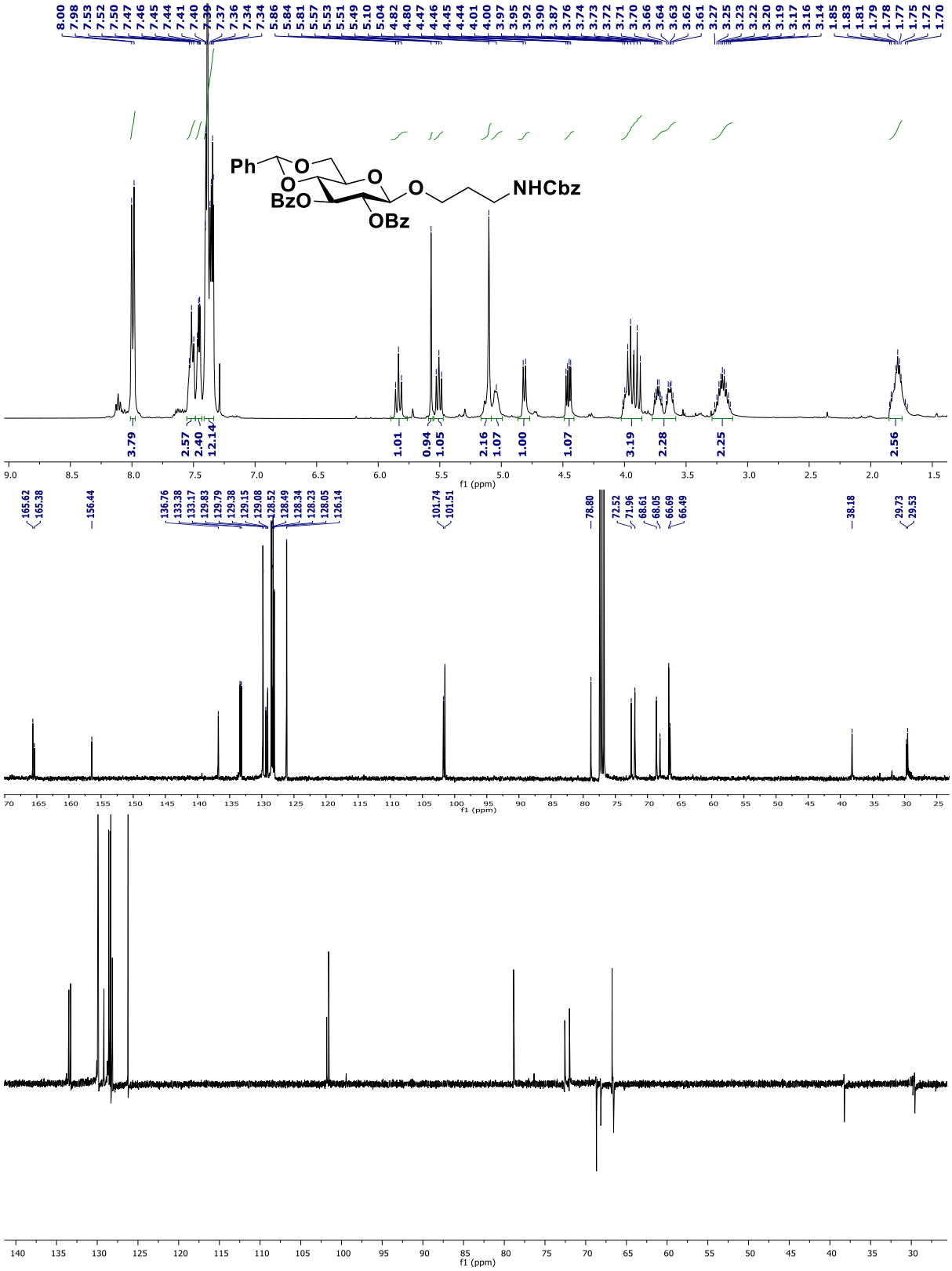
## $^{1}H$, $^{13}C$, and DEPT NMR spectrum of compound 44



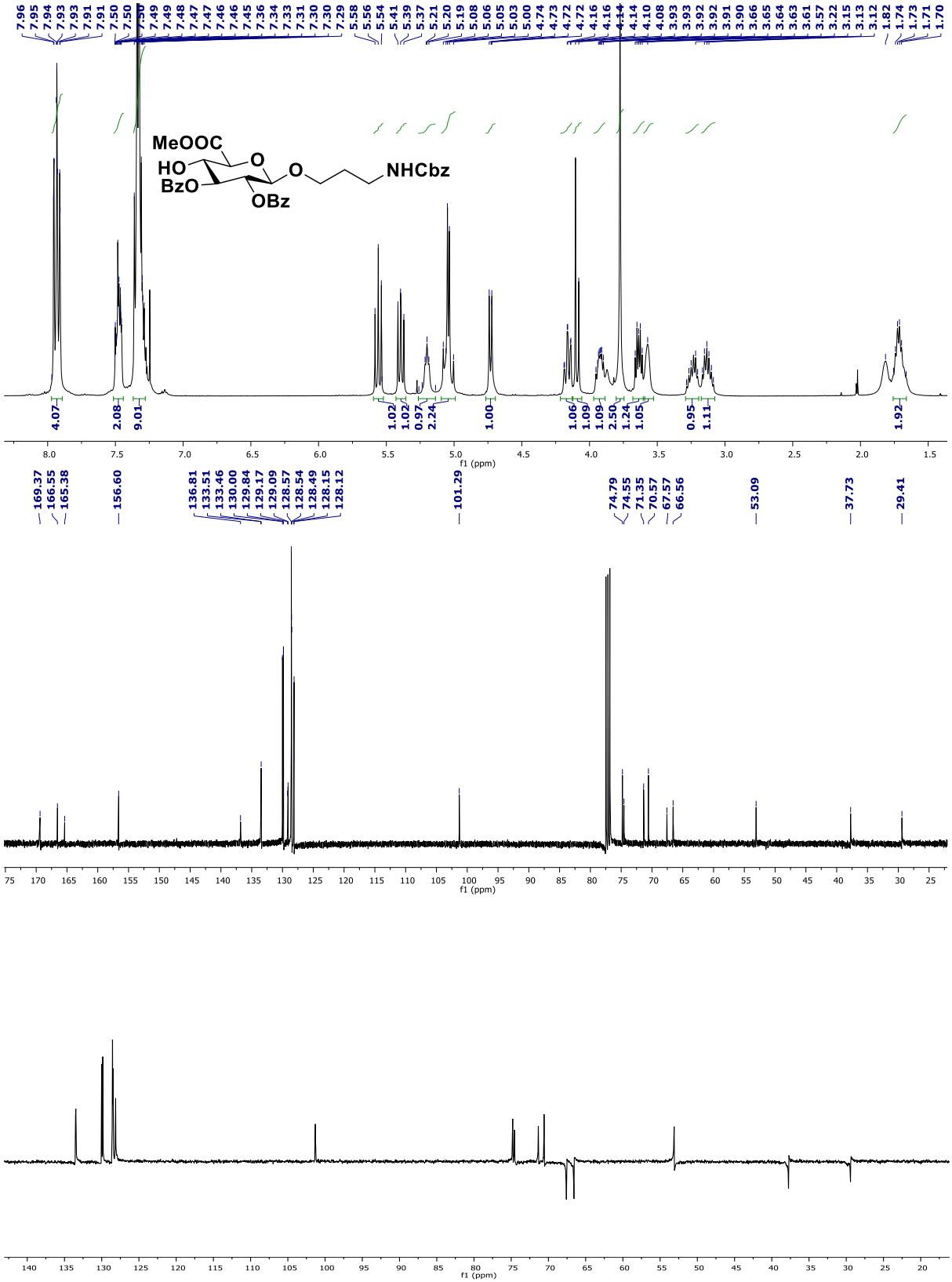
## $^{1}H$, $^{13}C$, and DEPT NMR spectrum of compound 48



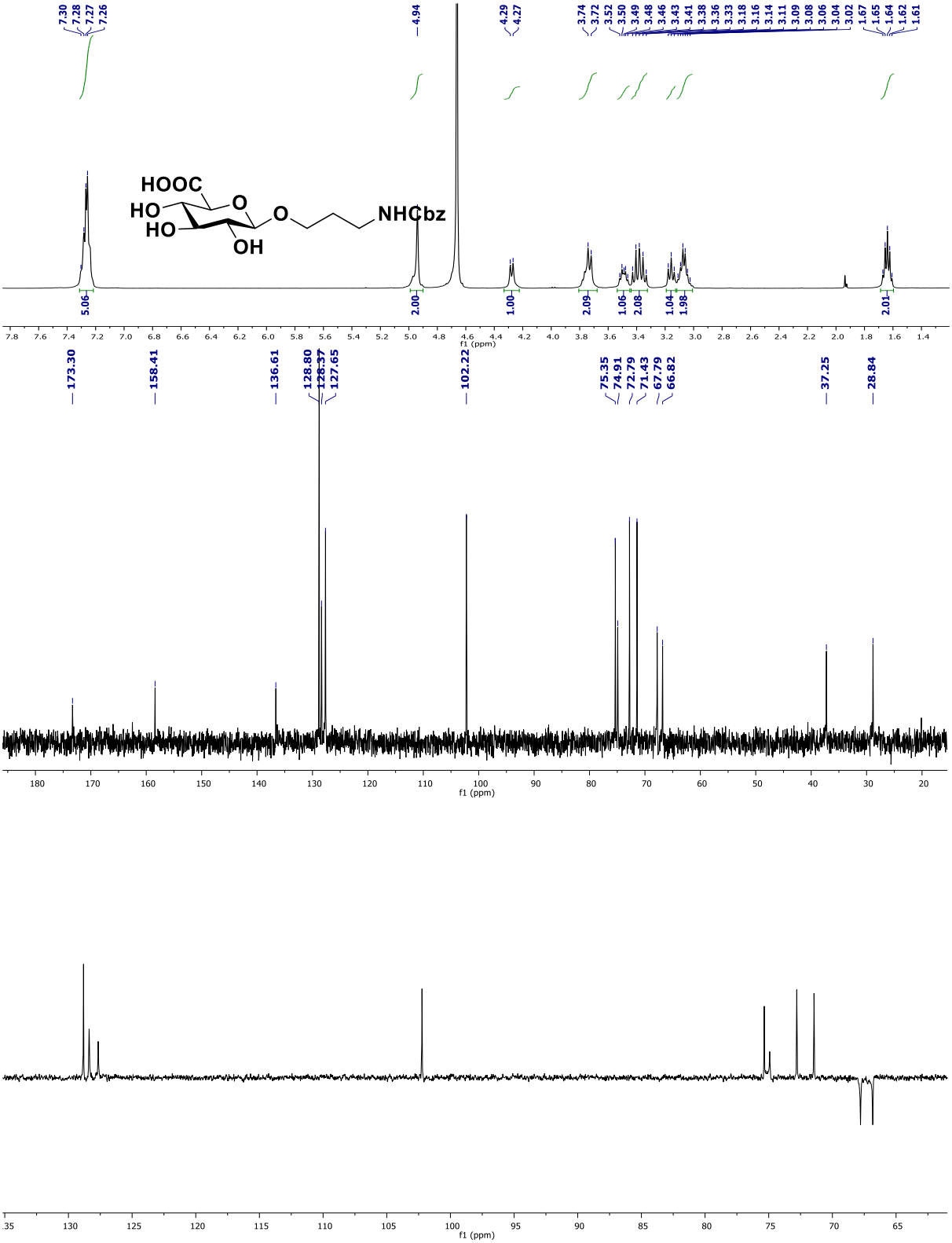
## $^{1}H$, $^{13}C$, and DEPT NMR spectrum of compound 50



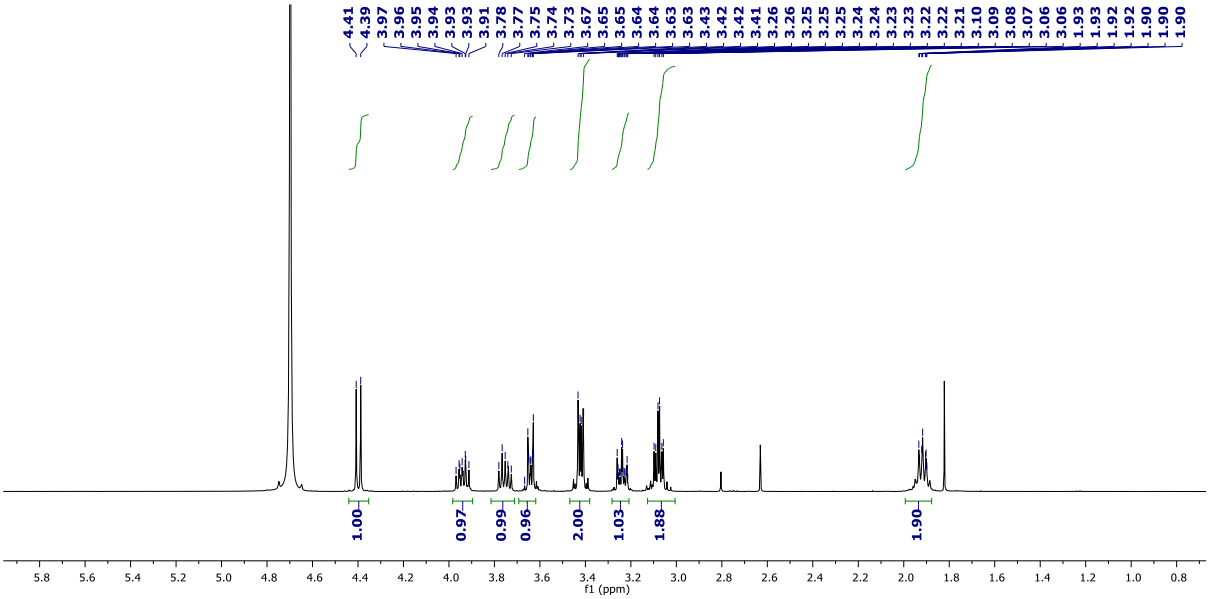
## $^{1}H$, $^{13}C$, and DEPT NMR spectrum of compound 51

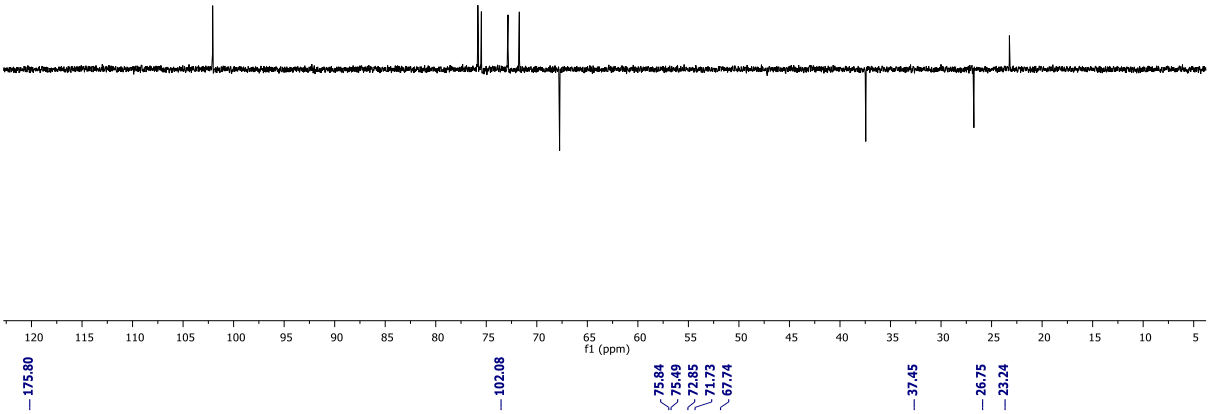


## $^{1}H$, $^{13}C$, and DEPT NMR spectrum of compound 52

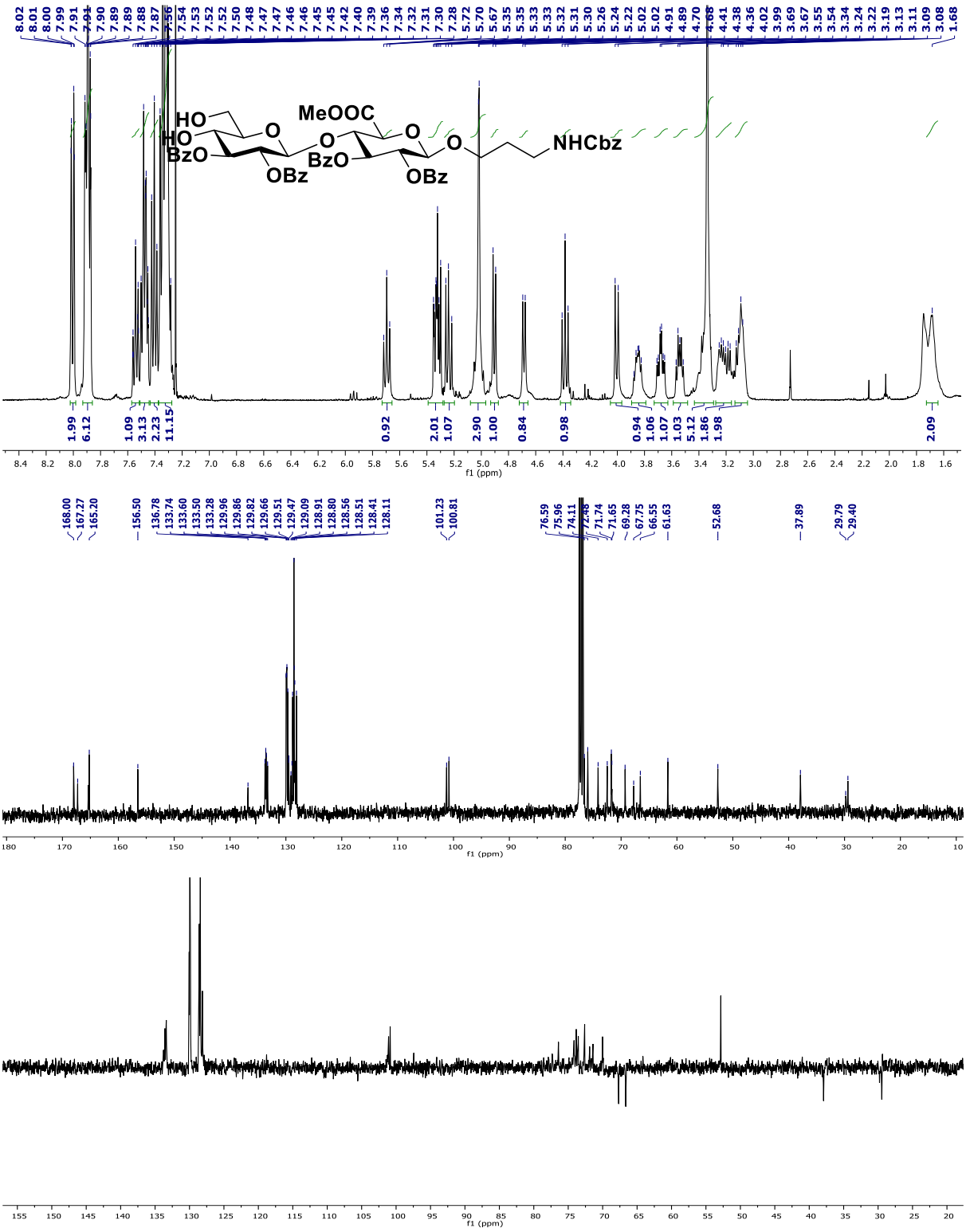


## $^{1}H$, $^{13}C$, and DEPT NMR spectrum of compound 53

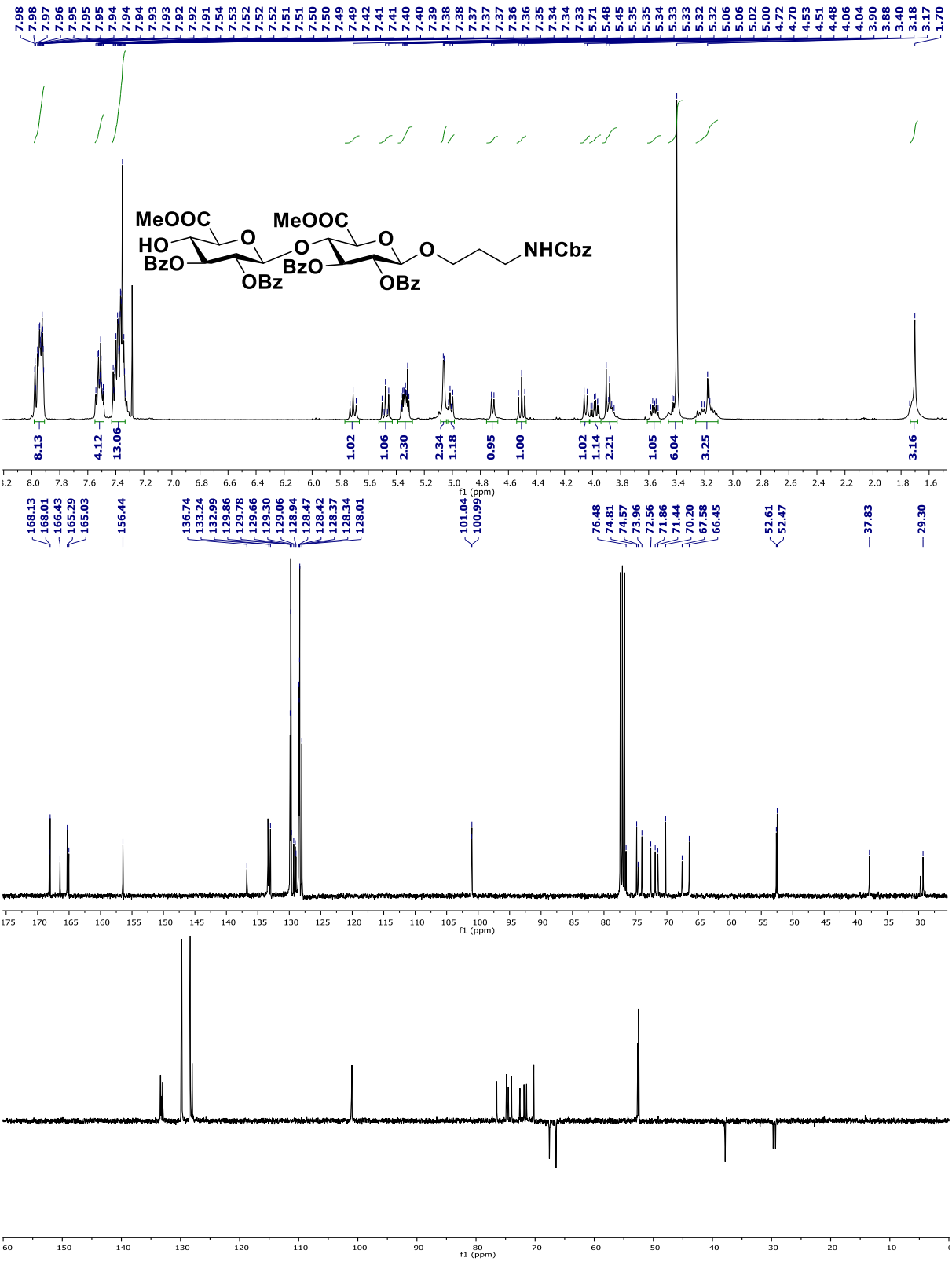


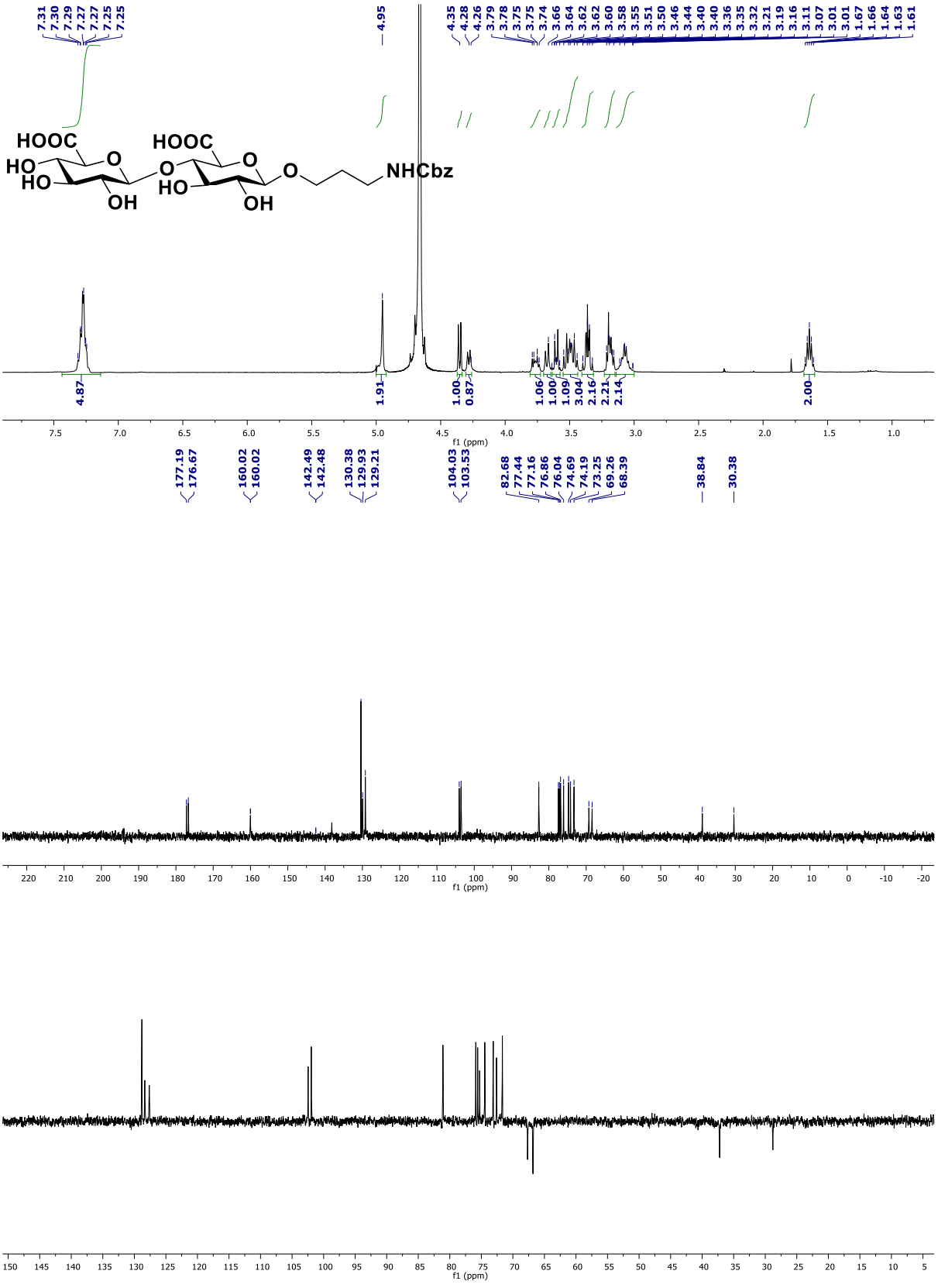
## $^{1}H$, $^{13}C$, and DEPT NMR spectrum of compound 54



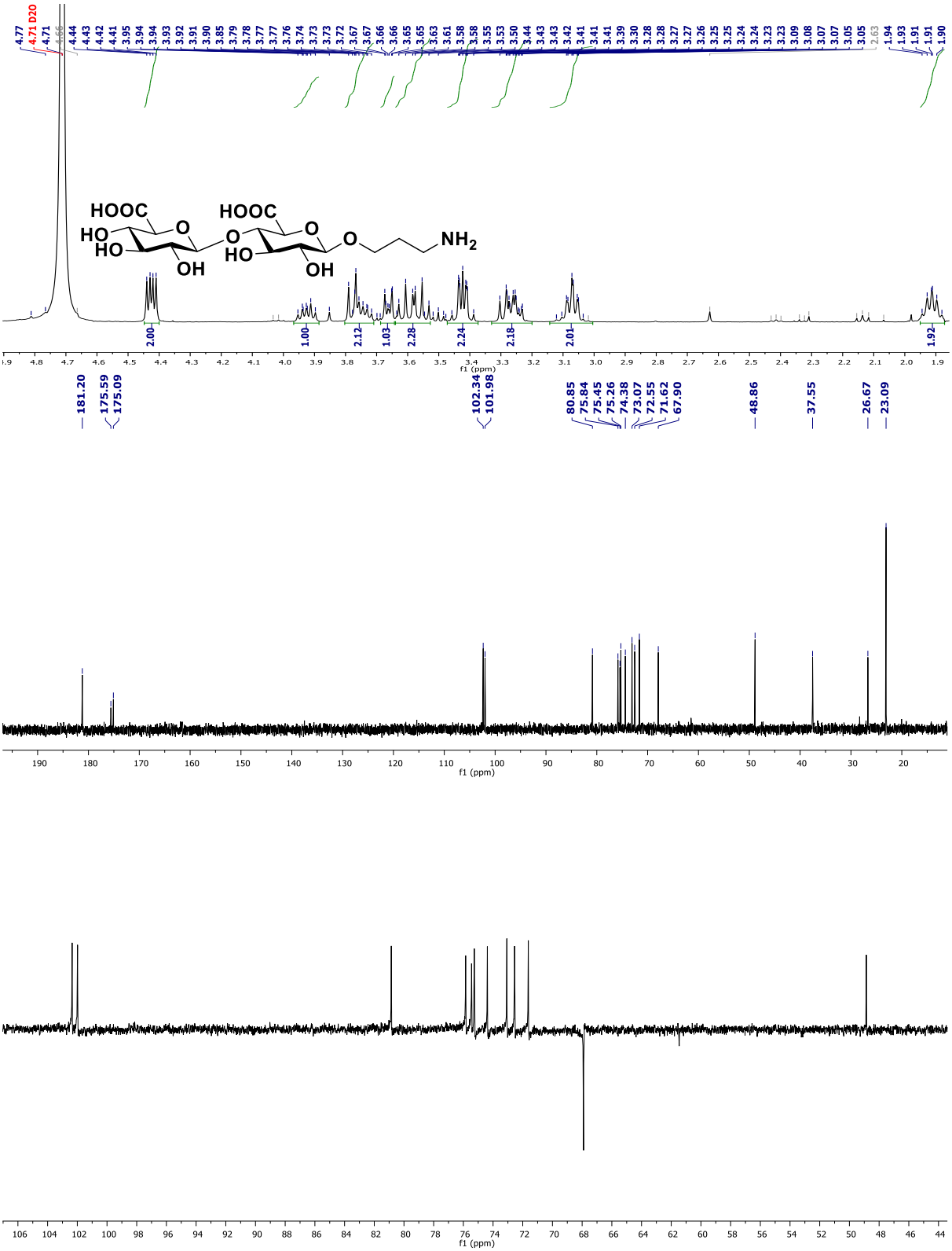
## $^{1}H$, $^{13}C$, and DEPT NMR spectrum of compound 55



## $^{1}H$, $^{13}C$, and DEPT NMR spectrum of compound 56



## $^{1}H$, $^{13}C$, and DEPT NMR spectrum of compound 57



## 4.7 References


1. J. H. Jang, H. W. Shin, J. M. Lee, H. W. Lee, E. C. Kim, S. H. Park, *Mediators of Inflammation*, **2015**, Article ID 794143.
2. H. Hatai, A. Lepelley, W. Zeng, M. S. Hayden, S. Ghosh, *PLoS One*, **2016**, *11*, e0148987.
3. T. Kawasaki, T. Kawai1, *Front Immunol*. **2014**, *5*, 461.
4. A. H. Dalpke, M. D. Lehner, T. Hartung, K. Heeg, *Immunology*. **2005**, *116*, 203–212.
5. M. G. Dorrington, I. D. C. Fraser, *Front Immunol.* **2019**, *10*, Article 705.
6. G. Y. Chen, G. Nuñez, *Nature Rev. immunol.* **2011**, *11*, 565.
7. D. A. S. Davis, C. R. Parish, *Front. Immunol*. **2013**, *4*, Article 470
8. L. T. H. Hsieh, M. V. Nastase, H. Roedig, J. Zeng-Brouwers, C. Poluzzi, S. Schwalm, C. Fork, Tredup, R. P. Brandes, M. Wygrecka, A. Huwiler, J. Pfeilschifter, L. Schaefer, *Int. J. Mol. Sci.* **2017**, *18*, 595.
9. S. Lees, S. B. Golub, K. Last, W. Zeng, D. C. Jackson, P. Sutton, A. J. Fosang, *Arthritis Rheum.* **2015**, *67*, 1240–9.
10. T. V. Stabler, Z. Huang, E. Montell, J. Verges, V. B. Kraus, *Osteoarthritis Cartilage*, **2017**, *25*,166-174.
11. T. V. Brennan, L. Lin, X. Huang, D. M. Cardona, Z. Li, K. Dredge, N. J. Chao, Y. Yang, *Blood*. **2012**, *120*, 2899–2908.
12. A. Adibekian, P. Bindschdler, M. S. M. Timmer, C. Noti, N. Schtzenmeister, P. H. Seeberger, *Chem. Eur. J*. **2007**, *13*, 4510-4522.
13. G. J. S. Lohman, D. K. Hunt, J. A. HOgermeire, P. H. Seenerger, *J. Org.Chem.* **2003**, *68*, 7559-7561.
14. S. Dey, C. H. Wong, *Chem Sci*. **2018**, *9*, 6685-6691.
15. Y. P Hu, Y. Q. Zhong,Z. G. Chen, C. Y. Chem, Z. Shi, M. M. Zuleta, C. C. Zu, P. Y. Lu, C. C. Wang, H. C. Hung, *J Am Chem Soc*. **2012**, *134*, 20722-7.
16. C. Zong, A. Venot, X. Li, W. Lu, W. Xiao, J. S. L. Wilkes, C. L. Salanga, T. M. Handel, L. Wang, M. A. Wolfert, G. J. Boons, *J. Am. Chem. Soc*. **2017**, *139*, 9534-9543.
17. S. Arungundram, K. Al-Mafraji, J. Asong, III. F. e. Leach, I. J. Amster, A. Venot, J. E. Turnbull, G. J. Boons, *J. Am. Chem. Soc.* **2009**, *131*, 17394-17405.

# CHAPTER- 5

## Pairing Nanoparticles Geometry with TLR Agonist to Modulate Immune Responses for Vaccine Development

## 5.1 Abstract

Nanotechnology-based vaccine development necessitates understanding the crucial biophysical properties of nanostructures that alter immune responses. In this study, we demonstrate the synergistic effect of gold nanoparticles (AuNPs) shapes with toll-like receptor (TLR) agonists in immune modulation activity. Our results showed that CpG- and imidazoquinoline-conjugated rod-shaped AuNPs display relatively fast uptake by bone marrow-derived macrophage cells, but secrete poor immunogenic responses compared to their spherical and star-shaped AuNP counterparts. Surprisingly, star-shaped AuNPs exhibited intense pro-inflammatory cytokine secretion. Further mechanistic studies showed that star-shaped AuNPs were abundantly localized in the late endosome and lysosomal regions, whereas rod-shaped AuNPs were majorly sequestered in the mitochondrial region. These findings reveal that the shape of the nanostructures plays a pivotal role in driving the adjuvant molecules toward their receptors and altering immune responses.

## 5.2 Introduction

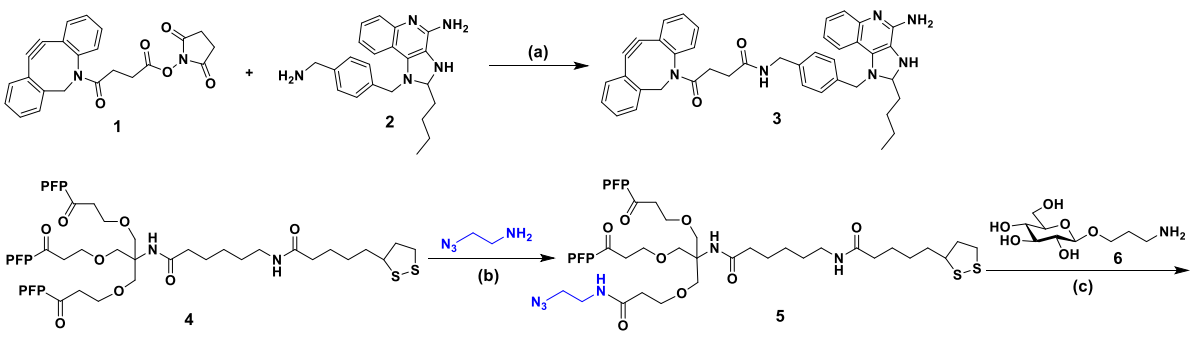
The importance of nanotechnology in vaccine development remains a powerful impetus for exploring new conceptual changes in nanostructures to generate an easy and efficient platform for developing antibodies against poor immunogenic antigens, such as tumor-associated carbohydrate antigens (TACAs).[1-6] Among various nanostructures, gold nanoparticles have attracted strong interest due to their facile synthetic methods, surface functionalization, and non-immunogenic and non-toxic nature.[7-10] Gold nanoparticle-based vaccine approaches frequently rely on decorating antigens and adjuvant molecules on nanoparticles and its access to immune cells and receptors.[11, 12] Consequently, understanding the impact of the geometry of the nanoparticles, the local concentration of the ligands, and the spacers between the nanostructures and ligands influencing the immune responses is persistently considered. [13-20] However, a head-to-head comparison of more than one adjuvant on a similar nanostructure platform is required to develop a broad immune-modulatory nanotechnology platform. To expand our knowledge of nanotechnology-based vaccine development, we studied the synthesis of spherical, rod-, and star-shaped gold nanostructures appended with CpG and imidazoquinoline ligands to evaluate shape-dependent immune cell uptake and immune modulation. Extensive live-cell imaging studies and fluorescent activated cell sorting assays (FACS) with murine bone marrow-derived macrophages (BMDMs) established the rate of uptake and sequestration of the nanostructures. Finally, cytokine secretion and co-localization studies of the BMDMs confirm the synergistic effect of the TLR agonists and the physical properties of AuNPs on endosomal secretion and their immune modulation.

### 5.3 Results and discussion

To explore this notion, TLR agonists, CpG, and imidazoquinoline derivatives were selected for our studies because they have a venerable history as vaccine adjuvants.[21, 22] CpGs are synthetic oligodeoxynucleotides that trigger toll-like receptor 9 and activate innate immune responses by producing Th1-associated cytokines.[23, 24] Whereas imidazoquinoline derivatives were identified as TLR 7/8 agonists, they induce pro-inflammatory cytokines such as TNF alpha and IL-12.[25] Both CpGs and imidazoquinoline have been extensively used as adjuvants in several vaccines.[26-33] However, to the best of our knowledge, they have never been studied together on a nanotechnology platform.

#### 5.3.1 Synthesis of tripodal derivative of imidazoquinolin

We first synthesized three standard shapes of AuNPs using the literature procedure.[34-36] More specifically, we synthesized spherical (**S-1**, 50 nm), rod-shaped (**R-1**, 45 nm × 6 nm), and star-shaped AuNPs (**St-1**, 70 nm spike-to-spike). The sizes and shapes were confirmed by a scanning electron microscopic (SEM) image and a UV-visible profile. The **S-1** AuNPs displayed a localized surface plasmon resonance peak at 532 nm, whereas the rod- and star-shaped AuNPs displayed LSPR peaks in the near-infrared region (**R-1** at 560 and 757 nm, and **St-1** at 641 nm, respectively). AuNPs were appended with the optimum amount of water soluble CpG, sufficient enough to induce immune responses and synthesized **S-CpG**, **R-CpG** and **St-CpG** nanoparticles. In contrast, Imidazoquinoline is a hydrophobic ligand and functionalizes as such on AuNPs' induced aggregation. Hence, we sought to synthesize hydrophilic imidazoquinoline ligands by using a tripodal system, where two arms were equipped with non-immunogenic glucose moiety and the third arm was equipped with imidazoquinoline moiety (Figure 1). The synthesis of the tripodal derivative (**T-1**) was carried out using our previous procedure.[14, 37]



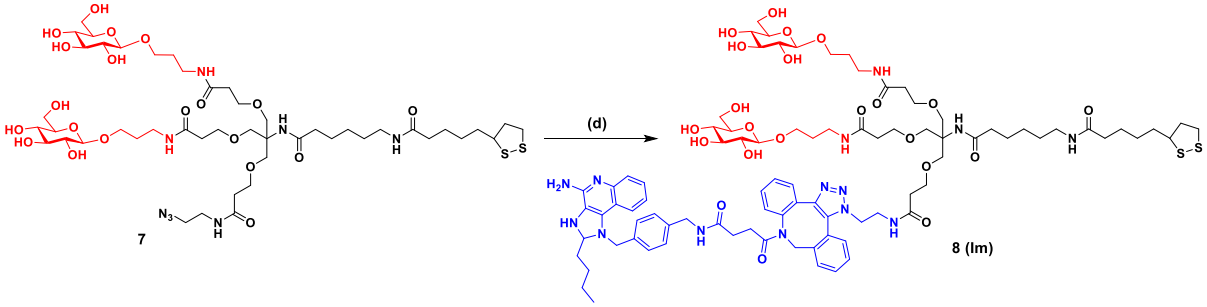



**Figure 1**. Synthesis of tripodal derivative of imidazoquinolin: (a) DCM, $Et_3N$, RT, 2 h, 87 %; (b) DMF, RT, 12 h, 55 %; (c) DCM, $Et_3N$, RT, 2 h, 62 %; (d) **3**, DMF, RT, 12 h, 58 %;

### 5.3.2 Synthesis, characterization and quantification of AuNP's conjugated with CpG and tripodal imidazoquinolin adjuvants

By using the ligand exchange process, we synthesized three nanostructures (**S-Im**, **R-Im,** and **St-Im**) (**Figure 2**).

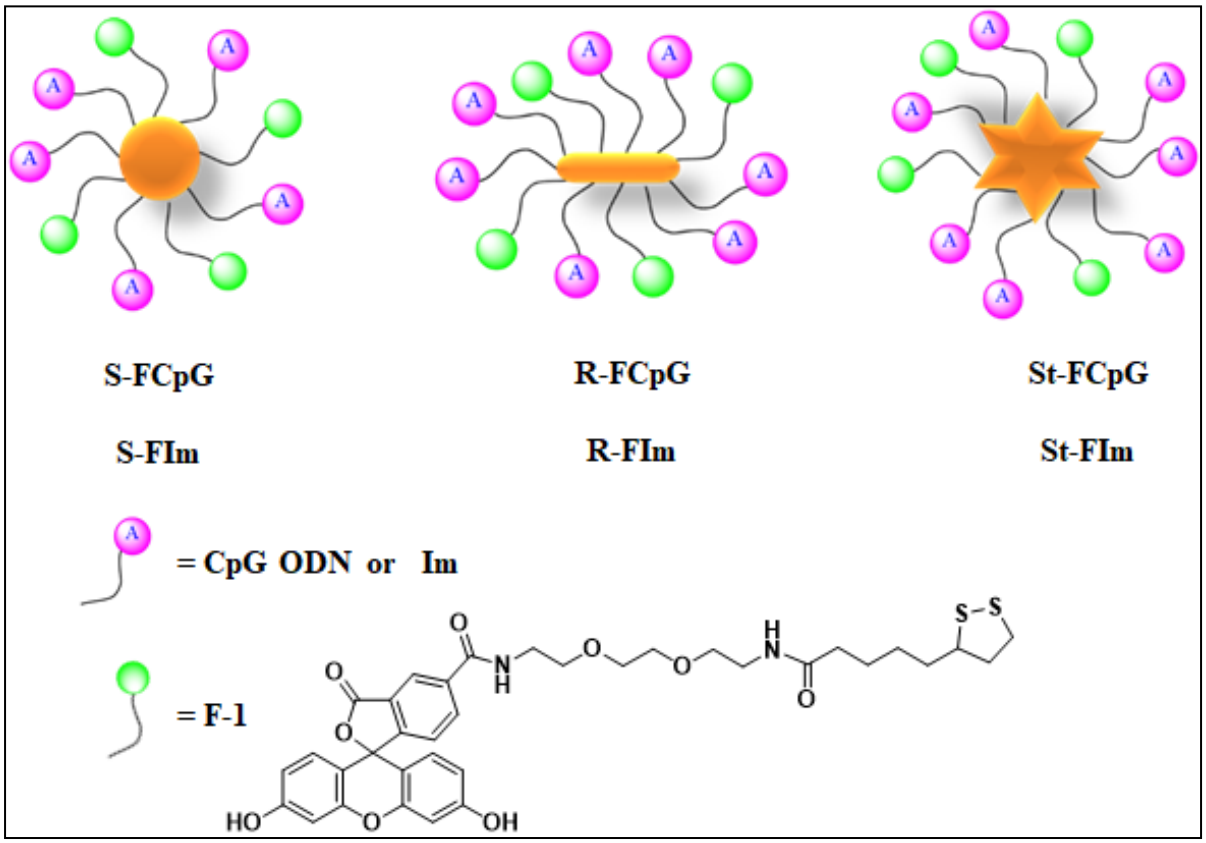



**Figure 2**. Schematic representation of AuNPs conjugated with CpG and tripodal imidazoquinolin adjuvants.

We characterized the nanoconjugation using zeta potential and UV-visible spectra (**Figure 3).** As expected, the incorporation of CpG and imidazoquinoline moieties decreased the zeta potential of the nanostructure; however, there was no significant difference in the UV-visible profile of the conjugation. To perform fluorescent imaging of the nanostructure, the AuNPs were again treated with fluorescent ligand (**F-1**), which was synthesized according to previously reported procedure.[14] Final nanostructures **S-FCpG**, **R-FCpG**, **St-FCpG,** **S-FIm**, **R-FIm,** and **St-FIm** were urified by cut-off filtration, and characterized by UV-visible, fluorescent spectra and zeta potential (**Figure 3**).

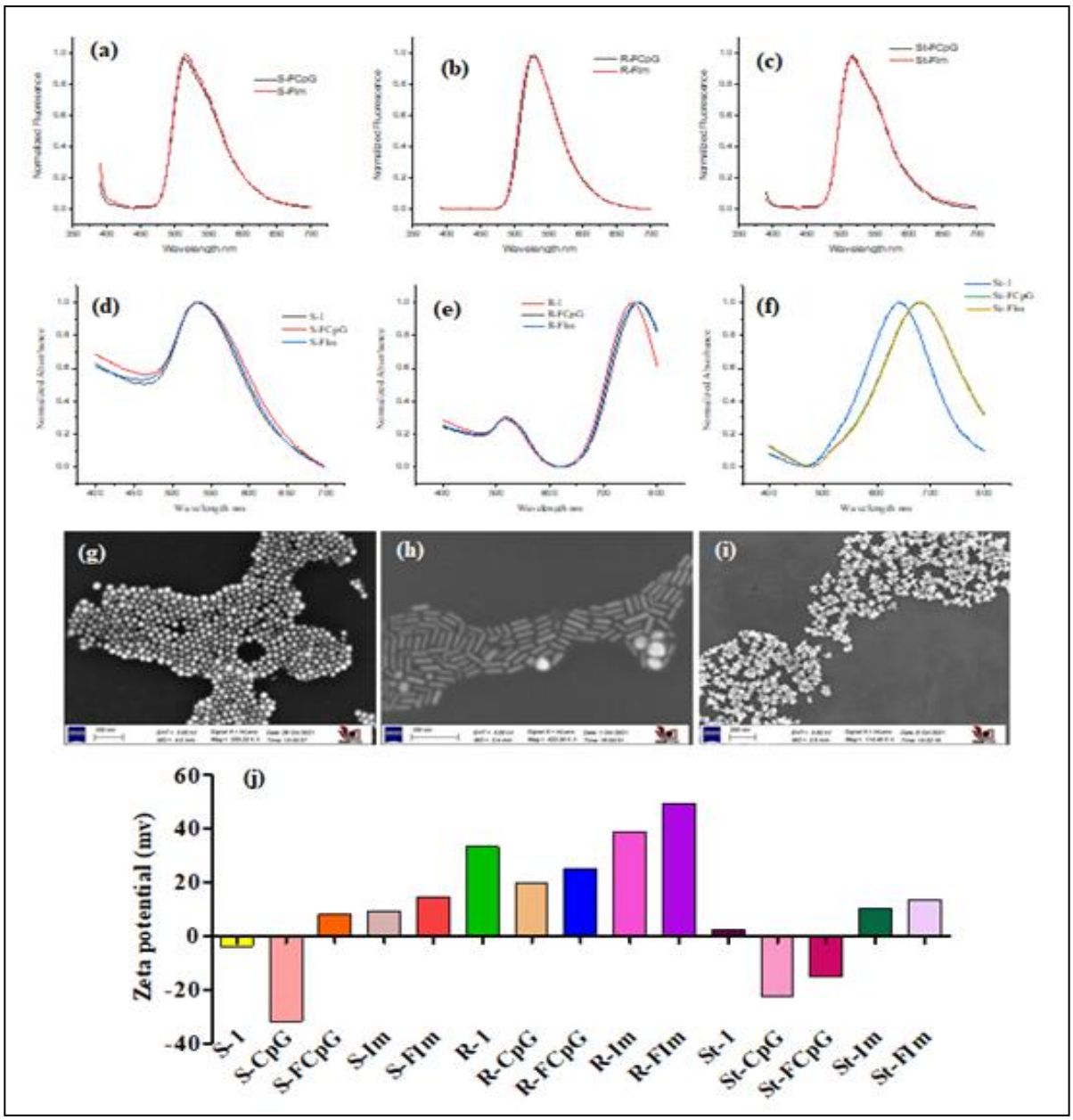


**Figure 3. Physical Characterization of adjuvant conjugated-nanoparticles** (a-c) Fluorescence spectra of AuNPs; (d-f) UV-visible spectra of AuNPs; (h-j) SEM images of all three shapes of AuNPs before conjugation; (k) zeta potential of functionalization of AuNPs.

Finally, the amount of CpG and imidazoquinoline on the nanostructure was quantified using a thio-detection assay kit. As Table 1 shows, there were nearly copmarable amounts of adjuvants on the nanoparticles.

| Sr. No. | AuNPs | CpG molecules/NP | Sr. No. | AuNPs | Im molecules/NP |
|---|---|---|---|---|---|
| **1** | S-CpG | 138 ± 24 | **1** | S-Im | 587 ± 28 |
| **2** | R-CpG | 196 ± 19 | **2** | R- Im | 780 ± 11 |
| **3** | St-CpG | 298 ± 10 | **3** | St-Im | 898 ± 23 |

**Table 1.** Quantification of CpG and tripodal Im adjuvant concentration on the surface of AuNPs.

### 5.3.4 Cytokine production Study

With access to six unique AuNPs (**S-FCpG**, **R-FCpG**, **St-FCpG, S-FIm**, **R-FIm,** and **St-FIm)**, we turned our attention to studying their immune modulation using macrophage cells. To this end, macrophage cells were isolated from the bone marrow of adult mice according to well-established protocols, and with the application of specific growth factors.[38] Following the isolation and differentiation of immune cells, CpG- and imidazoquinoline-conjugated AuNPs were independently added to the media with optimum concentration, which was standardized in our previous publication.[14, 39-41] After 4 h and 24 h of incubation, live images were captured and analyzed. Exposure of rod-shaped AuNPs (**R-FCpG** and **R-FIm**) resulted in a drastic increase in uptake after 4 h (Figure 4) compared to their spherical and star counterparts, and this trend continued after 24 h. This was further validated using the FACS measurement. All of these results correlate with our previous findings on shape-dependent studies.[14, 42] This indicates that the aspect ratio and trembling motion of the nanoparticles induce different uptake rates.

To evaluate the pro-inflammatory immune responses of TLR appended nanostructures, AuNPs were incubated in BMDM and enhancement in tumor necrosis factor TNF-α, Interleukin (IL)-6, and interferon (IFN)-γ; then, IL-10 level was evaluated. In general, the rate of uptake of nanoparticles correlates with cytokine secretion. However, we observed a completely different

cytokine secretion trend. The rod-shaped AuNPs (**R-FCpg** and **R-FIm**) displayed poor cytokine secretion, whereas the spherical AuNPs (**S-FCpG** and **S-FIm**) showed moderate immune responses (Figure 4 and Figure 5). This reiterates our previous finding that the uptake mechanism and TLR receptor activation are independent mechanisms.[14] However, to our surprise star-shaped AuNPs (**St-FCpG** and **St-FIm**) showed more robust Th1- and Th2-type immune responses.

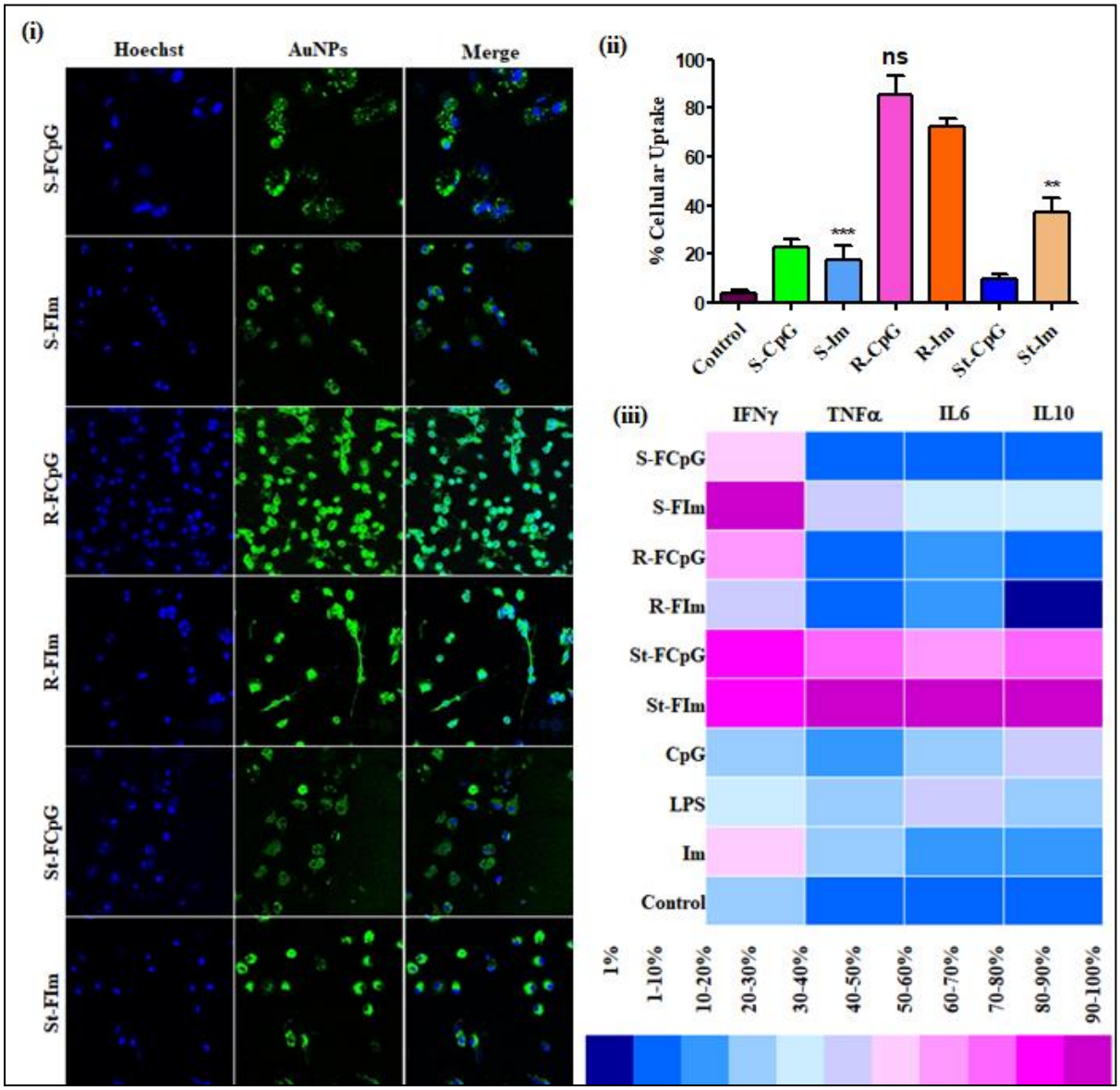



**Figure 4**. (i) Confocal images of CpG and Tripodal Im conjugated AuNPs internalization by mice bone marrow-derived macrophage after 4 h (scale bar: 20 μm); (ii) Quantification of cellular internalization of CpG and Tripodal Im conjugated AuNPs by mice bone marrow-derived macrophage after 4h based on FACS data; Asterisks indicate statistically significant differences ((*p < 0.05; **p < 0.001; ***p < 0.001; ns, not significant). Statistical analysis is between **R-FIm** and different AuNPs performed using a two-tailed Student t test; (iii) Hierarchical clustering

analysis (HCA) for cytokine secretion by mice bone derived macrophages after a 24 h treatment with CpG and Tripodal Im conjugated AuNPs based on ELISA cytokine secretion data (cytokine secretion for S-Im considered as 100% for IFNγ, while cytokine secretion for St-Im considered as 100% for rest of three cytokines).

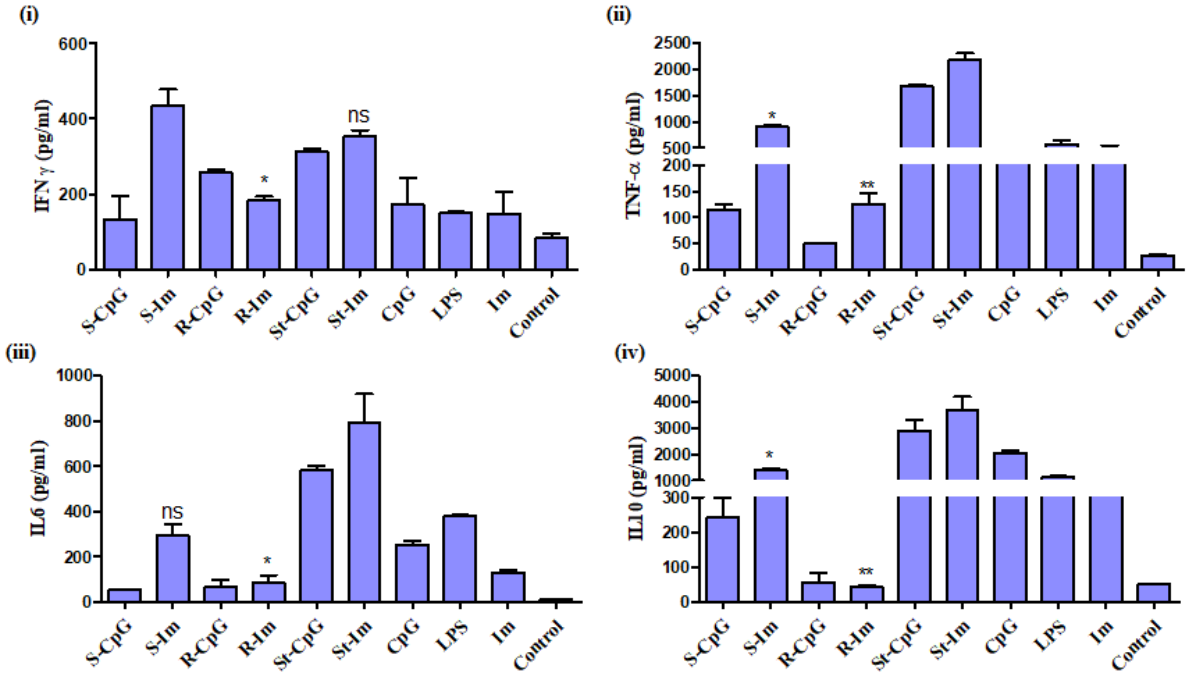



**Figure 5**. *In vitro* cytokine production by BMDM's pulsed with CpG and Im conjugated AuNPs. (i) Interferon-γ (IFN-γ); (ii) Tumor necrosis factor-α (TNF-α); (iii) Interleukin-6 (IL-6); (iv) Interleukin-10 (IL-10) production after 24 h; Asterisks indicate statistically significant differences ((*p < 0.05; **p < 0.01; ***p < 0.001; ns, not significant). Statistical analysis is between **St-FIm** and different AuNPs performed using a two-tailed Student t test.

### 5.3.5 Co-localization assay

To understand the mechanism, we performed co-localization assays using early, late endosome, lysosome, and mitotracker markers. To our further surprise, most of the **St-FIm** AuNPs were sequestered in the late endosome and lysosomal regions (Figure 6). It is hypothesized that TLR7/8 and 9 receptors are abundantly present in endosomal regions and **St-FIm** binds to these receptors and regulate immune responses.[43] Whereas, the nanoparticles in lysosomes may degrade and release the adjuvants molecules and activate the TLR receptors. However, the **R-FIm** was found majorly colocalized in the mitochondrial area, and **S-FIm** was found to be widely distributed in the early, late endosome, and mitochondrial regions. Hence, these nanoparticles might induce less immune response as compared to **St-FIm**. Similar trend was also observed

CpG-conjugated AuNPs (Figure 6). Overall, these results clearly illustrate that the shapes of AuNPs can drive TLR agonists to different cell compartments and modulate their immune modulation. Such disparity in cellular distribution contributes to vaccine development. Recently, we showed that the shapes of the CpG-AuNPs encapsulated with MUC1 peptides exhibited shape-dependent IgG responses. Spherical and star-shaped AuNPs have been proposed to modulate MUC1 peptide immune responses in dendritic cell/T-cell coculture systems and *in vivo* immune responses.[14] However, CpG is an expensive material for large-scale vaccine development. Alternatively, synthetic TLR agonists, such as imidazoquinoline, could be potential replacements. Thus, further elucidation of the connection between imidazoquinoline and antigens using star-shaped AuNPs will be a key consideration in the development of antibodies.

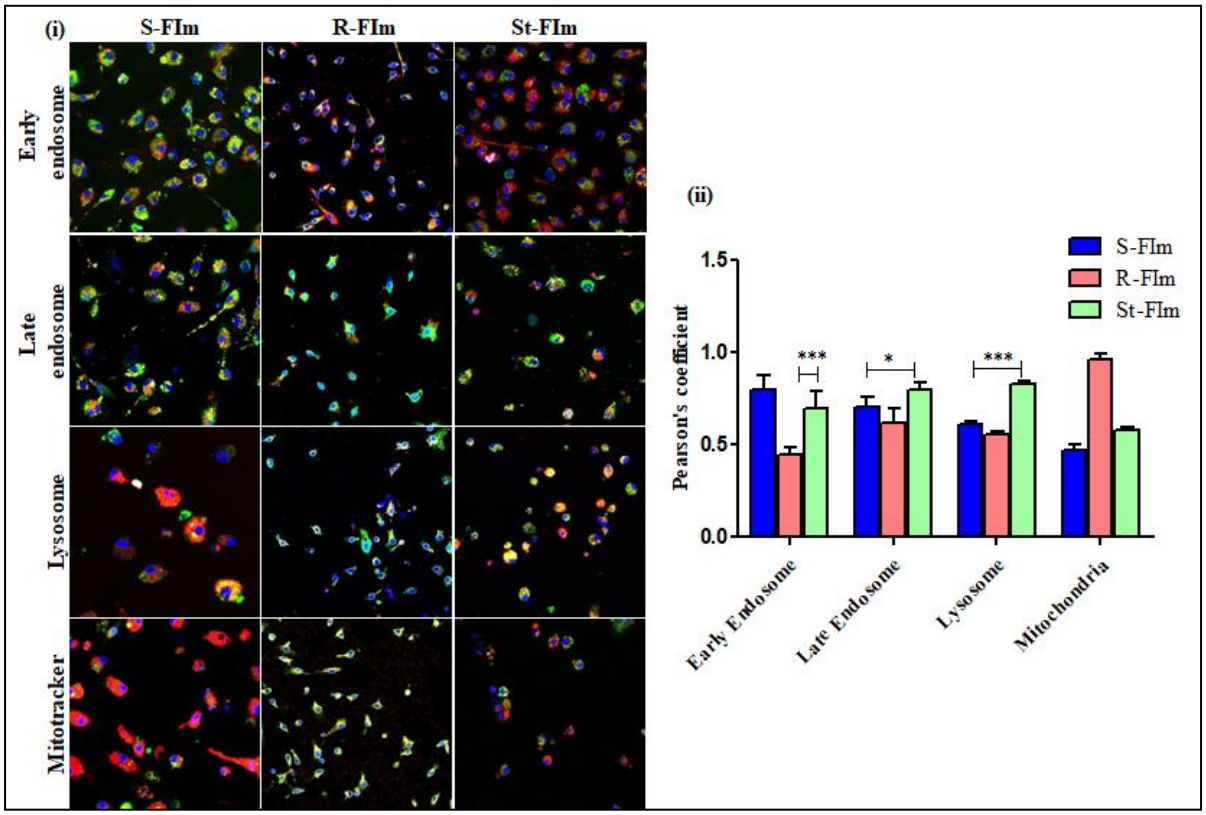



**Figure 6**. (i) Confocal microscopic images for trafficking of tripodal Im conjugated AuNPs (Green) in mitochondria (Mitotracker Deep Red), early (EEA1 antibody), late (LAMP2 antibody) endosomal compartments and lysosomes (lysotracker Deep Red) of mice bone derived macrophages after 4 h of treatment (scale bar: 20 μm); (b) Time point was assessed for >20 cells per treatment using Pearson's coefficient as determined by the just another co-localization plugin in Image J; Asterisks indicate statistically significant differences (*p < 0.05; **p < 0.01; ***p < 0.001; ns, not significant).

## 5.4 Conclusion

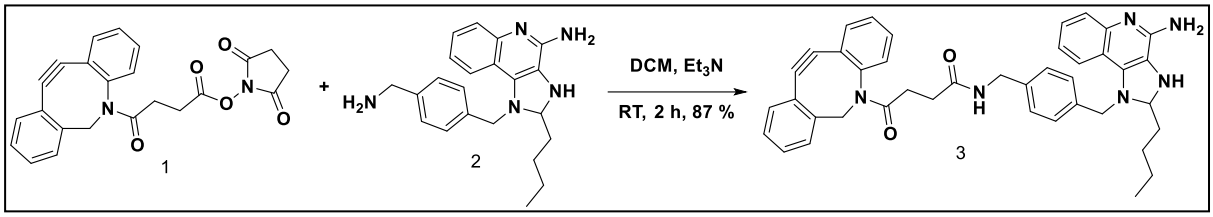
We synthesized a panel of TLR agonist-conjugated AuNPs with different geometries. Macrophage uptake and cytokine secretion showed that the geometry of AuNPs is key to organize adjuvant-conjugated AuNPs in endosomes and lysosomes, resulting in different inflammatory responses. More specifically, star-shaped AuNPs (**St-FCpG** and **St-FIm**) demonstrated an ideal platform for pursuing vaccine development, in contrast to rod-shaped AuNPs. Moreover, TLR agonists, such as CpG and imidazoquinoline, showed similar inflammatory responses, indicating that small molecule adjuvants have a potential role in vaccine development. Currently, *in vivo* studies of imidazoquinoline/antigen conjugation on star-shaped AuNPs are in progress.

## 5.5 Experimental part

### a) General Information

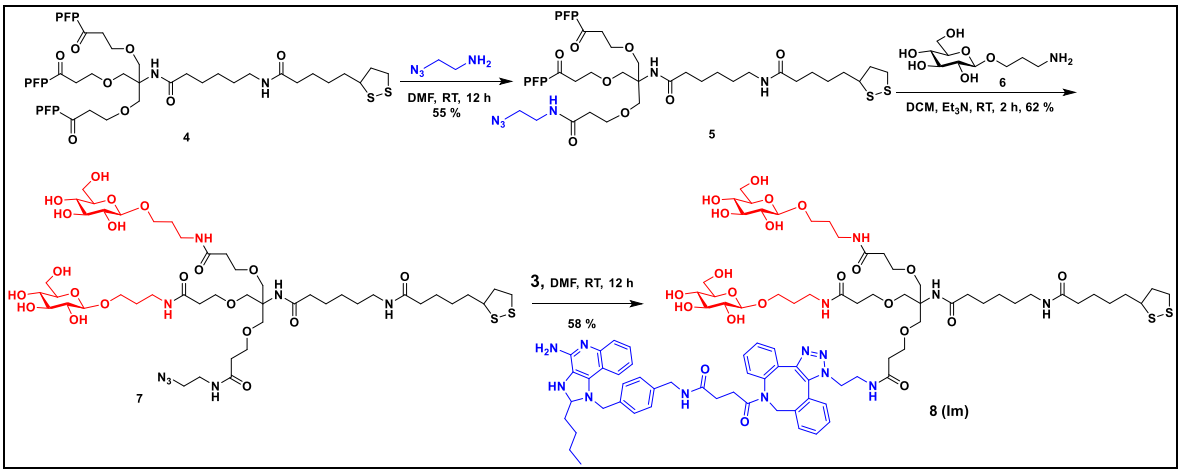
All chemicals were reagent grade and used without further purification unless otherwise noted. Reactions were carried out in anhydrous solvents under a nitrogen atmosphere. Reaction progress was monitored by analytical thin-layer chromatography (TLC) on Merck silica gel 60 $F_{254}$. Spots on TLC plate were visualized under UV light or dipping the TLC plate in CAM/ninhydrin solution followed by heating. Column chromatography was carried out using Fluka kieselgel 60 (230-400 mesh). Thiol modified oligodeoxynucleotide CpG ODN 1826 (5'-C6SS-TCCATGACGTTCCTGACGTT-3') was purchased from Genemed Synthesis Inc. USA. $^{1}H$ and $^{13}C$ NMR spectra of compounds were measured with Bruker 400 MHz, Bruker 600 MHz and Jeol 400 MHz using residual solvents as an internal reference ($CDCl_3$ δH 7.26 ppm, δC 77.3 ppm, $CD_3OD$ δH 3.31 ppm, δC 49.0 ppm, and $D_2O$ δH 4.79 ppm). The chemical shifts (δ) are reported in ppm and coupling constants (J) in Hz. UV-visible measurements were performed with Evolution 300 UV-visible spectrophotometer (Thermo Fisher Scientific, USA). Fluorescence spectra were measured with FluoroMax-4 spectrofluorometer (Horiba Scientific, U.S.A.). For colocalization studies mitotracker deep red (M22426), EEA1 antibody (MA5-31575, early endosomal marker), LAMP2 antibody (MA1-165, late endosomal marker), Donkey anti Rat IgG (H+L) highly cross absorbed secondary antibody, Alexa fluor 594 (A-21209) purchased from eBioscience™. All microscopy images were captured using Leica SP8 confocal microscope and processed using Image J software.

## b) Synthesis of imidazoquinolin tripod




## Synthesis of Compound 3

Compound **1** (20 mg, 49 µmol) and **2** (21.5 mg, 59 µmol) dissolved in anhydrous dichloromethane (200 µL) then added $Et_3N$ (20.7 µl, 149 µmol), The reaction mixture was stirred at room temperature for 2 h, concentrated and the residue was purified by silica gel column chromatography using a mixture of (1:5, v/v) ethyl acetate and hexane as eluent to afford the desired product **3** (28 mg, 87 %) as a white viscous liquid. $^1$H NMR (400 MHz, Methanol-$d_4$) δ 7.82 (d, *J* = 7.7 Hz, 1H), 7.64 (t, *J* = 7.9 Hz, 2H), 7.50 – 7.35 (m, 5H), 7.32 – 7.27 (m, 1H), 7.24 – 7.18 (m, 3H), 7.16 – 7.08 (m, 2H), 7.00 (s, 1H), 6.77 (d, *J* = 7.7 Hz, 1H), 6.16 (t, *J* = 5.9 Hz, 1H), 5.68 (s, 2H), 5.16 – 5.07 (m, 1H), 4.29 (m, 1H), 4.15 (m, 1H), 3.67 (m, 1H), 2.88 – 2.75 (m, 3H), 2.47 – 2.35 (m, 1H), 2.21 (m, 1H), 2.13 (s, 1H), 1.98 (m, 1H), 1.78 (m, 2H), 1.43 (m, 2H), 0.92 (t, 3H). $^{13}$C NMR (100 MHz, Methanol-$d_4$) δ 172.94, 172.81, 155.21, 151.12, 147.92, 139.90, 135.29, 132.06, 129.43, 129.24, 128.74, 128.43, 128.06, 127.93, 127.67, 127.07, 126.99, 125.36, 124.53, 123.92, 123.60, 123.10, 122.45, 120.40, 114.44, 114.03, 107.60, 55.64, 42.71, 30.55, 29.98, 29.48, 26.79, 22.24, 13.29. HRMS (ESI) m/z: calc'd for $[M-H]^-$ $C_{41}H_{40}N_6O_2$: 647.3213, Found: 647.3134.




## Synthesis of Compound 5

Compound **4** (10 mg, 8 µmol) in anhydrous DMF (100 µL) were added azidoethylamine (0.6 mg, 70 µmol). The reaction mixture was stirred at room temperature for 12 h and concentrated. The residue was purified by silica gel column chromatography using a mixture of (1:5, v/v) ethyl acetate and hexane as eluent to afford the desired product **5** (5 mg, 55 %) white solid. $^{1}$H NMR (400 MHz, Chloroform-*d*) δ 6.84 (s, 1H), 5.89 (s, 1H), 5.74 (s, 1H), 3.83 (t, *J* = 5.9 Hz, 4H), 3.80 – 3.73 (m, 4H), 3.70 (m, 2H), 3.61 – 3.53 (m, 1H), 3.44 (s, 3H), 3.22 (m, 2H), 3.18 – 3.14 (m, 1H), 3.14 – 3.08 (m, 1H), 2.98 – 2.87 (m, 5H), 2.47 (t, *J* = 5.9 Hz, 2H), 2.15 (m, 4H), 1.92 (m, 1H), 1.74 – 1.65 (m, 3H), 1.60 (m, 3H), 1.48 (m, 3H), 1.33 (q, *J* = 8.3 Hz, 2H). $^{13}$C NMR (100 MHz, Chloroform-*d*) δ 173.44, 172.91, 171.93, 142.47, 140.83, 139.93, 139.21, 138.31, 136.69, 124.93, 69.58, 69.50, 69.22, 67.28, 66.17, 66.12, 59.50, 56.53, 50.83, 40.33, 39.30, 39.03, 38.53, 36.89, 36.69, 36.55, 34.69, 34.30, 29.33, 28.99, 26.29, 25.52, 25.12. HRMS (ESI) m/z: calc'd for $[M+H]^+$ $C_{41}H_{48}F_{10}N_6O_{10}S_2$, 1039.2792, Found: 1039.2780.

## Synthesis of Compound 7

To the solution of compound **5** (5 mg, 4 µmol) in anhydrous dichloromethane (200 µL) was added $Et_3N$ (2 µl, 0.01 µmol), compound **6** (2.5 mg, 10 µmol). The reaction mixture was stirred at room temperature for 2 h, concentrated. The residue was purified using Bond elute C-18 column chromatography using a mixture of (1:2, v/v) water and acetonitrile as eluent. The purified fraction was lyophilized to afford compound **7** (3.41 mg, 62 %) white solid. $^{1}$H NMR

(400 MHz, Deuterium Oxide) δ 4.23 (d, *J* = 7.9 Hz, 2H), 3.85 – 3.76 (m, 4H), 3.65 – 3.47 (m, 24H), 3.36 (m, 2H), 3.31 – 3.26 (m, 3H), 3.19 – 3.01 (m, 8H), 2.35 (m, 6H), 2.08 (q, *J* = 7.3 Hz, 4H), 1.84 (m, 1H), 1.74 – 1.33 (m, 13H), 1.27 (m, 2H), 1.21 – 1.14 (m, 2H). $^{13}$C NMR (100 MHz, Deuterium Oxide) δ 176.63, 174.51, 174.07, 102.87, 75.16, 72.79, 70.79, 68.64, 67.62, 60.98, 60.12, 56.63, 50.04, 40.33, 38.78, 38.12, 36.39, 36.25, 36.18, 35.57, 33.75, 28.58, 27.84, 25.62, 25.14. HRMS (ESI) m/z: calc'd for $[M+H]^+$ $C_{47}H_{84}N_8O_{20}S_2$, 1144.5243, Found: 1144.5240.

## Synthesis of Compound 8

Compound **7** (3 mg, 4 μmol) and compound **3** (5.2 mg, 40 μmol) dissolved into DMF, stirred at room temperature for 12 h then concentrated, the residue was purified using Bond elute C-18 column chromatography using a mixture of (1:1, v/v) water and acetonitrile as eluent. The purified fraction was lyophilized to afford compound **8** (4.7 mg, 58 %) white solid. $^1$H NMR (400 MHz, Deuterium Oxide) δ 7.73 (d, *J* = 8.3 Hz, 1H), 7.65 – 7.45 (m, 4H), 7.30 (m, 3H), 7.15 (t, *J* = 8.3 Hz, 2H), 6.47 (s, 1H), 5.81 (s, 2H), 4.85 (d, *J* = 3.3 Hz, 1H), 4.29 (d, *J* = 7.9 Hz, 2H), 4.10 (s, 2H), 3.89 (s, 3H), 3.84 (d, *J* = 3.3 Hz, 3H), 3.70 (s, 2H), 3.67 (d, *J* = 3.7 Hz, 4H), 3.65 (d, *J* = 5.5 Hz, 9H), 3.59 (m, 11H), 3.55 (d, *J* = 3.4 Hz, 2H), 3.43 (m, 4H), 3.22 (t, *J* = 7.0 Hz, 5H), 3.09 (t, *J* = 6.8 Hz, 2H), 2.91 (s, 2H), 2.40 (t, *J* = 5.9 Hz, 6H), 2.18 – 2.12 (m, 5H), 1.98 (p, *J* = 3.4 Hz, 3H), 1.75 (p, *J* = 6.8 Hz, 6H), 1.58 (m, 4H), 1.47 (m, 7H), 1.32 – 1.21 (m, 6H), 0.74 (t, 3H). HRMS (ESI) m/z: calc'd for $[M+H]^+$ $C_{88}H_{124}N_{14}O_{22}S_2$, 1792.8456, Found: 1792.8458.

## c) Synthesis of different shapes and sizes of gold nanoparticles

### i) Synthesis of sphere gold nanoparticles

Sphere gold nanoparticles were synthesized according to the previously reported method.[1] In detail, to 30 mL of distilled water 300 µl of 1% chloroauric acid was added and brought to boil, on boiling 240 µl of 1% citric acid was added to it ot get 45 nm of sphere AuNPs. Refluxing continued until the colour changes from dark purple to the red wine. Then solution was cooled, centrifuged, and the pellet was washed with distilled water. Formation of AuNPs were characterized by SEM and UV-vis spectrophotometry.

### ii) Synthesis of rod gold nanoparticles

Large size nanorods were synthesized according to the previously reported producedure by seed mediated growth.[2]

Preparation of seed solution: To $HAuCl_4.3H_2O$ solution (5mL, 0.0005 M), CTAB solution (5 mL, 0.2 M) was added with moderate stirring at 25 ºC, to this solution an ice-cold solution of $NaBH_4$ (0.6 mL, 0.001 M) was added under vigorous stirring for 2 min. Then the solution was kept at 25 ºC and after 15 min used for the next step. Preparation of growth solution: To solution of CTAB in water (10 mL, 0.2 M), $AgNO_3$ (0.846 mL, 0.004 M) was added at 28 ºC under stirring followed by addition of $HAuCl_4.3H_2O$ solution (10 mL, 0.002 M) and ascorbic acid solution (0.23 mL, 0.0788 M). Finally, the seed solution (0.032 mL) was added, stirred for 2 min, and kept undisturbed at 27-30 º C for an hour. The nanoparticle solution was centrifuged, and the pellet of 45 nm gold nanorods was washed with distilled water and characterized by HRTEM and UV-vis spectrophotometry.

### iii) Synthesis of star nanoparticles

Star gold nanoparticles were synthesized by using the reported literature method.[3] Preparation of seed solution: Citrate solution (1%, 15 mL) was added to boiling solution of $HAuCl_4$ (100 mL) in water, boiling continued for 15 min, then cooled and filtered by a 0.22 µm nitrocellulose membrane and used for the next step.

Synthesis of Star nanoparticles: Seed solution (100 µL) and HCl (10 µL, 1 M) were added to stirring solution of $HAuCl_4$ (10 mL, 0.25 mM) at 25 ºC. Quickly, silver nitrate (100 µL, 20 µM) and ascorbic acid (50 µL, 100 mM) were added simultaneously. The resulting solution was stirred for 25 seconds as its colour was rapidly changed from light blue to greenish-black. Then the nanoparticles solution was immediately centrifuged to stop the nucleation. The pellet of nanoparticles was washed with distilled water and characterized by HRTEM and UV-vis spectrophotometry.

**d) CpG and imidazoquinolin tripodal derivative functionalization on a gold nanoparticle surface**

Thiol-modified tripodal imidazoquinoline and CpG ODNs were directly conjugated onto the surface of different shapes and sizes of gold nanoparticles using a simple ligand exchange method. Conjugation of these molecules and handling were done in sterile conditions.

**i) CpG-ODNs conjugation**

Prior to conjugation, the disulfide bond of CpG was reduced to thiol group in a TCEP solution (10 mM, 1 mL $H_2O$) at RT for an hour with constant shaking, followed by centrifugation with an amicon ultra centrifugal filter (cutoff size was 3 kD) to remove TCEP and linker by-product. The reduced CpG-ODN (100 µg) was mixed with gold nanoparticles in PBS pH 7.4 (0.5 mL, 0.1 M) at RT for 12 h with constant shaking, further the concentration of NaCl in the solution was slowly increased to 0.1 M over 2 h time window by stepwise addition of 2 M NaCl. The solution was further kept at RT for 12 h with constant shaking. Then the resulting solution was centrifuged, and pellet was washed three times with Mili Q water to remove the unbound antigen to get **S-CpG, R-CpG**, and **St-CpG**. The loading quantity of CpG-ODNs onto the surface of nanoparticles were determined by ssDNA assay kit (Thermo Fisher).

**ii) Imidazoquinolin tripod conjugation**

In brief, AuNPs (1000 µg) were dispersed in PBS buffer pH 7.4 (1 mL, 0.1 M), to this imidazoquinolin tripod **8** (100 µg) was added. The resulting solution was kept at 25 ºC for 24 h with constant shaking. Then the solution was centrifuged, and the pellet was washed three times with Mili Q water to remove the unbound antigen and get **S-Im, R-Im**, and **St-Im**, change in zeta potential confirmed the antigen (imidazolin tripod **8**) conjugation. The loading quantity of antigen onto the surface of nanoparticles was determined by a thiol detection kit (Cayman chemicals, USA).

Finally **S-CpG, S-Im, R-CpG, R-Im, St-CpG,** and **St-Im** AuNPs (each 100 µg) dispersed in PBS buffer pH 7.4 (1 mL, 0.1 M) followed by addition of fluorescent tag **F-1** (50 µg) and kept under constant shaking at RT for 24 h.then solution was purified by using 3 KD cutoff centrifugal filtration followed by washing with MiliQ water to get **S-FCpG, S-FIm, R-FCpG, R-FIm, St-FCpG,** and **St-FIm.**

## i) Isolation of mice bone marrow derived macrophages (BMDM)

All animal studies were performed with the approved protocol from the institutional animal ethical committee. Before the experiment, female C57BL/6 mice (6-8 weeks old) were maintained in pathogen-free condition with proper food supplements and day and night cycles. Macrophages were isolated from 6-8 weeks old female C57BL/6 mice.

**ii) Cell culture and differentiation of Bone marrow derived macrophages (BMDM)**

Euthanize mice by cervical dislocation and skin was peeled off from top up to hind leg followed by cutting off hip joint and hind leg with sterile scissors. Excess skin muscles were removed carefully from legs. Separated femur and tibia kept in sterile PBS and their ends were cut carefully using sterile blade. Bone marrow cavity was gently flushed out using 10 ml syringe with 25-G needle filled with DMEM media. The uniform suspension of cells were centrifuged at 300g for 5 min. Cell pellet was treated with RBC lysis buffer for 2 min at 0 ºC, on completion of incubation cells diluted four times with RPMI media and centrifuged at 300g for 5 min. Cells were suspended in RPMI media containing 50ng/ml m-CSF and plated in 100 mm plate and incubated at 37 ºC. On $4^{th}$ day of culture the media on plate was top up by addition of 3 ml fresh RPMI media containing 50ng/ml of m-CSF. On $6^{th}$ day the media was removed and cells washed with PBS followed by scraping in RPMI media. BMDM's were counted and used for the experiments.

## iii) Confocal Imaging

$2 \times 10^4$ BMDM's were seeded in 8 well plate in presence of RPMI media and incubated at 37 ºC for overnight. The cells were incubated with CpG (50 nmol) and tripodal Im (10 nmol) adjuvant functionalized AuNPs for 4 h. Then the cells were washed with the PBS and nuclei were stained with Hoechst. The fluorescent images were taken using Leica sp8 microscope.

## iv) FACS analysis

BMDMs ($2 \times 10^6$ cells) were seeded in 96 well plates in RPMI media and incubated at 37 ºC for overnight. The cells were pulsed with CpG (50 nmol) and tripodal Im (10 nmol) adjuvant functionalized AuNPs for 4 h. The BMDM's were washed with PBS to remove non-internalized AuNPs, then scraped using scraper and finally suspended in FACS buffer for analysis. Quantification of uptake was analysed by using Flowjo software.

## v) Cytokine secretion by BMDM's

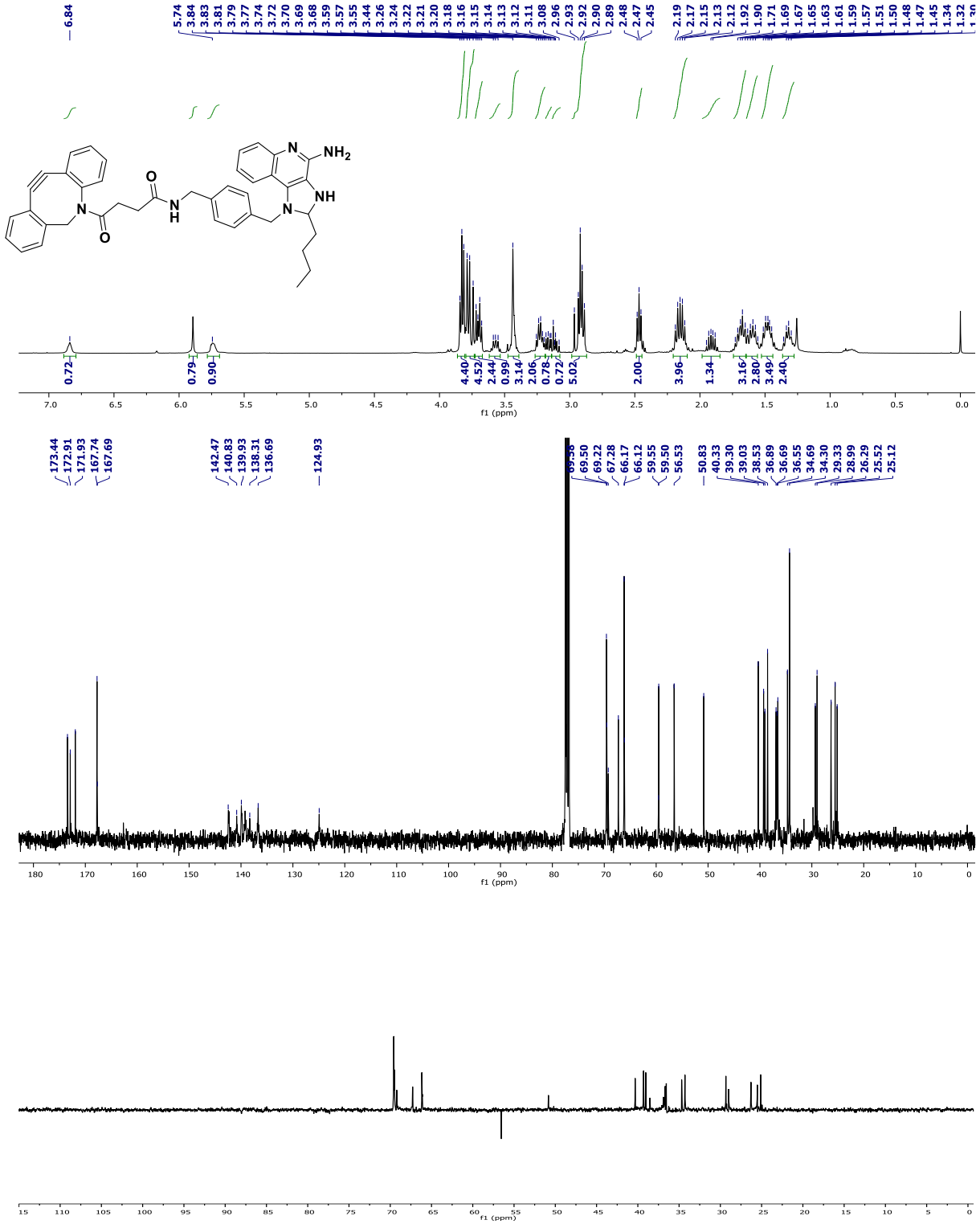
BMDMs ($2 \times 10^6$ cells/well) were seeded in 96 well-plate in presence of RPMI medium and incubated at 37 ºC for overnight. Then BMDMs were pulsed with the CpG and tripodal Im adjuvant functionalized AuNPs and incubated further for 24 h at 37 ºC. Supernatant was analysed for cytokine (IL6, IL10, TNFα, IFNγ) level using ELISA assay (R&D Systems).

## vi) Cellular trafficking studies

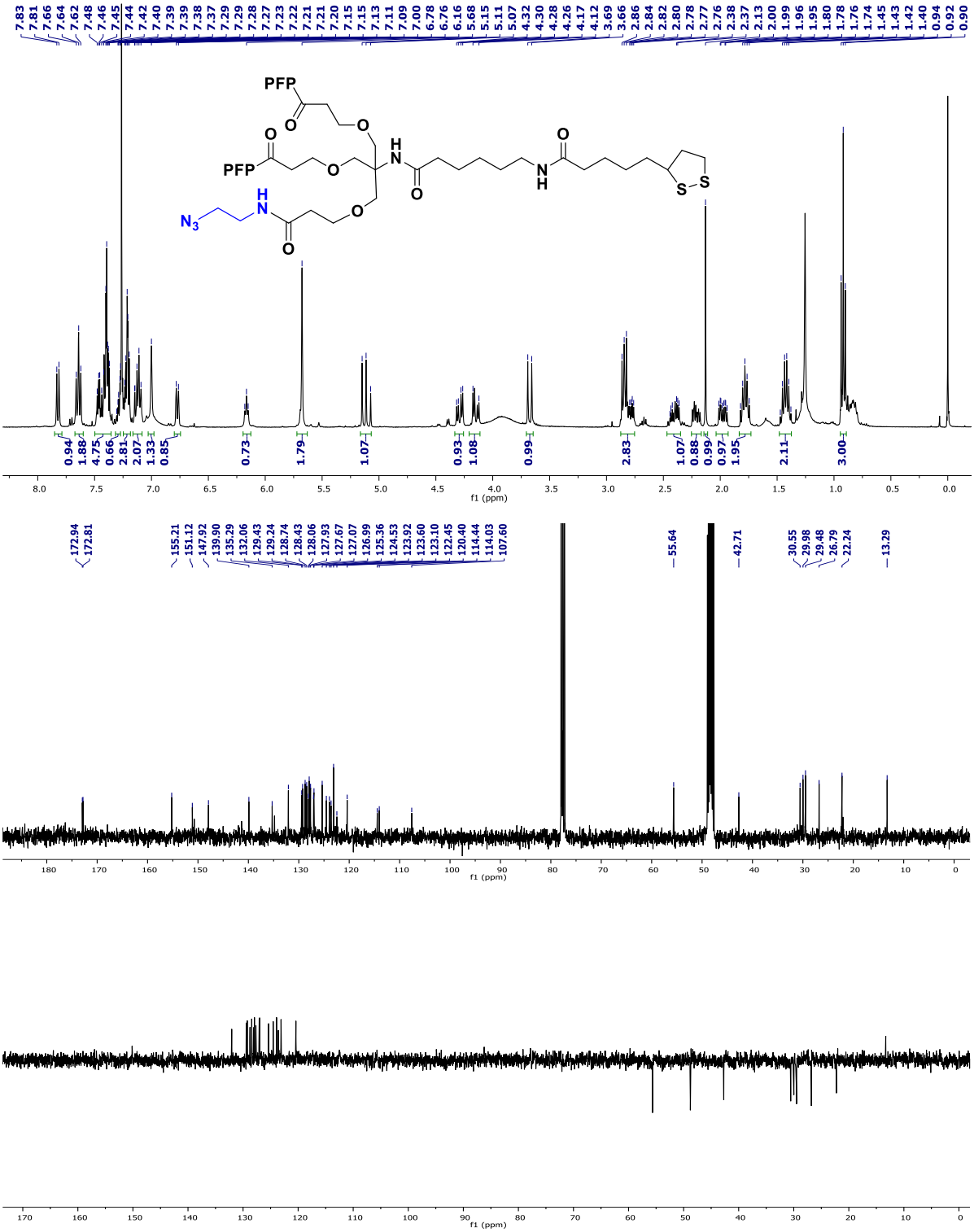
To study cellular co-localization of adjuvant conjugated AuNPs BMDM's were grown in an 8-well chamber cover glass ($1 \times 10^4$ cells per well) overnight. For early endosome co-localization cells treated with EEA1 antibody for 45 min then AuNPs were added and incubated further for 4h. For other organelle co-localization studies first cells treated with AuNPs for 4h, then LAMP2 antibody for late endosome, mitotracker deep red and lysotracker deep red was added and incubated further for 30 min. For early and late endosome secondary Goat anti rat Alex 594 antibody was added and incubated further for 30 min. Finally all cells stained with Hoechst, washed and taken for imaging.

# 5.6 NMRs

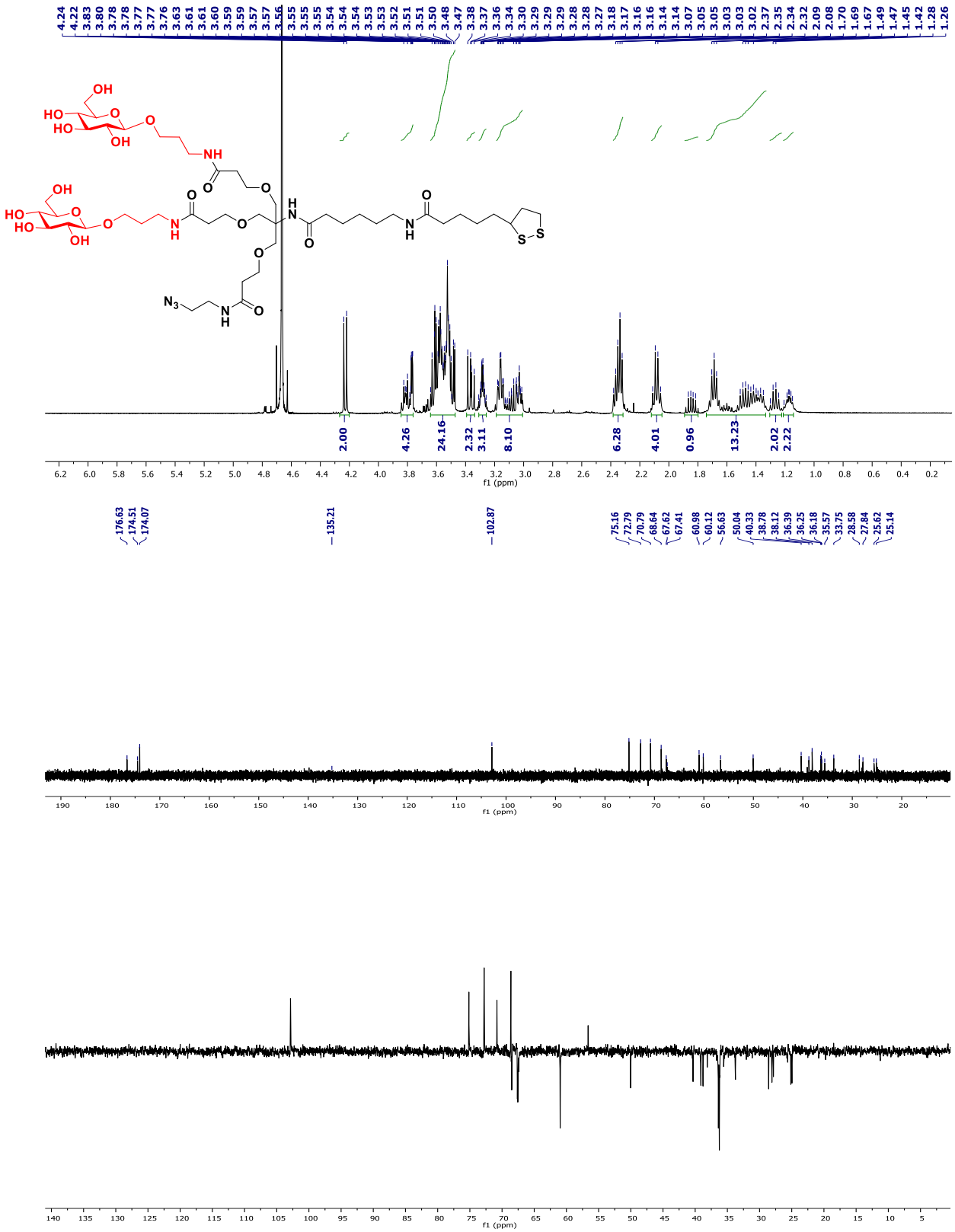
## $^{1}H$, $^{13}C$, and DEPT NMR spectrum of compound 3



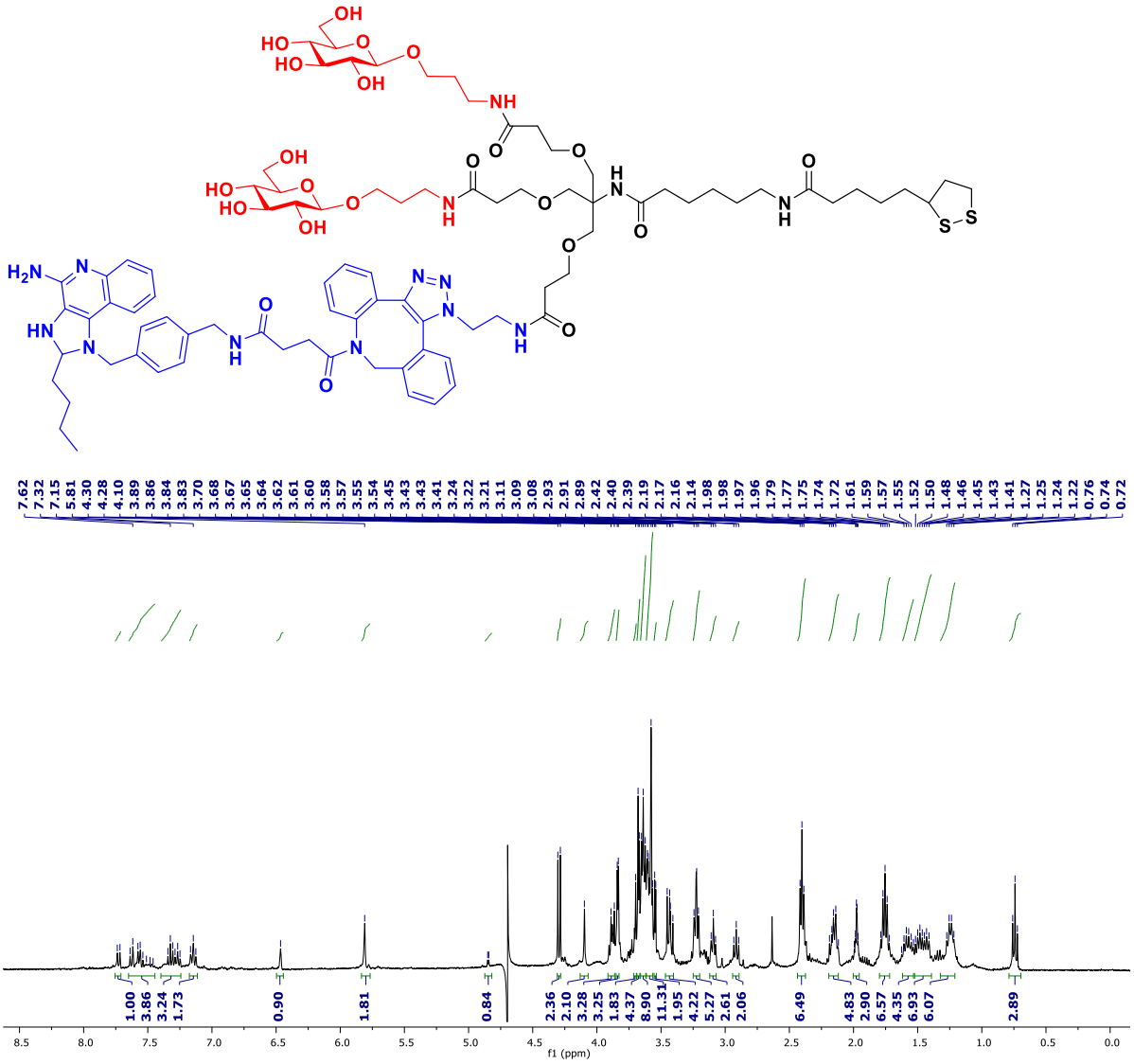
## $^{1}H$, $^{13}C$, and DEPT NMR spectrum of compound 5



## $^{1}H$, $^{13}C$, and DEPT NMR spectrum of compound 7



**$^{1}H$, $^{13}C$, and DEPT NMR spectrum of compound 8**



## 5.7 References


1. Mateu Ferrando, R.; Lay, L.; Polito, L. Gold nanoparticle-based platforms for vaccine development. *Drug Discov. Today Technol*. **2020**, *8*, 57-67.
2. Barchi, J. J. Jr. Glycoconjugate Nanoparticle-Based Systems in Cancer Immunotherapy: Novel Designs and Recent Updates. *Front Immunol*. **2022**, *13*, 852147.
3. Wu, X.; McFall-Boegeman, H.; Rashidijahanabad, Z.; Liu, K.; Pett, C.; Yu, J.; Schorlemer, M.; Ramadan, S.; Behren, S.; Westerlind, U.; Huang, X. Synthesis and immunological evaluation of the unnatural β-linked mucin-1 Thomsen-Friedenreich conjugate. *Org. Biomol. Chem*. **2021**, *19*, 2448-2455.
4. Wu, X.; McKay, C.; Pett C.; Yu, J.; Schorlemer, M.; Ramadan, S.; et al. Synthesis and Immunological Evaluation of Disaccharide Bearing MUC-1 Glycopeptide Conjugates with Virus-like Particles. *ACS Chem. Biol*. **2019**, *14*, 2176-2184.
5. Wang, P.; Huo, C. X.; Lang, S.; Caution, K.; Nick, S. T.; Dubey, P.; et al. Chemical Synthesis and Immunological Evaluation of a Pentasaccharide Bearing Multiple Rare Sugars as a Potential Anti-pertussis Vaccine. *Angew. Chem. Int. Ed. Engl*. **2020**, *59*, 6451-6458.
6. Yin, Z.; Wu, X.; Kaczanowska, K.; Sungsuwan, S.; Comellas, A. M.; Pett, C.; et al. Antitumor Humoral and T Cell Responses by Mucin-1 Conjugates of Bacteriophage Qβ in Wild-type Mice. *ACS Chem. Biol*. **2018**, *13*, 1668-1676.
7. Dykman, L. A. Gold nanoparticles for preparation of antibodies and vaccines against infectious diseases. *Expert Rev Vaccines*. **2020,** *5*, 465-477.
8. Sengupta, A.; Azharuddin, M.; Al-Otaibi,N.; Hinkula, J. Efficacy and Immune Response Elicited by Gold Nanoparticle Based Nanovaccines against Infectious Diseases. *Vaccines* **2022**, *10*, 505.
9. Krishnamachari, Y.; Geary, S. M.; Lemke, C. D.; Salem, A. K. Nanoparticle delivery systems in cancer vaccines. *Pharm Res.* **2011**, *28*, 215-36.
10. Brinãs, R. P.; Sundgren, A.; Sahoo, P.; Morey, S.; Rittenhouse-Olson, K.; Wilding, G. E.; et al. Design and synthesis of multifunctional gold nanoparticles bearing tumor-

associated glycopeptide antigens as potential cancer vaccines. *Bioconjug. Chem*. **2012**, *23*, 1513-1523.

11. Trabbic, K. R.; Kleski, K. A.; Barchi, J. J. Jr. A Stable Gold Nanoparticle-Based Vaccine for the Targeted Delivery of Tumor-Associated Glycopeptide Antigens. *ACS Bio Med Chem Au*. **2021,** *1*, 31-43.
12. Ghosh, C.; Priegue.; Leelayuwapan, H.; Fuchsberger, F. F.; Rademacher, C.; Seeberger, P. H. Synthetic Glyconanoparticles Modulate Innate Immunity but Not the Complement System. *ACS Appl. Bio. Mater*. **2022**, *5*, 2185-2192.
13. Niikura, K.; Matsunaga, T.; Suzuki, T.; Kobayashi, S.; Yamaguchi, H.; Orba, Y.; et al. Gold nanoparticles as a vaccine platform: influence of size and shapes on immunological responses *in vitro* and *in vivo*. *ACS Nano*. **2013**, *7*, 3926-3938.
14. Toraskar, S.; Chaudhary, P. M.; Kikkeri, R. The Shape of Nanostructures Encodes Immunomodulation of Carbohydrate Antigen and Vaccine Development. *ACS Chem Biol*. **2022**, *17*, 1122-1130.
15. Dykman, L. A.; Staroverov, S. A.; Fomin, A. S.; Khanadeev, V. A.; Khlebtsov, B. N. Bogatyrev, V. A. gold nanoparticles as an adjuvant: influence of size, shape, and technique of combination with CpG on antibody production. *Int. Immuno. Pharmcol.* **2018**, *54*, 163-168.
16. Lee, K.; Huang, Z. N.; Mirkin, C. A.; Odom, T. W. Endosomal Organization of CpG Constructs Correlates with Enhanced Immune Activation. *Nano Lett*. **2020**, *20*, 6170–6175.
17. Frey, M.; Bobbala, S.; Karabin, N.; Scott, E. Influences of nanocarrier morphology on therapeutic immunomodulation. *Nanomedicine (Lond)* **2018**, *13*, 1795-1811.
18. Parry, A. L.; Clemson, N. A.; Ellis, J.; Bernhard, S. S.; Davis, B. G.; Cameron, N. R. 'Multicopy multivalent' glycopolymer-stabilized gold nanoparticles as potential synthetic cancer vaccines. *J. Am. Chem. Soc*. **2013**, *135*, 9362-5.
19. Moyano, D. F.; Liu, Y.; Ayaz, F.; Hou, S.; Puangploy, P.; Duncan, B.; et al. Immunomodulatory effects of coated gold nanoparticles in LPS-stimulated in vitro and in vivo murine model systems. *Chem* **2016**, *1*, 320-327.
20. Zhang, G.; Yang, Z.; Lu, W.; Zhang, R.; Huang, Q.; Tian, M.; et al. Influence of anchoring ligands and particle size on the colloidal stability and *in vivo* biodistribution of

polyethylene glycol-coated gold nanoparticles in tumor-xenografted mice. *Biomaterials* **2009**, *30*, 1928-36.

21. Luchner, M.; Reinke, S.; Milicic, A. TLR Agonists as Vaccine Adjuvants Targeting Cancer and Infectious Diseases. *Pharmaceutics* **2021**, *13*, 142.
22. Yang, J. X.; Tseng, J. C.; Yu, G. Y.; Luo, Y.; Huang, C. F.; Hong, Y. R.; Chuang, T. H. Recent Advances in the Development of Toll-like Receptor Agonist-Based Vaccine Adjuvants for Infectious Diseases. *Pharmaceutics* **2022**, *14*, 423.
23. Bode, C.; Zhao, G.; Steinhagen, F.; Kinjo, T.; Klinman, D. M. CpG DNA as a vaccine adjuvant. *Expert. Rev. Vaccines* **2011**, *10*, 499-511.
24. Cheng, W. K.; Plumb, A. W.; Lai, J. C.; Abraham, N.; Dutz, J. P. Topical CpG Oligodeoxynucleotide Adjuvant Enhances the Adaptive Immune Response against Influenza A Infections. *Front Immunol*. **2016**, *7*, 284.
25. Torii, Y.; Ito, T.; Amakawa, R.; Sugimoto, H.; Amuro, H.; Tanijiri, T.; et al. Imidazoquinoline acts as immune adjuvant for functional alteration of thymic stromal lymphopoietin-mediated allergic T cell response. *J. Immunol*. **2008**, *181*, 5340-9.
26. Lin, A. Y.; Almeida, J. P.; Bear, A.; Liu, N.; Luo, L.; Foster, A. E.; Drezek, R. A. Gold Nanoparticle Delivery of Modified Cpg Stimulates Macrophages and Inhibits Tumor Growth for Enhanced Immunotherapy. *PLoS One* **2013**, *8*, e63550.
27. Wei, M.; Chen, N.; Li, J.; Yin, M.; Liang, L.; He, Y.; et al. Polyvalent Immunostimulatory Nanoagents with Self-Assembled CpG Oligonucleotide-Conjugated Gold Nanoparticles. *Angew. Chem. Int. Ed. Engl.* **2012**, *51*, 1202-1206.
28. Yue, J.; Pallares, R. M.; Cole, L.; Coughlin, E. E.; Mirkin, C. A.; Lee, A.; Odom T. W. Smaller CpG-conjugated Gold Nanoconstructs Achieve Higher Targeting Specificity of Immune Activation. *ACS Appl. Mater. Interfaces* **2018**, *26*, 21920–21926
29. Stickdorn, J.; Stein, L.; Arnold-Schild, D.; Hahlbrock, J.; Medina-Montano, C.; Bartneck, J.; et al. Systemically Administered TLR7/8 Agonist and Antigen-Conjugated Nanogels Govern Immune Responses against Tumors. *ACS Nano*. *2022*, *16*, 4426-4443.
30. Huppertsberg, A.; Kaps, L.; Zhong, Z.; Schmitt, S.; Stickdorn, J.; Deswarte, K.; et al. Squaric Ester-Based, pH-Degradable Nanogels: Modular Nanocarriers for Safe, Systemic Administration of Toll-like Receptor 7/8 Agonistic Immune Modulators. *J. Am. Chem. Soc*. **2021,** *143*, 9872-9883.

31. Nuhn, L.; Van Hoecke, L.; Deswarte, K.; Schepens, B.; Li, Y.; Lambrecht, B. N.; et al. Potent anti-viral vaccine adjuvant based on pH-degradable nanogels with covalently linked small molecule imidazoquinoline TLR7/8 agonist. *Biomaterials* **2018**, *178*, 643-651.
32. Jangra, S.; De Vrieze, J.; Choi, A.; Rathnasinghe, R.; Laghlali, G.; Uvyn, A.; et al. Sterilizing Immunity against SARS-CoV-2 Infection in Mice by a Single-Shot and Lipid Amphiphile Imidazoquinoline TLR7/8 Agonist-Adjuvanted Recombinant Spike Protein Vaccine. *Angew. Chem. Int. Ed. Engl.* **2021**, *60*, 9467-9473.
33. Li, Z.; Derking, R. Lee, W. H.; Bosman, G. P.; Ward, A. B.; Sanders, R. W.; Boons, G. J. Conjugation of a Toll-Like Receptor Agonist to Glycans of an HIV Native-Like Envelope Trimer Preserves Neutralization Epitopes. *Chembiochem* **2022,** e202200236.
34. Chaudhary, P. M.; Sangabathuni, S.; Murthy, R. V.; Paul, A.; Thulasiram, H. V.; Kikkeri, R. Assessing the effect of different shapes of glyco-gold nanoparticles on bacterial adhesion and infections. *Chem. Commun*. **2015**, *51*, 15669-15672.
35. Khanal, B. P.; Zubarev, E. R. Gram-Scale Synthesis of Isolated Monodisperse Gold Nanorods. *Chemistry* **2019**, *25*, 1595-1600.
36. Yuan, H.; Khoury, C. G.; Hwang, H.; Wilson, C. M.; Grant, G. A.; Vo-Dinh, T. Gold nanostars: surfactant-free synthesis, 3D modelling, and two-photon photoluminescence imaging. *Nanotechnology* **2012**, *23*, 075102.
37. Kikkeri, R.; Hossain, L. H.; Seeberger, P. H. Supramolecular one-pot approach to fluorescent glycodendrimers. *Chem. Commun. (Camb).* **2008**, *18*, 2127-2129.
38. Zhang, X.; Goncalves, R.; Mosser, D. M. The isolation and characterization of murine macrophages. *Curr Protoc Immunol*. **2008**, Chapter 14:Unit 14.1.
39. Nuhn, L.; Vanparijs, N.; De Beuckelaer, A.; Lybaert, L.; Verstraete, G.; Deswarte, K.; et al. pH-degradable imidazoquinoline-ligated nanogels for lymph node-focused immune activation. *Proc. Natl. Acad. Sci. U S A.* **2016**, *113*, 8098-103.
40. Albin, T. J.; Tom, J. K.; Manna, S.; Gilkes, A. P.; Stetkevich, S. A.; Katz, B. B.; et al. Linked Toll-Like Receptor Triagonists Stimulate Distinct, Combination-Dependent Innate Immune Responses. *ACS Cent. Sci*. **2019,** *5*, 1137-1145.

41. Krieg, A. M.; Wu, T.; Weeratna, R.; Efler, S. M.; Love-Homan, L.; Yang, L.; et al. Sequence Motifs in Adenoviral DNA Block Immune Activation by Stimulatory Cpg Motifs. *Proc. Natl. Acad. Sci. U.S.A.* **1998**, *95*, 12631-12636.
42. Sangabathuni, S.; Murthy, R. V.; Chaudhary, P. M.; Surve, M.; Banerjee, A.; Kikkeri, R. Glyco-gold nanoparticle shapes enhance carbohydrate-protein interactions in mammalian cells. *Nanoscale* **2016**, *8*, 12729-12735.
43. Sioud, M. Induction of Inflammatory Cytokines and Interferon Responses by Double-stranded and Single-stranded siRNAs is Sequence-dependent and Requires Endosomal Localization. *J. Mol. Biol*. **2005**, *348*, 1079–109.